Synthesis and Coordination Chemistry of Functionalised Phosphazanes

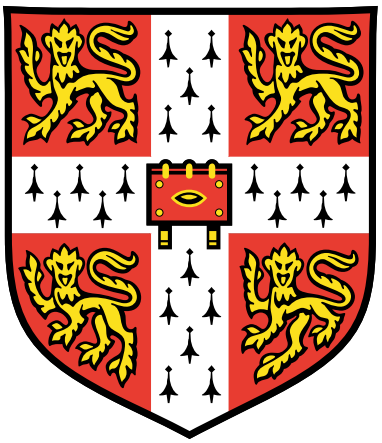

Callum G. M. Benson

Gonville and Caius College
Department of Chemistry
University of Cambridge
September 2016

This dissertation is submitted for the degree of Doctor of Philosophy.

Why did the Scarecrow pass his PhD?

Because he was outstanding in his field

Declaration

This dissertation is the result of my own work and includes nothing which is the outcome of work done in collaboration except where it is declared otherwise.

It is not substantially the same as any that I have submitted, or, is being concurrently submitted for a degree or diploma or other qualification at the University of Cambridge or any other Institution. I further state that no substantial part of my dissertation has already been submitted, or, is being concurrently submitted for any such degree, diploma or other qualification at the University of Cambridge or any other University of similar institution.

Signed……...

Callum G.M. Benson

Acknowledgements

I would first and foremost like to thank my supervisor, Dom. He has been an amazing help throughout, from making me a 30 g batch of starting material in my first week, to proof reading my thesis.

I have been lucky enough to supervise some incredible Masters and Part III students over the past 4 years. Thanks go to Vlad and Alex especially for their insightful ideas and hard-working nature.

All of lab 301 deserve generous praise for putting up with the incessant puns and jokes over the years, but also for all their help and the fun environment. Thanks go especially to Raúl, the NMR wizard. I would also like to thank the Gade group in Heidelberg who generously hosted me for three months during 2nd year. To all the technicians, crystallographers and support staff who have put up with me, I am extremely grateful for your help and patience.

Finally, I would like to thank my family for being so supportive and crazy, my friends for being the best one could wish for and Tamara, who has been amazingly helpful and patient.

List of Publications

C. G. M. Benson, A. J. Plajer, R. García-Rodríguez, A. D. Bond, S. Singh, L. H. Gade, and D. S. Wright, *Chem. Commun.*, 2016, **52**, 9683–9686.

C. G. M. Benson, V. Vasilenko, R. García-Rodríguez, A. D. Bond, S. González Calera, L. H. Gade, and D. S. Wright, *Dalt. Trans.*, 2015, **44**, 14242–14247.

T. Roth, V. Vasilenko, C. G. M. Benson, H. Wadepohl, D. S. Wright, and L. H. Gade, *Chem. Sci.*, 2015, **6**, 2506–2510.

M. L. Böhm, T. C. Jellicoe, J. P. H. Rivett, A. Sadhanala, N. J. L. K. Davis, F. S. F. Morgenstern, K. C. Gödel, J. Govindasamy, C. G. M. Benson, N. C. Greenham, and B. Ehrler, *J. Phys. Chem. Lett.*, 2015, **6**, 3510–3514.

Abstract

This thesis focuses on the chemistry of novel phosphazane species derived from the chloro-phosphazanes $[ClP(\mu\text{-}NR)]_2$ and their use as ligands and building blocks for macrocyclic compounds. The introduction (Chapter 1) surveys previous literature in the area, which is pertinent to the new studies. One of the most important issues is the various ways in which dimeric phosph(III)azanes can be employed as precursors for new ligands and in the design of new types of inorganic macrocycles. In Chapter 2 the synthesis of new chloro-dimers of the type $[ClP(\mu\text{-}NR)]_2$ is described, which are the primary starting materials. Chapter 3 concerns the substitution at the chlorine atoms of $[ClP(\mu\text{-}NR)]_2$ by LiSH to give a variety of sulfur-containing P^V species $[S{=}P(H)(\mu\text{-}NR)]_2$. The thermodynamic preference for the *cis* or *trans* isomers of the latter are explored by detailed NMR spectroscopic and DFT calculation investigations. Deprotonation of the ^{t}Bu derivative $[S{=}P(H)(\mu\text{-}N^tBu)]_2$ using organometallic bases (Chapter 3) led to the isolation of *s*-block salts (Mg^{2+}, Na^+, K^+) of the P^{III} dianion $[S\text{-}P(\mu\text{-}N^tBu)]_2^{2-}$. The Mg^{2+} salt was found to form a mononuclear complex in the solid state whereas the Na^+ salt formed a large cage comprising eight dianions and 16 Na^+ ions built around a NaSH core. These *s*-block metal salts were shown to be useful transfer reagents for the dianion towards complexation with main group metals (e.g., Sn and Ge). Chapter 4 explores the oxidation of the P^{III} dianions $[S\text{-}P(\mu\text{-}N^tBu)]_2^{2-}$ by chalcogens to give the more stable P^V species $[(E{=})P^v(\text{-}S)(\mu\text{-}N^tBu)]_2^{2-}$ (E = S, Se). The increase in stability and lower reducing ability of the P^V dianion allowed the formation of complexes with transition and main group metals. Reaction of $[(E{=})PS(\mu\text{-}N^tBu)]_2^{2-}$ with chloro-dimers $[ClP(\mu\text{-}NR)]_2$ led to the formation of homo- and heteroleptic P^{III}-P^V phosphazane macrocycles of the type $[\{S{=}P^V(\mu\text{-}N^tBu)\}_2(\mu\text{-}E)\{P^{III}(\mu\text{-}NR)\}_2]$. These can be oxidised to give air- and moisture-stable all-P^V species $[\{S{=}P^V(\mu\text{-}N^tBu)\}_2(\mu\text{-}E)\{S{=}P^V(\mu\text{-}NR)\}_2]$ by reaction with elemental sulfur. Finally, in Chapter 5 the substitution of the chlorine atoms in $[ClP(\mu\text{-}NR^1)]_2$ by amines (R^2NH_2) is explored, to give a range of bis(amino) cyclophosphazanes $[(R^2NH)P(\mu\text{-}NR^1)]_2$ containing chiral and non-chiral R^2 and R^1 groups. These species were used in the formation of early transition metal (Zr, Ti, Hf) complexes which are potential pre-catalysts for alkene polymerisation studies.

Abbreviations

Benz	Benzhydryl
Bn	Benzyl (-CH_2Ph)
bs	Broad Singlet
Calcd.	Calculated
Cp*	Pentamethylcyclopentadienyl
CV	Cyclic Voltammetry
d	Doublet
DCM	Dichloromethane
DFT	Density Functional Theory
Dipp	Diisopropylphenyl
DMSO	Dimethyl sulfoxide
dppe	Diphenylphosphineethylene
E	Chalcogen
equiv.	Equivalents
Et	Ethyl
FTIR	Fourier Transform Infrared
g	Grams
h	Hours
Hz	Hertz
I	Spin Quantum Number
^{i}Pr	isopropyl
K	Degree Kelvin
m	Multiplet (NMR)
m	Medium (IR)
Me	Methyl
Mes	Mesityl
MHz	Megahertz
min	Minutes
ml	Millilitres
mmol	Millimoles
*n*Bu	n-butyl
*n*BuLi	n-Butyllithium
NMR	Nuclear magnetic resonance
ºC	Degree Celsius

OTf	Triflate (CF_3SO_3)
Ph	Phenyl
$P^{III/V}$	Phosphorus in the oxidation state (III) or (V)
ppm	parts per million
R	Organic substituent
r.t.	Ambient temperature
s	Singlet (NMR)
s	Strong (IR)
^{t}Bu	Tertiary Butyl
TeCA	1,1′,2,2′-tetrachloroethane
Ter	Terphenyl
thf	Tetrahydrofuran
TMP	2,2,6,6-tetramethylpiperidide
TMS	trimethylsilyl ($(CH_3)_3Si$)
tol	Toluene
w	Weak
λ	Wavelength

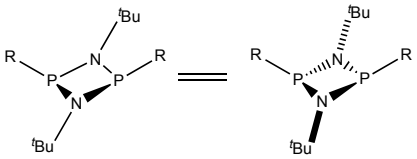

Colour codes for crystal structures

Phosphorus		Oxygen	
Nitrogen		Hydrogen	
Sulfur		Earth Metal	
Selenium		Gold	
Carbon		Gallium	
Chlorine		Bromine	
Iodine		Nickel	

Table of Contents

1. Introduction

1. Introduction

1.1 P-N Chemistry

The chemistry of phosphorus-nitrogen systems has been studied extensively and has led to a variety of thermodynamically-stable compounds used in organometallic, macrocyclic and biological chemistry, and they have also been studied in their own right. The stability of P-N systems is commonly attributed to the strength of the P-N σ bond (290 kJ mol^{-1}) which is comparable to that of a C-C single bond (346 kJ mol^{-1}). The P-N bonding interaction can also be strengthened further by combinations of σ*-π interactions and by the ionic contribution to the bond (owing to the difference in electronegativity between P and N). P-N compounds can therefore be formed of single P-N σ bonds or partial double π bonds. Rare examples of P-N (formally) triple bonds have also been isolated but are beyond the scope of this report.[1,2]

The ability of these species to form multiple bonded systems arises from the ability of phosphorus to adopt a variety of valence states (3 or 5). These factors combine to give rise to an extremely large set of structurally-diverse molecules. Of most interest to this thesis are the so-called cyclophosph(III)azanes, P^{III} analogues to the widely studied cyclophosphazenes which contain P^{V} centres, and which have been widely studied as ligand scaffolds, superbases and polymer precursors.

1.1.1 Phosphazenes

Phosphazenes, characterised by the presence of a formal P=N double bond, can be formed in linear or cyclic arrangements with a wide variety of substituents on both the N and P atoms. Depending on the steric bulk, cyclic phosphazenes form a range of different rings systems, ranging from small $[P_2N_2]$ units up to large $[P_8N_8]$ rings. The P=N bonding in these cyclic species has been a matter of much debate, with two main theories. One theory involves the negative hyperconjugation of the exocyclic P-R σ*-orbitals with the N-lone pairs within the ring system (Figure 1.1a). The other uses a zwitterionic model to describe the structure as alternating P cations and N anions within a zwitterionic arrangement (Figure 1.1b). Both have been debated and the subject of a number of computational

studies.[3] The reality is probably a combination of both the σ*-conjugation model and the zwitterionic one. Figure 1.1c shows the most common literature representation of cyclophosphazenes as the double bonded alternating motif. This explains the presence of alternating short (1.47-1.62 Å) and long (1.77 Å) P-N bonds. This model requires the involvement of P block d orbitals in a formally 6π aromatic system in which pπ-dπ bonding is occurring. However, it is now accepted that the d-orbitals on P are far too high in energy for this representation to be true.[4–6]

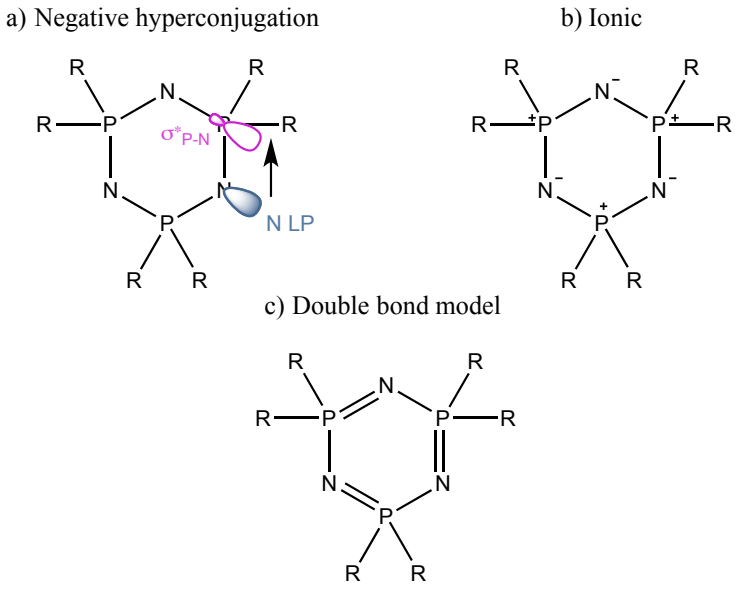

Figure 1.1: (a) negative hyperconjugation, (b) ionic, and (c) formally 6π aromatic system (involving dπ-pπ bonding).

The most common cyclophosphazene derivative is the easily synthesised $P_3N_3Cl_6$ (**1.1**). It is accessible by the simple reaction of PCl_5 and ammonium chloride and is an excellent building block for more elaborate materials (Scheme 1.1). An improved synthesis involving $N(SiMe_3)_3$ and PCl_5 is now more commonly employed.[7] The electrophilic phosphorus centre is readily modifiable by attack of a nucleophile (e.g. amines, alcohols, thiols, organometallic reagents) to give a large library of materials that can be used as ligands or polymer precursors. Using this method, thousands of compounds have been reported that contain the central P_3N_3 motif. The substituents can be added *geminally* or *non- geminally* to the phosphorus atoms of the P_3N_3 ring, depending on the nature of the substituting group. Substitution of the chlorine atoms by nucleophiles such as amines and alcohols can lead to complex frameworks centred around the cyclic P_3N_3 unit.[8]

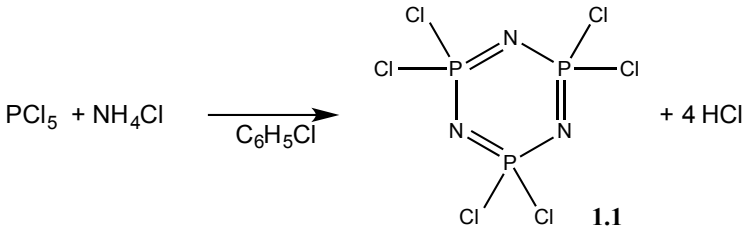

Scheme 1.1: Synthesis of $(NPCl_2)_3$

These materials are also important precursors to P-N polymers, which have found applications as flame retardant materials and battery coatings as well as medical devices and polymer dyes.[9] Their inherent conductivity and radiation resistance adds further diversity to their applications.[10] Two main methods used for PN polymerisation are thermal ring-opening polymerisation (heating to ~280 ºC) and cationic living polymerisation. The modifiable nature of these species and the variety of polymerisation methods available means they can form a host of polymers with a number of side groups. Figure 1.2 shows a typical P-N polymer (**1.2**) as well as an important precursor for living cationic polymerisation, the trichloro(N-silyl)phosphoranimine (**1.3**) characterised by Manners *et al.*[11,12]

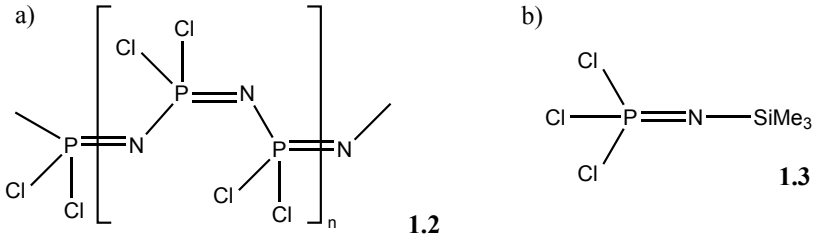

Figure 1.2: a) Simple P-N polymer framework. Further substitution at chloride gives immense structural diversity. b) Living-cationic polymerisation precursor, a trichloro(N-silyl)phosphoranimine 1.3.

Reaction of PCl_5 with bulkier primary amines gives rise to saturated phosph(V)azanes bearing three chlorides at P (**1.4**, Scheme 1.2).[13,14]

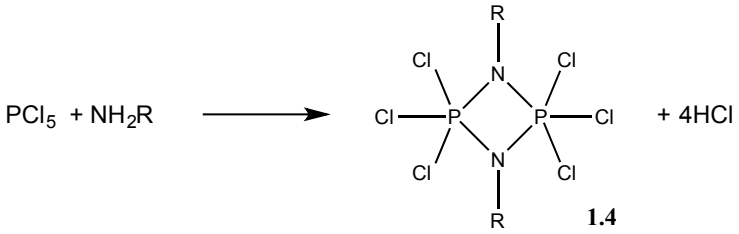

Scheme 1.2: Synthesis of cyclophosph(V)azanes.

The bonding in these compounds is strictly made up of a σ bond framework. The P-N ring is fully saturated and the reactivity of these species is therefore focused primarily on functionalisation by substitution at the phosphorus atoms using nucleophiles.[15] The species that come from reactions with $[PCl_3(\mu\text{-}NR)]_2$ tend to contain at least one chloride on phosphorus in the final products, and replacement of the final chlorine atom is only reported for a few cases. Furthermore, reduction to the corresponding P^{III} species has not yet been reported. The polymerisation behaviour seen for phosphazenes does not exist for these saturated analogues as heating generally leads to boiling or decomposition.

1.1.2 Phosph(III)azanes

As seen with the P^V systems mentioned at the end of the last section, saturated P-N rings or chains are known as phosph(III)azanes. The ring systems formed are found in a similar size range to their formally unsaturated P^V counterparts, ranging from P_2N_2 up to $P_{10}N_{10}$. Phosphorus(III) systems have been less studied than phosphorus(V) compounds, mainly due to their increased moisture sensitivity. The hydrolysis of P^{III} species **1.5** to form the P^V=O analogue **1.6** is driven by the formation of a very strong P=O bond upon (Scheme 1.3).

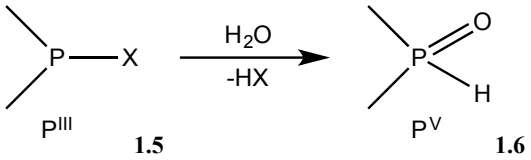

Scheme 1.3: Hydrolysis of P^{III} compound 1.5 to the P^V analogue 1.6 by H_2O with loss of HX (X= Halide, NR_2, OR, SR).

Bonding in phosph(III)azanes is composed of σ bonding between sp^3 hybridised phosphorus and sp^2 nitrogen atoms. Each heteroatom therefore has a lone pair available for bonding (i.e., donation). The saturated nature of these species gives them considerably more structural flexibility which, combined with the increased availability of the lone pair on phosphorus, makes them good candidates for coordination to metal centres. The four-membered P_2N_2 ring motif is the most prevalent structural type for phosph(III)azanes.

Phosphazanes can be formed *via* the simple condensation of PX_3 (X = Cl, Br) with amines (NR_3, R = H, alkyl, aryl) (normally in the presence of a Brønsted base), which gives a convenient synthetic procedure to obtain a variety of functionalised phosph(III)azanes. The majority of literature preparations of phosphazanes employ a primary amine in such a way that sequential Cl-substitutions occur with elimination of HCl as the thermodynamic driving force (Scheme 1.4) (normally eliminated as an ammonium salt upon reaction with a Brønsted base, such as Et_3N). These types of reactions can be performed in a variety of stoichiometric ratios to obtain the mono- (**1.7**), di- (**1.8**) tri- (**1.9**) and tetra- (**1.10**) substituted products $[YP(\mu\text{-}NR)]_n$ (Y = halogen, NHR).[16–18] This synthetic procedure can be extended to reactions with amine hydrochlorides, silylamines, and amides to give cyclophosph(III)azanes with a variety of R substituents.

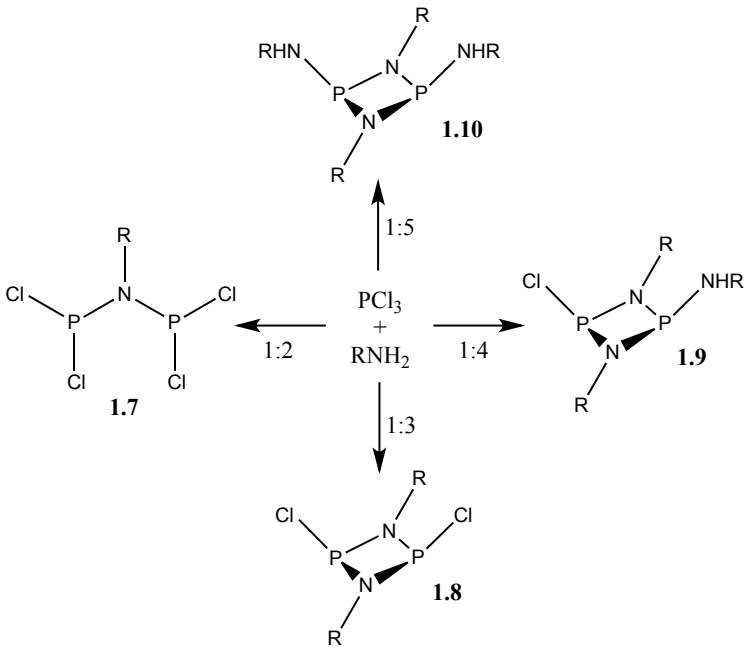

Scheme 1.4: Stoichiometric control in the synthesis of phosph(III)azanes.

Reactions of this type all require extremely slow addition of the amine to the PCl_3 at low temperatures to suppress any unwanted amine addition to phosphorus. This can be avoided, however, by using a separate non-coordinating Brønsted base such as Et_3N. A ten-fold excess is commonly employed in the improved synthesis of cyclodiphosphazanes and gives much higher yields of the desired materials.[19] It is important to note that the representation used throughout this thesis is for aesthetic purposes only, and that strictly speaking the P_2N_2 unit should be represented with forward and dashed bonds to emphasise the tetrahedral nature at phosphorus.

In the case of R = Ph (aniline) a carefully controlled ratio of 1:4.7 of PCl_3 to $PhNH_2$ gives an imido bridged phosphazane [{PhHNP(μ-NPh)$_2$P}$_2$(μ-NPh)]. Furthermore, less sterically hindered R groups (Me, Et) give rings of larger size. For example, reaction between $EtNH_3Cl$ and PCl_3 in 1,1′,2,2′-tetrachloroethane gives the cyclic trimer [ClP(μ-NEt)]$_3$ (**1.11**, Scheme 1.5).[20] Studies on [ClP(μ-NEt)]$_3$ showed that the ring can be contracted from the P_3N_3 trimer **1.11** (the thermodynamic product) to the dimeric ring compound [ClP(μ-NEt)]$_2$ (**1.12**) (the kinetic product) by simple distillation (Scheme 1.5). The process is reversed at ambient temperature.[21]

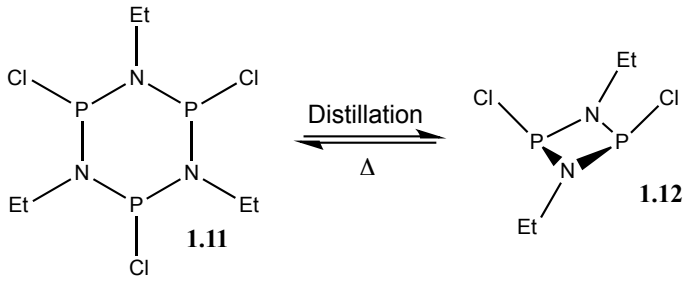

Scheme 1.5: Ring expansion and contraction of [ClP(μ-NEt)]$_3$ (1.11).

P_2N_2 rings of the type [ClP(μ-NR)]$_2$ (**1.8**) can be thought of as the [2+2] cyclo-addition products of two unsaturated P=N monomers. Studies have shown that there can be a dynamic equilibrium in solution between the monomeric and dimeric forms (which depends on the substituents). For example, the mesityl-substituted dimer [PCl(μ-NMes)]$_2$ (**1.13**) when reacted with one equivalent of a guanidinate species (**1.14,** Scheme 1.6) gives rise to the addition product **1.15** (Scheme 1.6).[22] When the steric bulk of the amine is increased even further, for example to accommodate the Mes* ligand, the 1:1 reaction between PCl_3 and Mes*NH_2 with Et_3N gives the iminophosphane ClP=NMes*.[1] The

much larger cone angle compared to the Mes substituent prevents the cyclo-addition of two ClP=NR monomers into a P_2N_2 dimer.[23]

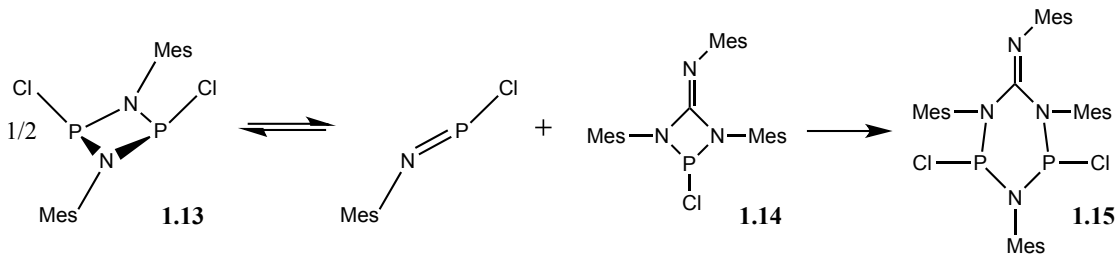

Scheme 1.6: Insertion of *in situ* generated monomer into a tris(Mes)guanidinato chlorophosphine (1.12) to give 1.13.

The presence of phosphorus in cyclophosphazanes allows for easy analysis of their formation and reactivity using ^{31}P NMR spectroscopy, taking advantage of the 100% natural abundance of ^{31}P (I = ½). Most reactions are easily followed by *in situ* NMR spectroscopy, which allows for mechanistic and kinetic elucidation. A good example is the analysis of the mechanism of reaction of $DippNH_2$ with PCl_3, where Burford *et al.* were able to identify nine separate species including six reactive intermediates during the successive addition of the amine in the generation of fully substituted bis(amino) species **1.10** (Scheme 1.3).[24] The number of environments and completeness of reaction can give valuable insight into the structure of the material obtained; however, X-ray crystallography remains the main diagnostic tool for phosphazane compounds.

X-ray crystallography allows for the characterisation of strain and steric effects on the P_2N_2 ring unit of phosphazane dimers. By measuring the P-N-N-P torsion angle, we can gain insight into how substituents affect the ring unit, which VSEPR would predict to be planar. *Cis*-conformers, in which the phosphorus substituents are on same face of the PN ring, tend to have a much more bent P_2N_2 core, whereas *trans*-analogues have nearly planar rings (for example *trans*-**1.16** and *cis*-**1.17**, Figure 1.3). Substituents on the nitrogen are typically in the mean plane of the ring whereas phosphorus substituents tend to lie almost perpendicular to the P_2N_2 ring, consistent with an sp^2 nitrogen and sp^3 phosphorus.

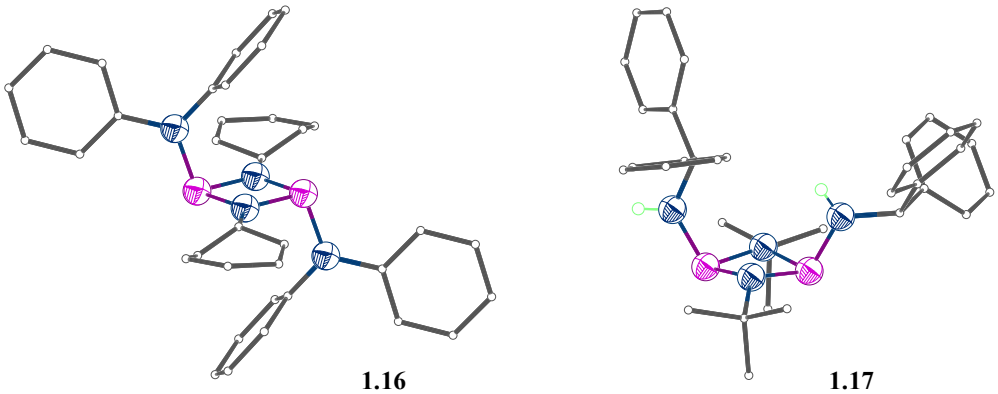

1.16 **1.17**

Figure 1.3: X-Ray structures of two amine-substituted phosphazanes. Left: *Trans*-conformation in $[Ph_2NP(\mu\text{-}NPh)]_2$.[25] Right: *Cis*-conformation in $[(Ph_2CH)NHP(\mu\text{-}N^tBu)]_2$.[26] Hydrogen atoms omitted for clarity.

Another important structural characteristic is the tendency for the adoption of the *cis* isomer formation in phosphorus(III) P_2N_2 rings of the type $[RP(\mu\text{-}NR)]_2$ (R = an organic substituent or halogen atom; CCDC search: 19 *trans* vs 151 *cis*).[25,27] Calculations have shown that the *trans* isomer is kinetically favoured whereas the *cis* is found to be thermodynamically favoured. However, the energy barrier between *cis* and *trans* isomers of a particular P_2N_2 ring compound is found to be low, and solution ^{31}P NMR spectroscopic studies show that the isomers can be present in equal amounts, and the adoption of the *cis* geometry in the crystalline state might well be the result of crystal packing forces alone.[28] Chloro-cyclophosph(III)azane dimers of the type $[ClP(\mu\text{-}NR)]_2$ are found to almost exclusively form *cis* isomers in the solid state.[19,29]

1.2 Reactivity of Chlorophosph(III)azanes $[ClP(\mu\text{-}NR)]_2$

The reactivity of halo-phosph(III)azanes has been widely explored in the past 50 years. Substitution is possible at the phosphorus centres by nucleophiles from across the periodic table. Furthermore, controlled oxidation of the phosphorus atom proceeds with a variety of main group oxidising agents. In this way, a variety of substituted phosph(III and V)azanes have been accessed.

1.2.1 Nucleophilic Substitution by NH_2R

Chloro-dimers of the general formula $[ClP(\mu\text{-}NR)]_2$ are readily transformed by substitution at the chlorine. Reactions with alcohols, amines, carbon nucleophiles and even sulfur compounds result in substitution of the chlorine atoms (OR, SR, NR_2, CR_3, R = H or Alkyl/Aryl). For example, Scheme 1.6 shows the reaction of mono- and di-chloro dimers (**1.8** and **1.9**) with an amine in presence of a Brønsted base to form either a symmetric or asymmetric bis(amino)cyclophosphazane **1.18** or **1.19** respectively.

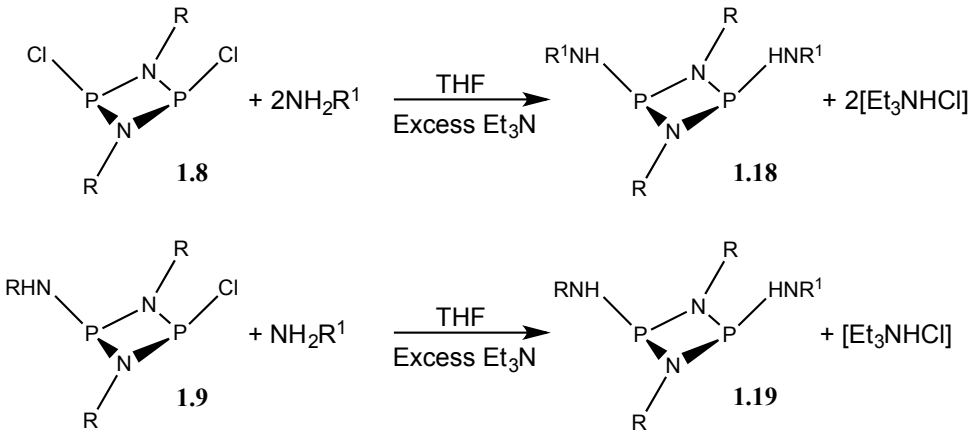

Scheme 1.6: Substitution of chlorides on $[ClP(\mu\text{-}NR)]_2$ and $NHRP(\mu\text{-}NR)PCl$ by amine to give bis(amino) cyclophosphazanes 1.18 or 1.19. Brønsted base used to control stoichiometry.

The substitution of the chlorine ligand with primary amino-groups is of particular interest. The resulting species of the type $[(RNH)P(\mu\text{-}NR)]_2$ have three types of donor atoms, Figure 1.4.

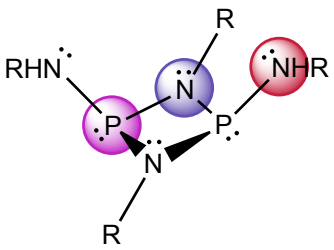

Figure 1.4: Representation of the different lone pairs in bis(amino)cyclophosphazanes. Amine lone pair (red), tertiary-amine (imido) lone pair (blue) and phosphorus lone pair (pink) highlighted.

The amino-substituents (red, Figure 1.4) can act as a bidentate nitrogen donor set and have been found to bond especially to early transition metals. Later transition metals (Au, Rh, Pd etc…) tend to coordinate *via* the softer phosphorus lone pair (pink, Figure 1.4) to give monodentate complexes. However, the imido-nitrogen atoms (blue, Figure 1.4) only participates weakly in bonding with heavier main group elements and some transition metals which coordinate primarily to the amino-substituents presumably due to lower steric hindrance at the amino position.[19,30,31] Work by Stahl and co-workers have explored the reactions of the dianion $[N^tBuP(\mu\text{-}N^tBu)]_2^{2-}$ with a range of transition metal and main group salts (e.g. Sn, As, P, Ti, Zr).[19,30,32–34] Typical complexation reactions involving these species proceed *via* either direct reaction with a metal dichloride/amine group species in the present of a Brønsted base, or *via* a first step involving lithiation to form the dianion $[NRP(\mu\text{-}NR)]_2^{2-}$, followed by transfer of the dianion to the metal.

In the case of main group elements, the structures all fall into three main categories, based on the typical cubane unit (Figure 1.5). The elements (generally metal ions) occupy either both (**I**) or just one corner of the unit (**II**), or bridge the P_2N_2 ring (**III**), depending on the nature of E (e.g., charge and ionic size). Complexes have been obtained for all Group 13, 14 (except Pb) and 15 elements, as well as a number of Group 16 elements.[19,35] These coordination studies show the variety and complex structures that can be obtained from a relatively simple ligand set, especially since these complexations are primarily limited to a small range of R groups, mainly species containing ^{t}Bu, Ph or Cy as amino substituents have been characterised.

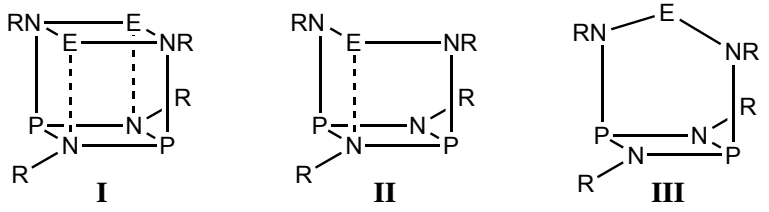

Figure 1.5: Three typical ligand configurations of main group elements (E) with bis(amino) diphosphazanes. I: Occupying both corners of a cubane unit, II: Occupying one corner of a cubane unit, and III: Bridging *via* amino groups.

1.2.2 Substitution Using Main Group Acids/Nucleophiles.

Another recently developed field is the substitution of dichloro-dimers $[ClP(\mu\text{-}NR)]_2$ using simple main group nucleophiles. The use of main group nucleophiles (or acids in conjunction with a suitable base, to generate a nucleophile) leads to substitution at phosphorus. Scheme 1.7 shows a summary of the different main group substitutions that have been incorporated in this way.[36–38] The resulting compounds can either contain a P^V or P^{III} unit, depending on the relative bond strengths of the π vs σ bonds.

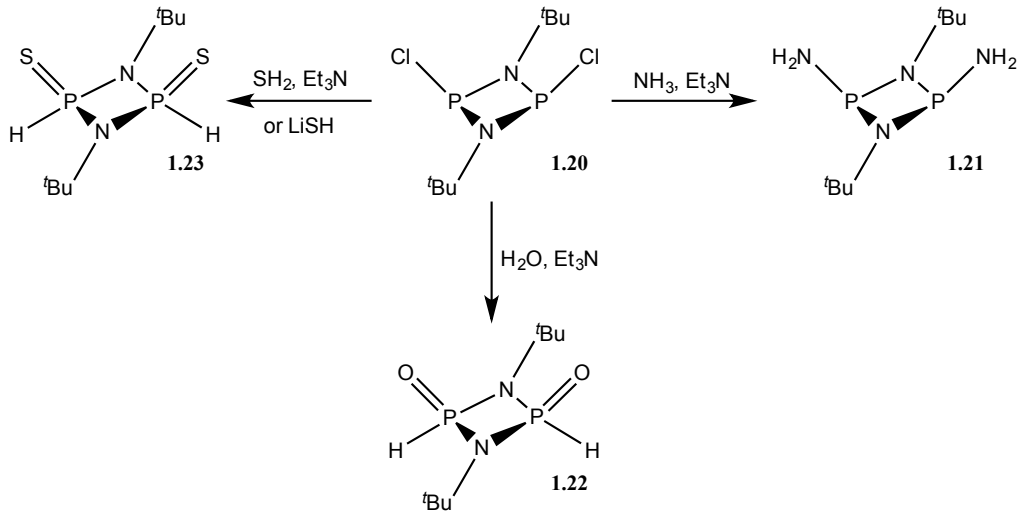

Scheme 1.7: Synthesis of main group element substituted diphosph(III)azanes 1.21,[39] 1.22,[40] and 1.23[37] from 1.20.

These molecules are precursors to a variety of metal complexes but have been most valuable in the formation of inorganic macrocycles (see Section 1.3.2). The lack of steric bulk at the P atom can lead to thermal instability, for example, the oxo-derivative $[O=(H)P(\mu\text{-}^tBu)]_2$ **1.22** readily condenses with another molecule of **1.22** at temperatures >5 ºC and needs to be handled carefully in order to be used as a the single phosphazane (Scheme 1.8).[38]

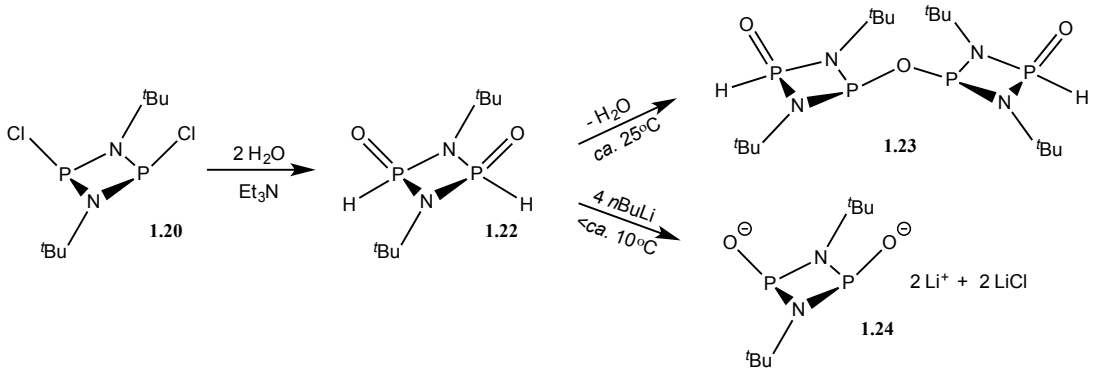

Scheme 1.8: Synthesis of the oxo-substituted dimer [O=P(H)(μ-^{t}Bu)]$_2$ (1.22) and subsequent condensation at ambient temperature to give 1.23 or deprotonation to give 1.24.

This condensation to **1.23** is avoided by *in situ* lithiation using *n*BuLi. The resulting cage complex that is formed is made up of three [O-P(μ-N^{t}Bu)]$_2^{2-}$ anions with a core structure based around a cage of two interlocked Li_4Cl_4 cubane units (Figure 1.6).

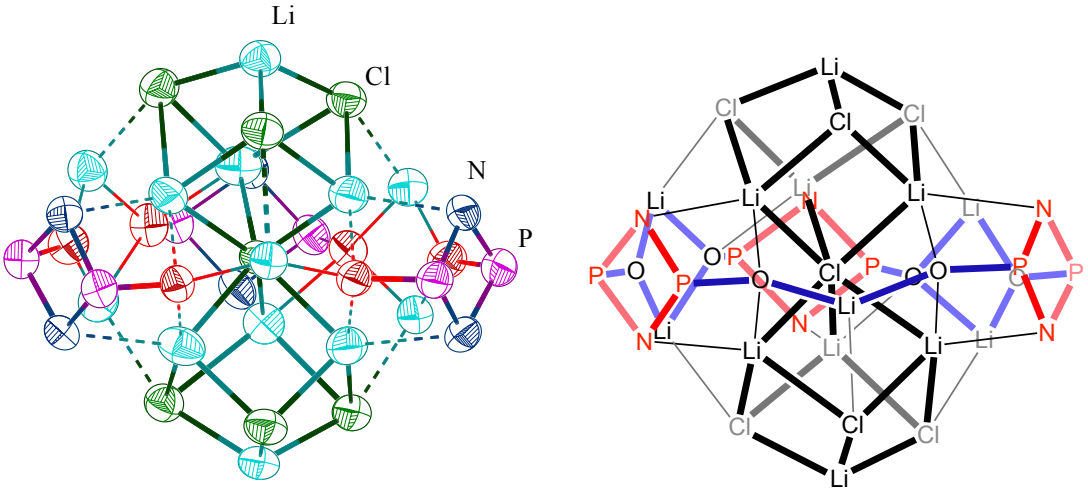

Figure 1.6: Left: Core structure of the Li_{13} cage containing the [O=P(H)(μ-^{t}Bu)]$_2^{2-}$ dianion 1.24. ^{t}Bu units and Hydrogen atoms omitted for clarity Right: Line drawing of the structure, central ring highlighted in blue and phosphazane units in red.

Another way of suppressing the self-condensation of the oxo species was to form the asymmetric species [O=(H)P(μ-N^{t}Bu)$_2$PNH^{t}Bu] (**1.25**) where one O(H) is replaced with N^{t}Bu. Starting from the readily synthesised mono(amino) chloro dimer [ClP(μ-N^{t}Bu)$_2$PNH^{t}Bu] (**1.9**), reaction with H_2O gives **1.25** which was not found to aggregate in the same manner as the di-oxo species [O=(H)P(μ-N^{t}Bu)]$_2$.[40]

Despite their interesting reactivity and potential as sterically unhindered building blocks, only a few examples of these simple main group substituted phosphazanes exist. As seems to be the common trend with phosphazanes, only the ^{t}Bu derivatives have been synthesised and their full reactivity scope has not been explored.

1.2.3 Reactions at Phosphorus

The generation of new species by substitution at the chlorine at the phosphorus atoms of the dimers $[ClP(\mu\text{-}NR)]_2$ with nucleophiles is an important area. Another theme in current research on phosphazanes is the abstraction of the halide ion or halogen atom from these dimers. The resulting species are the P^+ cation or $P\cdot$ radical (Figure 1.7). Weigand and coworkers used strong Lewis acids ($GaCl_3$) to extract the chloride from the phosph(III)azane dimer $[ClP(\mu\text{-}NDipp)]_2$, to give the corresponding di-cation $[P(\mu\text{-}NDipp)]_2^{2+}$ (**1.26**).[41] The use of stoichiometric amounts of Lewis acid also allows the formation of the mono-cation **1.27**. The addition of 3:2 $GaCl_3$ to $[ClP(\mu\text{-}NDipp)]_2$ leads to the insertion of *in situ* generated P^+=NDipp into a $[ClP(\mu\text{-}NDipp)]_2$ moiety to give the six membered cation **1.29**.[42]

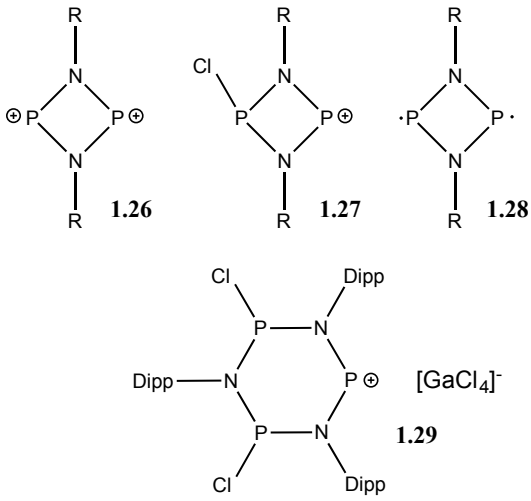

Figure 1.7: Range of cations and radicals resulting from halide abstraction of a chloro-cyclodiphosphazane dimer (R= Dipp, Ter).

Both the *bis*- (**1.26**) and *mono*- (**1.27**) cations are reactive species that can be used for activation of P_4 or coordination of weakly-coordinating anions, such as triflate or azide, to the phosphazane moiety.[43]

The generation of the biradical **1.28** proceeds *via* a similar route, however, the R substituents on the nitrogen have to be bulky in order to prevent P-P bond formation. Schulz *et al.* have undertaken exhaustive studies on the reduction of $[ClP(\mu\text{-NTer})]_2$ by $[CpTiCl_2]$ to give the biradical **1.28** (R = Terphenyl).[44–47] The generated species is diamagnetic even at high temperatures and is therefore referred to as a *biradicaloid*. It reacts with a variety of main group and organic substrates in the manner of a traditional biradical, to form a variety of cyclodiphosphazane cages.[48] Recent computational and synthetic studies on its coordination to AuCl showed that it has zwitterionic character and serves as a P^- source to coordinate two AuCl atoms to one phosphorus atom (**1.30**, Figure 1.8) or a P^+ source when reacted with NHC's to give the adduct $[(NHC)_2P]^+[TerNPNTer]$.

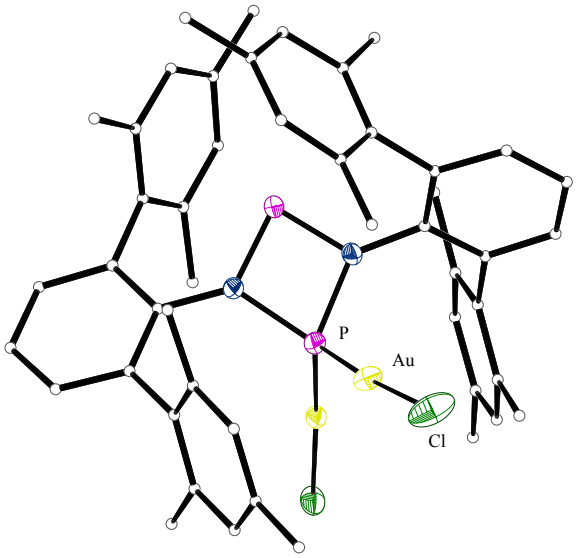

1.30

Figure 1.8: X-ray structure of the di-gold adduct 1.30, product of a 2:1 reaction of DMSAuCl with 1.28.

The saturated nature of the bonding in phosph(III)azane systems allows for further diversification. As previously mentioned, sp^3 P^{III} systems can undergo oxidation to form phosphorus(V) species. This can be achieved using variety of common oxidants, such as H_2O, elemental S, Se, and Te. P^V compounds have the advantage of being significantly more stable than their P^{III} analogues.[49] Furthermore, the addition of an electron-rich main group element on the phosphazane ring gives another potential coordination site. Figure 1.9 shows the three types of unique lone pairs present in an oxidised bis(amino) cyclophosphazane.

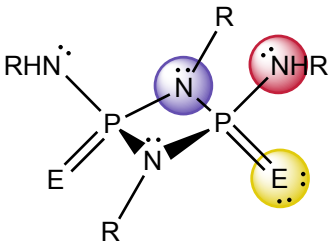

Figure 1.9: Lone pairs present in an oxidised bis(amino) cyclophosphazane. Imido (Blue), amino (Red) and main group substituent E (E= O, S, Se, Te, Yellow).

The first oxidised phosph(V)azane rings reported by Weiss *et al.* in the 1960's were prepared by reaction of PCl_5 with amines followed by oxidation with a sulfur source, SH_2 or SO_2.[50] Ten years later, further studies incorrectly characterised similar compounds as six-membered $(PSN)_2$ heterocycles, generated from the thermal condensation of amines with PhPS.[51] Finally, determination of the crystal structure of one of the products, $[S=(Ph)P(\mu\text{-}NR)]_2$ (**1.31**), showed that it is a *trans* phosph(V)azane containing P=S bonds (Scheme 1.9).[52] This was the first identification of a *trans* P_2N_2 ring and also the first structural determination of an oxidised phosphazane.

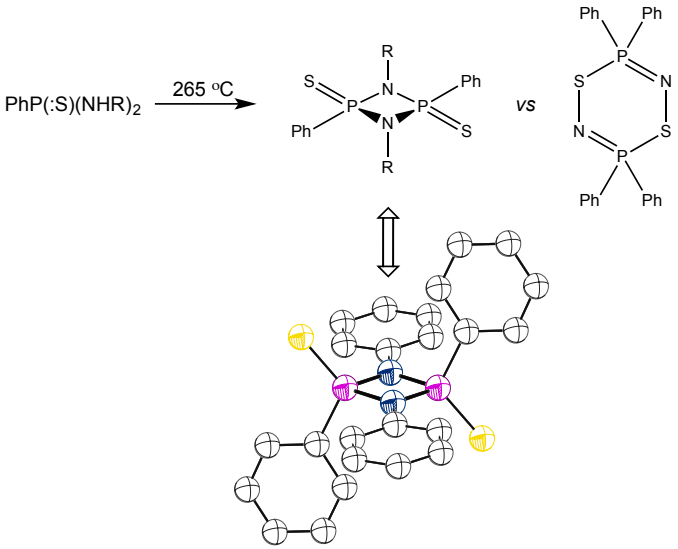

1.31

Scheme 1.9: Synthesis of the first main group oxidised phosph(V)azane 1.31 and structural determination by X-ray crystallography. Hydrogen atoms omitted for clarity.

The first reports of direct oxidation of phosph(III)azanes to the corresponding P^V species were by Keat *et al.* in the early 80's. The work was focused primarily on oxo-substituted rings of the type

$[ROP(\mu\text{-}N^tBu)]_2$ and their transformation into main group oxidised species $[RO(E{=})P(\mu\text{-}N^tBu)]_2$ (E = O, S), by reaction with elemental sulfur, or with primary alcohols followed by reduction with MeI.[53,54] More recent studies have focused on the transformation of P^{III} species to the P^V in order to stabilise and functionalise the P_2N_2 ring. Swamy and co-workers pioneered the reaction of amine and oxo-substituted phosphazane macrocycles with either elemental sulfur, or a diol ligand to form air-stable addition products **1.32** and **1.33** (Figure 1.10).[55–57]

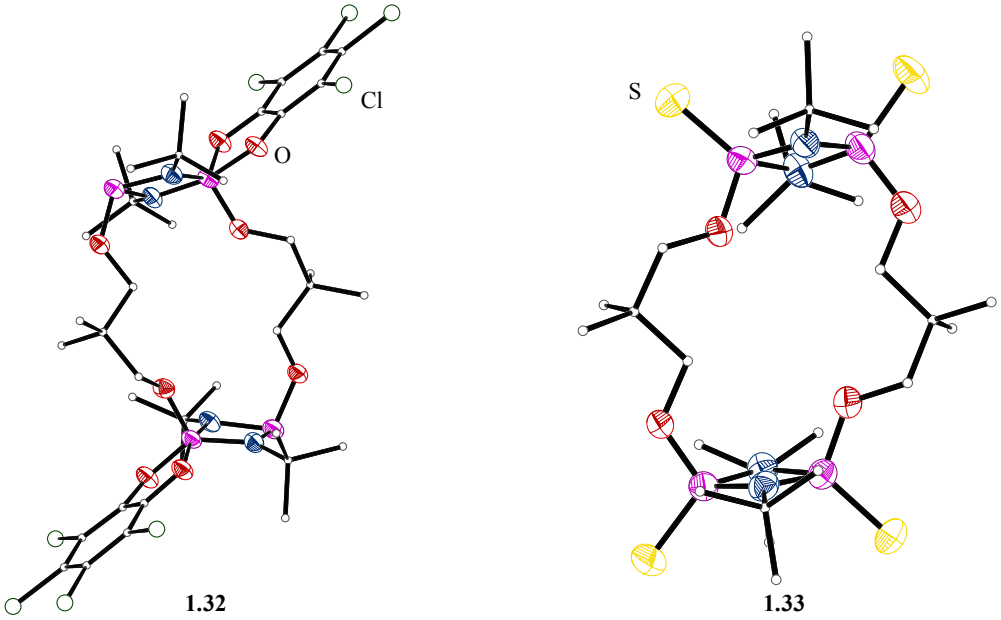

Figure 1.10: X-ray structures of oxidised phosphazane species (Swamy *et al.*), Left: *mono*-diol oxidised bridged phosphazane 1.32, Right: *bis*-sulfur oxidised O-Bridged phosphazane 1.33.

Interestingly, in the case of the diol oxidation product **1.32**, only one side of the phosphazane unit within the macrocycle is oxidised. This is most likely to be due to steric factors since in almost all other cases bis-oxidation occurs.[57] These simple transformations paved the way for extensive work on the coordination of oxidised dianions to main group elements and transition metals. Work by Chivers *et al*. using bis(amino)cyclophosphazanes $[RNHP(\mu\text{-}N^tBu)]_2$ showed the diversity of phosphazanes as ligands. Starting from the common ^{t}Bu-substituted chloro dimer $[ClP(\mu\text{-}N^tBu)]_2$, condensation with amine gives the bis(amino) substituted phosphazane ring $[RNHP(\mu\text{-}N^tBu)]_2$ (**1.34**).[58] As previously mentioned, these di-amines are easily deprotonated (Stahl *et al*,[19] Section 1.1.3), however, *in situ* oxidation using S_8, Se, or Te gives the oxidised species $[RNH(E{=}P)(\mu\text{-}N^tBu)]_2$ (**1.35**) which can be

deprotonated using a variety of organometallic reagents to give the dianions $[RN(E=P)(\mu\text{-}N^tBu)]_2^{2-}$. The coordination of the metal cations to these anions is complicated. The possibility for the cation to bridge either over the face of the P_2N_2 ring (E,E'/N,N' mode, **1.36**) or side-on (E,N mode, **1.37**) through the groups on one phosphorus gives rise to a variety of solid-state structures. Some contain mixed motifs of both side-on and face-on cation coordination (Scheme 1.10).

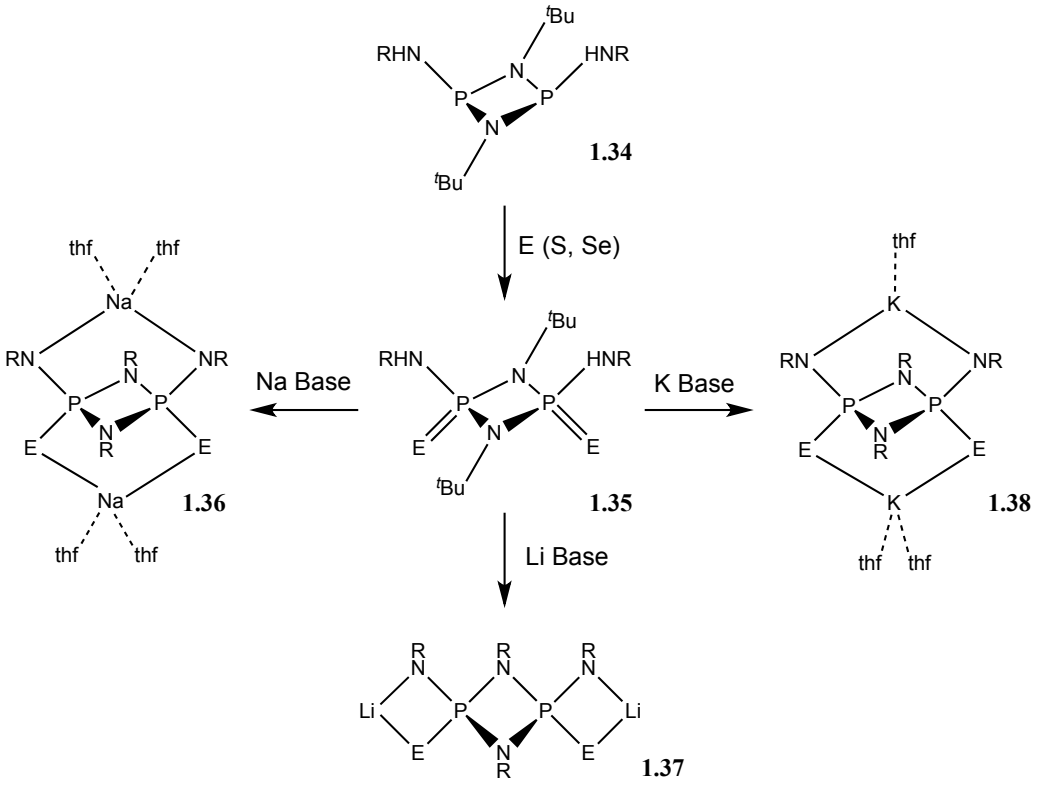

Scheme 1.10: Deprotonation of oxidised bis(amido) cyclophosphazanes, showing the variety of coordination modes of the counterions.

In the case of the Te-oxidised species, it is necessary to first deprotonate the bis(amino) cyclophosphazane before oxidation. Similarly to the S or Se oxidised analogues, cations can bridge over the face of the P_2N_2 ring (**1.39**, Scheme 1.11) but mix-bridged species have also been observed (**1.40**), where one cation sits side-on and the other over the face (i.e., a combination of Te,Te' and Te,N coordination modes).

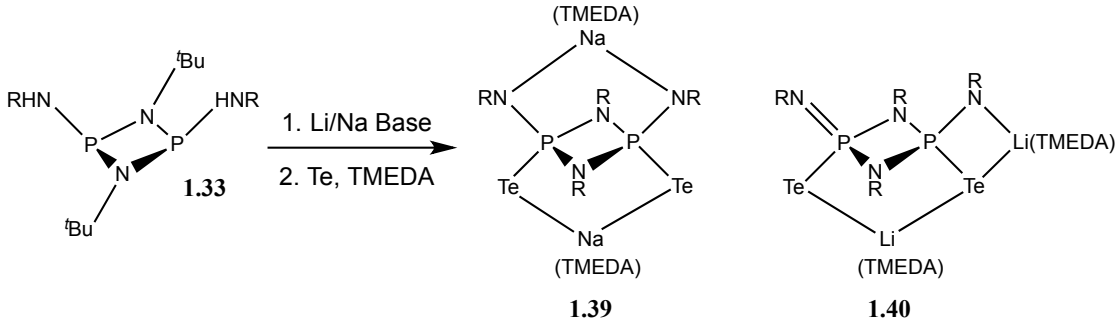

Scheme 1.11: Formation of the Te-oxidised bis(amino) cyclophosphazane by deprotonation followed by *in situ* oxidation. Depending on the base, the counterion can reside over the face of the ring (1.39), side-on, or both (1.40).

One interesting example is the result of a reaction of $[^t\text{BuN(Te-P)}(\mu\text{-N}^t\text{Bu})]_2^{2-}$ (**1.40**, Scheme 1.11) with $GaCl_3$ or $InCl_3$. The bi-spirocyclic product (**1.41**) consists of one dianionic ditelluro phosphazane coordinated to Ga^{III} in a Te,Te' manner, and the Te,N coordination of a monotelluro anion $[(^t\text{BuN(Te)P}^V(\mu\text{-N}^t\text{Bu})_2\text{P}^{III}\text{N(H)}^t\text{Bu})]^-$, resulting from the loss of Te and mono-protonation from solvent. The loss of Te from phosphorus accompanied by protonation of the amine is a common feature of these P-Te compounds.[59–62]

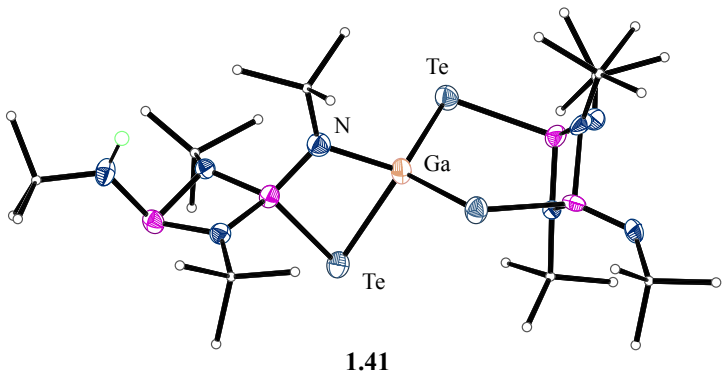

1.41

Figure 1.11: X-ray structure of the Ga^{III} complex of the Te-dianion 1.41.

The solid state structures of the dianions $[^t\text{BuN(E=)P}(\mu\text{-N}^t\text{Bu})]_2^{2-}$ vary hugely depending on the metal base and the cation and can lead to complex structures. For example, the potassium salt of $[^t\text{BuN(E=)P}(\mu\text{-N}^t\text{Bu})]_2^{2-}$ generated from the reaction of **1.35** and $2KN(SiMe_3)_2$ exists as an extended

ladder structure **1.42** (Figure 1.12) in the solid state.[63] This structure contains two separate intramolecular K-Se interactions, *mono* and *bis*, to form a 20-membered extended structure.

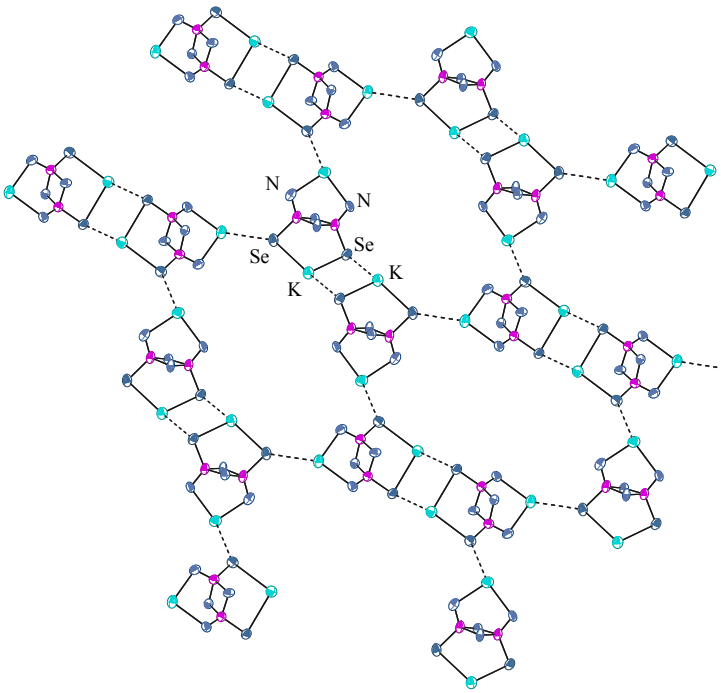

1.42

Figure 1.12: The extended structure of 1.42 showing the two types of K···Se interactions. ^{t}Bu groups and thf are omitted for clarity.[63]

Dianions of the type $[^t\text{BuN(E=)P}(\mu\text{-N}^t\text{Bu})]_2^{2-}$ undergo a variety of polar additions, and have interesting oxidative behaviour. The reaction between I_2 and the S and Se dianions $[^t\text{BuNH(E=P)}(\mu\text{-N}^t\text{Bu})]_2^{2-}$ gives E-E bonded products, either trimeric macrocycles (2:1 in I_2, **1.43,** Figure 1.13a) or E_4-bridged phosphazane rings (in the presence of excess I_2, **1.44** Figure 1.13b). These compounds both result from a one-electron oxidation and subsequent formation of the main group element bond.

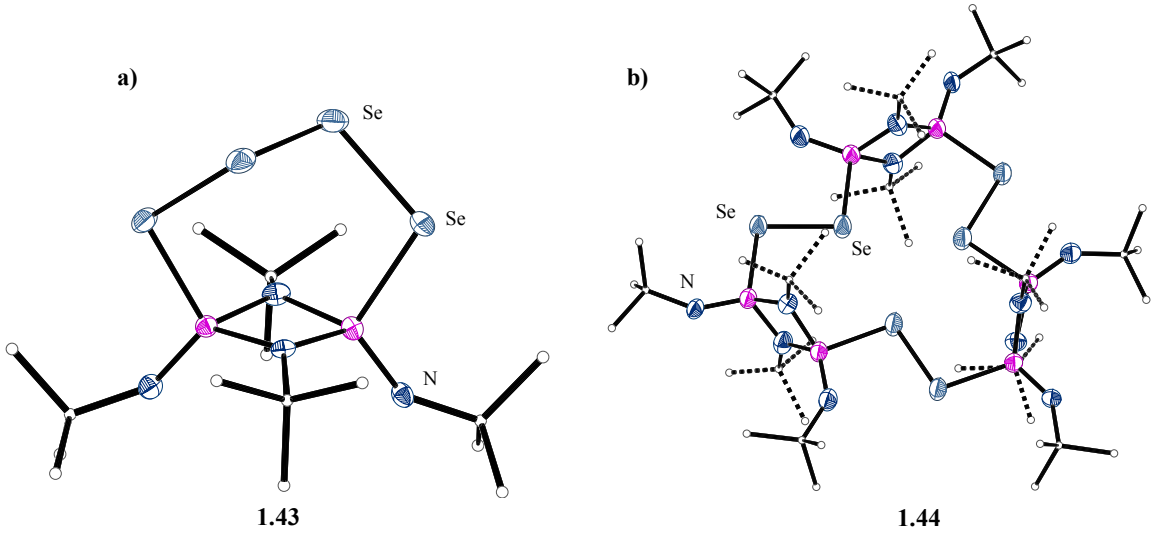

1.43 **1.44**

Figure 1.13: Structures of a) Se_4-bridged species 1.43 and b) Se-Se bridged macrocycle 1.44, formed upon reaction of dianion $[RNH(Se{=}P)(\mu\text{-}N^tBu)]_2^{2-}$ with different stoechiometries of I_2.

The tellurium anions **1.39** however form a spirocyclic Te_5 dianion $[\{^tBuN(Te)\text{-}P(\mu\text{-}N^tBu)_2P(Te)N^tBu\}_2\mu\text{-}Te]^{2-}$ upon reduction with iodine.[64] However, as is the case with most reactions of the oxidised tellurium species, the yields are very low and loss of elemental Te is observed.[65]

The oxidation of cyclophosphazane dianions and neutral species therefore allows for unprecedented stabilisation of the systems and can lead to remarkable coordination structures and environments. This could be used to our advantage in the use of novel systems containing smaller main group substituents at the phosphorus atoms as well as in cyclophosphazanes containing R groups other than ^{t}Bu.

1.3 P-N Ligands in Catalysis

Despite the numerous reports of complexes of phosphazane ligands with metals and main group elements throughout the periodic table, there have been relatively few studies of these species as ligands in single-site catalysts. This might stem from the relatively air- and moisture-sensitive nature of PN compounds, making them particularly tricky ligands to handle, but with advances in techniques and the need to develop modular approaches to a broad range of supporting ligands there has been some focus on this area recently. Phosphorus-based ligands have found extensive use in catalysis in transition metal mediated transformations. Several Nobel prizes have been awarded for the synthesis

and design of phosphorus-based ligands for enantioselective hydrogenation, hydroformylation, carbon-carbon bond formation and carbon heteroatom cross coupling.[66–69]

The broad spectrum of phosphorus-based ligands has been dominated by so-called “privileged ligands” (Figure 1.14).[70]

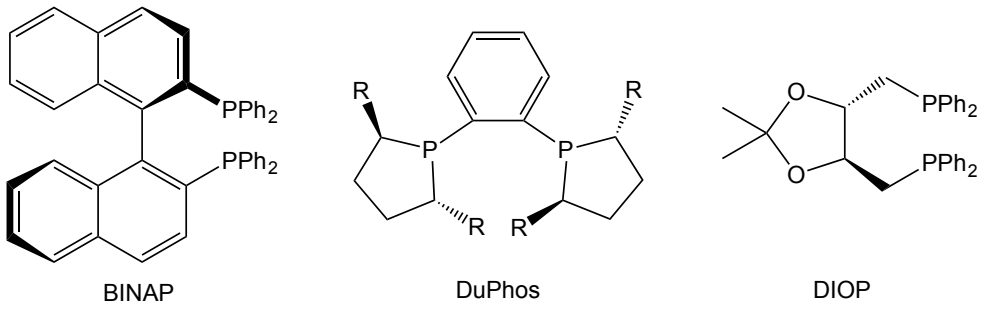

Figure 1.14: So-called "privileged" chiral phosphorus ligands used widely in catalysis.

These ligands have found a very wide use in asymmetric catalysis.[71] They benefit from low flexibility and C_2 symmetry which limits the possibility of numerous isomeric complexes forming. Their wide range of applications from asymmetric allylic substitution to hydroformylation makes them excellent benchmarks for the performance of novel systems, particularly in the case of BINAP. Although there are a number of well-studied ligand systems of this type that are commercially available, there is still an important need for the design of new frameworks. A number of monodentate ligands have been developed that give similar activities to the C_2 symmetrical bidentate privileged systems. Most notably monodentate phosphoramidite,[72–74] -diamide[75] and phosphonite[76] ligands.

Cyclophosph(III)azanes have rarely been used as supporting ligands in catalysis, and only once as asymmetric ligands. Building on work by Stahl and co-workers on the complexation of bis(amino) phosphazanes (Section 1.1.3), Repo *et al.* successfully synthesised a range of novel bulky amino-substituted cyclophosphazanes[26] and showed that their complexes with $ZrCl_2$ and $TiCl_2$ could be used in polymerisation catalysis (Scheme 1.12).[77,78] This was the first study to employ phosphazane ligands in a catalytic system.

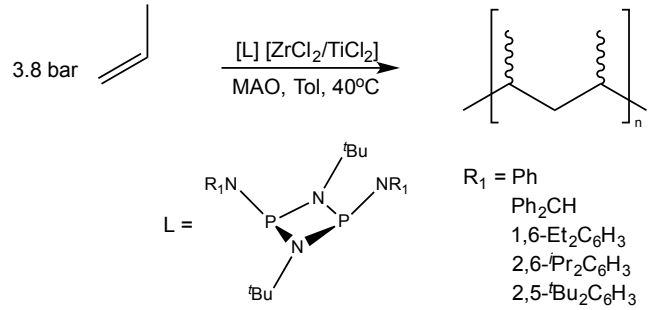

Scheme 1.12: Polymerisation of ethene by Zr^{IV} or Ti^{IV} catalysts supported by bis(amino) cyclophosphazane ligands.

There were, however, a number of flaws in this study, most importantly the use of a highly-oxidising MAO (general formula $(Al(CH_3)O)_n$) pre-catalyst. In particular, it is very unclear what the nature of the catalysts actually is, or whether it even has an intact phosphazane ligand attached at all. Although some combinations showed initial high activity for polymerisation at the initial stage of the reaction, the authors noted the "stench of phosphine" emanating from the reaction vessels after catalytic studies (suggesting significant breakdown of the ligand framework).

More recent work has focused on the design of chiral phosphazane systems towards asymmetric gold catalysis. Building on work by Swamy *et al.* where the reaction of a dichloro dimer **1.20** with bidentate alcohols gave biaryl diol derivatives such as **1.47**,[55] a range of dichlorophosphazanes containing chiral (BINOL) and non-chiral substituents led to a large library of chiral ditopic cyclophosph(III)azanes and corresponding transition metal complexes (Figure 1.15).

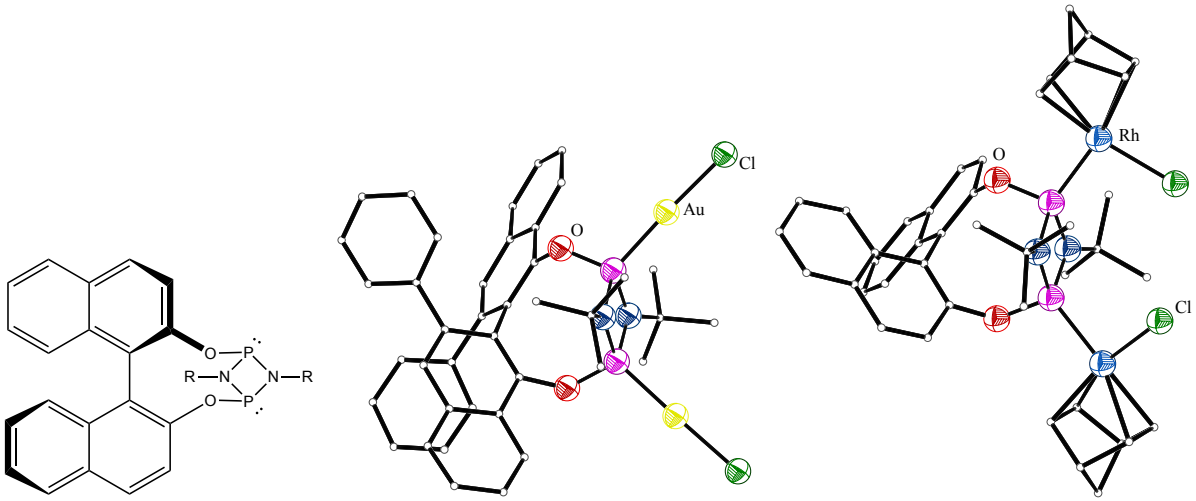

1.45 **1.46** **1.47**

Figure 1.15: Chiral bis(oxy) diphosphazane (1.45), Complex of a chiral bis(oxy) diphosphazane with AuCl (1.46) and a chiral ditopic complex with Rh(nbd)Cl (1.47).

This study took advantage of the lone pair on phosphorus as a donor to support transition metal-mediated catalysis. The unique properties of these ligands leads to both phosphorus lone pairs pointing in different directions and therefore the formation of bis-monodentate metal complexes such as **1.46**, and **1.47** which contain gold and rhodium centres respectively. Although this behaviour was well known for phosphazanes since the 1980's, no studies had taken advantage of the modifiable nature of the phosphazane ring and its donor capabilities in catalytic studies.[79] The potential of these complexes was tested in gold catalysed hydroamination and in a nickel catalysed three component coupling. Although the reactions were efficient, the enantiomeric excesses (ee) ranged from poor to average compared to conventional systems.[31] It is clear that the metal centres attached to the P-atoms are too remote from the chiral group for good transfer of chirality in this type of ligand.

It is apparent that for phosphazane species to be used successfully in asymmetric catalysis the chiral centres need to be in close proximity to the metal centre. Furthermore, coordination through phosphorus is unlikely to achieve chiral control. The use of oxidising pre-catalysts should be avoided, as this is likely to lead to breakdown of ligands.

1.4 Macrocyclic Chemistry

A macrocycle is defined as "a cyclic macromolecule or a macromolecular cyclic portion of a macromolecule", that is a molecule of high molecular mass made up of repeating units or "monomers".[80] The need for high molecular weight is largely ignored in the literature, where any cyclic species comprising of at least nine atoms in a ring (including three or more donor atoms) is defined as a macrocycle.[81] The key difference between smaller cyclic molecules and macrocycles is the ability to encapsulate and coordinate species within the cavities. These are primarily charged molecules or atoms although many species also have the ability to incorporate neutral guests. Macrocycles play important roles in many biological systems. Through the ability to act as ligands and chelating agents they can selectively bind guest molecules *via* non-covalent interactions. Metallo-porphyrins, which incorporate Fe^{II}, for example, are involved in numerous biological functions in animals and plants, from the transport of oxygen to muscles to the oxidation of water in photosynthesis. Compared to many other complex biological systems, macrocycles can be synthesised with relative ease. This has led to a much greater understanding of biological processes where macrocyclic systems are involved. Not only can we now synthesise the naturally-occurring species, but fine tuning and simple modifications are possible which can lead to important clinical and technological advantages.

1.4.1 Organic Macrocycles and Gas Storage

The strength of the covalent C-C, C-O and C-N bonds in common organic macrocycles gives these systems good stability. The donor atoms (N, O) are usually incorporated into a carbon framework that can be saturated or unsaturated. Some common organic macrocycles are shown in Figure 1.16.

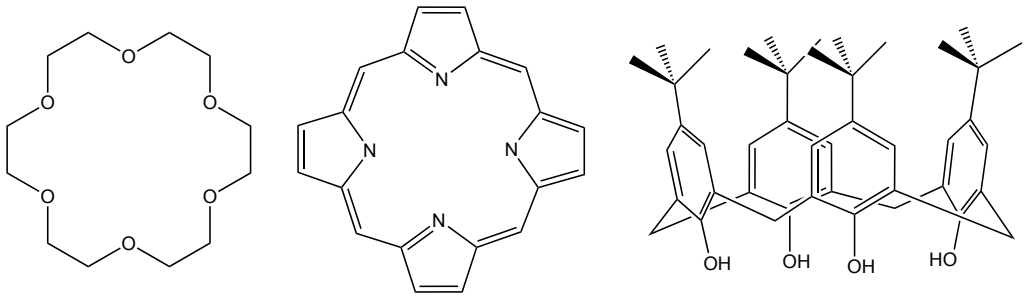

A **B** **C**

Figure 1.16: Common organic macrocycles. A) 18-crown-6, a crown ether, B) unsubstituted porphyrin, C) tert-butyl calix[4]arene.

The functionalisation of these sorts of macrocycles determines their chemical and physical properties. For example, changing the backbone groups can decrease or increase solubility. Organic molecules such as those shown above have the ability to coordinate a wide range of cationic and neutral guests using cation/lone-pairs, H-bonding and π-π aromatic interactions, as well as the size of the macrocyclic cavity. Crown ethers, which contain donor -atoms, coordinate a broad range of metal ions, where the selectivity of coordination depends on the number of O-donor atoms available and the size of the metal ion. 18-crown-6, for example, encapsulates larger K^+ selectively, whereas 12-crown-4 binds Li^+ selectively.

Although the bulk of the literature relating to macrocyclic chemistry focuses on metal coordination, there has been increased interest in anion coordination as well as gas encapsulation and storage.[82,83] Anion guest binding is important for a variety of applications relating to amino acid binding and transport[84] as well as analytical chemistry[85] and anion-templated reactions.[86] The main challenge in coordinating anions is the necessity for the host to contain H-bonding functional groups.

Gas storage applications on the other hand rely on a much broader range of characteristics, including pore size and packing of the molecules in the solid state. Another important factor that needs to be considered is the gas being stored and the target storage capacity/weight of the material, depending on its application. The identification and mitigation of the effects of climate change has led to the development of so-called "green technologies." An important aspect of some green technologies is the need to encapsulate and trap greenhouse gasses, known as carbon-capture storage.[83] Another important area is the storage and transport of "green fuels" such as H_2. Hydrogen has the highest

energy per unit mass of any fuel, equal to about three times as much as that generated from gasoline and almost seven times as much obtained from coal. However, the big problem with hydrogen as a fuel is its low volumetric density, in other words very little energy is stored per unit volume for H_2 gas. Current methods of storage and transportation are either very dangerous or the storage materials themselves are too heavy for vehicular applications.[87] The American Department of Energy (D.O.E.) has set a requirement that a material should be able to store 5.5 w.t% H_2 (revised down from 7.5% in 2012) for applications in transportation.[88] The current method for hydrogen gas storage for automotive applications is the use of high-pressure Kevlar-lined tanks containing the gas at 350-700 bar.

CO_2 capture technologies have also been developing rapidly. In order to maintain current power generation methods, technologies to mitigate their effects on global climate change are necessary. One of the main culprits in climate change is CO_2. It is a potentially useful gas, as it can readily be converted into a range of hydrocarbons and feedstocks, but high purity material is required and its separation from other compounds in the gas phase can be difficult.[89] Leading current technologies involve metal organic frameworks (MOFs) or the use of catalytic converters.[90–92]

Studies on small organic molecules have shown that they possess the potential to store gases under relatively low pressures, and have enough capacity to theoretically meet the regulatory standards.[93,94] Macrocycles such as calix[4]arene have been shown to store gases by adsorption into the interstices of their crystal lattice. Studies of tert-butyl calix[4]arene, for example, have shown that CH_4 is trapped in the interstices of the crystals in the voids made by two macrocycles (Figure 1.17).[87,94]

a)

b)

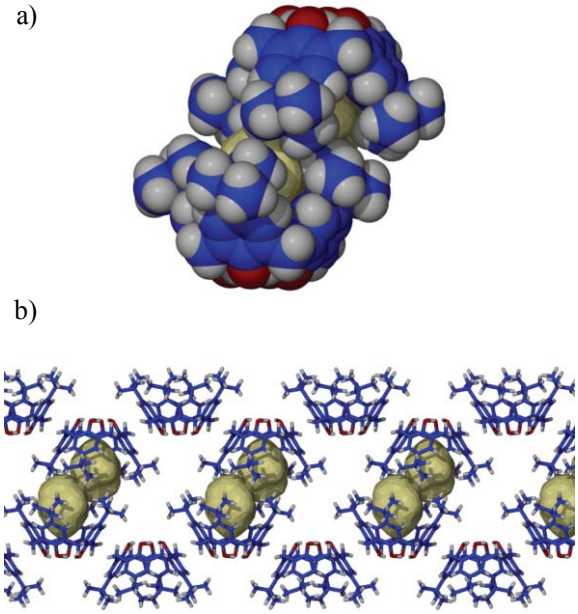

Figure 1.17: a) Space filling diagram showing tert-butyl calix[4]arene encapsulating two CH_4 molecules b) Crystal-packing diagram of the CH_4 contained in the lattice. Image from studies by Atwood *et al.*[95]

However, in practice the storage capabilities of these organics struggle to exceed 1 w.t.%, far below the 5 w.t.% required for example by the D.O.E. for H_2 storage. Importantly, theoretical studies have shown that the introduction of greater polarity into such macromolecular storage molecules and aromatic substituents may increase the H_2 gas storage capability significantly.[96–98]

1.4.2 Inorganic Macrocycles

The stability of organic macrocycles arises from the high thermodynamic stability of the carbon-bonded backbones. Bonds to carbon bonds have greater stability compared to the vast majority of main group element bonded systems, especially homo- and hetero-bonded systems beyond the second row of the periodic table.[99] These weaker bonds are the main challenge to overcome in the synthesis of inorganic macrocyclic systems based on non-carbon frameworks. Other issues arise when considering the potential oxidation states and a wider range of formal hybridization states that are available to main group elements other than carbon. The weaker covalent bonds lead to thermodynamic instability, which combined with instability towards oxidation and hydrolysis, has led to a lack of general synthetic techniques for the synthesis of inorganic macrocycles.

Although more synthetically challenging, inorganic macrocycles are attractive targets, not least for their potential as polar hosts gas storage (mentioned in the previous section). A wide variety of inorganic macrocycles have been synthesised and characterised, although still comparatively few to the huge library of organic counterparts.

Acceptor macrocycles have been developed by Mulvey *et al.*, primarily in the form of ionically-bonded metallocyclic species referred to as "inverse crowns".[100] These metallocycles act as acceptors to a wide range of organic, inorganic and organometallic anions. Their ability to stabilise unusual anions, such as the tetraanionic ferrocenyl $[(C_5H_3)_2Fe]^{4-}$, arises from the incorporation of cyclic heterometallic s-block imido frameworks, as shown in Figure 1.18a.[101]

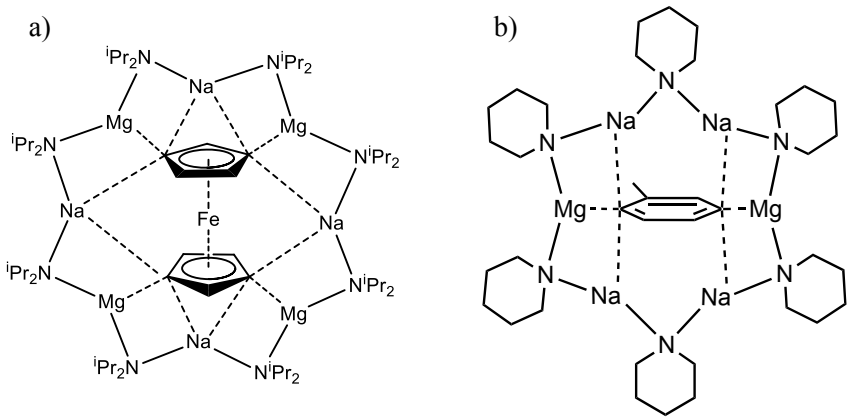

Figure 1.18: a) Structure of the "inverse crown" complex of the ferrocenyl tetraanion and b) Deprotonation of toluene by an inverse crown, Me groups on Cy omitted for clarity.

The coordination of aromatic ions by inverse crowns of this type shows their potential in synthetic applications. The double-deprotonation of toluene to give the inverse crown shown in Figure 1.18b occurs regioselectively on the -2 and -5 position, rather than the apparently more acidic CH_3 position in order to incorporate it within the cavity.[102]

Despite the wide range of inorganic acceptor macrocycles which have now been reported, comparatively few inorganic macrocycles are known to possess donor type behaviour, making them able to incorporate cations in a similar manner to crown ethers.[103–106] The chance discovery of an antimony (Sb^{III}) based macrocycle $[\{Sb(\mu\text{-Nma})\}_2(\mu\text{-Nma})]_6$ (**1.49**) (ma = methoxyaniline 2-MeO-C_6H_4N) by Wright *et. al.* in 1996 led to large developments in both acceptor and donor

macrocycles.[107] The deprotonation of a stannate complex [Sn(NHma)$_3$Li.thf] (**1.48**, Scheme 1.13) with the strong base Sb(NMe$_2$)$_3$ leads to the hexameric macrocycle **1.49**, formed from six Sb_2N_2 ring units bridged into a macrocyclic arrangement by the μ-Nma groups.

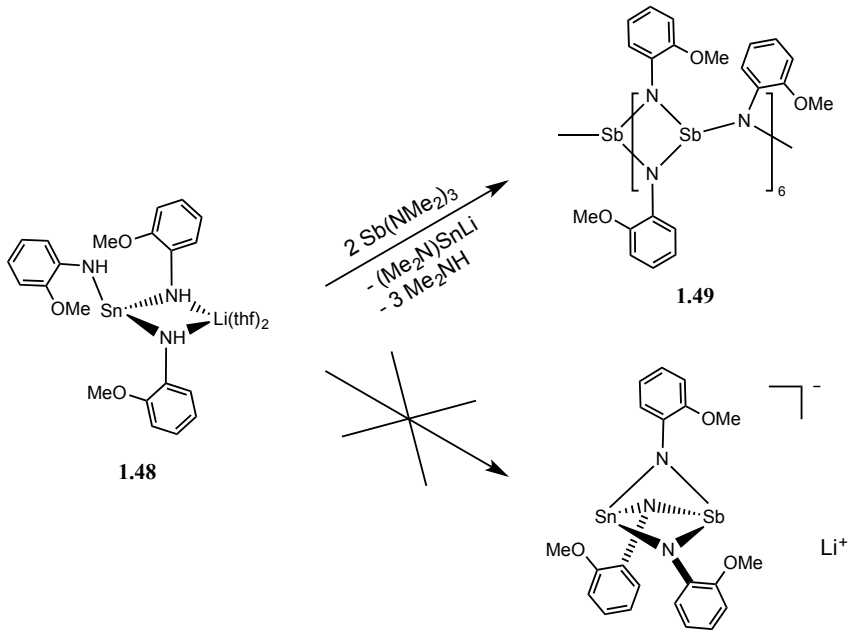

Scheme 1.13: Deprotonation of the stannate complex 1.48 leads to the formation of an antimony-nitrogen hexameric macrocycle 1.49.

The macrocycle **1.49** is closely related to another Sb^{III} macrocycle [{Sb(μ-Ph)}$_2$(μ-Ph)]$_6$ reported later by Norman *et. al.* obtained from direct reaction of $SbCl_3$ with PhNHLi.[108] These types of macrocycle are similar in shape to many organic macrocycles (having a toroidal shape), notably calixarenes, and have the potential to coordinate cations and anions in the cavity through N-bonding and Sb-bonding respectively. The observation of such coordination was seen in the reaction of the dimer [Me$_2$NSb(μ-NCy)]$_2$ (**1.50**) with $LiNH_2$ which led to the formation of [{{Sb(NCy)}$_2$(μ-N)}$_3$(Li·thf)$_2$.LiN=NH] (**1.51**, Scheme 1.14). This reaction involves the complete deprotonation of the NH_2^- unit to N^{3-}.[109] The trimeric macrocycle coordinates one Li^+ ion in its void, and the remaining Li^+ cations lie above the cavity coordinated by the neutral nitrogen centres and the $[N{=}NH]^-$ fragment.

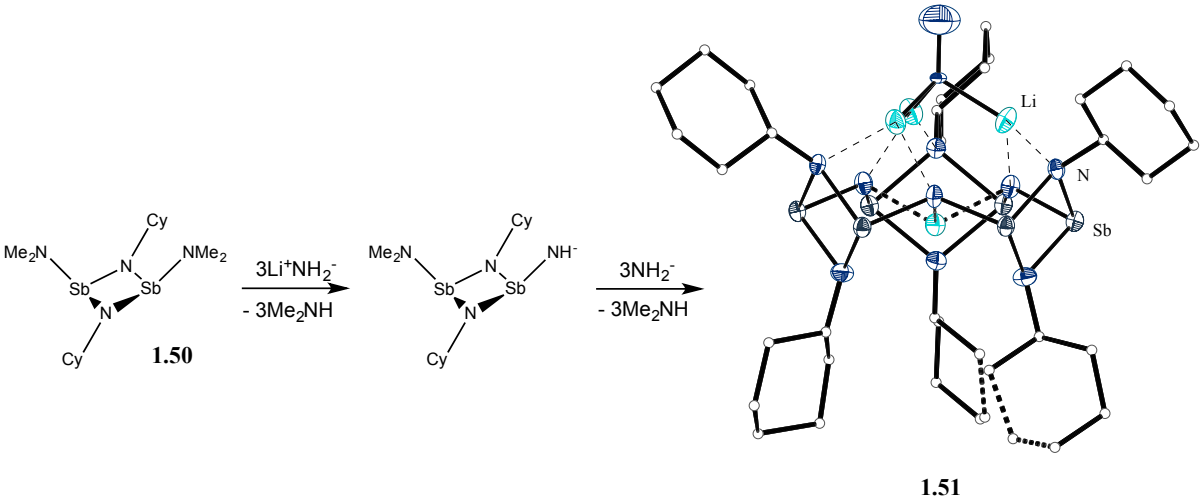

Scheme 1.14: Synthesis of trimeric antimony trianionic macrocycle 1.51 *via* total deprotonation of NH_2^-.

Although initial studies showed great promise in developing an extended family of inorganic macrocycles based on antimony and nitrogen, general synthetic strategies proved to be hard to develop. As mentioned earlier, the weakness of main group heteroatom bonds, as well as the reactivity of the higher oxidation states can make the structures and outcomes of reactions much harder to predict and control, especially where manipulation of molecular architecture is key.

1.4.3 P-N Macrocycles

P^{III}-N dimers are of particular interest due to the increased stability (compared to other main group dimers) that arises from the P^{III}-N bond energy (290 kJ mol^{-1}), which is comparable to that of C-C bonds (346 kJ mol^{-1}).[110] The first macrocyclic ligand based on phosphorus and nitrogen to be found to incorporate guests was the large crown-like hexamer $[(Me_2)_2PN]_6$ which forms $[\{(Me_2)_2PN\}_6 \cdot CuCl]^+$ $[CuCl_2]^-$ (**1.52**) upon reaction with $CuCl_2$ and CuCl (Figure 1.19).[105,111] The Cu^{II} centre is coordinated by four of the six nitrogens in the macrocycle framework. Cobalt and palladium complexes have also been synthesised.[112,113]

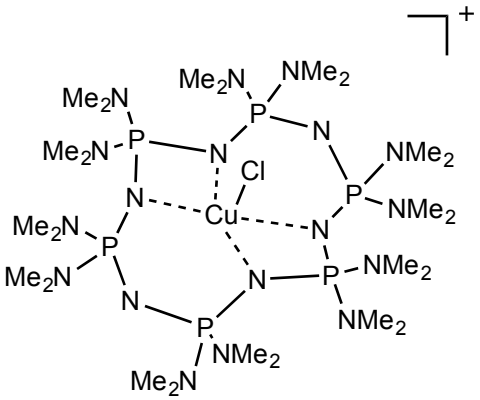

1.52

Figure 1.19: P_6N_6 phosphazene macrocycle encapsulating Cu^{II}.

A pivotal moment in the development of PN macrocycles was the realisation that the dimeric macrocycles $[\{P(\mu\text{-}NR')\}_2(\mu\text{-}NR)]_2$ (**1.53**) are valence-isoelectronic with a range of main group relatives, such as the Sb^{III} species (**1.54**) and Al^{III} phosphide (**1.55**) shown in Figures 1.20.[114–117] The dimeric macrocycles **1.53** are in effect the first macrocyclic homologues of an extended series of related macrocycles $[\{P(\mu\text{-}NR)\}_2(NR)]_n$ which were targeted in later studies.

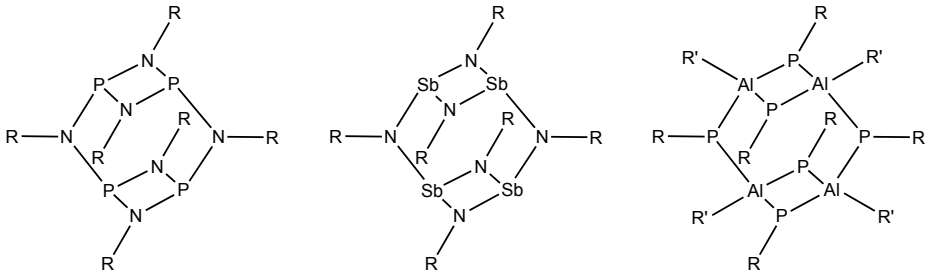

1.53 **1.54** **1.55**

Figure 1.20: Neutral and isovalent main group macrocyclic dimers based on phosphorus (1.53), antimony (1.54) and aluminium (1.55).

The dimer $[\{P(\mu\text{-}NR')\}_2(\mu\text{-}NR)]_2$ (**1.53**), was obtained from the thermolysis reaction of $[ClP(\mu\text{-}N^iPr)_2PN(^iPr)(SiMe_3)]$ (Scheme 1.15).[114] This class of dimeric macrocycle can also be synthesised in a more targeted manner by combining the bis(amido) dimer $[(^tBuN)P(\mu\text{-}NR)]_2^{2-}[2Li^+]$ with $[ClP(\mu\text{-}N^tBu)]_2$.[115] Since they contain only eight atoms in their frameworks these species are not technically

macrocycles, but the synthetic procedure is important as it paved the way to significant advances in phosph(III)azane macrocyclic chemistry.

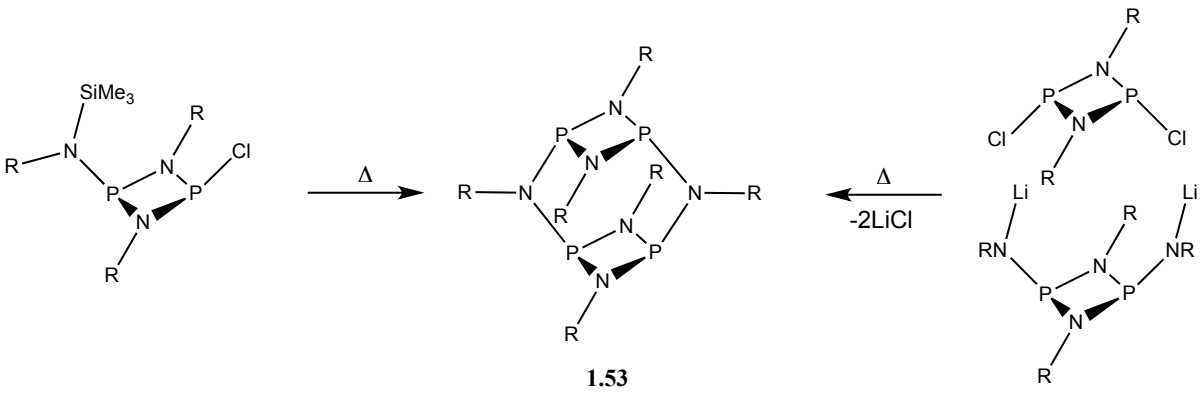

Scheme 1.15: Synthesis of the dimeric cyclodiphosph(III)azane macrocycle [{P(μ-NR′)}$_2$(μ-NR)]$_2$ (1.53).

Consideration of the structurally related antimony systems **1.49** and **1.54**, suggests that there are certain important characteristics governing the structure and size of main group macrocycles of this type. The size of the nitrogen substituents (R) play a large role in controlling ring size on the basis of the sterics and the existence of *cis* and *trans* isomers in the starting dimers can pre-organise certain configurations. There is also another important structural factor, and that is the nature of the bridging groups. Phosphazane macrocycles can be separated into three categories, macrocycles built using hybrid organic linkers [{P(μ-NR)}$_2$(μ-LL´)]$_n$ (Figure 1.21a),[118,119] more recently developed macrocycles containing transition metal linkers (Figure 1.21b),[120–122] and wholly inorganic-based macrocycles using heteroatom linkers of the type [{P(μ-NR)}$_2$(μ-X)]$_n$ (X = NH, O, S, Se) (Figure 1.21c).[123]

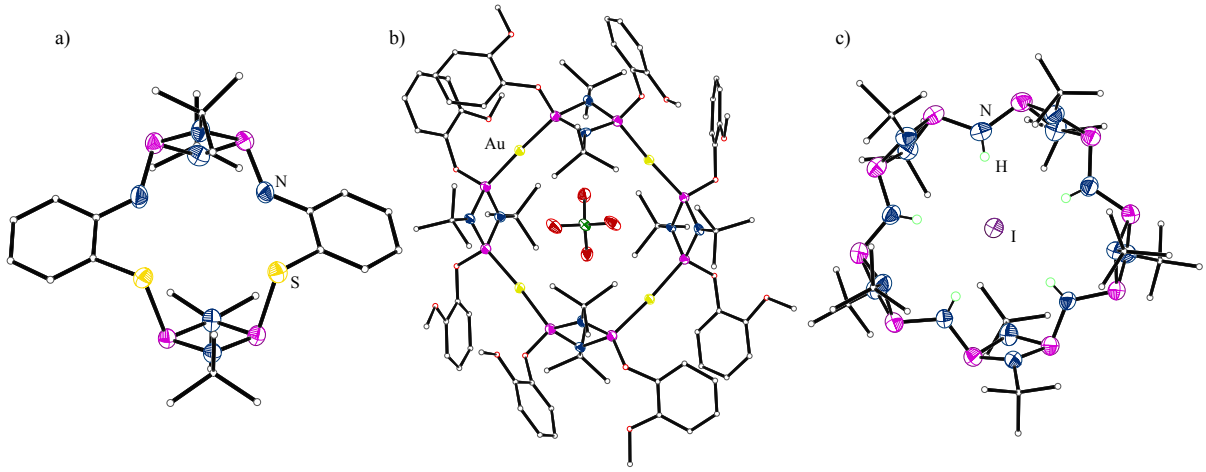

Figure 1.21: Examples of phosph(III)azane macrocycles: a) hybrid organic linked (N-S) b) transition metal linked (Au), and c) Inorganic linked (NH).

By reducing the size of the R group in the linking group, larger systems become readily available. Using NH groups as opposed to bulky NR groups allowed for the synthesis of a tetrameric macrocycle. Reaction of $[P(\mu\text{-}N^tBu)Cl]_2$ (**1.20**) with the diamino-dimer $[P(\mu\text{-}N^tBu)NH_2]_2$ (**1.21**) in the presence of Et_3N as a Brønsted base gave $[\{P(\mu\text{-}N^tBu)\}_2(\mu\text{-}NH)]_4$ (**1.56**) in excellent yield.[39] ^{31}P NMR spectroscopy showed that the bulk of the product was the tetramer **1.56**. However, at lower temperatures ^{31}P NMR studies showed that another product was formed in very low yields (1-5%). This was isolated by fractional crystallisation and found to be the pentamer $[\{P(\mu\text{-}N^tBu)\}_2(\mu\text{-}NH)]_5HCl$ (**1.57-HCl**, Scheme 1.16).[36] This complex is a host-guest complex reminiscent of sappharins, particularly the pentaporphyrin complex $[\{3\text{-Me-4-Et-pyrNH}\}_5(CH_2)_4F][PF_6]$ (**1.58**), which has five NH groups coordinating to a fluoride anion (Figure 1.22).[124] In a similar manner, the pentameric phosphazane complex **1.57-HCl** has a guest chloride anion coordinating *via* H-bonding to the NH linkers.

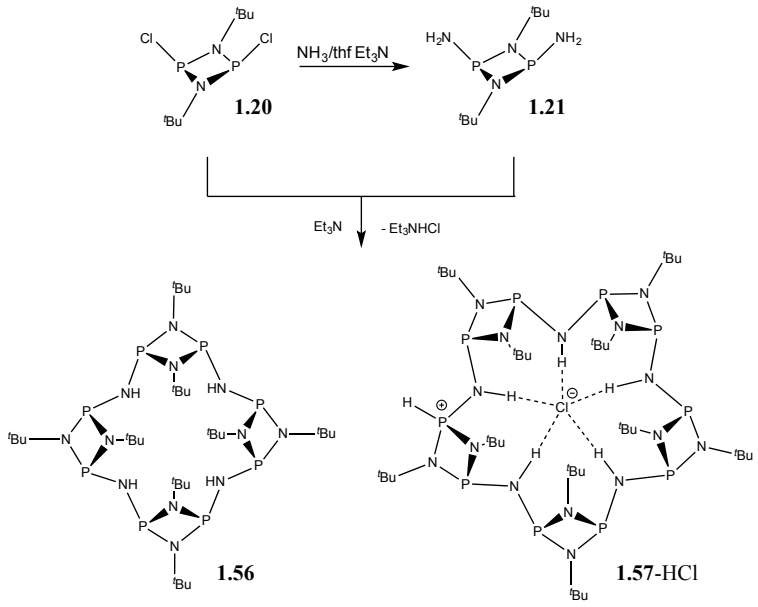

Scheme 1.16: Synthetic strategy for phosph(III)azane macrocycles containing NH bridges.

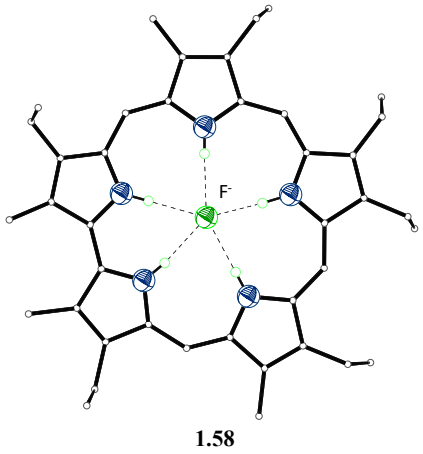

Figure 1.22: Pentapyrrol complex 1.58, coordinating F^- *via* five N-H groups.

The formation of exclusively macrocyclic complexes in these reactions can be attributed (at least in part) to the *cis*-conformation of the dimeric precursors, i.e., pre-organisation. However, this does not explain the different sizes of the tetrameric (**1.56**) and pentameric (**1.57-HCl**) macrocycles formed. Extensive studies of the reaction of **1.56** and **1.57-HCl** suggested a stepwise growth of the final macrocyclic products *via* condensation reactions. Scheme 1.17 describes the stepwise growth, and shows the key step that the templating ion Cl^- anion plays in forming **1.57-HCl** *vs* formation of the tetramer **1.56**. The structurally-determining step depends on self-condensation between the two ends

of the intermediate **1.57** with the loss of Et_3NHCl to give **1.56**, or further reaction with another equivalent of $[P(\mu\text{-}N^tBu)NH_2]_2$ (**1.22**) to give **1.57-HCl**.[125]

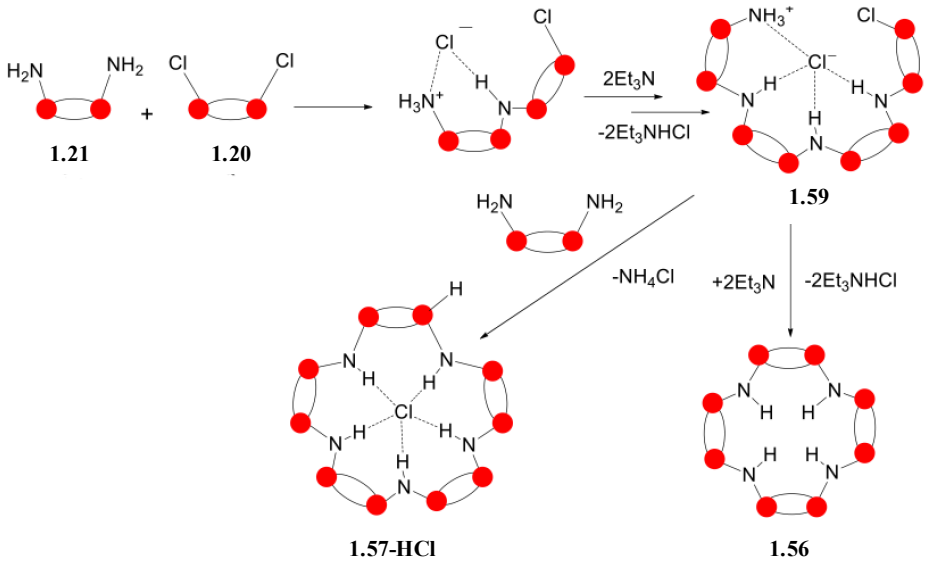

Scheme 1.17: Proposed templating mechanism for the formation of the pentamer 1.57-HCl over the tetramer 1.56 *via* addition of one amino dimer 1.21 to the intermediate 1.59.[36]

Studies of the same reaction in the presence of different halide ions in the form of the lithium salts (LiX; X – Cl, Br, I), show that the formation of the pentameric arrangement **1.57-HCl** is amplified in the order I >> Br > Cl. The solid-state structure of **1.57-HBr** shows distortion from planarity of the pentameric macrocyclic ring compared to the flat arrangement seen for **1.57-HCl**. Using a ten-fold excess of lithium iodide, as well as a 3:2 stoichiometric ratio of the starting dimers, leads to *exclusive* formation of the pentameric host-guest complex **1.57-ILi(thf)$_4$**, which is easily isolated in crystalline form.[125] The solid-state structure shows an even more distorted pentameric ring, in which the iodide is coordinated outside of the macrocyclic ring plane. A comparison of the distortion seen between these three coordinated halide complexes is shown in Figure 1.23.

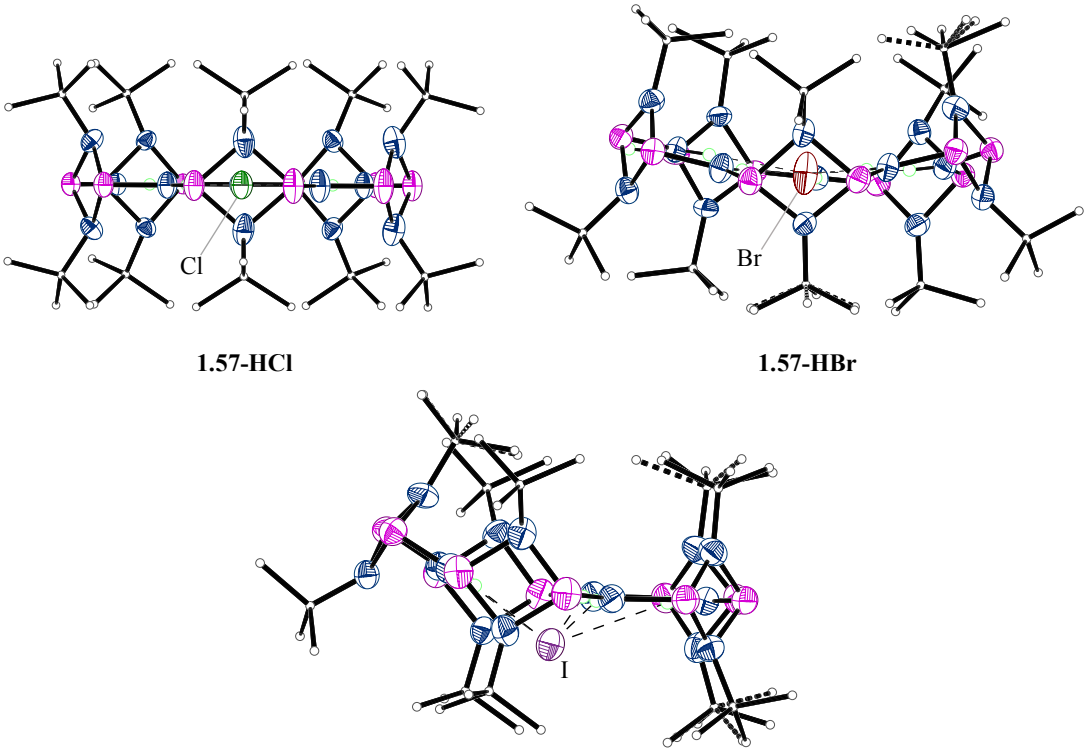

1.57-HCl **1.57-HBr**

1.57-ILi(thf)$_4$)

Figure 1.23: A comparison of 1.57-HCl, 1.57-HBr and 1.57-ILi(Thf)$_4$ showing increasing distortion from Cl to I. The Li(thf)$_4^+$ cation is omitted for clarity in the case of 1.57-ILi(thf)$_4$.

Reaction of the chloro-phosphazane dimer [ClP(μ-N^{t}Bu)]$_2$ (**1.20**) with water gives the di-oxo dimer [O=(H)P(μ-^{t}Bu)]$_2$ **1.22** (described in Chapter 1.2.2).[126] This compound can be isolated as the dianion [O-P(μ-N^{t}Bu)]$_2^{2-}$ by *in situ* lithiation, and further reaction with [ClP(μ-N^{t}Bu)]$_2$ (**1.20**) produces the oxygen bridged tetramer [P(μ-O)(μ-N^{t}Bu)$_2$]$_4$ (**1.60**, Scheme 1.18).[127]

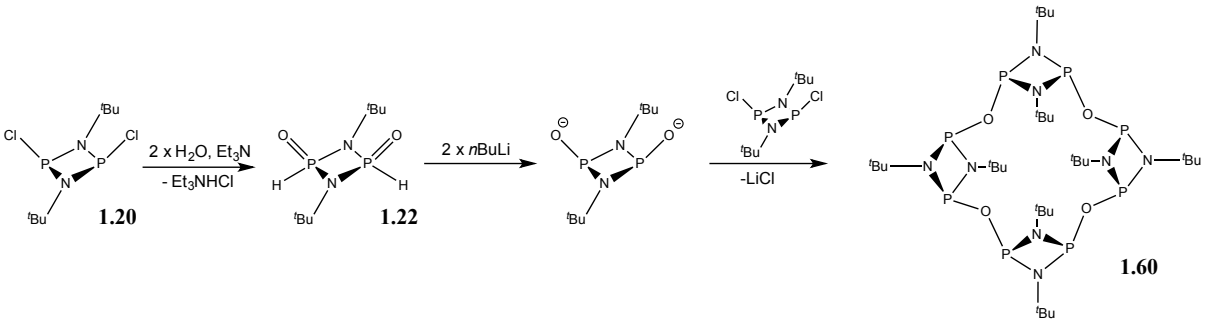

Scheme 1.18: Formation of the oxygen-bridged tetramer (1.60) from the dianionic di-oxo-dimer [O=P(μ-N^{t}Bu)]$_2^{2-}$.

This structure of **1.60** is very similar to the NH bridged tetramer **1.56**, however, it has a slightly smaller cavity due to the shorter P-O bonds.[39] Attempts to expand the size of this type of arrangement using cation templating (with alkali metal cations) were unsuccessful, and only the tetramer could be isolated.[128]

The Se-bridged P^{III}-P^{V} hexamer (Scheme 1.19) was prepared by Wurtz-like coupling of a selenium dimer [Se=P(μ-N^{t}Bu)Cl]$_2$ (**1.61Se**) with sodium metal in toluene under reflux.[129] The resulting planar macrocycle [(μ-Se)P(μ-N^{t}Bu)$_2$P(=Se)]$_6$ (**1.62Se**) is formed *via* a head-to-tail reaction, and was found to have a very large cavity measuring 8.2 Å in diameter and 6.1 Å in depth.

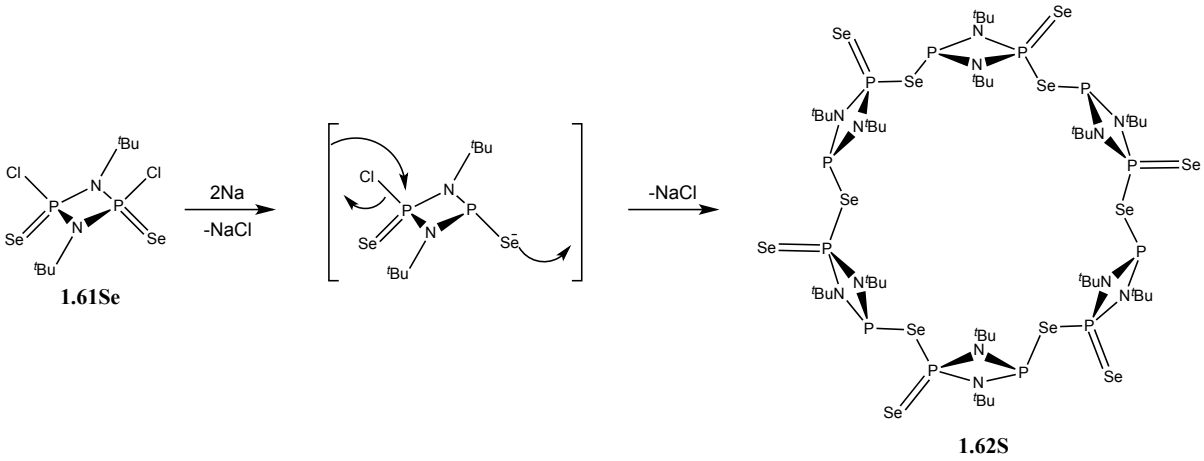

1.61Se **1.62S**

Scheme 1.19: Head-to-tail cyclisation formation of a Se-linked hexamer 1.62Se.[123]

Recently, the sulfur analogue of this species was also synthesised by Singh *et al.*[130] Unlike the selenium derivative, the synthesis of the sulfur hexamer **1.62S** also leads to the formation of a radical species [S(Cl)P(μ-N^{t}Bu)]$_2^{2-}$ (**1.63**), which arises from the double-reduction of the starting material [S=P(μ-N^{t}Bu)Cl]$_2$ (**1.61S**).

This background gives a great deal of scope for the development of phosphazane macrocycles based on simple main group linkers, as well as the use of phosphazanes as ligands in transition metal mediated catalysis, which are both addressed in this thesis.

1.5 Aims and Objectives

The aim of this thesis is to make use of the modular nature of the phosphazane unit in the synthesis of novel building blocks for ligand design and new macrocyclic species.

The development of novel macrocycles based on the phosphazane unit requires the design of a systematic synthetic method that will allow for the incorporation of a variety of linker atoms as well as modification of the R groups on the phosphazane backbone. The different approaches to varying the linker atom have so far been partly successful, giving macrocyles with N, O, S and Se linkages; however, none have taken advantage of the variety of possible R groups on the phosphazane. Moreover, macrocycles bridged by lower chalcogens (S, Se) have so far only been synthesised by less systematic methods.

The steps to achieve these aims were:

(i) Develop novel precursors based on sulfur; $[S=P(H)(\mu\text{-}NR)]_2$ towards developing macrocycles using lower chalcogen linkages as well as different R groups

(ii) Explore the use of these species as ligands, due to their relatively sterically unhindered nature and presence of "soft" coordination sites.

(iii) Study the reactivity, notably deprotonation to generate P^{III} dianions, as well as oxidation to give the P^{V} species, adding a further level of variation.

(iv) Use these P^{III} and P^{V} species as building blocks in macrocycle formation.

In the same vein of taking advantage of the modularity and diversity of the P_2N_2 unit, we are interested in diversifying the library of bis(amino) cyclophosphazanes $[R^2NHP(\mu\text{-}NR^1)]_2$, which has been limited to a small number of R groups. We are interested in systematically introducing chiral groups into the R^1 and R^2 positions and exploring the formation of chiral-bis(amino) phosphazane metal complexes to test their ability in asymmetric catalysis.

2. Synthesis of Novel Chloro-phosphazanes

2. Synthesis of Novel Chloro Cyclophosphazanes

The large bulk of studies involving phosph(III)azane species $[P(\mu\text{-}NR)Cl]_2$ have been conducted using relatively few substituents (R). The literature is dominated by the use of the tertiary butyl derivative $[ClP(\mu\text{-}N^tBu)]_2$ as the principle starting material. This is primarily due to the ease of synthesis of this particular derivative, its solubility and steric characteristics. In order to design syntheses that take advantage of the modularity of the phosphazane unit, we synthesised a range of chloro-cyclophosphazanes based on previous literature procedures (Figure 2.1). The first examples of cyclophosphazanes bearing chiral R groups were prepared by Gade *et al.*[31] In collaboration with their laboratory in Heidelberg (Germany), a series of novel chloro-dimers containing a range of R groups was prepared as starting materials for future studies (presented in Chapter 5). These were fully characterised by ^1H, ^{13}C and ^{31}P NMR spectroscopy, as well as elemental analysis, single-crystal X-ray diffraction, and in selected cases ESI mass spectrometry.

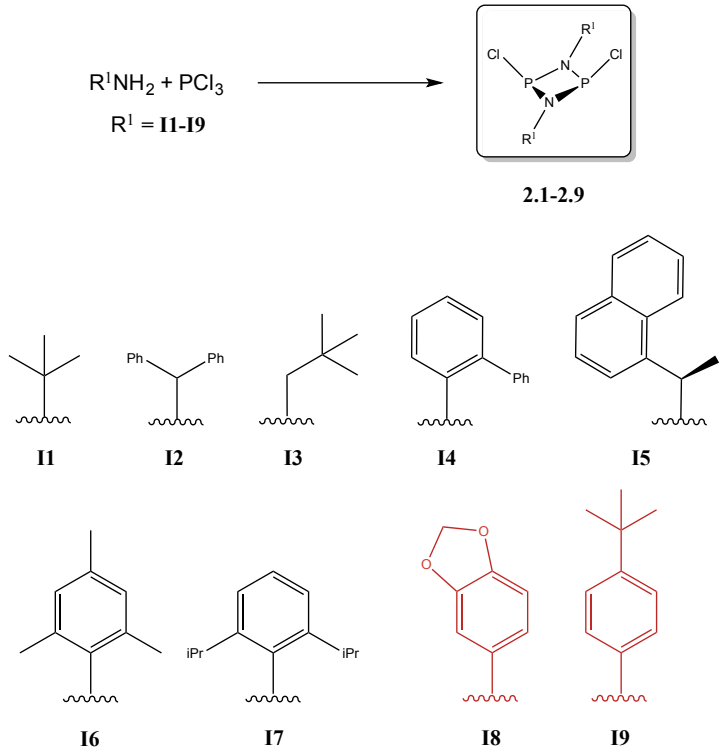

Figure 2.1: Imido substituents (I1-I9) of the dichloro precursors used in this work. Colour coding indicates preparation method: Black = condensation method, Red = reflux method.

The use of chiral substituents (like **I5**, above) is particularly important for obtaining ligands for asymmetric catalysis and, in particular, for incorporating chirality into macrocyclic systems (see later Chapter 4). The opportunity to select from a library of chloro-dimer starting materials based on steric bulk and electronic parameters is obviously advantageous.

The bulk of the syntheses of the chloro-dimers were performed according to the general procedure illustrated in Scheme 2.1. A solution of RNH_2 was added dropwise to a stirred solution of PCl_3 and Et_3N in thf at low temperature. After filtration to remove the triethylamine hydrochloride salt, the products were (in most cases) crystallised from a concentrated toluene solution and isolated as white to green/white powders). In the case of **2.1** (R = **I1**) and **2.3** (R = **I3**) it was possible to distil the crude product, ultimately producing crystalline materials of high purity. In most cases the products **2.1**-**2.7** (R = **I1**-**I7**) are obtained in excellent yields >80% and are of very high purity. However, the neopentyl species $[P(\mu\text{-}N(CH_2{}^tBu)Cl]_2$ (**2.5**, R = **I3**) was obtainable in a yield of only 28%.

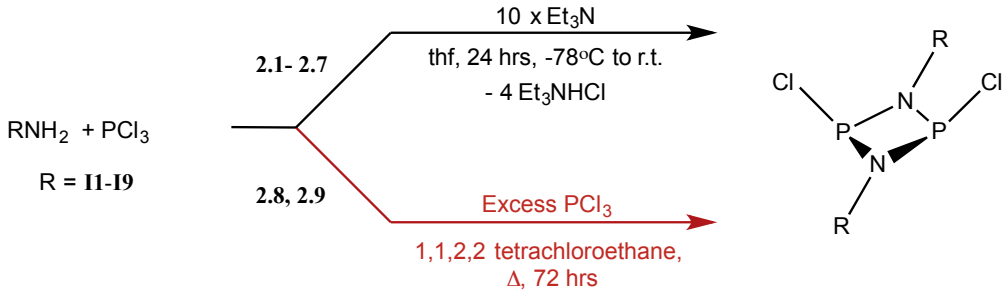

Scheme 2.1: Synthesis of the dichloro precursors *via* condensation of PCl_3 and amine (black), or reflux in high boiling point solvent (red).

This procedure was used to synthesise dimers **2.1**-**2.7** containing the imido R groups **I1**-**I7**, respectively. In the case of **2.8** and **2.9** (**I8** and **I9**, respectively) the condensation method produced a mixture of products. Unpublished work from our group had shown that other synthetic routes to cyclophosphazanes could be employed in selected cases.[131] Reflux of the amine in a solution of PCl_3 (10 x excess) in the high boiling point solvent 1,1′,2,2′-tetrachloroethane for 72 hours followed by removal of the solvent and unreacted PCl_3 gave viscous yellow materials. Extraction with toluene followed by filtration and removal of the solvent gave the desired products (**2.8** and **2.9**) as white powders in moderate yields (30-40 %).

All of the new dimers were characterised by ^{31}P, ^{1}H and ^{13}C NMR spectroscopy and show characteristic peaks between δ = 205-250 ppm in their ^{31}P NMR spectra. This range is indicative of a *cis*-configuration of the Cl-groups relative to the P_2N_2 units, as *trans*-chloro-dimers have an approximate shift range δ = 80–90 ppm upfield.[119] The ^{31}P NMR shifts of the chloro-dimers are compiled in Table 2.1. ^{31}P NMR spectroscopy is an especially valuable tool in the evaluation of these materials to determine their purity and the completeness of the reactions.

Table 2.1: ^{31}P NMR spectroscopic shifts of chloro dimers used in this work.

Compound	**2.1**	**2.2**	**2.3**	**2.4**	**2.5**	**2.6**	**2.7**	**2.8**	**2.9**
^{31}P Shift (ppm), C_6D_6	207.6	223.8	240.9	217.4	221.0	211.0	211.0	208.4	201.3

Crystals of **2.2** and **2.8** suitable for X-ray diffraction were obtained from saturated toluene solutions at -16 ºC.

The three dimensional geometry of **2.2** and its packing are illustrated in Figure 2.2. The asymmetric unit is made up of 1.5 phosphazane molecules as well as one toluene molecule. Each phosphazane features the typical *cis* configuration of the halogen substituents at the phosphorus atom and a relatively flat P_2N_2 ring (PNNP torsion angle 172.69º). The Ph groups of the benzhydryl group on the endocyclic nitrogens are rotated so as to accommodate the toluene molecules and are on the same side of the P_2N_2 ring plane, with the bridging hydrogens pointing towards the same face as the halogens. The molecules pack to form C-H···π interactions between adjacent aromatic groups (CH-C distance 2.85 Å based on fixed hydrogens). It is interesting to note that the P-N distances in this compound are not all equal, with the P(1)-N(1) and P(2)-N(2) bonds being shorter than the respective P(1)-N(2) and P(2)-N(1).

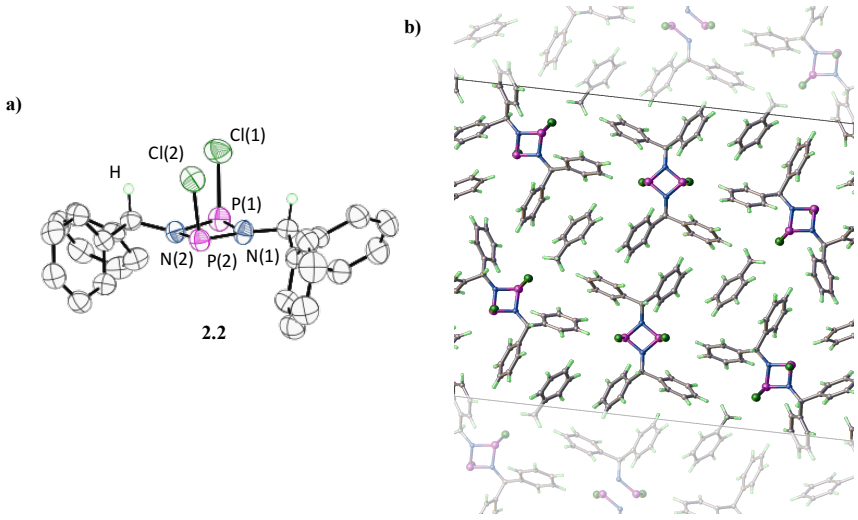

Figure 2.2: a) Crystal structure of 2.2; b) Packing diagram of 2.2. Thermal ellipsoids set at the 50% probability level. Hydrogen atoms on phenyl rings omitted for clarity. Selected bond lengths (Å) and angles (°); P(1)-N(1) 1.687(4), P(1)-N(2) 1.717(3), P(1)···P(2) 2.5789 (16), P(2)-N(2) 1.6804(11), P(2)-N(1) 1.697(3), P(1)-Cl(1) 2.1215(19), P(2)-Cl(2) 2.1428(17), N-P-N mean 80.72, P-N-P mean 98.98, N-P-Cl mean 102.9, PNNP torsion 172.69.

The structure of **2.8** shows one molecule in the asymmetric unit (Figure 2.3a). The 3,4(methylenedioxy)aniline substituents do not lie in the same plane, with one twisted out of the plane of the P_2N_2 ring. Analysis of the packing diagram (Figure 2.3c) shows that this is probably to accommodate neighbouring groups and to allow the alignment of the halogen atoms throughout the structure. The molecules pack to form C-H···π interactions between the CH_2 groups and adjacent aromatic groups (Figure 2.3b, CH-π distance 2.85 Å).

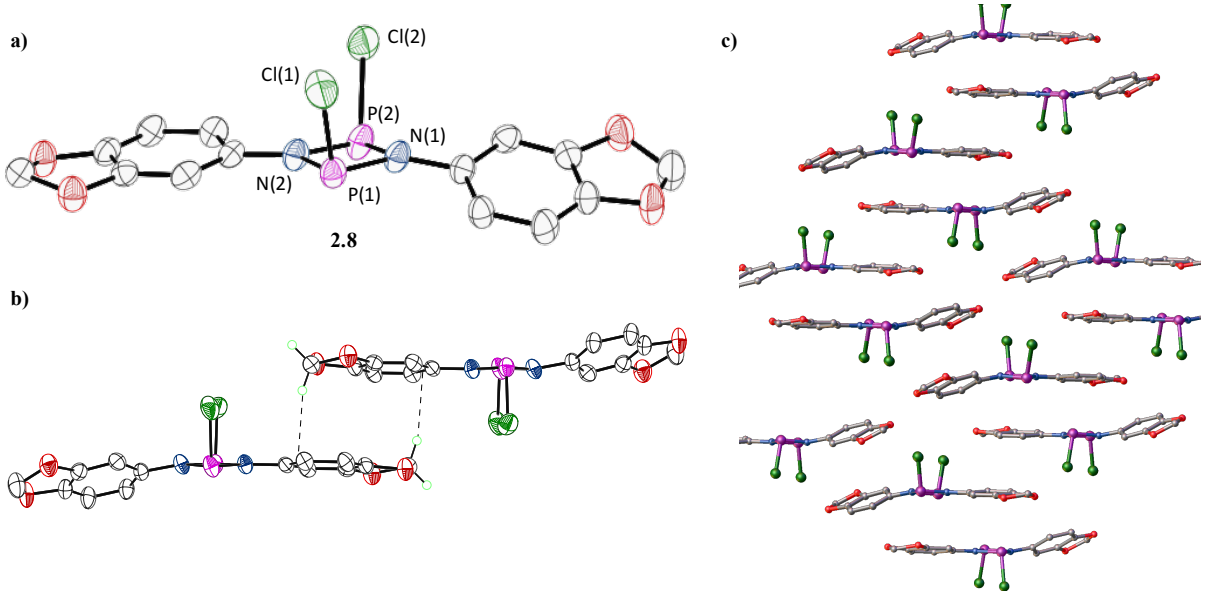

Figure 2.3: a) Solid State structure of 2.8; b) overlay of two independent molecules of 2.8 in the structure showing CH-π interactions; c) Packing diagram of 2.8. Thermal ellipsoids set at the 50% probability level and Hydrogen atoms (other than CH_2 in b) omitted for clarity. Selected bond lengths (Å) and angles (°); P(1)-N(1) 1.706(2), P(1)-N(2) 1.705(2), P(1)···P(2) 2.590, P(2)-N(2) 1.698(2), P(2)-N(1) 1.705(2), P(1)-Cl(1) 2.0949(11), P(2)-Cl(2) 2.0968(11), N-P-N mean 80.98, P-N-P mean 98.97, N-P-Cl mean 102.97.

The variety of steric bulk and chirality of these chloro-dimers was exploited in the following chapters, which involve core modification of the P_2N_2 rung units, complexation, and macrocycle formation, and also the attempted synthesis of novel bis(amido)-cyclophosphazane complexes. Due to the low yields of **2.8** and **2.9**, these were not employed as starting materials in further studies.

3. Sulfur Substituted Cyclophosphazanes

3. Sulfur Substituted Cyclophosphazanes

3.1 Background

In stark contrast to organic macrocycles, which have a variety of widely established synthetic routes using carbon-based building blocks, inorganic macrocycles have been far less studied and general synthetic routes have yet to be developed. Phosph(III)azane macrocycles of the type $[\{P(\mu\text{-}NR)\}_2(\mu\text{-}Y)]_n$, in which dimeric ring units are linked into toroidal cyclic arrangements *via* a bridging group (Y = NH, O, S, Se), have been explored in recent years. They are one of the few inorganic macrocyclic systems where modular synthesis can be employed in a logical manner.

The synthetic approach to nitrogen-bridged species $[\{P(\mu\text{-}N^tBu)\}_2(\mu\text{-}NH)]_n$ (e.g., Chapter 1.4.3 tetramer **1.56** and pentamer **1.57**) relies on the condensation of $[(NH_2)P(\mu\text{-}N^tBu)]_2$ with the parent chloro-dimer $[ClP(\mu\text{-}N^tBu)]_2$.[39] The outcome of this reaction can be controlled by templating using a halide anion (e.g., I^-) to give the pentameric species **1.57-ILi(thf)$_4$** exclusively.[36,125] This species encapsulates an iodide anion which can be removed by reaction with MeOH/MeONa in DCM to give the guest-free neutral macrocycle **1.57** and NaI (Scheme 3.1).

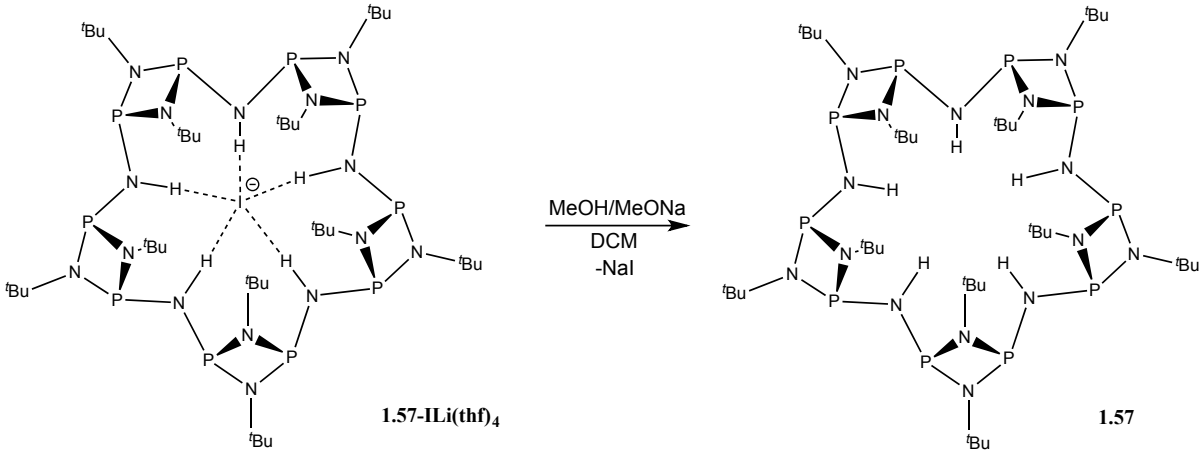

Scheme 3.1: Synthesis of the open-cavity neutral pentamer 1.57.

The synthesis of crown ether-like species containing oxygen linkers $[\{P(\mu\text{-}NR)\}_2(\mu\text{-}O)]_4$ (**1.60**) proceeds *via* a different pathway. Due to the reactivity and thermal instability of the oxygen substituted precursor $[O=(H)P(\mu\text{-}N^tBu)]_2$ (the key starting material), it was necessary to first lithiate it to obtain the more stable dianion $[O\text{-}P(\mu\text{-}N^tBu)]_2^{2-}$ before *in situ* condensation with the chloro-dimer $[ClP(\mu\text{-}N^tBu)]_2$.[40,127]

The extension of the O-bridged systems to S and Se was desirable in order to explore the expansion of the macrocyclic cavity, as well as the incorporation of a softer ligand set. Taking the chloro-dimer $[ClP(\mu\text{-}N^tBu)]_2$, oxidation at phosphorus by elemental sulfur or selenium gives the P^V chalcogeno-chloro species $[E=(Cl)P(\mu\text{-}N^tBu)]_2$ (E = S, Se, **1.61**).[54] Reaction of these species with Na metal in a Wurtz-type coupling reaction was found to give hexameric macrocycles $[(\mu\text{-}E)P(\mu\text{-}N^tBu)_2P(=E)]_6$ (**1.62**).[129,130] In the case of the S species $[S=(Cl)P(\mu\text{-}N^tBu)]_2$ (**1.61S**), the reaction with Na gave a mix of hexameric species $[(\mu\text{-}S)P(\mu\text{-}N^tBu)_2P(=S)]_6$ (**1.62S**) and the biradicaloid $[S\text{-}P(Cl)(\mu\text{-}N^tBu)]_2^{2-}$ (**1.63**), whereas the Se analogue **1.61Se** gave the hexamer $[(\mu\text{-}Se)P(\mu\text{-}N^tBu)_2P(=Se)]_6$ (**1.62Se**) exclusively (Scheme 3.2).

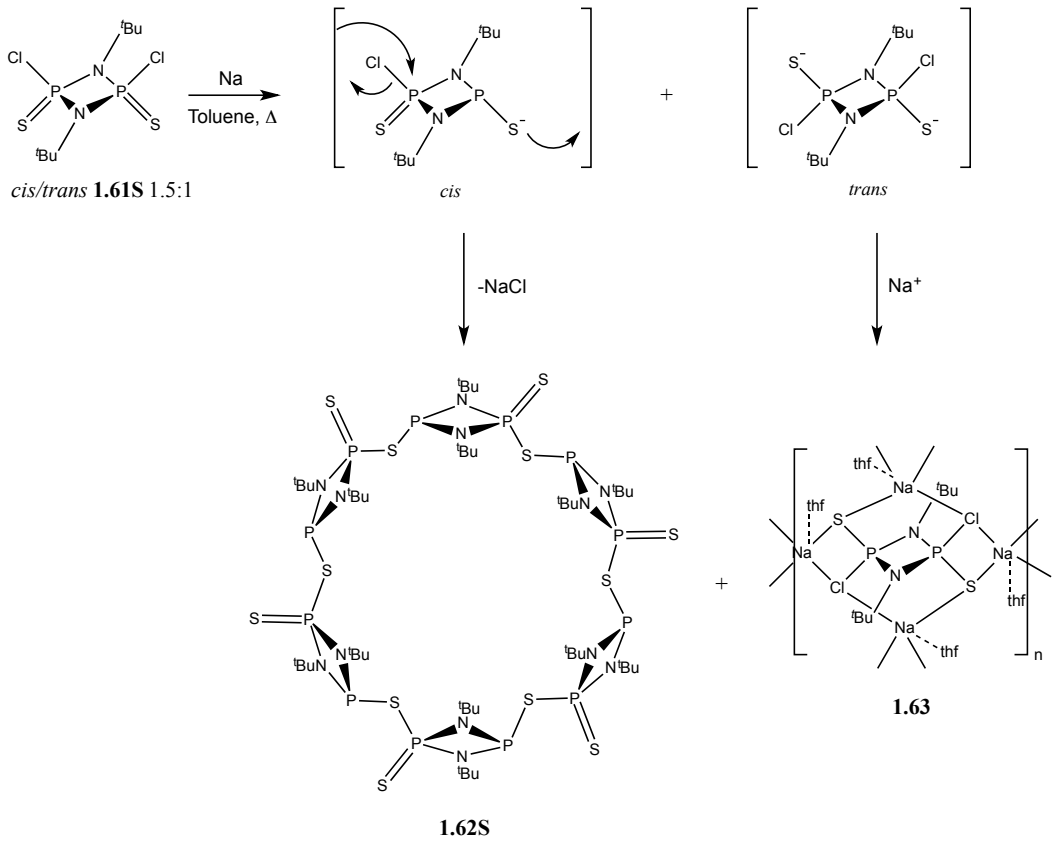

Scheme 3.2: Synthesis of sulfur hexamer 1.62S with side reaction giving biradicaloid 1.63. Image adapted from work by Singh *et al.*[130]

There are therefore three different methods for forming macrocycles based on cyclophosphazane species, the condensation method using a protic nucleophilic species and a Brønsted base (used to form NH-bridged macrocycle), the nucleophilic substitution method using a dianionic nucleophilic species (used for O-bridged macrocycles), and the Wurtz coupling method (used to obtain the P^{III}-P^{V} containing hexamers bridged by sulfur and selenium). A common theme in these reactions is the modification of the chloro-dimer $[ClP(\mu\text{-}N^tBu)]_2$ to give 'nucleophilic' variants $[EP(X)(\mu\text{-}N^tBu)]_2$ (E = NH_2, O, S, Se X = -, H, Cl). These nucleophiles are then reacted with the electrophilic chloro-dimer $[ClP(\mu\text{-}N^tBu)]_2$ to give the macrocycles. Although these approaches allow the incorporation of different linking atoms (NH, O, S, Se), there is still no general method that has allowed the introduction of different R groups, to create heteroleptic macrocycles or the tuning of the macrocycle cavity size. The systematic introduction of new R groups into the macrocyclic unit could be a

significant advantage in terms of the applications of these species, producing a range of steric characteristics, solubilities and cavity sizes.

The main group substituted species used as nucleophilic precursors in macrocycle formation are structurally related to the oxidised P^V dianions synthesised by Woollins *et al.* and Chivers *et al.*, $[RN(E=)P(\mu\text{-}N^tBu)]_2^{2-}$ (R = alkyl, E = S, Se, O) (**1.36-1.38**, Chapter 1.3). Their coordination chemistry has been studied extensively, however, all involve the use of sterically bulky substituents at the amino position (NR).

In this chapter, the synthesis, coordination chemistry and reactivity of the new dianionic ligands $[E=P(H)(\mu\text{-}N^tBu)]_2$ or $[E\text{-}P(\mu\text{-}N^tBu)]_2^{2-}$ are explored.

3.2 Synthesis and Characterisation of S/H phosph(V)azanes

This section focuses on the synthesis of sulfur phosph(V)azane dimers of the type $[S=(H)P(\mu\text{-}NR)]_2$ and investigates the influence of the steric bulk of the R-group on the preference for the formation of *cis* and *trans* isomers and their stability towards decomposition and oligomerisation.

3.2.1 Preliminary Studies on $[S=(H)P(\mu\text{-}N^tBu)]_2$

Pilot studies focused on the dimer $[ClP(\mu\text{-}N^tBu)]_2$ (**2.1**) as the precursor in order to establish the best experimental protocol for the synthesis of the sulfur dimer $[S=(H)P(\mu\text{-}N^tBu)]_2$ (**3.1**). Following an analogous procedure to that employed earlier in the synthesis of the diamino-dimer $[NH_2P(\mu\text{-}N^tBu)]_2$ **1.21**, a thf solution of $[ClP(\mu\text{-}N^tBu)]_2$ was added dropwise to a thf solution of H_2S at −78 ºC. Stirring the reaction at ambient temperature, removal of the solvent under vacuum and extraction of the solid residue with toluene produced variable yields of **3.1** as a powder after evaporation of the solvent under vacuum (10–38%). However, the reaction of $[ClP(\mu\text{-}N^tBu)]_2$ with an *in situ* prepared solution of LiSH in thf at −78 ºC, followed by the same work up produced significantly higher yields of pure **3.1** (83%) (Scheme 3.3).

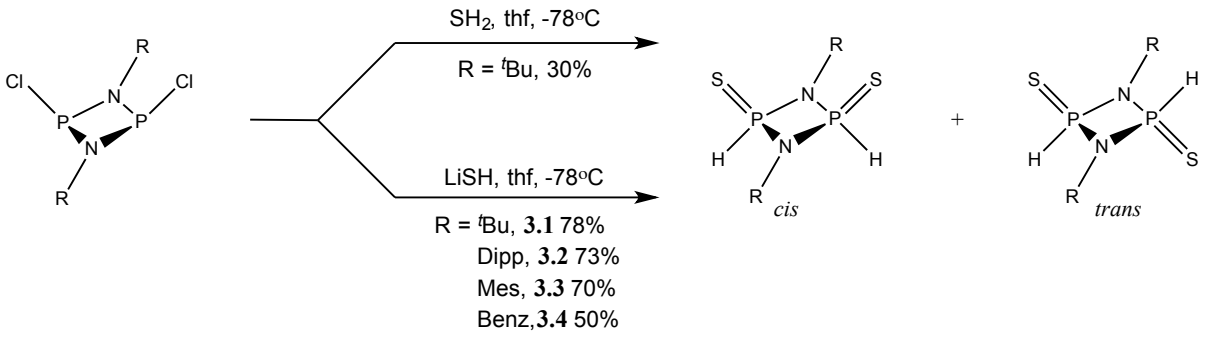

Scheme 3.3: Synthetic procedures for sulfur dimers [S=(H)P(*μ*-NR)]$_2$ (3.1-3.4) .

The identity of **3.1** was confirmed by multinuclear NMR (^{31}P, ^{1}H) and IR spectroscopy. The predominant *cis* isomer of **3.1** was structurally characterised by X-ray diffraction of a crystal grown from a toluene solution at −5 ºC (Figure 3.1).

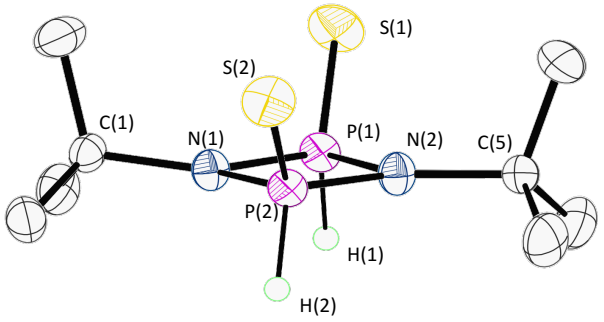

Figure 3.1: X-ray crystal structure of 3.1. Hydrogen atoms (except those attached to P) have been omitted for clarity. Thermal ellipsoids set at the 50% probability level. Selected bond lengths (Å) and angles (°); P(1)-N(1) 1.6785(11), P(1)-N(2) 1.6817(11), P(1)···P(2) 2.4991(4), P(2)-N(2) 1.6804(11), P(2)-N(1) 1.6799(11), P(1)-S(1) 1.9167(5), P(2)-S(2) 1.9143(5), P(1)-H(1) 1.322(17), P(2)-H(2) 1.314(18), N-P-N mean 83.88, P-N-P mean 96.10, N-P=S mean 122.15.

The solid-state structure of *cis*-**3.1** shows that it adopts the expected P^{V}(H)=S (rather than P^{III}–SH) tautomer and has a planar P_2N_2 core arrangement. This isomer appears as a second-order AA′XX′ multiplet centred at δ = 36.3 ppm in the fully-coupled, ^{31}P NMR spectrum of **3.1**, which contains only about 1% of the *trans* isomer (at δ = 40.7 ppm, see Figure 3.2). The ratio of *cis*/*trans* varies depending on the batch of material, but the ratio never exceeds 1-2% of the *trans*-species.

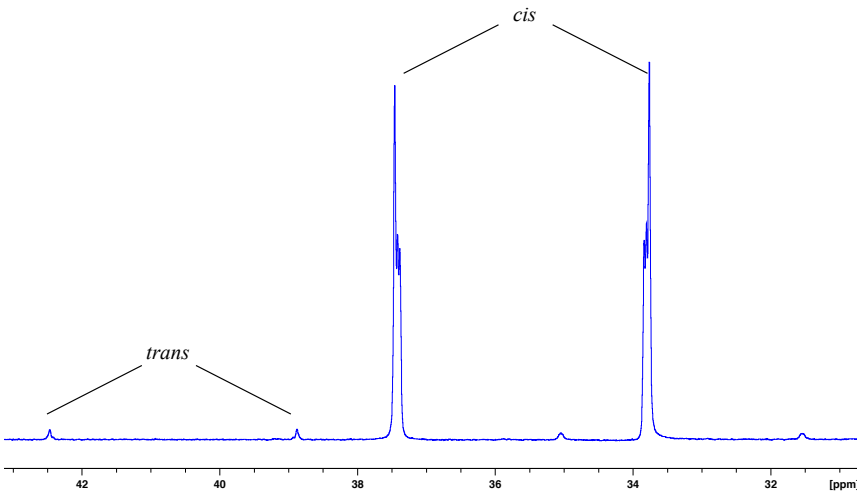

Figure 3.2: ^{31}P-^{1}H NMR (202.5 MHz, C_6D_6) spectrum showing AA'XX' signal for *cis*-3.1 and minor amounts of *trans*-3.1.

The assignments of the ^{31}P resonances for the *cis* and *trans* isomers are supported by DFT chemical shift calculations (carried out by Vladislav Vasilenko, Heidelberg) which show that the *trans* isomer should have a chemical shift *ca.* 2.7 ppm higher than the *cis* (experimental value $\Delta\delta$ = 4.4 ppm). The calculated values for all the possible tautomers of **3.1** are shown in Table 3.1. The calculations were performed and correlated relative to the experimental value of *cis*-**3.1**.

Table 3.1: Full ^{31}P chemical shift calculations for the possible tautomers of 3.1. Correlated shifts based on measured value for *cis*-3.1 highlighted in red.

Gen Basis TZ/5Z			Tautomer			
	Reference Peak					
	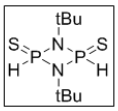	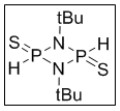	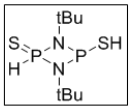	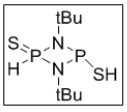	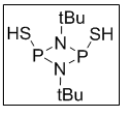	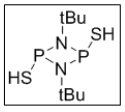
NMR Signals						
Shift P1	244,2510	236,4770	228,0600	221,7200	57,0164	-19,8018
Shift P2	244,4150	246,8430	91,9633	93,8062	57,3398	4,2690
Avarage Shift	244,3330	241,6600	160,0117	157,7631	57,1781	-7,7664
Relative Shift (Ref Cis) 1	0,0000	--	16,2730	22,6130		
Relative Shift (Ref Cis) 2	0,0000	--	152,3697	150,5268		
Relative Avarage Shift	0,0000	2,6730			187,1549	252,0994
Correlated Shifts	34,8100	37,4830	51,0830 187,1797	57,4230 185,3368	221,9649	286,9094

The lower chemical shift found for the *cis* compared to the *trans* isomer is similar to the trend observed in bis(amino) cyclophosph(III)azanes $[R^2NHP(\mu\text{-}NR^1)]_2$.[19] The presence of two isomers is also apparent in the room-temperature ^{1}H NMR spectrum, which shows two ^{t}Bu resonances (δ = 1.38 (*cis*), 1.36 (*trans*) ppm) and two second-order P-H multiplets (δ = 8.40 (*cis*), 8.75 (*trans*) ppm).

Relative $^{1}J_{P\text{-}H}$ coupling constants can be observed in the $^{31}P\text{-}^{1}H$ NMR as well as the ^{1}H NMR spectrum and are within the expected range for P^{V}-H species (*cis*-$^{1}J_{P\text{-}H}$ = 598 Hz and *trans*-$^{1}J_{P\text{-}H}$ = 574 Hz).

An *in situ* ^{31}P NMR spectroscopic study of a sample of **3.1** in toluene shows that it is gradually converted into *trans*-**3.1** at higher temperature, but starts to decompose at *ca.* 333 K into a number of unidentified products (Figure 3.3). Decomposition can be characterised by a change of colour from white/transparent solution to yellow with formation of a yellow solid as well as a variety of peaks throughout the ^{31}P NMR spectrum. The final ratio of *cis*:*trans* isomers is *ca.* 7:1 at 333 K. However, the thermal decomposition of **3.1** made van't Hoff analysis of the data unreliable. One noticeable feature of this process is that the conversion of *trans*-**3.1** back to *cis*-**3.1** is irreversible once the temperature is returned to ambient temperature.

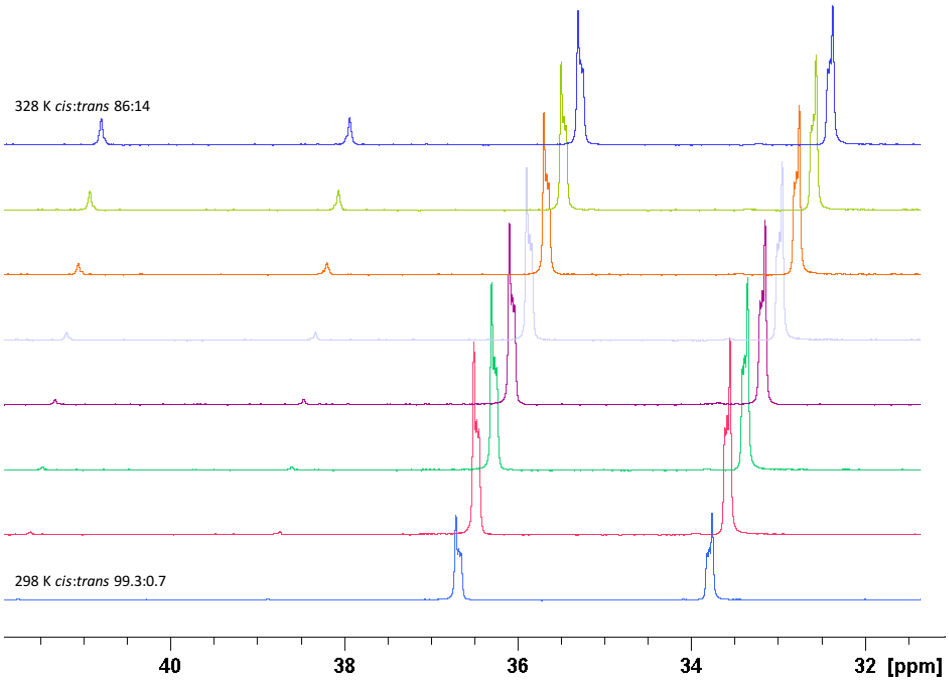

Figure 3.3: $^{31}P\text{-}^{1}H$ VT NMR (202.5 MHz, d_8-toluene, 298→328 K in 5 K increments) study of 3.1 showing conversion of *cis* to *trans* isomer.

3.2.2 *Cis/Trans* Isomerism in $[S{=}(H)P(\mu\text{-}NR)]_2$

Following the successful synthesis and isolation of the ^{t}Bu derivative **3.1** we attempted to explore the LiSH reaction using other chloro-dimers $[ClP(\mu\text{-}NR)]_2$ from Chapter 2, bearing different R substituents. Attempts to extend the same synthetic method to other dimers of this type (R = Dipp

(**2.7**, 2,6-$^{i}Pr_2C_6H_3$), Mes (**2.6,** 2,4,6-$Me_3C_6H_2$), Benz (**2.4**, Ph_2CH–), Neopent (**2.3**, $^{t}BuCH_2$–) and the chiral species **2.5** ((R)1-isoproylenapthalene)) were hampered either by the instability of the product in solution at ambient temperature or the rapid formation of a variety of by-products. However, in some cases if worked up immediately after warming the reaction mixture to ambient temperature, then decomposition can be minimised. The new dimers $[S=(H)P(\mu\text{-}NR)]_2$ (R = Mes (**3.3**), Benz (**3.4**)) can be obtained in moderate to good yields (55–73%) as powders using this method after removal of the solvent under vacuum. However, for R = Dipp (**3.2**) the low purity of the powder obtained meant that a further crystallisation step was required, resulting in a lower final yield of 12%. The ^{31}P and ^{1}H NMR spectra of **3.2**, **3.3** and **3.4** indicate that samples are of >95% purity. This synthetic approach is not reliable for less sterically bulky R groups (e.g., R = $^{t}BuCH_2$, 2-biphenyl and (R)1-isoproylenapthalene (**I3**, **I4** and **I5**, Chapter 2.2)), for which only minor yields of the products are obtained amongst a large number of impurities.

Variable-temperature ^{31}P NMR spectroscopic studies illustrate that the thermal stabilities of the sulfur dimers are in the order **3.2**, **3.3** > **3.1** > **3.4**. For example, whereas **3.2** and **3.3** are stable up to *ca.* 353 K, **3.4** decomposes significantly into other products at *ca.* 308 K. The ^{1}H-coupled ^{31}P NMR spectra of these species at ambient temperature shows a further effect of the general reduction in the steric demands of the R-group. There is a change in the relative ratios of the isomers from the *cis* isomer in the case of **3.1** (1% *trans*, 99% *cis*), to a mixture of *cis* and *trans* for **3.2** and **3.3** (*ca.* 60% *cis*, 40% *trans* in **3.2**, *ca.* 50% *trans*, 50% *cis* in **3.3**) to predominantly the *trans* isomer in the case of **3.3** (*ca.* 90% *trans* and 10% *cis*) (Figure 3.4). A comparison of the ^{31}P and ^{1}H NMR shifts of **3.1**-**3.4** as well as their relative *cis*:*trans* ratios can be found in Table 3.2.

Table 3.2: Summary of the ^{31}P (202.26 MHz) and ^{1}H NMR (400 MHz) spectroscopic data for compounds 3.1-3.4, as well as relative *cis/trans* isomer ratios observed and their calculated energy differences (discussed in further detail in Chapter 3.2.3).

Compound	^{31}P NMR (PH, ppm)	^{1}H NMR (PH, ppm)	$^{1}J_{P-H}$ (Hz)	*cis:trans*	ΔG *cis*→*trans* (calc, k*J* mol^{-1})
***cis*-3.1**	36.3	8.4	598	50:1	9.04
***trans*-3.1**	40.7	8.75	574		
***cis*-3.2**	45.0	9.04	593	3:2	1
***trans*-3.2**	53.1	9.32	591		
***cis*-3.3**	36.7	9.07	592	1:1	-4.22
***trans*-3.3**	44.6	9.29	593		
***cis*-3.4**	38.2	-	579	1:9	-11.6
***trans*-3.4**	40.0	7.44	556		

Unlike **3.1**, the ^{31}P NMR spectra of **3.2** and **3.3** show no changes in the ratios of the *cis*:*trans* isomers with increased temperature. As in the case of **3.1**, the P–H region of the ^{1}H NMR spectra of **3.2**–**3.4** show similar second-order patterns for the P–H protons of their *cis* and *trans* isomers as well as similar $^{1}J_{P-H}$ coupling constants.

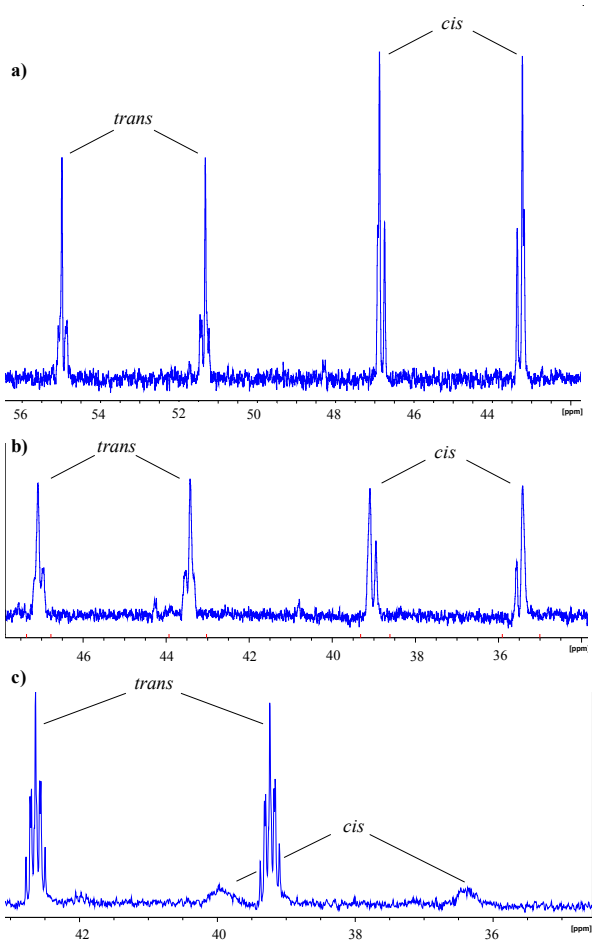

Figure 3.4: The fully H-coupled ^{31}P NMR (202.5 MHz, C_6D_6, 298 K) spectra of (a) 3.2, (b) 3.3, and (c) 3.4.

The assignment of the ^{1}H NMR spectrum of **3.2** is particularly informative and was supported by a 2D ^{31}P/^{1}H HMBC NMR experiment (Figure 3.5d). For the *cis* diastereomer (Figure 3.5b) the two methyl groups of each ^{i}Pr group are enantiotopic, whereas diastereotopic methyl groups are found for the *trans* diastereomer (Figure 3.5a). Consequently, the ambient temperature ^{1}H NMR spectrum displays one septet resonance for the C–H protons of the ^{i}Pr groups and two 1:1 Me resonances for the Me-groups of the ^{i}Pr substituents of the *trans* isomer. This is consistent with the C_2 symmetric structure of the *trans*-**3.2** (Figure 3.5a) revealed by single-crystal X-ray analysis (Figure 3.7), and results from restricted rotation of the C_{aryl}–N and C_{aryl}–C(^{i}Pr) bonds. In contrast, *cis*-**3.2** shows two C–H resonances for the ^{i}Pr groups and two 1:1 resonances for the Me groups of the ^{i}Pr substituents. The ^{1}H–^{1}H NOESY NMR spectrum (Figure 3.5c) provides further support for the rigid structures of both isomers in solution by confirming that only one of the C–H (^{i}Pr) environments in the *cis* isomer is in

close proximity to the P–H protons, whereas, for symmetry reasons, all of the C–H (^{i}Pr) protons of the *trans* isomer are close to the P–H protons.

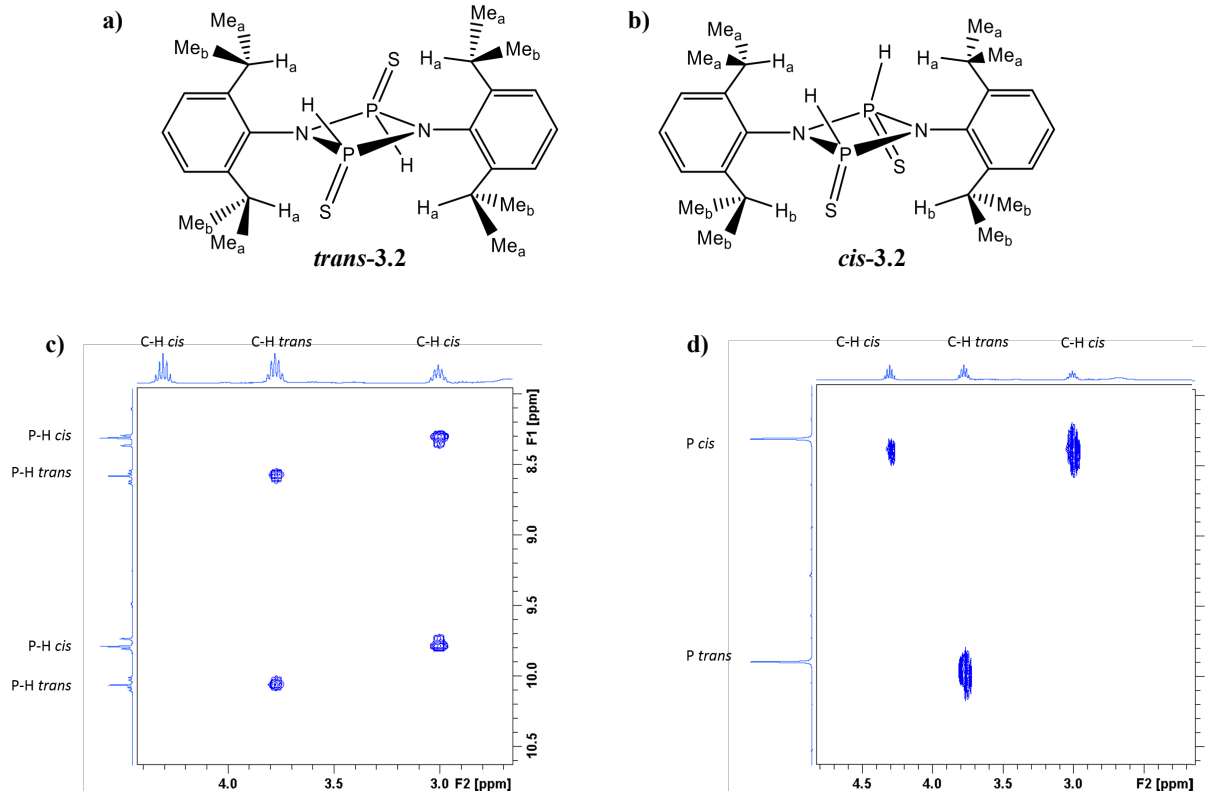

Figure 3.5: a) Idealized C_{2h} structure for *trans*-3.2 b) Idealised C_{2v} structure for *cis*-3.2 c) ^{1}H-^{1}H NOESY spectrum (d_8-toluene, 298 K, mixing time = 1000 ms) of 3.2 expanded to show through-space correlation between P-H *cis* and P-H *trans* with the corresponding CH protons of the ^{i}Pr groups d) ^{1}H-^{31}P HMBC spectrum of 3.2 expanded to show coupling between inequivalent Ha and Hb in the *cis* species and Ha *trans* with their respective ^{31}P resonances.

Similar restricted rotation was seen for **3.3** where two separate broad signals are seen for the *o*-Me in the *cis* isomer whereas only one sharp signal is observed for the *trans* (Figure 3.6). Evidence for the less restricted nature of the C_{aryl}–N bonds within the dimer **3.3** was found by ^{1}H-^{1}H NOESY (Figure 3.6c) and ^{1}H-^{1}H EXSY (Figure 3.6d) NMR as well as a variable-temperature NMR experiment. In **3.3**, the *trans* isomer was revealed to have a C_{2h} symmetric centre (Figure 3.6a) as evidenced by a single peak for the *o*-Me hydrogens in the ^{1}H NMR and the structure was also confirmed by X-ray crystallography. Crystals of *cis*-**3.3** (Figure 3.6b) could not be obtained, but a ^{1}H-^{1}H NOESY experiment (Figure 3.6c) revealed through-space correlation between the P-H protons and the two separate *o*-Me groups on either face of the C_{2v} symmetric ring. Rotational equivalence between the *o*-

Me groups in *cis*-**3.3** was shown by ^{1}H-^{1}H EXSY NMR (Figure 3.6d) where positive cross peaks between the *o*-Me groups indicate exchange between the groups.

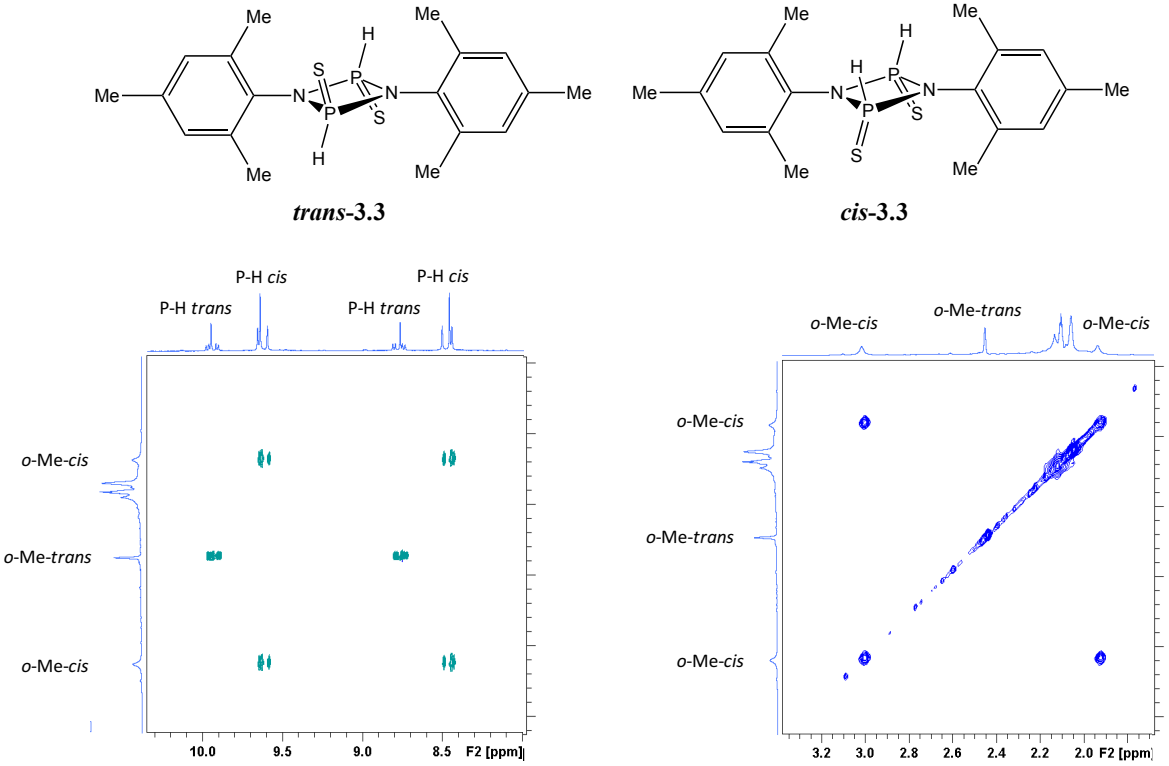

Figure 3.6: a) Idealized C_{2h} structure for *trans*-3.3 b) Idealised C_{2v} structure for *cis*-3.3 c) ^{1}H-^{1}H NOESY spectrum (C_6D_6, 298 K, mixing time = 1000 ms) of 3.3 expanded to show through-space correlation between P-H *cis* and P-H *trans* with the corresponding CH protons of the *o*-Me groups d) ^{1}H-^{1}H EXSY spectrum of 3.3 expanded to show rotational equivalence between the two *o*-Me groups in *cis*-3.3.

Crystals of *trans*-**3.2** and *trans*-**3.3** were grown from saturated *n*-hexane/thf solutions at ambient temperature (Figures 3.7a and b, respectively). Although the solutions contained mixtures of *cis* and *trans* isomers, no crystals of the *cis* isomers could be obtained. The two species have very similar structures, both lying on a crystallographic inversion centre and having C_{2h} symmetry. The P_2N_2 ring is planar and the aromatic rings of the R groups lie perpendicular to the ring plane, placing the *ortho* substituents over the face of the phosphazane unit.

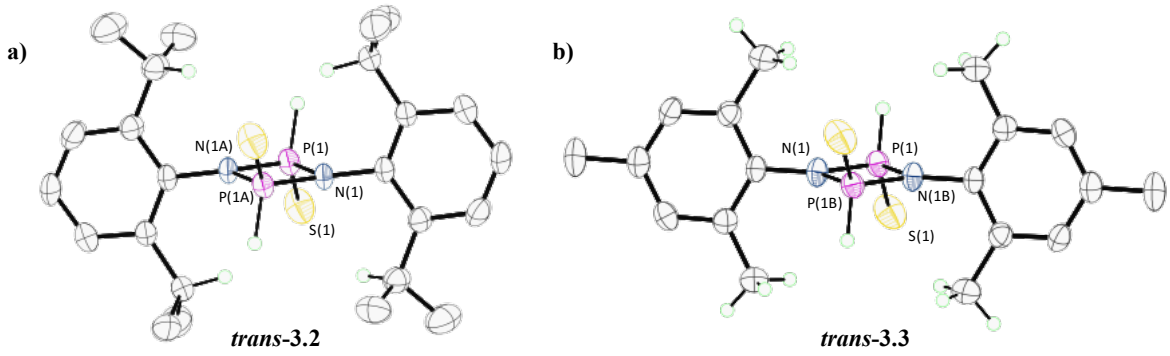

Figure 3.7: X-ray crystal structures of a) *trans*-3.2 and b) *trans*-3.3. Hydrogen atoms (except those discussed in NMR data) omitted for clarity. Thermal ellipsoids set at the 50% probability level. 3.2: P(1)-N(1) 1.679(2), P(1)-N(1A) 1.676(2), P(1)···P(1A) 2.5055(16), P(1)-S(1) 1.8875(12), P(1)-H(1) 1.35(3), N-P-N 83.38(12), P-N-P 96.62(12), N-P=S mean 122.17; 3.3: P(1)-N(1) 1.680(3), P(1)-N(1A) 1.691(3), P(1)···P(1A) 2.5322(17), P(1)-S(1) 1.9084(13), N-P-N 82.63(13), P-N-P mean 97.38(13), N-P=S mean 121.2.

3.3 contains a minor disordered component (site occupancy major: 0.923(3) minor: 0.077(3)) (Figure 3.8) which could also be found in some crystals of **3.2**. The dihedral angle between the Mes substituent and the P_2N_2 plane is 55.6º in the minor component *vs.* 82.2º in the major component.

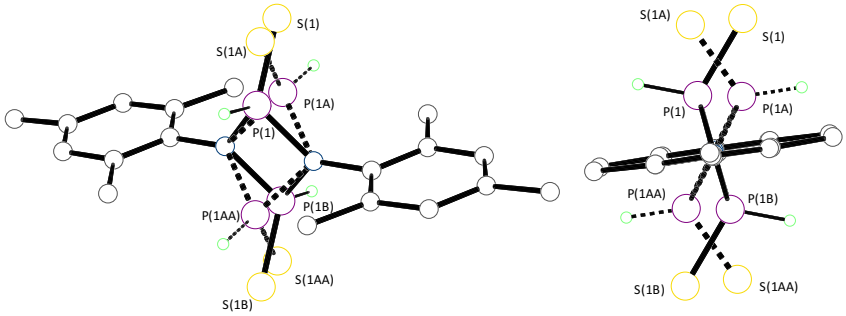

Figure 3.8: X-ray structure of *trans*-3.3 showing major and minor crystallographic components. Major: P(1),S(1),P(1B),S(1B) (suffix B generated from P(1),S(1) by inversion centre), solid bonds. Minor: P(1A),S(1A),P(1AA),S(1AA) (suffix AA generated from P(1A),S(1A) by inversion centre), dashed bonds.

3.2.3 Computational Studies of $[S=(H)P(\mu\text{-}NR)]_2$

In order to understand the *cis/trans* isomerism and relative ratios of the products better, DFT calculations were performed (Vladislav Vasilenko, Heidelberg) modelling the *cis* and *trans* isomers of **3.1-3.4** using the B3LYP/cc-pVTZ level of theory in thf solvent (PCM model) using Gaussian 09.[132–136] Frequency calculations of the optimized geometries were carried out, confirming the absence of imaginary frequencies. Thermodynamic parameters of the reaction energy for conversion between the

cis→*trans* isomers are provided for 298 K and standard pressure (Table 3.3), further details for individual tautomers can be found in the Appendices.

Table 3.3: Reaction energies (E, H, G, in kJ mol^{-1}) for the conversion *cis* → *trans* for compounds 3.1–3.4. Thermodynamic parameters H and G were calculated for 298 K and standard pressure.

Compound	Δ*E*	Δ*H*	Δ*G*
3.1	8.52	8.42	9.04
3.2	-0.05	-0.88	1
3.3	-0.58	-1.03	-4.22
3.4	-10.31	-4.62	-11.6

The calculated thermodynamic data support the experimental observation from ^{31}P NMR spectroscopy that the *cis* isomer is the most stable for bulkier R-groups (^{t}Bu, Dipp) but the *trans* isomer becomes most stable for less sterically encumbered R-groups (Mes, Ph_2CH). Depending on the steric demands of the substituents, the calculated *cis*/*trans* ratios range from strongly favoured *cis* (ΔG = 9.0 kJ/mol^{-1} for **3.1**) to strongly favoured *trans* isomer (Δ*G* = −11.6 kJ mol^{-1} for **3.4**). It is clear, however, that the steric effect is a subtle one since the trend in the relative stabilities of the *cis* vs. *trans* isomers does not follow that expected on the basis of Tolman cone angle completely (for which the preference for the *cis* isomer should be **3.2** > **3.3** > **3.1** > **3.4**). Although we cannot discount electronic factors as an influence on the preference for either isomer, I believe that the lower than expected steric influence of the Dipp and Mes groups of **3.2** and **3.3** is due to their perpendicular orientation with respect to the P_2N_2 rings. In order to probe the potential tautomerism of the dimers between the P^{V}=S to the P^{III}-SH species, calculations on the various energies of the possible tautomers were performed. The tautomers containing an SH group are all much higher in energy, regardless of the substituents attached to the P_2N_2-ring (e.g., **3.1** and derivatives in Figure 3.9, further details for **3.2**-**3.4** can be found in appendix 8.2).

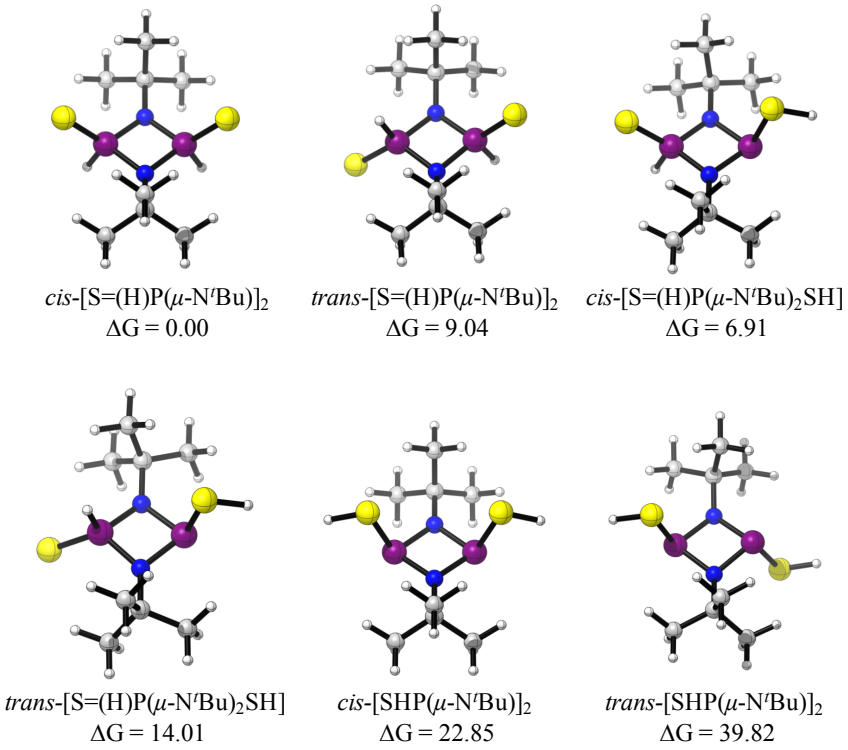

Figure 3.9: Calculated geometries of the possible tautomers of 3.1 and their relative energies (ΔG in kj mol^{-1}) compared to *cis*-[S=(H)P(μ-N^{t}Bu)]$_2$.

In order to understand the apparent irreversibility of the isomerism seen in **3.1**, we investigated possible mechanisms for the conversion of the *cis* isomer of **3.1** to the *trans* isomer. The analysis of typical intramolecular isomerization mechanisms such as (i) a concerted pathway in which *cis*-**3.1** is converted into *trans*-**3.1** directly *via* rotation of one P(H)=S fragment (Red *via* TS1, Figure 3.10) and (ii) a stepwise pathway involving P(H)=S/P-SH tautomerism and phosphorus lone pair inversion (Black, *via* TS3, Figure 3.10) were found to involve very high activations barriers (> 150 kJ mol^{-1}) and are therefore unlikely. In view of the findings in variable-temperature NMR experiments, it is probable that the relative *cis*/*trans* ratios of the different isomers are in part influenced by kinetic factors. Further mechanistic studies are required to resolve the nature of the transition states (intra- *vs.* intermolecular) that might be involved in this process. Previous studies on the isomerism of bis(amino) species might suggest that dissociation of the dimer and intermolecular re-association is most likely.[19,137]

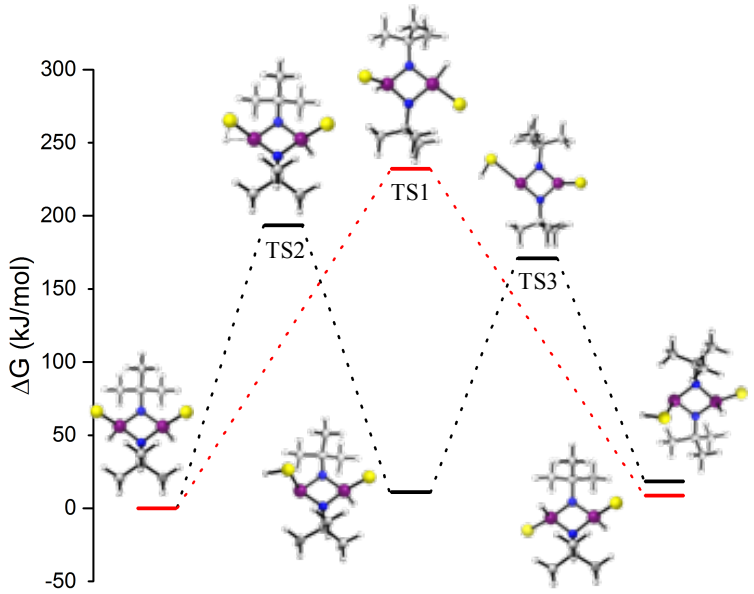

Figure 3.10: Transition state calculations - (i) a concerted pathway in which *cis*-3.1 is converted into *trans*-3.1 directly *via* rotation of one P(H)=S fragment (red); (ii) a stepwise pathway involving P(H)=S/P-SH tautomerism and phosphorus lone pair inversion (black).

Complete experimental data and calculated configurations can be found in the Appendix (Chapter 8.2).

These studies show that the sulfur derivatives $[S=(H)P(\mu\text{-}NR)]_2$ can be obtained from a simple reaction of $[ClP(\mu\text{-}NR)]_2$ with LiSH to give potential building blocks for the synthesis of S-bridged macrocycles. Reactions of these species with the chloro dimers in presence of a Brønsted base in an analogous manner to the formation of the N-bridged species **1.56/1.57** gave no pure species, rather solutions containing multiple phosphorus products were observed by ^{31}P NMR spectroscopy. Although some peaks appear in the ^{31}P NMR spectrum in the range where macrocycles might be expected, it was impossible to separate or characterise any single species.

3.3 Generation and Characterisation of $[S\text{-}P(\mu\text{-}N^tBu)]_2^{2-}$

Unlike the oxygen counterparts $[O=(H)P(\mu\text{-}N^tBu)]_2$ (**1.22** Chapter 1.4.3) which are thermodynamically unstable with respect to dimerisation into $\{[O=(H)P(\mu\text{-}N^tBu)]_2\}_2(\mu\text{-}O)$, the stability of **3.1-3.3** allows them potentially to be used as storable sources of the dianions $[(S)P(\mu\text{-}NR)]_2^{2-}$. The interest in these as novel ligands concerns (i) the fact that they would be valence-

isoelectronic with the well-known family of $[(RN)P(\mu\text{-}NR)]_2^{2-}$ phosph(III)azane ligands used extensively in coordination studies (see Introduction 1.3.3), but contain a mixed (hard-soft) donor set (Scheme 3.4), and (ii) they should be easily elaborated, especially in respect to the incorporation of chiral R-groups. This section focuses on the coordination characteristics of the first example of this new ligand, the dianion $[(S)P(\mu\text{-}N^tBu)]_2^{2-}$ (**3.5**), and show that it not only has adaptable hard-soft ligand properties but also can be applied in the construction of large supramolecular cage architectures.

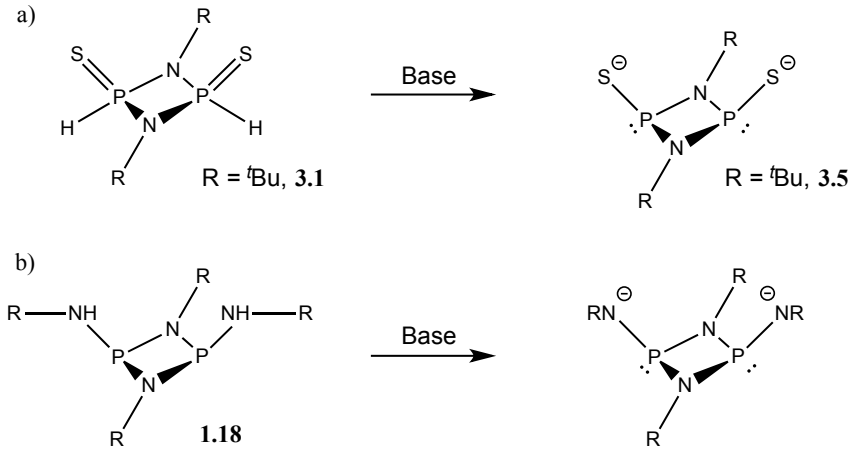

Scheme 3.4: a) Deprotonation of 3.1 to give the anion $[(S)P(\mu\text{-}N^tBu)]_2^{2-}$ (3.5), b) Generation of the valence-isoelectronic nitrogen ligands $[(RN)P(\mu\text{-}NR)]_2^{2-}$.

3.3.1 Formation and Characterisation of $[(S)P(\mu\text{-}N^tBu)]_2[Mg\cdot 2thf]$

The precursor $[S{=}(H)P(\mu\text{-}N^tBu)]_2$ (**3.1**) was chosen in trial reactions because it is easily prepared in gram quantities as a crystalline material from the reaction of the chloro-diphosphazane $[ClP(\mu\text{-}N^tBu)]_2$. Initial attempts to deprotonate **3.1** at -78°C using *n*BuLi failed, the isolated powder showing a broad range of products in the ^{31}P NMR spectrum, implying total breakup of the P_2N_2 phosphazane ring. The high nucleophilicity and basicity of organolithium reagents is likely to be the cause of this decomposition. We therefore moved on to explore other less nucleophilic organometallic bases. The 1:1 stoichiometric reaction of **3.1** with Bu_2Mg in thf was followed in an *in situ* ^{31}P NMR spectroscopic study, which showed clean quantitative formation of the dianion $[S\text{-}P(\mu\text{-}N^tBu)]_2^{2-}$ (**3.5**) (Scheme 3.5). The change in valency of the P atoms from V to III is accompanied by a large change in chemical shift from δ = 35 ppm for **3.1** to a broad singlet at δ = 186.5 ppm for the dianion **3.5**

(Figure 3.11). Related diphosph(V)azanes exhibit resonances in the range δ = 30–60 ppm whereas trivalent diphosph(III)azanes are found in the range δ = 150–210 ppm. It is interesting to note that any *trans*-**3.1** that is present in the reaction mixture is also converted into **3.5**, which shows no *cis*/*trans* isomers.

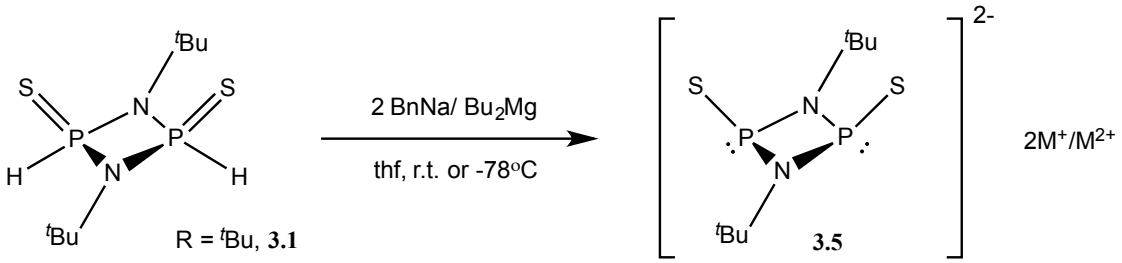

Scheme 3.5: Deprotonation of 3.1 to generate the dianion [S-P(μ-N^{t}Bu)]$_2^{2-}$ (3.5).

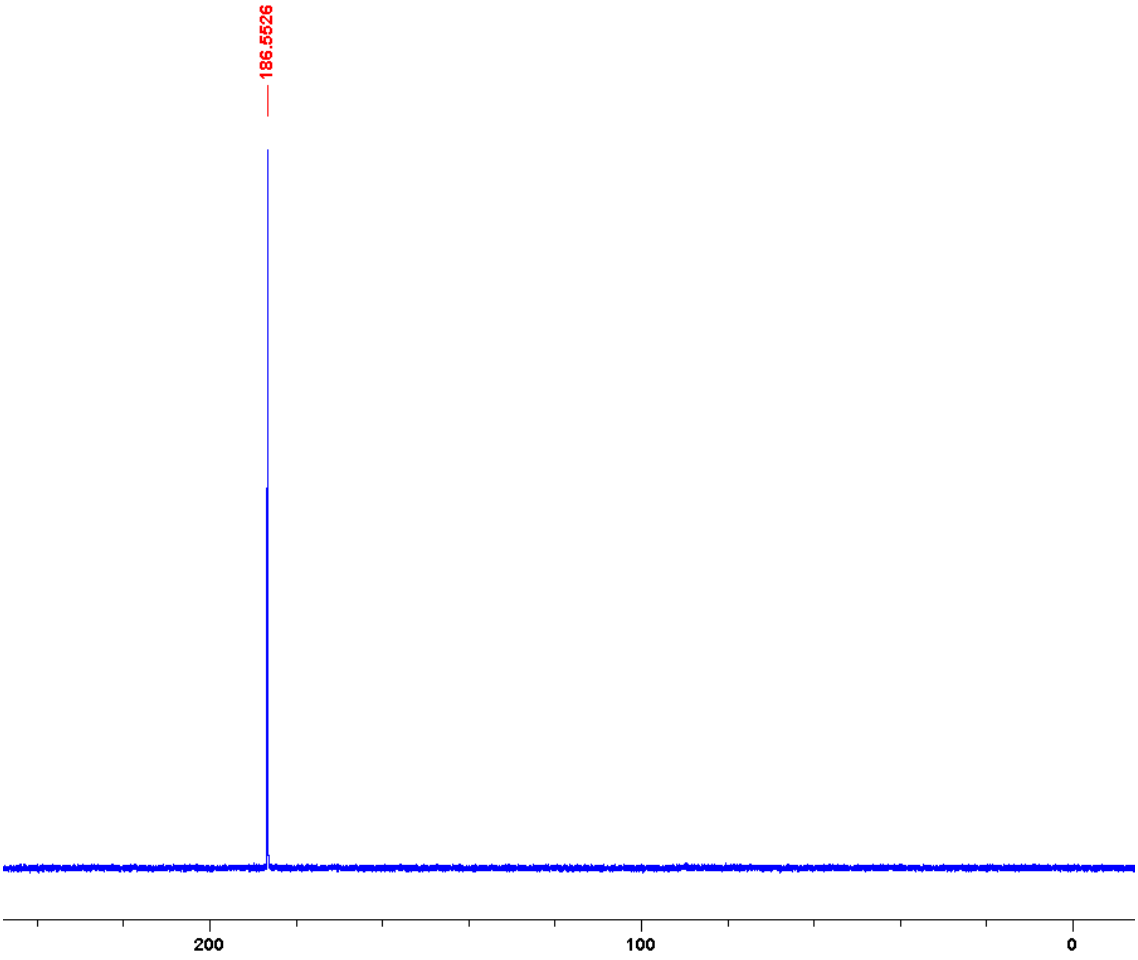

Figure 3.11: ^{31}P NMR (202.5 MHz, d$_8$-thf, 298 K) spectrum of [Mg(3.5)·2thf] (3.6).

Crystals of [Mg(**3.5**)·2thf] (**3.6**) suitable for X-ray diffraction were obtained from a scaled-up reaction (70 % yield) after storage of a toluene solution at -12 ºC (16 h).

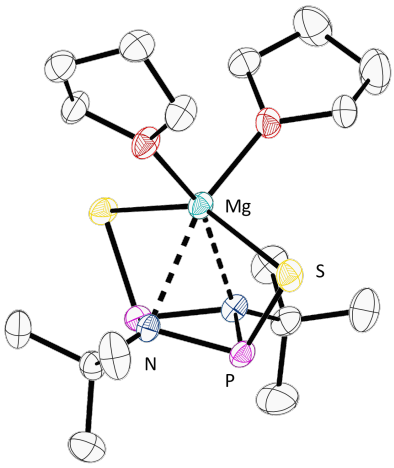

Figure 3.12: X-ray crystal structure of [Mg(3.5)·2thf] (3.6). Hydrogen atoms are omitted and thermal ellipsoids are set at the 30% probability level. Selected bond lengths (Å) and angles (º); P-N average 1.773(1), P-S average 2.060(6), Mg-S range 2.4979(6)-2.5030(6), N···Mg range 2.391(2)-2.437(2), P-N-P range 97.14(7)-97.46(7), N-P-N range 78.28(6)-78.57(6), PNNP torsion angle 156(1).

The solid-state structure of **3.6** is that of a mononuclear Mg complex (Figure 3.12). As expected, there is a significant increase in the P–S bond length in **3.6** compared to that in the starting material **3.1** (from mean 1.92 Å in **3.1** to mean 2.06 Å in **3.6**), accompanying the reduction in multiple bond character. The Mg^{2+} cation of **3.6** is coordinated by both the terminal S-atoms and the μ-N(^{t}Bu) groups of the *cis*-anion **3.5**, giving a highly distorted six-coordinate metal geometry. While the S–Mg bond lengths (2.4979(6)-2.5030(6) Å) are typical for bonding between a sulfur anion and Mg^{2+}, the Mg···N bond lengths (2.391(2)–2.437(2) Å) are consistent with a neutral N lone-pair interaction with Mg^{2+} (literature range 1.95–2.47 Å).[27] Although similar Mg···N distances have been noted in related Mg complexes,[32,138] the striking feature in the structure of **3.6** is the extreme distortion of the P_2N_2 ring of the anion **3.5** (with a PNNP torsion angle of 156º), which results from the orientation of the N-lone pairs towards the Mg^{2+} cation. This contrasts with all other anions of the $[(^t\text{BuN})\text{P}(\mu\text{-N}^t\text{Bu})]_2^{2-}$ family in which the P_2N_2 rings are almost planar (as in compound **3.7**, later), and suggests that Mg–N bonding in **3.6** is much more significant than in these previous examples. There is also a noticeable

elongation in the P–N bonds in the P_2N_2 ring unit of the anion **3.5** compared to those in **3.1** (mean 1.77 Å in **3.6**, cf mean 1.68 Å in **3.1**), associated with the weakening of P–N bonding.

3.3.2 Potassium and Sodium Salts of the Dianion $[S\text{-}P(\mu\text{-}N^tBu)]_2^{2-}$

After the successful isolation of the Mg salt of the dianion **3.5**, we attempted the synthesis of complexes containing monocations. As previously stated, attempted deprotonation with *n*BuLi appeared to result in extensive decomposition of **3.1**, even at low temperatures. The addition of **3.1** in thf to a solution of less nucleophilic NaBn (Bn = $PhCH_2$) in thf at ambient temperature results in an immediate colour change to deep blue, which then fades after a few minutes of stirring to colourless/pale green. Storage of the reaction mixture at -12 ºC (16h) gives the sodium complex, which is shown in the following section to have the formula $[Na_{16}(\mathbf{3.5})_8 \cdot NaSH \cdot 8thf]$ (**3.7**), in 90% yield, as a powder after removal of the solvent. *In situ* NMR spectroscopy indicated that the deprotonation reaction is essentially quantitative, showing the presence of the dianion **3.5** as the only product in the ^{31}P NMR spectrum (singlet, δ = 190 ppm, Figure 3.13), as well as only one ^{t}Bu environment in the ^1H NMR spectrum in solution at ambient temperature.

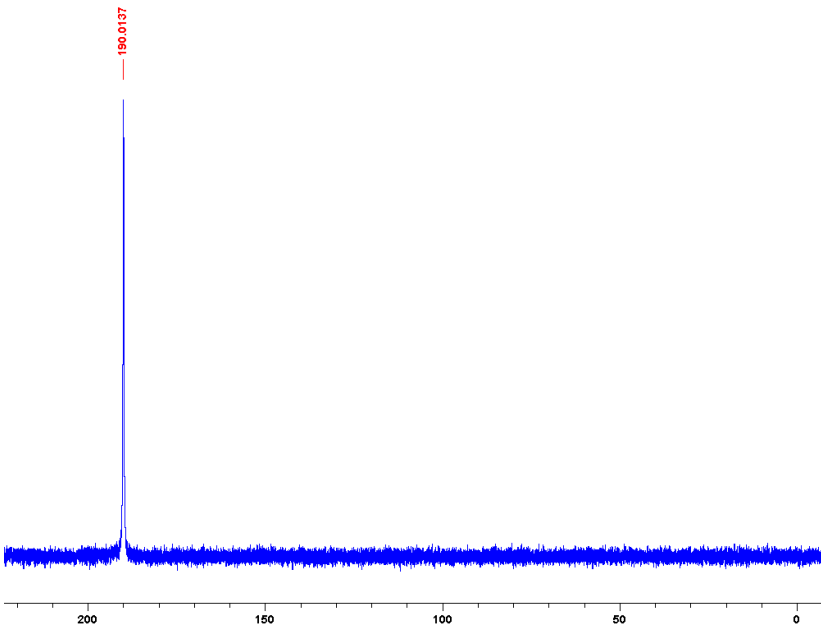

Figure 3.13: ^{31}P NMR spectrum of (202.5 MHz, d_8-thf, 298 K) spectrum of Na_2(3.5) (3.7).

The complicated nature of the structure of **3.7** could not be guessed at from initial spectroscopic and analytical analysis. The single-crystal X-ray diffraction study shows that it is a large cage of overall formula [Na_{16}(**3.5**)$_8$·NaSH·8thf] (Figure 3.14). The core structure of **3.7** is composed of eight interlocked [Na_2(**3.5**)] cubane units built around the central NaSH monomer, which is aligned along the principal rotational axis of the cage. The Na^+ cations have distorted 4-, 5- and 6-coordinate geometries within the core, with four other 4-coordinate, thf-solvated Na^+ cations located at the periphery of the cage. A particularly interesting feature of the structure of **3.7** is that the central Na_9S_9 fragment of the cage (composed of the eight interlocked Na_4S_4 cubanes) has the same NaCl-structural motif as found in the high-temperature phase of NaSH itself (Figure 3.15).[139] Although the bond lengths and angles in the dianions **3.5** are similar to those observed in the Mg complex **3.6**, the P_2N_2 rings are far less puckered, with a PNNP torsion angle of *ca.* 170º.

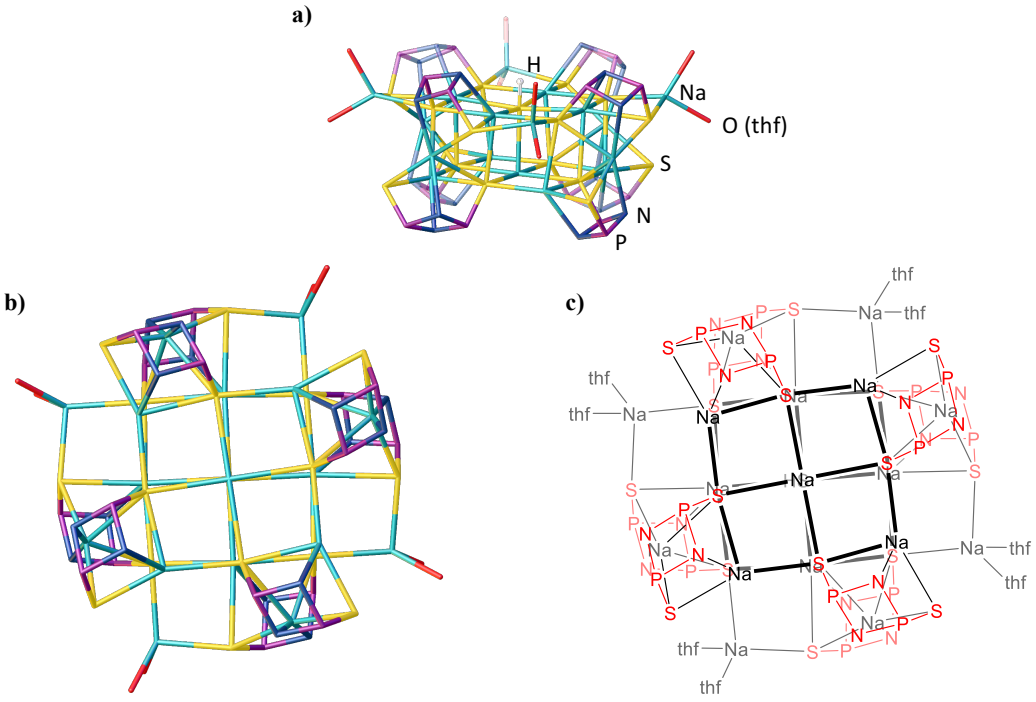

Figure 3.14: Cage structure of 3.7 with Hydrogen atoms other than the central SH group omitted. Only one of two independent molecules in the crystal structure is shown; (a) view from the side (at 90º to the principal axis), (b) from the bottom (along the principal axis) and (c) schematic diagram showing the same orientation as in (b) with the framework of the dianions 3.5 shown in red. Selected bond lengths (Å) and angles (º); P-N range 1.708(13)-1.786(10), P-S range 2.037(7)-2.112(5), Na-SH range 2.88(1)-2.91(1). P-N-P range 96.8(5)-98.9(6), N-P-N range 80.2(5)-83.4(4), PNNP torsion angles average value 170.4(5).

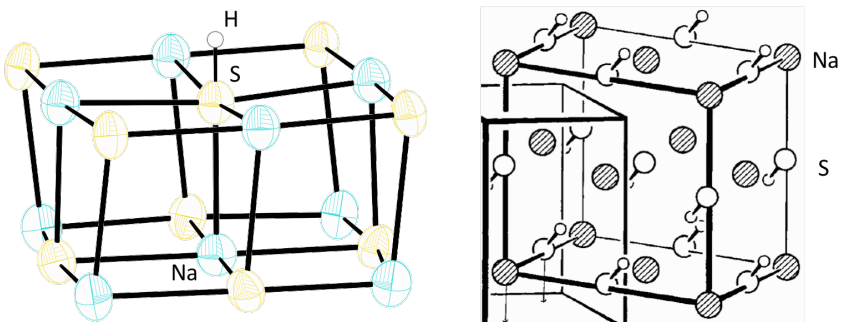

Figure 3.15: Na-S core of the solid-state structure of 3.7 (left) showing close relation to the Na-SH high temp phase as characterised by Jacobs *et al* (right).[139]

The crystals of **3.7** contained a substantial solvent (thf) quantity that was handled by application of the SQUEEZE procedure (See Experimental).[140] The void volume within the crystal, with an estimate of 125 $Å^3$ per non-coordinated thf molecule, suggests *ca.* 14 thf molecules per cage.

The identity and connectivity of the cage is clear, although the SH^- anion could not be established from the X-ray data alone and its identity was confirmed by infrared, ^{31}P and ^1H NMR spectroscopy as well as elemental analysis techniques. The S-H proton resonance can be observed in the ^1H NMR spectrum at δ = 3.4 ppm (Figure 3.16a), where it is found in the expected 1:144 ratio (experimentally 1.4:144) with respect to the ^{t}Bu groups. A variable temperature ^1H NMR experiment confirmed that the resonance exhibits a downfield shift with decreased temperature that is characteristic of an acidic H-atom (Figure 3.16b). A ^1H-^{13}C HSQC 2D NMR experiment showed no corresponding cross peak which would indicate an attached carbon for the signal at δ = 3.47 ppm for the SH H-atom.

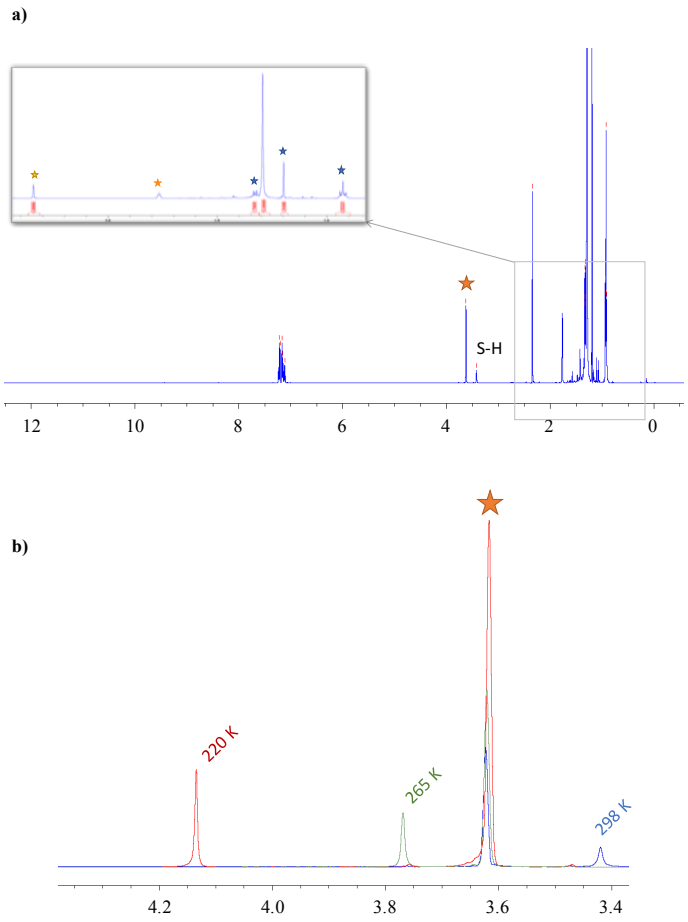

Figure 3.16: a) ^{1}H *in situ* NMR spectrum (500.2 MHz, d_8-thf, 298 K) of 3.7 with residual *n*-hexane (from BnNa purification step, blue), thf (orange) and toluene (yellow) solvent marked with stars. b) Variable-temperature ^{1}H NMR spectrum (500.2 MHz, d_8-thf 298->220 K) of 3.7 expanded to show movement of Na-SH peak at 3.47 ppm (298 K) with decreasing temperature, thf solvent marked with orange star.

The IR spectrum of solid **3.7** also shows a characteristically weak S-H stretching band at 2579 cm^{-1} (cf literature range of 2540-2600 cm^{-1}) (Figure 3.17).[141]

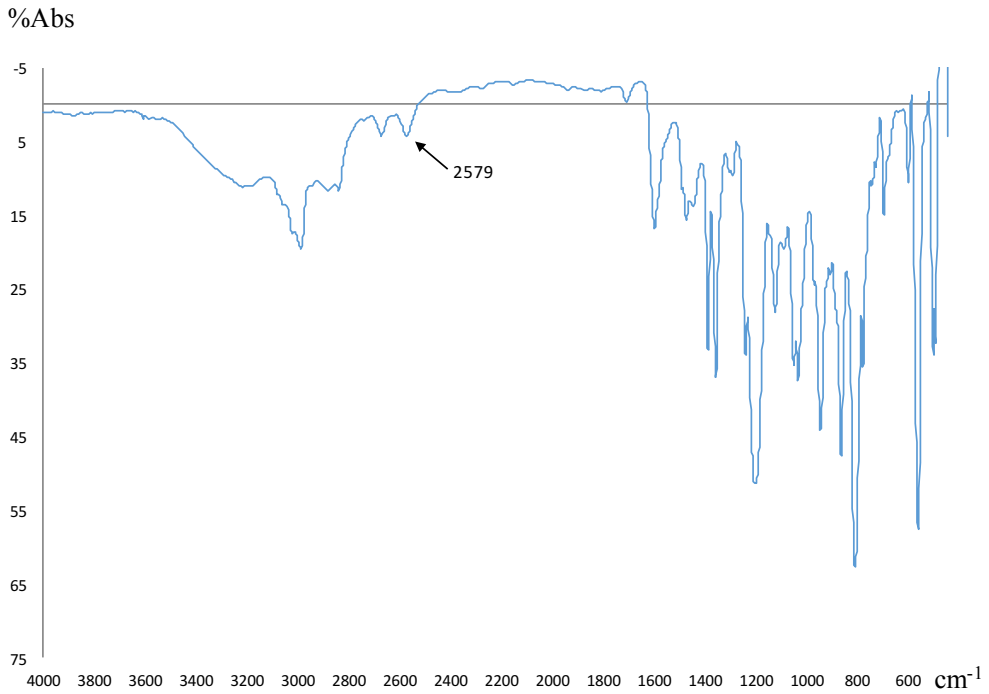

Figure 3.17: FTIR (NaCl windows) of 3.7 with Nujol spectrum subtracted, showing S-H stretch at 2579 cm^{-1} (N.B. the deformed baseline between 2750 cm^{-1} and 3250 cm^{-1} is due to strong Nujol C-H absorptions).

Chlorine elemental analysis was used to rule out any potential presence of Cl^-. Chloride is a potential contaminant in precursor **3.1** (synthesised from $[ClP(\mu\text{-}N^tBu)]_2$ and LiSH), and the X-ray structure could be refined equally well with Cl^- rather than SH^- at the specific site. Cl was found to be present only at a trace level (*ca.* 0.2 wt%) and the purity of the samples were further verified by C, H, N analysis. A clue to the origin of the SH^- anion in **3.7** is the deep blue colour that is observed immediately on reaction of **3.1** with BnNa. This colour is typical of sulfur radicals such as S^{2-} and S^{3-} and presumably arises from radical cleavage of the P–S bond of the precursor **3.1**.[142,143] Attempts to perform UV-Vis analysis of the initial stages of the reaction were hampered by the air-sensitive nature of the reagents and the products, as well as the incomplete dissolution of NaBn in thf.

Reactions of **3.1** with KBn were also performed initially in an *in situ* NMR study. A solution of **3.1** in thf was added dropwise to a solution of KBn and the reaction mixture turned rapidly from orange to clear. The ^{31}P NMR spectrum showed complete conversion to the potassium adduct of the dianion **3.5**

at a slightly different shift than the sodium derivative **3.7** (191.6 ppm and 190.0 ppm, respectively, in d_8-thf). Attempts to scale up the reaction were successful, however, the potassium salt K_2[**3.5**] (**3.8**) precipitates rapidly from solution (after *ca.* 5min with stirring) as a white powder and although it could be isolated in good yields and in apparently high purity after washing with thf and DCM, it is insoluble in most solvents except DMSO and sparingly in DMF and CH_3CN. No crystals of **3.8** suitable for X-ray diffraction could be obtained (despite numerous diffusion, layering and variable-temperature attempts). Satisfactory C, H, N analysis corresponding to K_2[**3.5**] and clean ^{31}P and ^{1}H NMR spectra were obtained after washing the product thoroughly with thf/DCM. The ^{31}P NMR signal shifts upfield in DMSO solvent (191.6 ppm to 188.0 ppm) accompanied by a sharpening of the signal, presumably due to increased donation of the solvent to the K^+ cations.

It has been shown that the dianion **3.5** is obtainable as the Mg^{2+}, Na^+ or K^+ complexes in good yields. Deprotonation reactions using main group metal bases, however, gave different results. Less basic aluminium organometallics such as $AlMe_3$ showed no reaction. In contrast, an *in situ* ^{31}P NMR study of the reaction of $ZnEt_2$ with **3.1** showed that reaction occurred, however, the product could not be identified in initial studies. The species was shown later (Chapter 3.4) to be {[S=PH(μ-N^{t}Bu)P]$_2$}$_2$(μ-S) (**3.9**, Figure 3.18) analogous to the oxo species {[O=PH(μ-N^{t}Bu)P]$_2$}$_2$(μ-O) (**1.23**) formed when the oxo-dimer [O=PH(μ-N^{t}Bu)]$_2$ is warmed to ambient temperature.[40] The formation of **3.9** appears to be encouraged by the presence of Lewis acidic metals and occurs *via* cleavage of one of the P-S bonds in **3.1** (and removal of S).

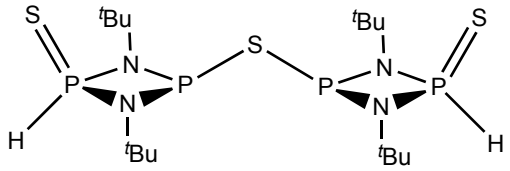

3.9

Figure 3.18: 3.9 as identified and characterised in Chapter 3.4.

3.3.3 Synthesis and Deprotonation of [(RNH)P(μ-N^{t}Bu)$_2$PSH]

The asymmetric sulfur dimer [S=(H)P(μ-^{t}Bu)$_2$PNH^{t}Bu] (**3.11**) was prepared starting from the mono-amino-chloro species [ClP(μ-N^{t}Bu)$_2$PNH^{t}Bu] (**3.10**), which can be made on a large scale,[21,144] using a similar synthetic strategy as previously used in the formation of **3.1**. A solution of LiSH was added dropwise to a stirred solution of **3.10** at -78 ºC. After stirring for 5 minutes the solvent was removed and the residue taken into *n*-hexane and filtered to remove LiCl (Scheme 3.6). Colourless crystals suitable for X-ray diffraction were grown from a saturated toluene solution at -12 ºC in *n*-hexane. ^{31}P-^{1}H coupled NMR spectrum of the product shows a doublet of doublets signal at δ = 50.7 ppm corresponding to the P^V-H centre ($^1J_{PH}$ = 532 Hz, $^2J_{P\text{-}P}$ = 4 Hz) as well as a broad singlet at δ = 128.7 corresponding to the P^{III}-NH^{t}Bu centre (Figure 3.19a). The ^{1}H NMR spectrum shows the accompanying P-H doublet of doublets at δ = 9.62 ppm as well as a broad signal for the N-H proton (δ = 2.5 ppm) (Figure 3.19b). The two ^{t}Bu resonances are distinguishable, with the ^{t}Bu group of the ^{t}BuNH due to coupling to the NH proton at δ = 0.99 ($^4J_{HH}$ = 1.7 Hz). The imido ^{t}Bu group appears at δ = 1.38 ppm as a singlet. The signals are directly comparable to the oxo-species [O=(H)P(μ-^{t}Bu)$_2$PNH^{t}Bu] with a downfield shift of Δδ ≈ 50 ppm and similar $^2J_{P\text{-}P}$ and $^1J_{P\text{-}H}$ coupling constants.

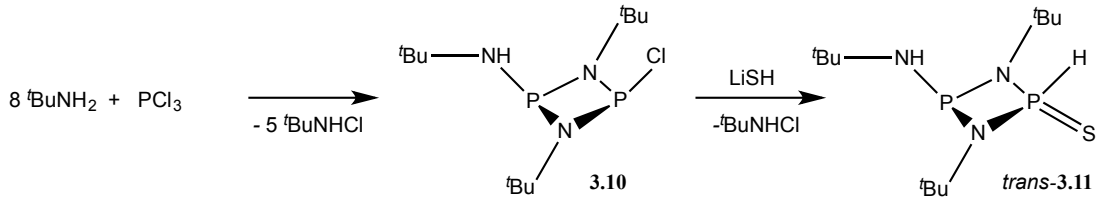

Scheme 3.6: Synthesis of 3.10 from ^{t}BuNH$_2$ and PCl$_3$ followed by reaction with LiSH to generate 3.11.

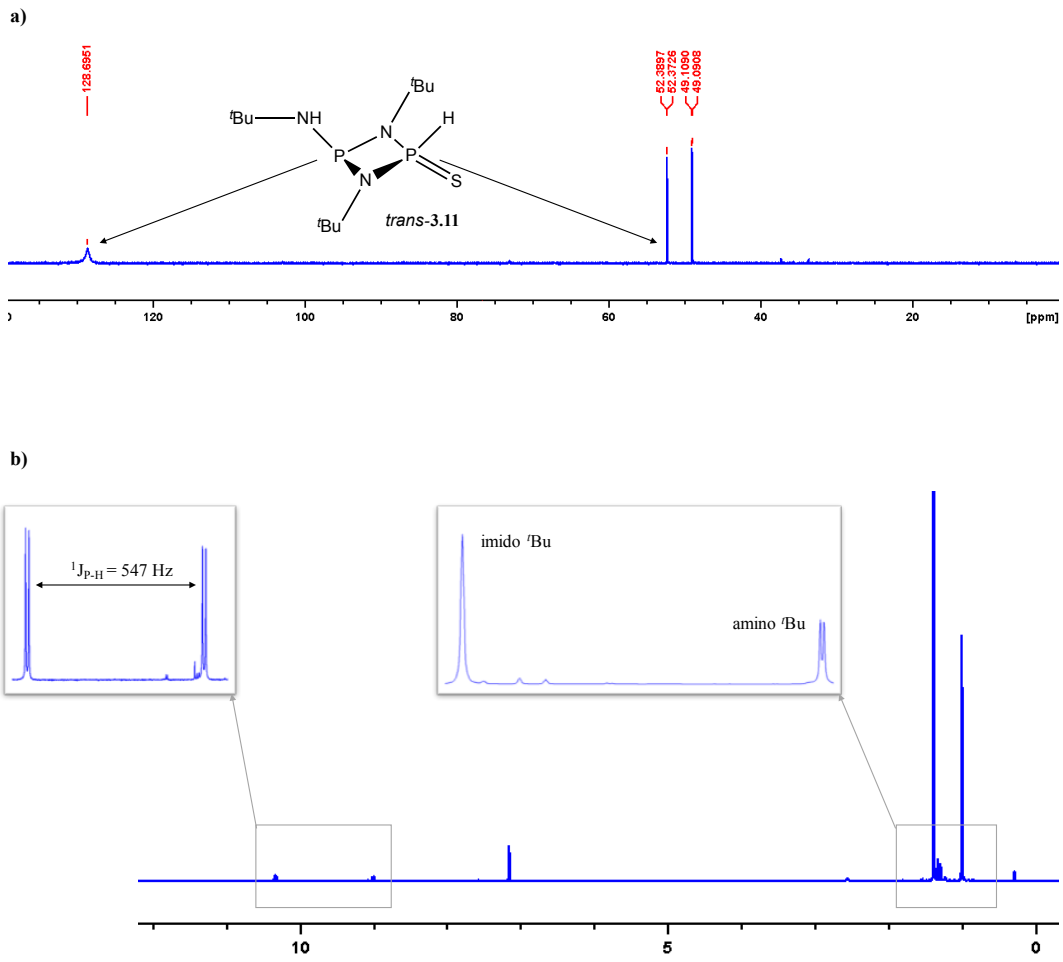

Figure 3.19: a) ^{31}P-^{1}H NMR spectrum (161.7 MHz, C_6D_6, 298 K) of 3.7, b) ^{1}H NMR spectrum (400 MHz, C_6D_6, 298 K) of 3.11.

In contrast to the oxygen analogue [(RNH)P(μ-N^{t}Bu)$_2$P(H)=O] (R = ^{t}Bu[40], Cy[145]) where the *cis* conformation is found to form exclusively, **3.11** was found to adopt the *trans* configuration in the solid state (Figure 3.20a). The *trans* conformation of **3.11** allows hydrogen bonding of the sulfur atom of one molecule to the acidic P-H, N-H protons of another in the solid state (Figure 3.20b). The *cis* conformation of the oxygen species, however, leads to only one intramolecular hydrogen bond between molecules, forming end-to-end chains.

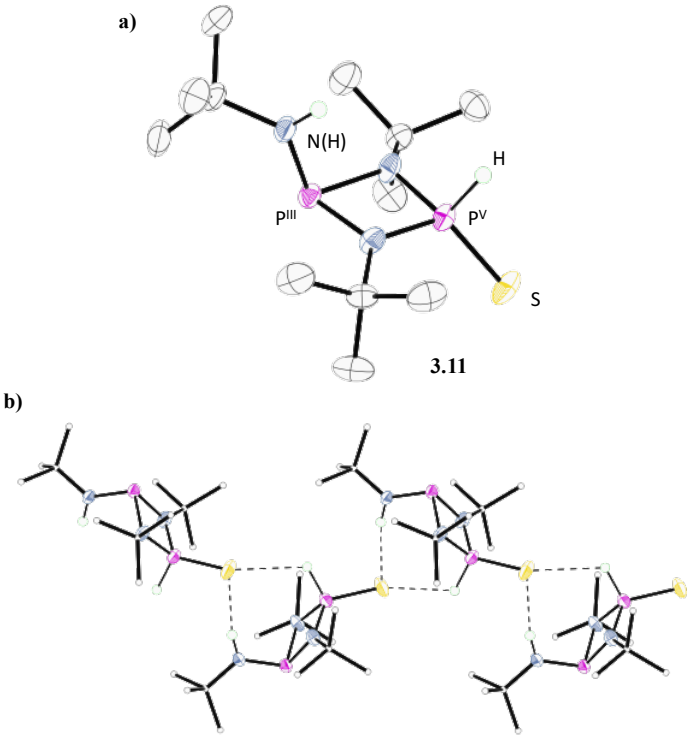

Figure 3.20: a) Solid-state structure of 3.11, Hydrogen atoms (except those attached to the ^{t}BuNH and P(H)=O groups) have been omitted for clarity, thermal ellipsoids set at the 50% probability level, (b) association of molecules of 3.11 *via* H-bonding in the crystal lattice. Selected bond lengths (Å) and angles (°): P-N(exo) 1.651(3), P-N(endo) average 1.756, P^V-S 1.9422(13), P^V-H 1.33(4), N-H 0.91(5), N(exo)-P^{III}-N(endo) 103.28(16), N(endo)-P^V-N(endo) 79.18(14), S-P^V-P^{III} 132.87(6).

In order to probe the acidity of this species, a range of bases were used to attempt the deprotonation of the NH and/or PH positions (blue and yellow respectively, Scheme 3.7). *In situ* ^{31}P NMR experiments of the reaction of **3.11** with Bu_2Mg, BnNa and *n*BuLi are shown in Figure 3.21a, Figure 3.21b and Figure 3.21c, respectively.

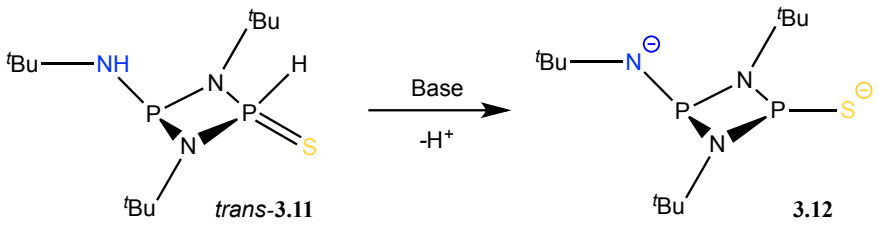

Scheme 3.7: Deprotonation of 3.11 at the N position (blue) and S (yellow) to generate the mono- or dianion 3.12.

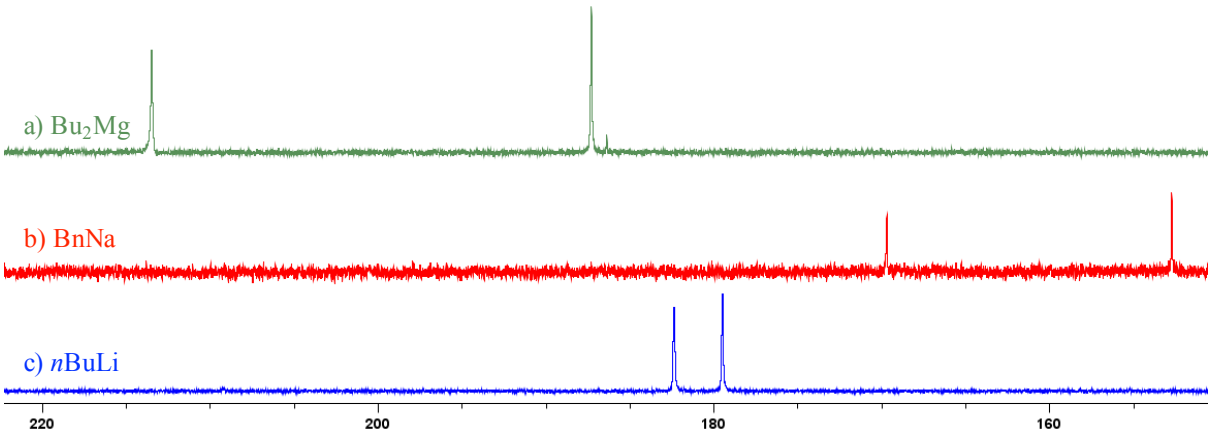

Figure 3.21: ^{31}P NMR spectra of the products of the deprotonation of 3.11 by a) Bu_2Mg (d_8-thf), b) 2BnNa (*n*-hexane, d_6-acetone capillary) and c) 2*n*BuLi (d_8-thf) to give the dianion 3.12.

The downfield shift of the products and the preserved asymmetry of the phosphazane ring suggests that all three bases give quantitative conversion to the dianionic species [S-P(μ-N^{t}Bu)$_2$PN^{t}Bu]$^{2-}$ (**3.12**). Most notably, the use of a nucleophilic lithium base *n*BuLi does not lead to decomposition as it did with the sulfur species **3.1**. In contrast, the oxo-species [O=P(H)(μ-N^{t}Bu)$_2$PNH^{t}Bu] (**1.25**) was only found to form the mono-anion [O-P(μ-N^{t}Bu)$_2$PNH^{t}Bu]$^-$ when reacted with excess *n*BuLi *via* deprotonation only at the phosphorus position. Attempts to generate the mono-anion of **3.11** by reactions with one equivalent of base (BnNa, *n*BuLi) gave mixtures of products containing the mono-anion [S-P(μ-N^{t}Bu)$_2$PHN^{t}Bu]$^-$ and starting material amongst other products.

The dianion **3.12** is particularly interesting as it provides a further location for the introduction of chiral centre (through the NR group) close to the potential coordination sphere of a metal centre. This gives the opportunity for matching/mismatching configurations.

3.3.4 Attempted Complexation of **3.5** with Transition and Main Group Metals

In order to extend the potential applications of the new dianion [S-P(μ-N^{t}Bu)]$_2^{2-}$ (**3.5**), I was interested in applying the s-block metal complexes **3.6** and **3.7** as transfer reagents. The potassium complex **3.8** was deemed unsuitable for use due to its poor solubility. *In situ* ^{31}P NMR studies of the reactions of **3.6** or **3.7** with Ph_2SnCl_2 (Scheme 3.8) showed complete conversion to the Sn^{IV} complex [Ph_2Sn(**3.5**)]

(**3.13**), indicated by the formation of a sharp singlet at δ = 206.7 ppm at ambient temperature (including $^{117/119}$Sn satellites) (Figure 3.22a).

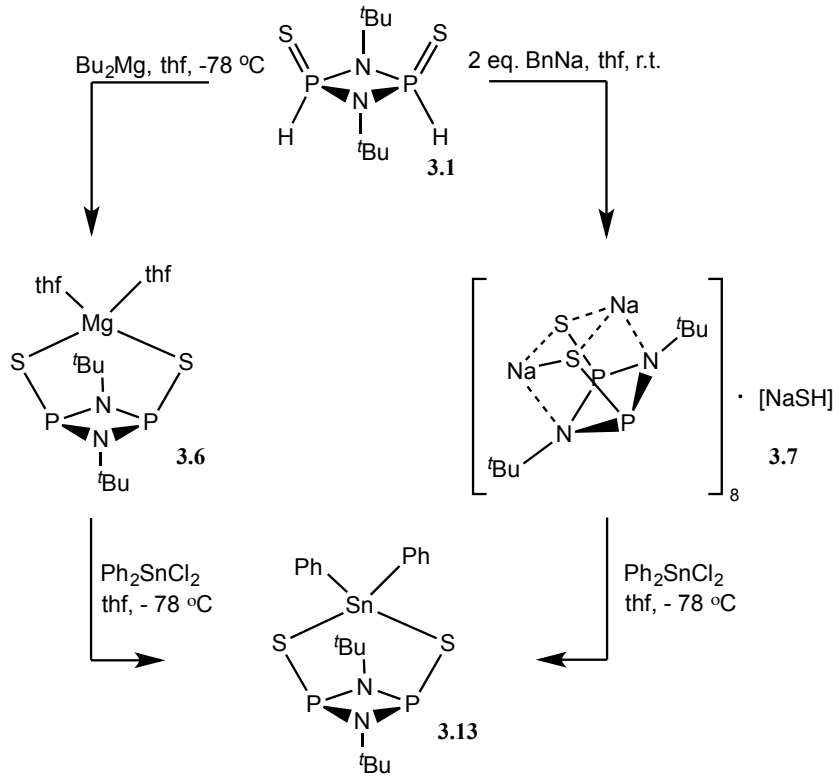

Scheme 3.8: Deprotonation of 3.1 with metal bases (producing the Mg and Na complexes 3.6 and 3.7) and transmetallation to give the Sn^{IV} complex 3.13.

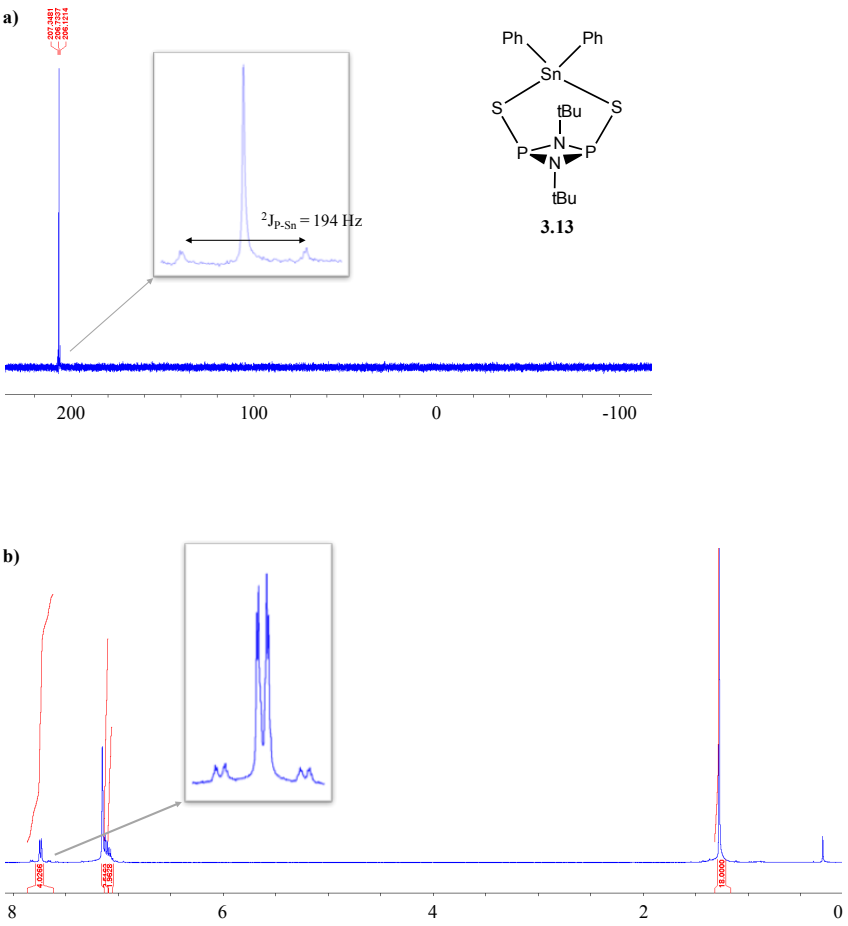

Figure 3.22: a) $^{31}P\{^1H\}$ (161.7 MHz, d_6-benzene, 298 K) NMR of 3.13 in showing $^2J_{P\text{-}Sn}$ coupling; b) ^1H (400 MHz, d_6-benzene, 298 K) NMR of 3.13 showing $^2J_{H\text{-}Sn}$ coupling.

[Ph_2Sn(**3.5**)] (**3.13**) was isolated as a powder in 88% yield after extraction with *n*-hexane and removal of the solvent. Crystals of **3.13** were grown from a concentrated *n*-hexane solution and the solid-state structure is shown in Figure 3.23. The overall features of the structure of **3.13** are similar to those of the Mg complex **3.6**. However, the coordinative saturation of the Sn^{IV} centre combined with the steric influence of the Sn-bonded Ph groups, preclude any significant N···Sn interactions. As a result, the P_2N_2 ring unit in **3.13** is almost planar. This is despite the fact that steric crowding of the Sn-bonded Ph and ^{t}Bu groups results in conformational readjustment elsewhere in the molecule, with the Sn^{IV} centre pivoting towards one side of the P_2N_2 ring of the dianion **3.5**.

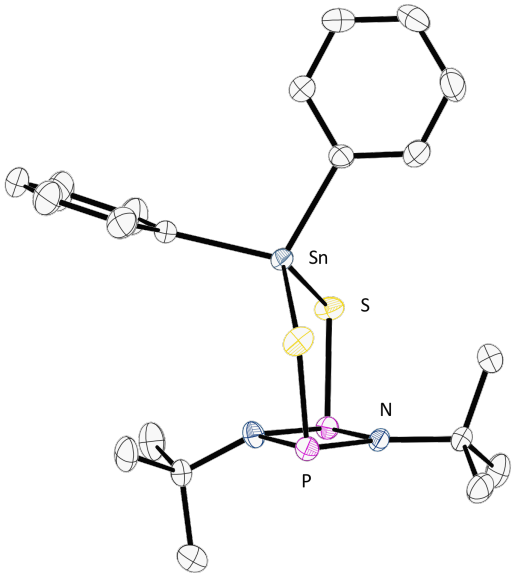

Figure 3.23: X-ray crystal structure of [Ph_2Sn(3.5)] (3.13), with Hydrogen atoms omitted and thermal ellipsoids set at the 30% probability level. Selected bond lengths (Å) and angles (°); Sn-S average: 2.4125(5), C-Sn average 2.135(2), P-N range 1.708(2)-1.726(2), P-S range 2.1601(7)-2.1646(8), N-P-N range 81.79(8)-82.00(8), P-N-P average angle 98.09(9).

Reaction of **3.6** or **3.7** with $GeCl_2Ph_2$ also gives the $GePh_2$-bridged species [Ph_2Ge(**3.5**)] (**3.14**) in a directly analogous reaction to that of $SnCl_2Ph_2$. The ^{31}P NMR spectrum at ambient temperature shows a singlet at δ = 215.4 ppm and the product can be isolated in good yields, however, no crystals suitable for X-ray diffraction could be obtained.

Interestingly, prolonged storage of a thf solution of **3.13** at ambient temperature results in the formation of the sulfur-bridged species $\{[S{=}PH(\mu\text{-}N^tBu)]_2\}_2(\mu\text{-}S)$ (**3.9**), the same species generated by attempted deprotonation of **3.1** with $ZnEt_2$. Compound **3.9** is also commonly observed in the reactions of the dianion **3.5** with a range of Lewis acidic metal ions. For example, *in situ* ^{31}P NMR studies of the reaction of **3.5** with $ZnCl_2$ shows quantitative conversion to a Zn complex of **3.5** (δ = 213 ppm) that decomposes to **3.9** in a matter of minutes at ambient temperature (Figure 3.24). This decomposition was observed for any complexation reaction involving transition or main group Lewis acidic metals (e.g. FeX_2 (X = Cl, Br, I), $CoCl_2$, CuCl, AgCl, DMSAuCl, $ZnCl_2$, $AlCl_3$) and is usually accompanied by the precipitation of elemental metal in the reaction vessel.

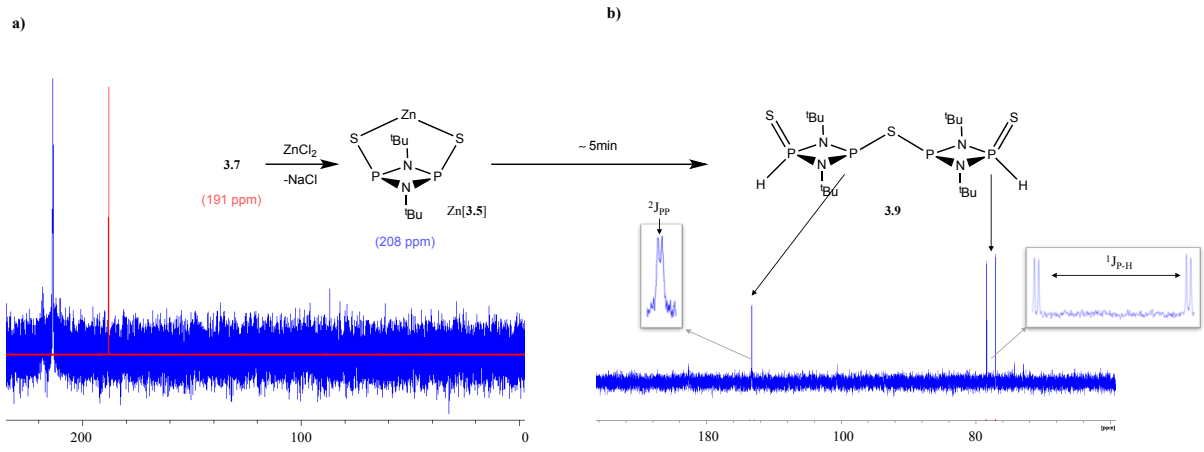

Figure 3.24: a) *In situ* ^{31}P NMR spectrum (161.7 MHz, d_6-acetone capillary, 298 K) of the reaction between 3.9 (red) and $ZnCl_2$, b) *In situ* ^{31}P NMR spectrum after 5min showing decomposition to 3.9.

Table 3.4 gives a comparison of the spectroscopic data for **3.9** with the oxygen analogue **1.23**. The downfield shift of $\Delta\delta \approx 40$ ppm is also comparable with the difference seen between the dimers **3.1** and **1.22**. For further comparison, the spectroscopic data for the oxo and sulfur species [O=(H)P(μ-^{t}Bu)$_2$PNH^{t}Bu] (**1.25**) and [S=(H)P(μ-^{t}Bu)$_2$PNH^{t}Bu] (**3.11**) are also shown.

Table 3.4: comparison of the ^{31}P NMR shifts of sulfur species 3.1, 3.9, 3.11 and their oxygen analogues.

Compound	P^V shift (ppm)	P^{III} shift (ppm)	$^1J_{P\text{-}H}$ (Hz)	$^2J_{P\text{-}P}$ (Hz)
1.22	-8.3	-	585.0	-
3.1	36.3	-	598.4	-
1.23	-3.2	98.7	590.0	14.7
3.9	44.4	133.23	547.6	15.0
1.25	-8.6	73.6	575.2	8.0
3.11	50.7	128.7	532.1	4.0

The assumed mechanism for the formation of **3.9** involves the elimination of a tin sulfide. Indeed, when Ph_3SnCl (2 equiv.) was reacted with the sodium salt **3.7** in an attempt to form the di-$SnPh_3$ adduct, the sulfur-bridged product Ph_3Sn-S-$SnPh_3$ was isolated in significant yields (>20%) and characterised by X-ray crystallography. Although there is a chance that some of the tin sulfide formed might be from reaction with residual NaSH that is generated in the formation of **3.7**, the relatively high yield obtained suggests otherwise.

3.4 Attempted Synthesis of Phosphorus(III) Macrocycles

All attempts to use the precursor **3.1** as a precursor to macrocycles (according to Scheme 3.9) were unsuccessful.

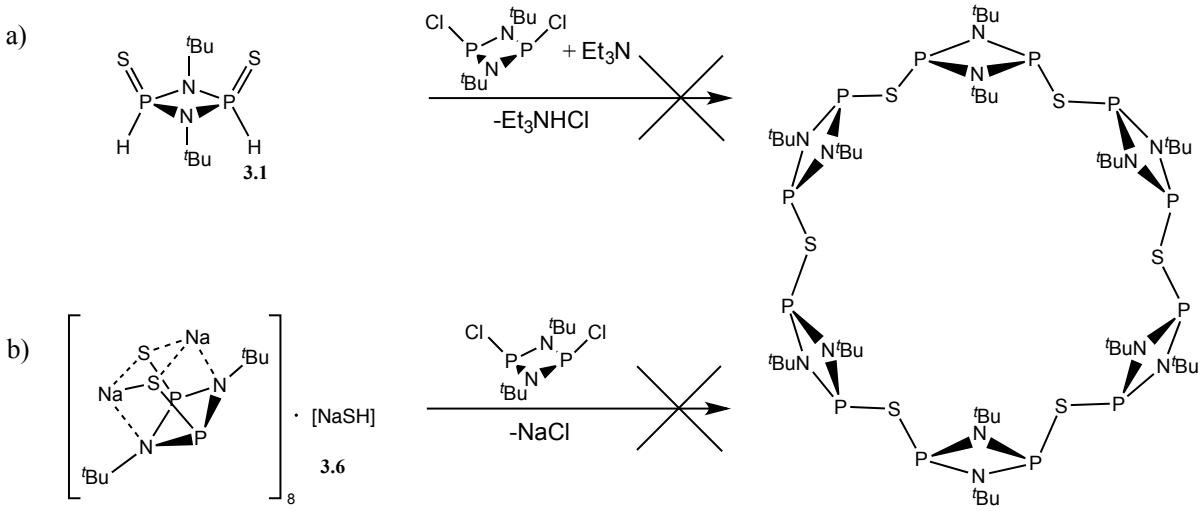

Scheme 3.9: Attempted macrocycle formation reactions using 3.1.

The first approach (Scheme 3.9a) was followed by *in situ* $^{31}P\{^{1}H\}$ NMR spectroscopy. A mixture of **3.1**, $[ClP(\mu\text{-}N^tBu)]_2$ (**2.1**) and excess Et_3N (as a Brønsted base) in d_8-toluene showed complete consumption of the starting material $[S{=}(H)P(\mu\text{-}N^tBu)]_2$ (**3.1**) (δ = 35 ppm) after 15min and the generation of a mixture of a range of products as shown by *in situ* ^{31}P NMR spectroscopy - multiple singlets between δ = 190-230 ppm.

The synthesis depicted in Scheme 3.9b was based on the successful synthesis of the oxygen bridged tetrameric macrocycle $[\{P(\mu\text{-}N^tBu)\}_2(\mu\text{-}O)]_4$ (**1.60**). The *in situ* generated species **3.6** was reacted with $[ClP(\mu\text{-}N^tBu)]_2$ (**2.1**) in an attempted cyclisation, with NaCl elimination. The *in situ* ^{31}P NMR spectrum shows numerous overlapping signals, which indicate the formation of oligomeric chains of various lengths. The dianion **3.5** seems to have a tendency to form these oligomeric adducts, as seen in the reactions with Lewis acidic metals to give **3.9**. Further attempts to crystallise products from the reaction mixtures were unsuccessful.

3.5 Conclusions

It has been shown that the sulfur dimer $[(S=)HP(\mu\text{-}N^tBu)]_2$ can be used as source of the dianion $[S\text{-}P(\mu\text{-}N^tBu)]_2^{2-}$, as exemplified by the quantitative formation of $[S\text{-}P(\mu\text{-}N^tBu)]_2^{2-}$ (**3.5**) with certain alkali metal bases. Attempts to extend the synthesis of the sulfur derivatives **3.1**-**3.4** to chiral variants $[(S)P(\mu\text{-}NR^*)]_2^{2-}$ were not succesful, possibly due to the lower steric bulk of the chiral derivatives used. Reactions of the protic sulfur species **3.1** (Scheme 3.8a) or the dianion **3.5** (Scheme 3.8b) with the electrophilic species $[ClP(\mu\text{-}N^tBu)]_2$ in reactions analogous to the nucleophilic pathways that gave NH or O bridged macrocycles respectively were unsuccessful leading to a mix of products in the ^{31}P NMR spectrum of the isolated species.

The dianion **3.5** presents an interesting hard/soft combination with respect to metal coordination, which can respond to the nature of the metal coordinated (involving S- and N- or solely S-bonding modes). In addition, the lower steric demands of ligands like **3.5** compared to valence-electronic amido counterparts such as the extensively studied dianion $[(^t BuN)P(\mu\text{-}N^tBu)]_2^{2-}$ (in which S is replaced by ^{t}BuN) can lead to the formation of larger cages (beyond the formation of dimeric metal complexes), as seen in the case of **3.7**. In related studies it was shown that it is possible to form a mono-amino sulfur dianion $[(^t BuN)P(\mu\text{-}N^tBu)P\text{-}S]^{2-}$ (**3.11**) which shows increased stability compared to dianion **3.5**. Finally, attempts to obtain macrocycles using **3.1** as the precursor gave only mixtures of various products.

The dianion **3.5** was found to be extremely air- and moisture-sensitive and in order to develop a more suitable ligand set, stabilisation of this dianion by using more sterically protecting R groups on the imido nitrogen or oxidation at the phosphorus atoms might be advantageous. Furthermore, oxidation would have the effect of reducing the tendency for reduction of metals hindered the formation of transition metal complexes.

4. Oxidative Stabilisation of Phosphazanes

4. Oxidative Stabilisation of Phosphazanes

4.1 Background

As previously mentioned in the introduction (Chapter 1), there exist numerous derivatives of P^{III} and P^{V} cyclophosphazanes. In general, the P^{V} congeners have increased stability and are much easier to handle due to their decreased moisture- and air-sensitivity. Studies have explored this increase in stability, notably in the case of moisture- and air-sensitive [(4-CN-PhO)P-(μ-N^{t}Bu)]$_2$ which upon oxidation by chalcogens O, S or Se to the P^{V} cyclophosphazanes gave the air-stable products [(4-CN-PhO)(E)P(μ-N^{t}Bu)]$_2$ [E = O, S, and Se] (Scheme 4.1).[49]

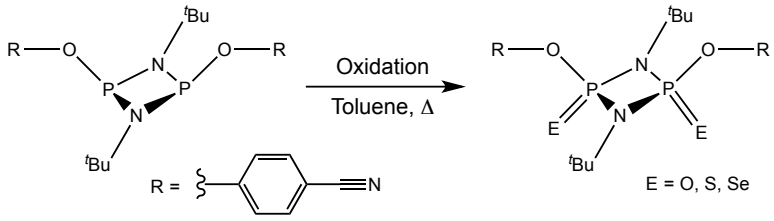

Scheme 4.1: Oxidation of air- and moisture-sensitive P^{III} species to stable P^{V} species.

Despite this increased stability, however, there are many more examples of phosph(III)azane complexes with metals from across the periodic table have been structurally characterised than phosph(V)azanes (CCDC search of metal/main group bridged phosphazanes: P^{III}: 53 complexes, P^{V}: 12 complexes[27]).

The interest in P^{V} species stems not only from the stabilisation, but also from the presence of lone pairs on the chalcogen substituent. Depending on the donor functionality prior to oxidation this can lead to elaborate ligand sets that contain numerous coordination sites and resulting coordination geometries, as explained in Chapter 1.3.2. Notably, chalcogens such as S, and Se provide soft donor substituents that can help stabilise complexes with softer metals.[122,146]

Extensive work by Swamy *et al.*,[56,145] Stahl *et al.*,[35] and Chivers *et al.*[63,147] has taken advantage of such oxidation to create geometries based on oxidised phosphazane units of the type [(G)(E=)P(μ-N^{t}Bu)]$_2$ (G = RNH, RO, RS. E = O, S, Se, Te). In the case of secondary amine substituents containing a

proton (NHR), there is also the possibility of deprotonating these species to generate dianions with delocalised charge (Scheme 4.2).[146–148] The same dianions can also be generated by deprotonation to generate the intermediate salts $[(RN)P^{III}(\mu\text{-}N^tBu)]_2^{2-}$ $2[M^+]$, followed by *in situ* oxidation with the chalcogens.

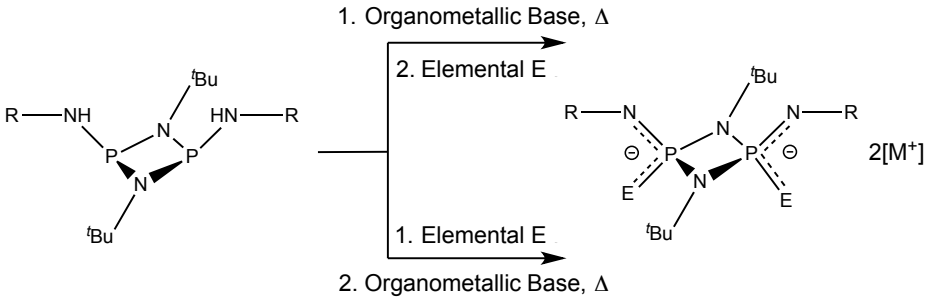

Scheme 4.2: Two different routes to the salts $[(RN)(E=)P(\mu\text{-}N^tBu)]_2^{2-}$ $2[M^+]$ (M = e.g., alkali metal).

As described previously (Chapter 1.4.3), the oxidation of chloro-dimers $[ClP(\mu\text{-}N^tBu)]_2$ with S or Se occurs readily to give $[Cl(E=)P(\mu\text{-}N^tBu)]_2$ (E= S, Se), from which Wurtz coupling reactions with sodium can be used to obtain the give hexameric macrocycles **1.62S/Se** (containing with S and Se linkages, Scheme 1.19).[129,130] Similarly, reduction of the S- and Se-dianions $[^tBuN(E=)P(\mu\text{-}N^tBu)]_2^{2-}$ with I_2 has been shown to generate E-E bonded cyclic trimers (**1.45**, Chapter 1.2.3).[149]

4.2 Oxidation of Dianionic Sulfur Dimers

In this section reactions of the sulfur dianions $[(S\text{-})P(\mu\text{-}NR)]_2^{2-}$ presented in Chapter 3.3 with chalcogens are explored. Oxidation was found to proceed readily at ambient temperature and gave increased stability to the resulting P^V dianion.

4.2.1 Oxidation of $[S\text{-}P(\mu\text{-}N^tBu)]_2^{2-}$ (**3.5**)

The oxidation studies presented in this chapter were carried out in collaboration with Alex Plajer (MSci, Cambridge), and are partially published elsewhere.[150]mu

Based on previously published synthetic procedures for the oxidation of dianions $[(RNH)P(\mu\text{-}N^tBu)]_2^{2-}$ to $[RN(E=)P(\mu\text{-}N^tBu)]_2^{2-}$, the dianion $[S\text{-}P(\mu\text{-}N^tBu)]_2^{2-}$ (**3.5**) was successfully oxidized by the addition of two equivalents of S, Se or Te to a solution of the sodium salt **3.7** (Scheme 4.3). The

dianions [S-P(E)(μ-N^{t}Bu)]$_2^{2-}$ (E = S **4.1**, Se **4.2**, Te **4.3**) were isolated as their sodium salts Na$_2$[S-(E=)P(μ-N^{t}Bu)]$_2$ **4.1·Na$_2$**, **4.2·Na$_2$** and **4.3·Na$_2$.** In contrast, the neutral precursor [(S=)(H)P(μ-NR)]$_2$ (**3.1**) was found to decompose upon reaction with the elemental chalcogens, to give a mix of products (as observed by *in situ* ^{31}P NMR spectroscopic studies).

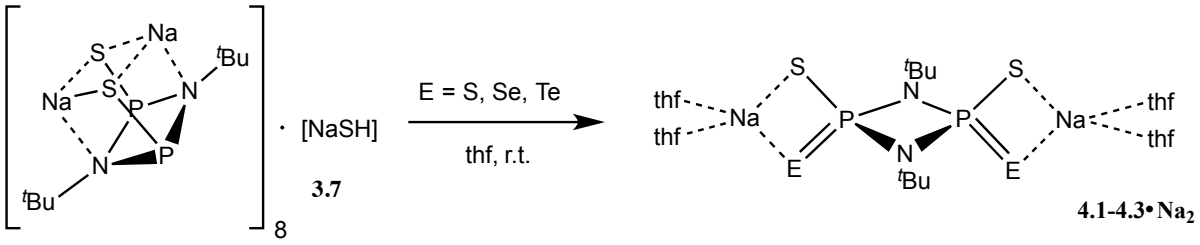

Scheme 4.3: Oxidation of 3.5 by elemental chalcogens, to generate the sodium complexes of the P^V dianions [S-(E=)P(μ-N^{t}Bu)]$_2^{2-}$ (4.1-4.3).

In all cases, the generation of the dianions **4.1-4.3** causes a significant shift of the resonance for **3.7** in the ^{31}P NMR spectrum. The formation of [S(S-)P(μ-N^{t}Bu)]$_2^{2-}$ (**4.1**) is accompanied by a significant upfield shift of a broad signal at δ = 190 ppm in the dianion **3.7** to a sharp singlet at δ = 87 ppm in **4.1** in the ambient temperature ^{31}P{^{1}H} NMR spectrum (Figure 4.1a). This change (Δδ = 107 ppm) is indicative of the change in oxidation state of the phosphorus from P^{III} to P^V.[49,151]

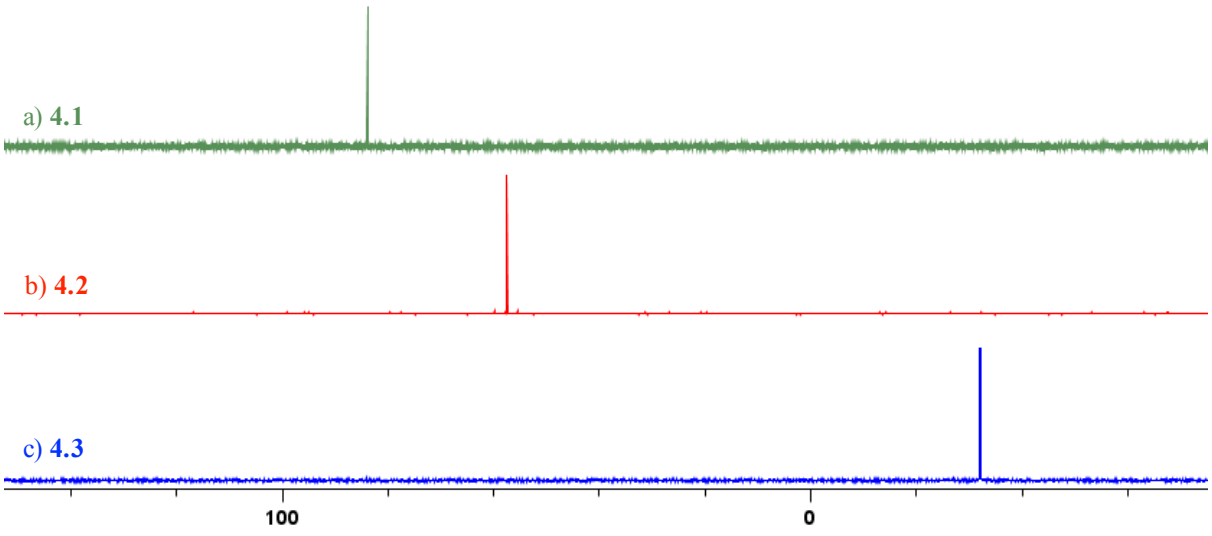

Figure 4.1: Comparison of the ^{31}P NMR (161.7 MHz, d$_8$-thf, 298 K) spectrum of a) 4.1·Na$_2$, b) 4.2·Na$_2$ and c) 4.3·Na$_2$.

In a similar manner, the oxidation of **3.7** by excess selenium (10 equiv.) occurs readily at ambient temperature and within 5 minutes in thf. A similar change in the shape of the ^{31}P NMR signal and upfield shift is seen for [S(Se-)P(μ-N^{t}Bu)]$_2^{2-}$ (**4.2**), with the appearance of a sharp signal at δ = 57.5 ppm which is accompanied by two ^{77}Se satellites ($^1J_{P\text{-}Se}$ = 703 Hz) (Figure 4.1b). This is due to the presence of an isotopomer [S(^{77}Se-)P(μ-N^{t}Bu)$_2$P(-^{80}Se)S]$^{2-}$ (also present in Cl(S=)P(μ-N^{t}Bu)]$_2$ (**1.61S**)[129]) which leads to inequivalence of both phosphorus centres, causing a $^2J_{P\text{-}P}$ coupling of 10.1 Hz. The corresponding $^1J_{PSe}$ coupling is also observed in the ^{77}Se spectrum of **4.2**, as a doublet at δ = 295.9 ppm ($^1J_{P\text{-}Se}$ = 695.5 Hz) (Figure 4.2).

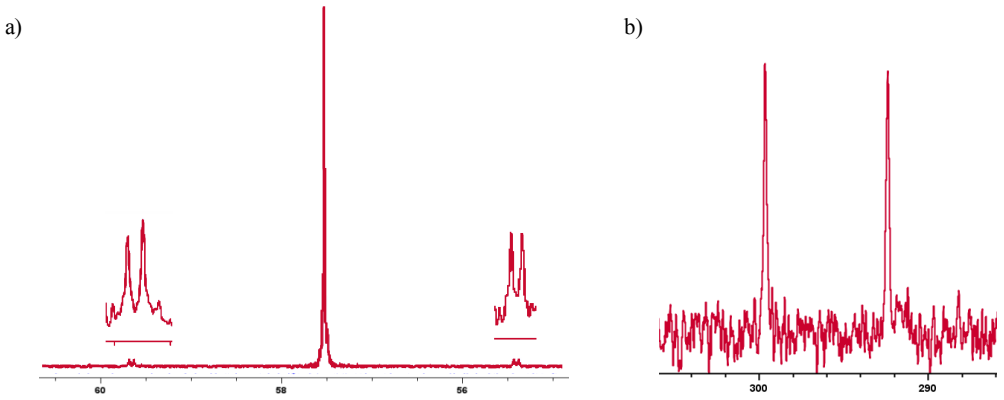

Figure 4.2: a) Expansion of the ^{31}P NMR (161.7 MHz, d$_8$-thf, 298 K) of 4.2·Na$_2$ showing ^{77}Se satellites; b) Expansion of the ^{77}Se NMR (95.4 MHz, d$_8$-thf, 298 K) of 4.2·Na$_2$.

The oxidation reactions of **3.7** with S and Se are scalable up to gram quantities giving almost quantitative yields of **4.1·Na$_2$** and **4.2·Na$_2$**. Oxidation of **3.7** with elemental Te (10 equiv.) at ambient temperature gives the telluride salt Na$_2$[S(Te-)P(μ-N^{t}Bu)]$_2$ (**4.3·Na$_2$**) as indicated by an increased upfield shift of the signal in the ^{31}P NMR spectrum to δ = -32.2 ppm with accompanying ^{125}Te satellites (Figure 4.2c). The formation of the asymmetric isotopomer [S(^{125}Te-)P(μ-N^{t}Bu)$_2$P(-^{130}Te)-S]$^{2-}$ is again seen for this species, giving a $^2J_{P\text{-}P}$ coupling constant of 18.8 Hz. The negative value of the shift is expected based on a similar Te dianion for [^{t}BuN(Te-)P(μ-N^{t}Bu)]$_2^{2-}$ reported by Woollins *et al.* which appears at δ = −74.9 ppm in the ^{31}P NMR spectrum (d$_8$-toluene).[137,148] The ^{125}Te NMR spectrum shows a doublet at δ = 420.1 ppm with a corresponding $^1J_{Te\text{-}P}$ coupling constant of 1644.2 Hz. Furthermore, analysis of the ^{125}Te and ^{77}Se NMR shifts shows that the shift for **4.3** is exactly 1.6

times that of **4.2** (420/260 = 1.6), which is a well-known correlation between ^{77}Se and ^{125}Te NMR signals ($\delta(^{125}Te) = 1.6 \times \delta(^{77}Se)$) found for isostructural species.[152]

4.3 was found to be extremely unstable with respect to decomposition to elemental tellurium. This decomposition happens even with rigorous exclusion of light, air and moisture, within a few days. This behaviour, as well as the lower yield compared to the S- and Se- counterparts, has frequently been reported for P^V=Te bonded species and results from the lability of the P=Te bond.[65,153]

Although crystals of **4.1** and **4.2** could be grown from thf solutions none were suitable for X-ray analysis.

In stark contrast to the starting material **3.7**, which is only stable for a few days, both **4.1**·**Na$_2$** and **4.2**·**Na$_2$** were found to be stable at ambient temperature under inert atmosphere for several months. This makes them excellent candidates for the transfer of their [S-P(E)(μ-N^{t}Bu)]$_2^{2-}$ dianions to other metals/main group elements or for the formation of macrocyclic species.

4.2.2 Metal Complexes of [S-P(E)(μ-N^{t}Bu)]$_2^{2-}$ (E = S **4.1**, Se **4.2**)

A range of ligand-transfer reactions was attempted with variety of transition metals and main group elements. In background studies, voltammetry was also carried out in order to compare redox behaviour of the dianions **3.5**, **4.1** and **4.2**.

The dianions **4.1** and **4.2** have slightly different coordination geometries. **4.1** is fully symmetrical, with both faces of the phosphazane ring allowing for S,S-bridging or S′S′-bridging (Figure 4.3a). On the other hand **4.2** bind either *via* the Se,Se-face or the S,S-face of the ring (Figure 4.3b). In both cases, bonding in a side-on fashion, orthogonal to the P_2N_2 ring *via* the S,S' or S,Se face in **4.1** and **4.2**, is also possible.

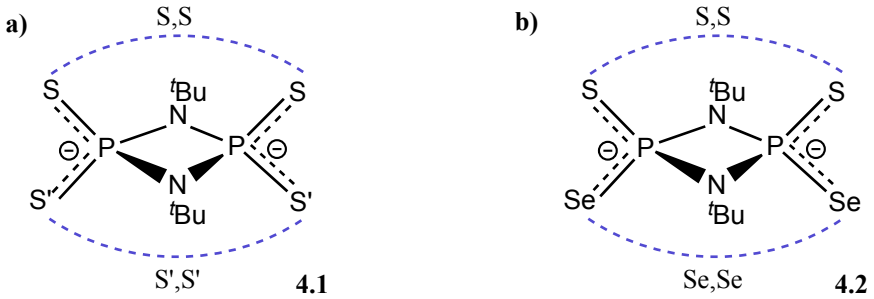

Figure 4.3: Possible coordination modes of the P^V dianions, a) S,S face or S',S'-face in 4.1, b) S,S-face or Se,Se face in 4.2.

4.1 and **4.2** reacted with Ph_2SnCl_2 in a similar manner to the P^{III} species **3.5**. The sodium salts were transmetallated with one equivalent of Ph_2SnCl_2 in thf at ambient temperature (Scheme 4.4) and followed by *in situ* ^{31}P NMR spectroscopy, which showed quantitative conversion to a single product in both cases. After scale-up, the products could be isolated in good yields and crystals suitable for X-ray diffraction were grown from *n*-hexane solution.

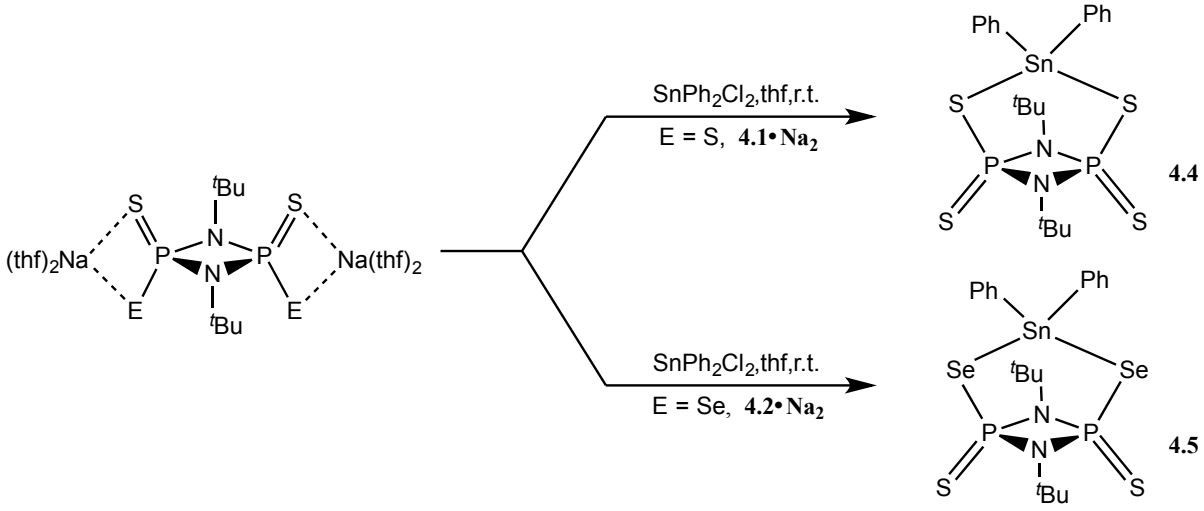

Scheme 4.4: Reaction of $4.1 \cdot Na_2$ and $4.2 \cdot Na_2$ with $SnPh_2Cl_2$ to generate the Sn bridged species 4.4 and 4.5.

The generation of the Sn complex [Ph_2Sn(**4.1**)] (**4.4**) is indicated in the room-temperature ^{31}P NMR spectrum in thf by a singlet at δ = 58.1 ppm which is consistent with a P^V species. The ^{31}P NMR spectrum of [Ph_2Sn(**4.2**)] (**4.5**) in thf shows a singlet with accompanying ^{77}Se and $^{117/119}Sn$ satellites at δ = 34.9 ppm. The corresponding ^{119}Sn spectrum shows a triplet resonance with a coupling constant consistent with $^2J_{Sn\text{-}P}$ coupling ($^2J_{Sn\text{-}P}$ = 69 Hz). The spectral data does not, however, allow the

identification of the bridging mode of the $SnPh_2$ group in the complex, as the spectra for both binding modes (S,S, or Se,Se) would be similar.[146] The only data that provides an indication of the mode is the ^{77}Se NMR spectrum, which shows a doublet at δ = 171.4 ppm ($^1J_{P\text{-}Se}$ = 465 Hz) and which is more consistent with a P-Se bonded species present in a Se,Se-bridging mode rather than a P=Se species in a S,S-bridging mode (which would most likely appear between 300-500 ppm and have a P-Se coupling constant $^1J_{P\text{-}Se} > 600$ Hz).[147,154]

The solid-state structures of both complexes were obtained and are shown in Figure 4.4. As suspected, **4.5** is a mononuclear complex in which the metal bridges the phosphazane *via* the Se,Se-mode. This result is somewhat surprising, as it involves the formation of less thermodynamically favoured Se-Sn bonds. However, this mode also involves the formal formation of strong P=S bonds, which may counteract the effect of the lower Se-Sn bond energy.

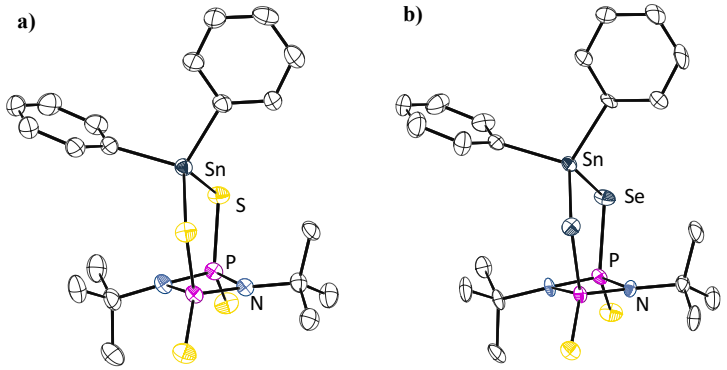

4.4 **4.5**

Figure 4.4: Solid-state structures of a) 4.4 and b) 4.5, showing one of two independent molecules in the respective unit cells. Hydrogen atoms omitted for clarity and thermal ellipsoids set at the 50% probability level. Selected bond lengths (Å) and angles (°): 4.4: Sn-S 2.4468(11), P-S(endo) 1.9132(15), P-S(exo) 2.0861(14), P-N 1.689(3), S-Sn-S 111.61(4), P-S(endo)-Sn 100.36(5), S(endo)-P-S(exo) 109.35(7), P-N-P 94.94(17) 4.5: Sn-Se 2.5570 (7), Se-P 2.2229(15), P-N 1.681(4), P-S 1.9174(19), Se-Sn-Se 112.88(2), P-Se-Sn 98.92(4), S-P-Se 108.37(8), N-P-Se 109.49(15).

4.4 shows the expected S,S-bridging mode, with the Sn located over the face of the phosphazane ring causing the *exo* sulfurs to splay out, with the S···S distances on each side of the ring increasing from 4.89 Å (bridged) to 5.34 Å (non-bridged). The distortions seen in the Sn complex of the P^{III} derivative [Ph_2Sn(**3.5**)] (**3.13**) are once again present in both of these complexes, with one ^{t}Bu group being pushed away from the plane of the P_2N_2 ring in order to accommodate the steric bulk of the Ph groups on the bridgehead. The only other main structural difference between [Ph_2Sn(**3.5**)] (**3.13**) and

[Ph_2Sn(**4.1**)] (**4.4**) is the shortening of the P-S σ bonds of the bridgehead, from 2.1601(7) Å in the P^{III} complex to 2.0861(14) Å in the P^{V}.

Reaction of **4.1·Na$_2$** with two equivalents of Ph_3PAuCl led to the formation of a single product, [Ph_3PAuS-(S=)P(μ-N^{t}Bu)]$_2$ (**4.6**) which was characterised by ^{31}P, ^{1}H NMR spectroscopy and X-ray crystallography. The ^{31}P NMR spectrum at ambient temperature shows a singlet at δ = 78.7 ppm, corresponding to the P^{V} centres of the phosphazane ring, and a signal at δ = 31.1 ppm for the coordinated Ph_3P ligand. The structure of the product was shown to be the di-gold complex by X-ray crystallography. The solid-state structure (Figure 4.5) shows that the $AuPPh_3$ units are coordinated *trans* to each other on opposite sides of the P_2N_2 ring and are bonded to sulfur atoms. The ^{31}P NMR signals for this species are broadened significantly, presumably due to *exo/endo* rotation about the P-S σ bonds (Scheme 4.5).[19,137]

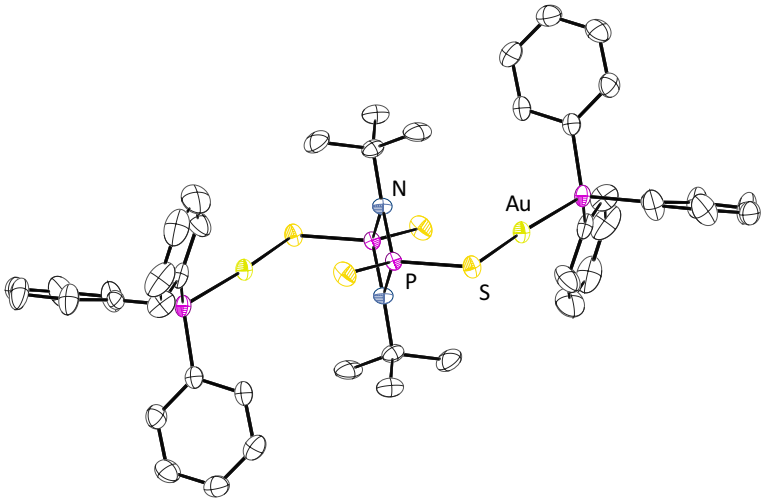

Figure 4.5: Solid-state structure of 4.6. Hydrogen atoms omitted for clarity, thermal ellipsoids set at the 50% probability level. Selected bond lengths (Å) and angles (°): Au-P 2.2639(11), Au-S 2.3164(10), P-S 1.9431(14), P-S(Au) 2.0356(14), P-N 1.688(3), P-Au-S 168.79(4), S-P-S 110.52(6), P-S-Au 104.47, P-N-P 96.02(17).

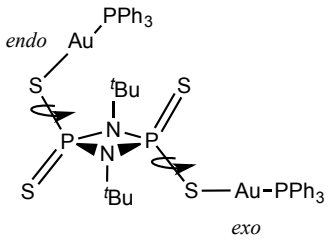

Scheme 4.5: *exo*/*endo* rotation of the AuPPh$_3$ groups in 4.6.

4.6 decomposes when exposed to light for extended periods of time, with precipitation of colloidal gold. The same decomposition process occurs even more rapidly for the Au complex of the Se oxidised dianion $[S\text{-}(Se{=})P(\mu\text{-}N^tBu)]_2^{2-}$ (**4.2**).

The reaction of **4.2·Na2** with $dppeNiCl_2$ in thf gave a red solid that precipitates after 10 minutes of stirring. The ^{31}P NMR spectrum of the product [dppeNi(**4.2**)] (**4.7**) contains a second order AA'XX' signal at 31.1 ppm in that was fully modelled using the program WinDNMR.[155] The deep red colour of the product in solution indicates the presence of square planar Ni^{II}.[156] The ^1H NMR spectrum shows no paramagnetic shifting of the signals, which again suggests a diamagnetic low-spin d_8-configuration of the nickel centre. The $^{31}P\{^1H\}$ NMR spectrum at ambient temperature showed signs of the desymmetrisation of the P_2N_2 phosphorus centres, characterised by a multiplet at δ = 39.7 ppm and a doublet at δ = 65.2 ppm as well as a second-order multiplet at δ = 66.1 ppm for the dppe ligand. The solid-state structure confirmed this desymmetrisation, which is the result of side-on coordination by the ligand to the Ni^{II} centre (Figure 4.6).

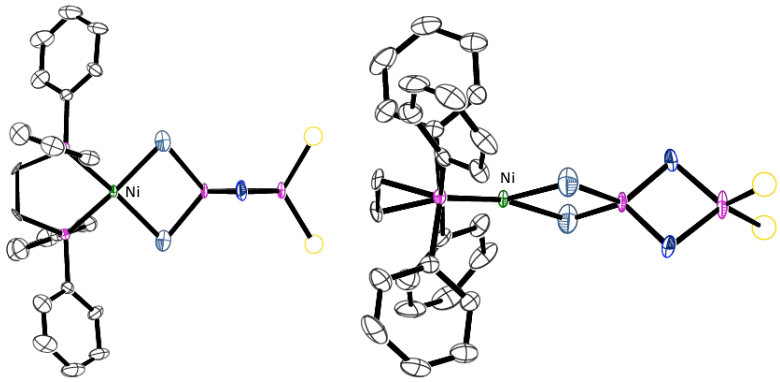

Figure 4.6: Solid-state structure of 4.7. DCM molecules and disordered ^{t}Bu groups have been omitted for clarity. Full interpretation of the data is not possible due to poor quality of the data set. Disorder between the Se and S positions could not be resolved.

In order to probe why the dianions **4.1** and **4.2** are capable of forming stable complexes with main group elements and transition metals whereas the P^{III} counterpart **3.5** decomposed, cyclic voltammetry (CV) studies were undertaken. The CV oxidation and reduction curves of the three anions are shown in Figure 4.7.

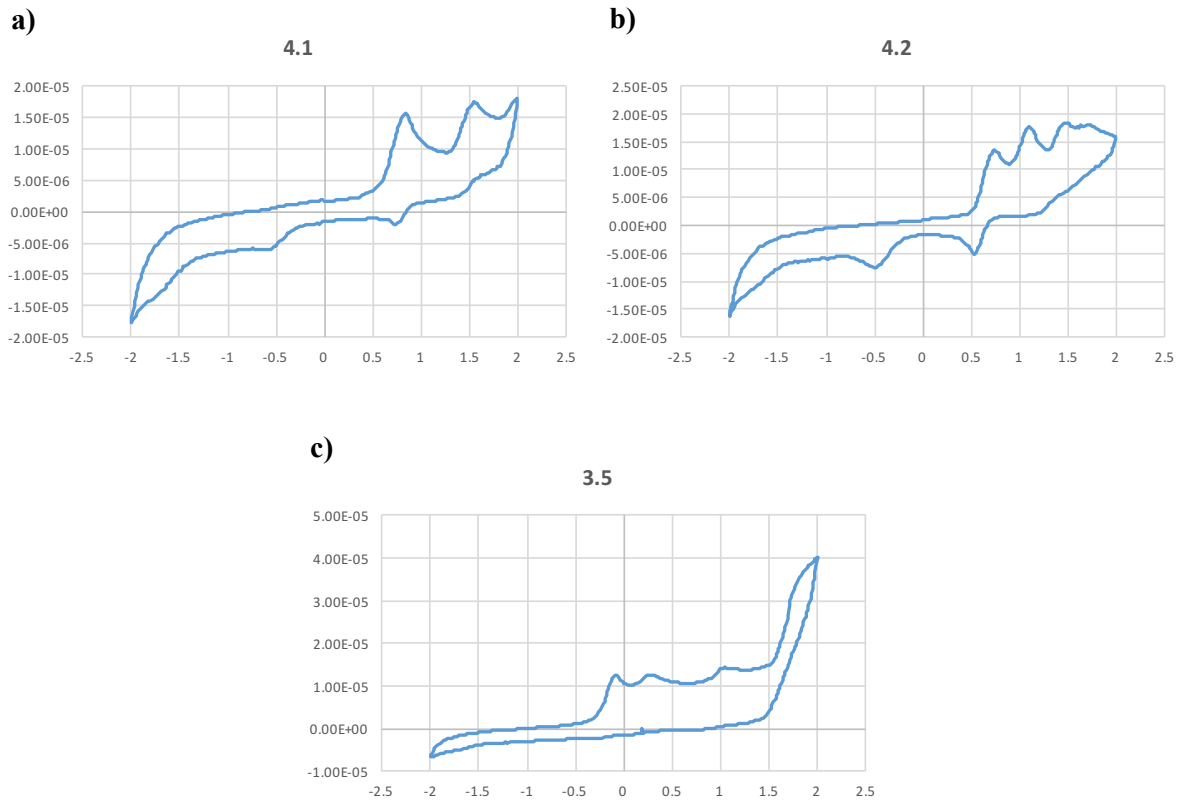

Figure 4.7: Cyclic voltammetry curves (1mM in 0.1M Bu_4NBF_4 in thf rel. $Fe(Cp)_2$) of the sodium salts of, a) 4.1, b) 4.2, and c) 3.5 showing decreased reduction potential of 3.5.

It is clear that the reduction potential for the P^{III} species **3.5** is far lower than the P^{V} species **4.1** and **4.2** (*ca*. 1 mV lower). It is also interesting to note the two separate oxidation pathways for the Se-anion **4.2** compared to the presence of only one pathway for the S-anion **4.1**. These measurements support the experimental observations from coordination studies that the P^{III} dianion **3.5** is much more reducing than the P^{V} counterparts.

4.3 Formation of Novel S and Se Bonded Macrocycles

In light of the increased stability observed for the dianions **4.1** and **4.2** compared to P^{III} counterparts, interest turned to the attempted synthesis of macrocycles in an analogous manner to the formation of the oxygen bridged tetramer **1.59** (Chapter 1.4.3). It can be noted that the attempted formation of macrocycles using P^{III} dianion (**3.5**) did not result in the selective formation of any macrocyclic species, as revealed by studies presented at the end of the previous chapter.

The sodium salts of the dianions $[S\text{-}P(E)(\mu\text{-}N^tBu)]_2^{2-}$ (E = S **4.1**, Se **4.2**) were reacted with $[ClP(\mu\text{-}NR)]_2$, with elimination of NaCl (Scheme 4.6).

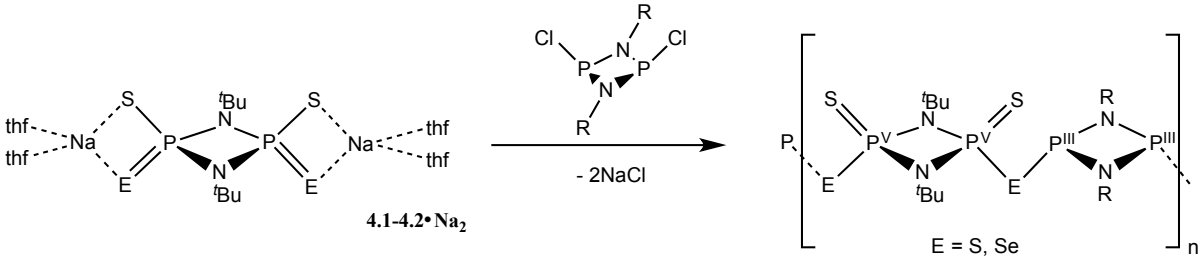

Scheme 4.6: Reaction of 4.1 and 4.2 with chlorophosphazanes to give macrocyclic systems containing alternating P^{III} and P^V rings bridged by either S or E.

An *in situ* ^{31}P NMR study of the reaction of the sodium salt **4.1·Na₂** with **2.1** in d_8-toluene shows quantitative conversion of the dianion (δ = 34.4 ppm) to a species **4.8** containing P^{III} and P^V centres at ambient temperature, and in a matter of minutes. The phosphorus centres in the species are magnetically inequivalent leading to two doublets of doublets at δ_{PIII} = 225.2 ppm and δ_{PV} = 56.1 ppm, with $^2J_{P\text{-}P}$ coupling constants of 16.7 and 27.2 Hz, respectively. The measured $^2J_{P\text{-}P}$ coupling constants are smaller than those previously reported for phosph(III/V)azanes, which are typically in the range of 40-50 Hz.

Crystals of **4.8** suitable for X-ray diffraction were grown from *n*-hexane. The solid-state structure of **4.8** showed an alternating P^{III}-P^V motif for the backbone and that a hexameric macrocycle has been formed, consisting of six P_2N_2 ring units linked by bridging S atoms $[\{P^{III}(\mu\text{-}N^tBu)_2\}(\mu\text{-}S)\{(S=)P^V(\mu\text{-}N^tBu)\}_2]_3$ (Figure 4.8).

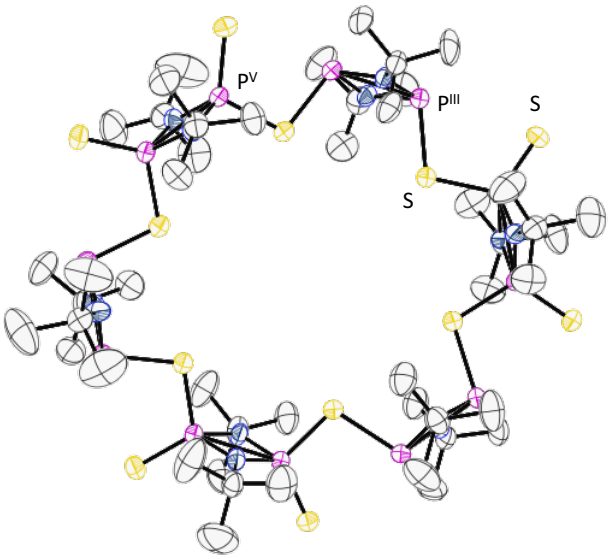

Figure 4.8: Solid state structure of 4.8. Hydrogen atoms omitted for clarity, thermal ellipsoids set at the 50% probability level. Selected bond lengths (Å) and angles (°): S(endo)-P^V 2.0823(17), S(endo)- P^{III} 2.2279(18), P^V-S(exo) 1.9224(19), P^{III}-N 1.706(4), P^V-N 1.689(4), P^V-S(endo)-P^{III} 105.08(7), S(exo)-P^V-S(endo) 113.93(8), N-P^{III}-S(endo) 102.48(16).

The structure of **4.8** differs from that of the sulfur-bridged macrocycle $[(\mu\text{-S})P(\mu\text{-N}^t\text{Bu})_2P(=S)]_6$ (**1.62S**) recently reported by Singh *et al.*[130] in that it is almost planar, with all eighteen atoms of the backbone deviating only 0.26 Å on average from the mean plane of the hexamer. Furthermore, the cavity of the macrocycle (measured between opposite S atoms) is 8.3 Å across, and 6.5 Å deep (^{t}Bu to ^{t}Bu), making it slightly larger than **1.62S**.

Reaction of **4.1·Na$_2$** with chloro-phosphazanes $[ClP(\mu\text{-NR})]_2$ containing other R groups, to produce heteroleptic macrocycles of the type $[\{P^{III}(\mu\text{-NR})_2\}(\mu\text{-S})\{(S=)P^V(\mu\text{-N}^t\text{Bu})\}_2]_3$, was also successful (Scheme 4.7). The reactions of **4.1** with less sterically bulky $[ClP(\mu\text{-NCH}_2{}^t\text{Bu})]_2$ (**2.3**) and the chiral $[ClP(\mu\text{-N(}\mathbf{I5}\text{)})]_2$ (**2.5**) gave the heteroleptic macrocycles **4.9** and **4.10,** respectively. Both show two doublets of doublets in their ^{31}P NMR spectra (P^V 61.7; P^{III} 249.7 ppm in toluene) with similar chemical shifts and coupling constants. A comparison of the ^{31}P/^{1}H NMR data for **4.8**, **4.9** and **4.10** can be found in Table 4.1. The similarity of these data suggests that the structure of the macrocycles is the same; a hexamer formed of alternating P^{III} and P^V phosphazanes bridged by S.

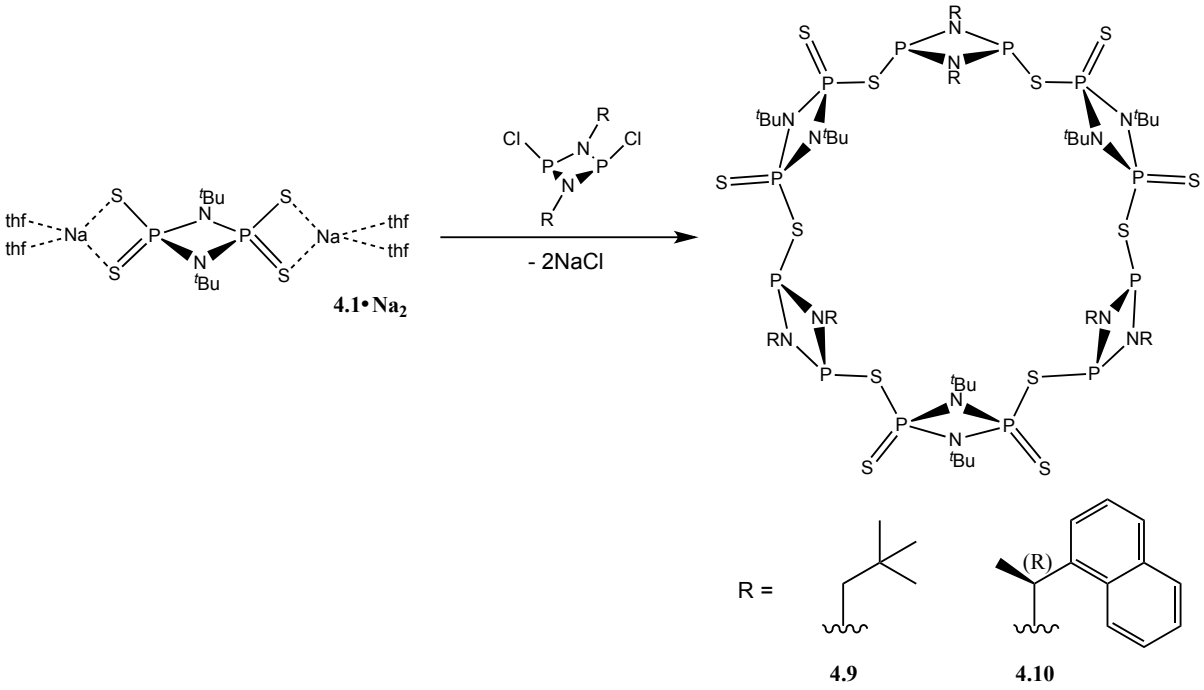

Scheme 4.7: Synthesis of heteroleptic S-bridged hexamers 4.9 and 4.10.

Table 4.1 ^{31}P NMR shifts (161.7 MHz, non-donor solvent, 298 K) and coupling constants of the P^{III} units in the macrocycles.

Compound	**4.8**	**4.9**	**4.10**	**4.12**
P^{V}/P^{III} ^{31}P shift (ppm)	60.7; 229.8	61.7; 249.7	61.7; 249.7	43.5; 252.4
P^{III} $^{2}J_{P\text{-}P}$ (Hz)	16/27	21/30	21/30	20/-

The structure of **4.9** was determined by X-ray crystallography, which showed that this has a very similar arrangement to the homoleptic macrocycle **4.8**. However, due to the decreased steric bulk of the $CH_2{}^t$Bu group now incorporated, there is greater distortion of the ring plane, leading to a chair-like conformation similar to the S-bridged macrocycle $[(\mu\text{-S})P^{III}(\mu\text{-N}{}^t\text{Bu})_2P^{V}(=S)]_6$ (**1.61S**) characterised by Singh *et al*. (Figure 4.9a).

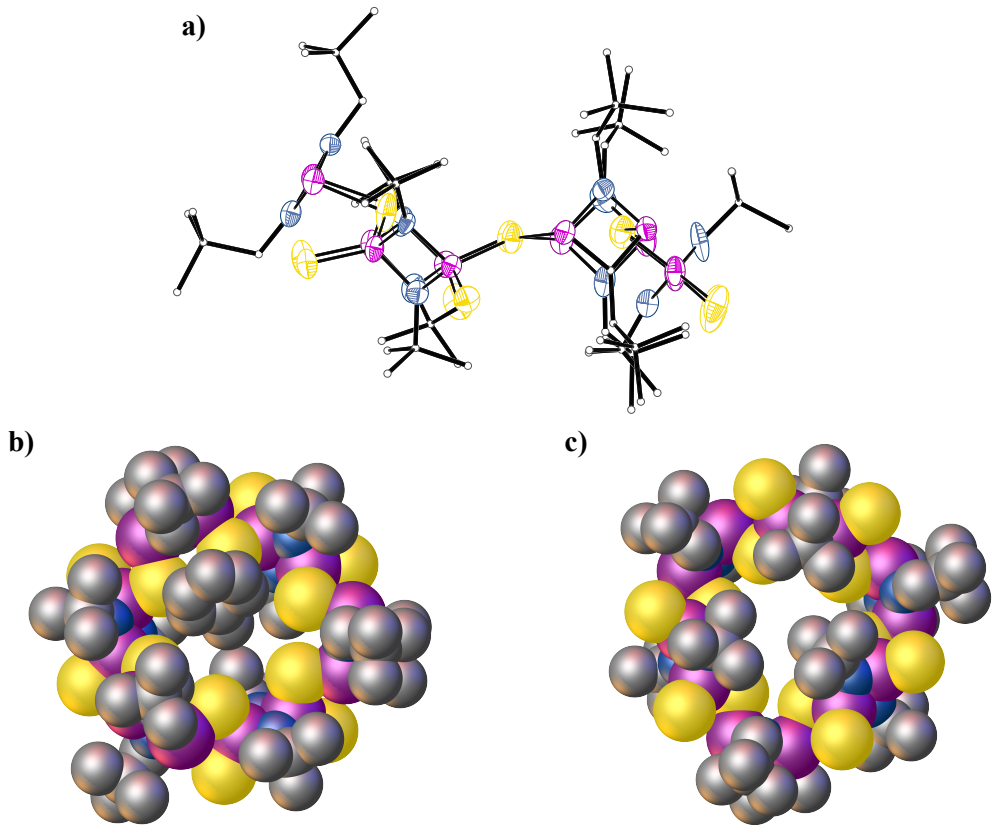

Figure 4.9: a) Side-view of 4.9 showing chair-like structure; b) Space filling diagram showing "open" face of 4.9 and toluene guest molecule; c) Space filling diagram showing "closed" face of 4.9. Hydrogen atoms and lattice solvent molecules have been omitted for clarity, thermal ellipsoids set at the 50% probability level in (a); thermal and geometrical constraints were used to facilitate anisotropical refinement hence no bond lengths or angles are shown here.

The distortion in **4.9** leads to the presence of two different faces in the macrocycle, one "open" face, (Figure 4.9b) and one "closed", where the R groups are over the cavity (Figure 4.9c). A toluene molecule is located within the cavity of **4.9** at the open face.

No X-ray structure of **4.10** could be obtained, however, the previously discussed NMR spectroscopic data suggests a similar structure. These heteroleptic macrocycles are the first examples of phosphazane macrocycles to contain organic substituents other than ^{t}Bu and **4.10** is also the first chiral macrocycle of this type. The introduction of new R groups into the structure not only modifies the solid-state properties but also their behaviour in solution. For example, the $CH_2{}^t$Bu bearing macrocycle **4.9** is highly soluble even in *n*-pentane whereas **4.8** and **4.10** are not. More sterically bulky groups, such as Mes, were found by *in situ* NMR studies to form the desired macrocyclic species upon reaction with **4.1**, however, these could not be isolated in the solid state.

Another important modification that is possible with macrocycles such as **4.8**-**4.10** is the oxidation of the remaining P^{III} centres. Reaction of **4.8** with stoichiometric amounts of elemental sulfur gives quantitative conversion to the all-P^V macrocycle $[(\mu\text{-S})\{(S=)P^V(\mu\text{-N}^t\text{Bu})\}_2]_6$ (**4.11**, Scheme 4.8). The presence of the fully-symmetric core structure is evident in the ^{31}P NMR spectrum in toluene which contains a singlet peak at δ = 66.5 ppm at ambient temperature. The fully-oxidised macrocycle **4.11** is air- and moisture-stable for several months, whereas **4.8** decomposes in a matter of hours under the same conditions. The presence of a pair of P=S stretching bands for P^A=S and $P^{A'}$=S (600-750 cm^{-1}) containing alternating P^{III}-P^V centres compared to only one for the all P^V macrocycle **4.11** gives another indication of the structural difference between these species.

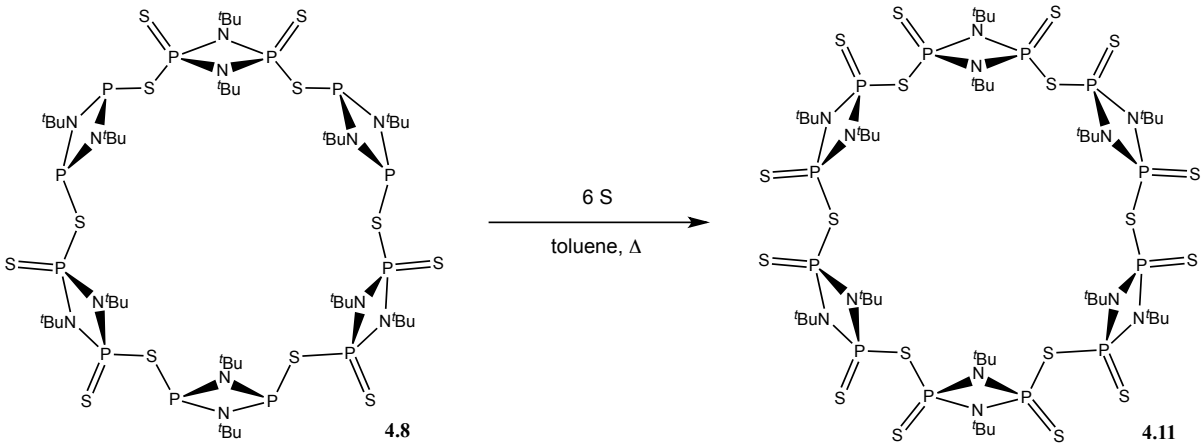

Scheme 4.8: Oxidation of the P^{III} positions in 4.8 by S to give the all-P^V species 4.11.

The oxidation of the P^{III} positions proceeds smoothly with S, however, reactions with Se were more complicated. Reaction with Se under the same conditions as S (refluxing thf) gave little to no reaction, and reflux in toluene lead to decomposition. Oxidation with Se has been shown recently to lead to rearrangements in phosphazanes, due in part to the change in geometry at the phosphorus atoms and to the sometimes harsh conditions employed.[157]

Reaction of **4.2·Na₂** with $[ClP(\mu\text{-N}^t\text{Bu})]_2$ (**2.1**) gives the mixed chalcogen macrocycle $[(\mu\text{-Se})\{(S=)P^V(\mu\text{-N}^t\text{Bu})\}_2]_6$ (**4.12**). The room-temperature ^{31}P NMR spectrum in toluene shows two doublet of doublet signals at δ = 43.5 ppm and δ = 252.4 ppm for the P^V and P^{III} centres, respectively,

which are both accompanied by ^{77}Se satellites ($^{2}J_{PSe}$ = 484.7 and 227.0 Hz respectively). The downfield shift of the P^{III} signal by $\Delta\delta$ = 30 ppm compared to the S-bridged macrocycle **4.8** indicates that the bridging of the P_2N_2 ring units occurs *via* Se.

Crystals of **4.12** suitable for X-ray diffraction were grown from a saturated *n*-hexane solution. The solid-state structure showed a similar P^{III}-P^{V} arrangement to that seen in **4.8** and **4.9** (Figure 4.10). The bridging of the P_2N_2 ring units was shown to occur *via* the Se atoms rather than the S. The dimensions of the macrocyclic cavity are almost identical to **4.8**, with an average diameter of 8.3 Å and a depth of 6.6 Å.

The core of **4.12** is less distorted than the S-analogue **4.8**, with an average deviation of the Se atoms of only 0.22 Å from the mean plane of the ring atoms. The increased length of the P-Se bonds (ranging between 2.2332(8) and 2.3701(7) Å in **4.8**) *vs.* P-S bonds (between 2.10914(6) and 2.228(2) Å in **4.8**) is presumably the reason for the lower distortion of the macrocycle, resulting from the lower steric repulsion between the peripheral ^{t}Bu and S groups. The increased P=S bond energy vs P=Se also gives a further thermodynamic preference for the Se bridging.

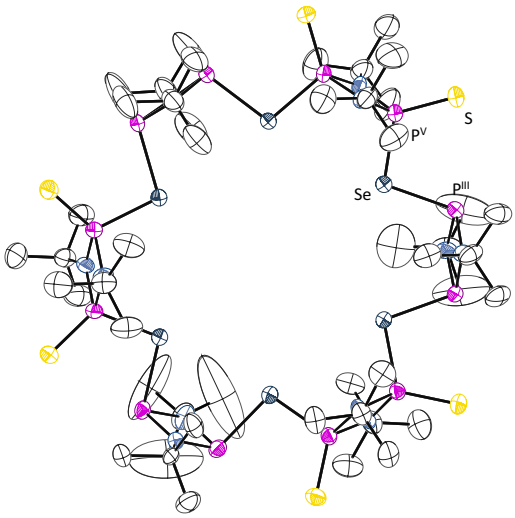

Figure 4.10: Solid-state structure of the Se-bridged hexamer 4.12. Hydrogen atoms omitted for clarity and thermal ellipsoids set at the 50% probability level. Selected bond lengths (Å) and angles (°): Se-P^{V} 2.228(2), Se-P^{III} 2.378(2), S-P^{V} 1.928(3), N-P^{V} 1.681(7), N-P^{III} 1.710(7), P^{III}-Se-P^{V} 102.16(7), S-P-Se 113.62(11), N-P^{V}-N 83.7(3), N-P^{III}-N 81.9(3).

4.4 Conclusions

Results presented in this chapter have shown that the general trend in the increase in stability of phosphazanes going from P^{III} to P^{V} holds true for the dianions $[S\text{-}P^{III}(\mu\text{-}N^{t}Bu)]_2^{2-}$. Oxidation with elemental chalcogens gives the dianions $[S\text{-}P(E)(\mu\text{-}N^{t}Bu)]_2^{2-}$ (E = S, Se, Te), which are interesting new ligands for a range of metals. In contrast to the P^{III} counterparts, reaction of the P^{V} dianions with chloro-dimers $[ClP(\mu\text{-}NR)]_2$ showed quantitative formation of hexameric macrocycles $[\{P^{III}(\mu\text{-}NR)_2\}(\mu\text{-}E)\{(S=)P^{V}(\mu\text{-}N^{t}Bu)\}_2]_3$. This approach allows the incorporation of a number of R groups into the backbone of the macrocycles as well as a range of linker atoms (S, Se). Furthermore, in some cases these alternating P^{III}-P^{V} macrocycles can be fully oxidised to air- and moisture-stable all-P^{V} macrocycles $[\{(S=)P^{V}(\mu\text{-}NR)_2\}(\mu\text{-}S)\{(S=)P^{V}(\mu\text{-}N^{t}Bu)\}_2]_3$. A summary of the reactions involved is shown in Scheme 4.9.

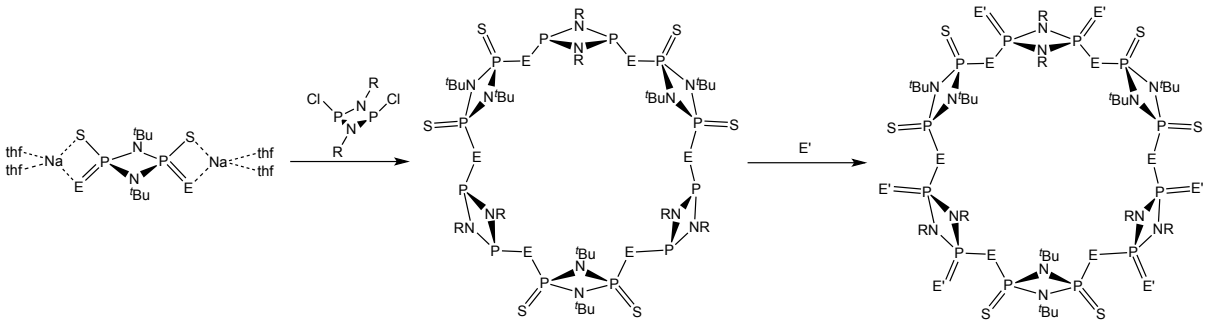

Scheme 4.9: Formation of E-bridged macrocycles and subsequent oxidation.

5. Complexes of Bis(amino) Cyclophosphazanes

5. Complexes of Bis(amino) Cyclophosphazanes

5.1 Olefin Polymerisation – Background

Alkene polymerisation using Zr or Ti catalysts is part of an array of well-established polymerisation methods used on an industrial scale by many companies. Typically, a metal chloride sandwich-type precatalyst is activated using long chain aluminium oxide MAO (Scheme 5.1), this is known as Ziegler-Natta polymerisation.

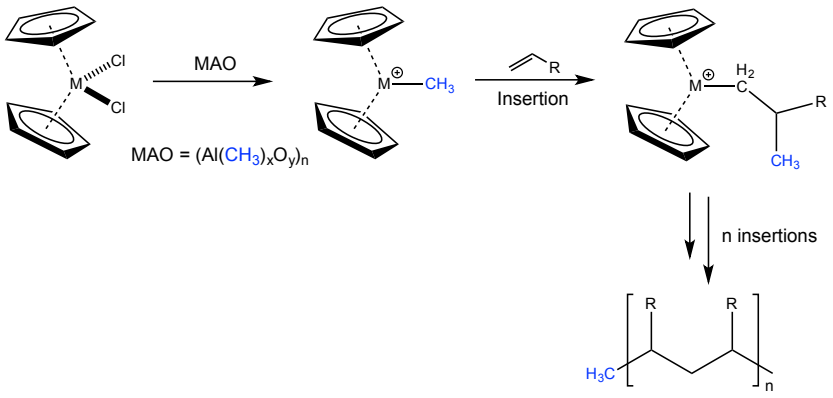

Scheme 5.1: Ziegler-Natta polymerisation of 1-alkene by MAO activated metallocene catalyst. M = Zr/Ti or other early transition metal.

However, controlling the tacticity of the polymer as well as the chain length among other parameters means that there is always room for improvement and room for catalyst and ligand optimisation.[158] "Atactic" olefin polymers (Figure 5.1a) are readily obtained using simple early transition metal catalysis. However, in order to obtain "isotactic" (Figure 5.1b) or "syndiotactic" (Figure 5.1c) polymers, that is ones with alternating or same side chain groups, more elaborate ligand sets are necessary. The use of bidentate or tridentate ligands containing nitrogen and oxygen donors, rather than the classical sandwich metallocenes have shown excellent potential in chiral Ziegler-Natta polymerisation.[159]

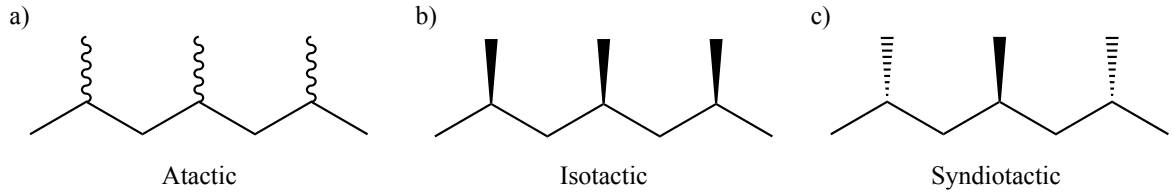

Figure 5.1: Polypropylene polymer geometries: a) Atactic, b) Isotactic and c) Syndiotactic.

The discovery of precatalysts based on alkyl transition metal complexes that can be activated with weakly coordinating ions in the late 80's was the first major step in improving the rational design of catalysts based on those designed by Ziegler and Natta.[160] Generation of a 'naked' metal cation by de-alkylation with the formation of 'non-coordinating' anions gives catalysts with extremely high activities.[161] The main advantage of this route comes from the weakly coordinating anion, but in the case of more sensitive ligand sets the use of a less reactive species than MAO could be an advantage. Typically, the alkyl abstraction is done *in situ* by a sterically protected boron species such as $B(C_6F_5)_3$.

Studies by Repo *et al.* on a variety of bulky bis(amino) cyclophosphazanes $[P(\mu\text{-}N^tBu)HNR]_2$ (R = alkyl, aryl) showed their potential to coordinate to early transition metals (Zr, Ti, Hf), with the resulting complexes performing as catalysts in alkene polymerisation studies.[78] There are a variety of synthetic routes used to obtain metal complexes of bis(amino) cyclophosphazanes. The simplest, also employed by Stahl *et al.,* is the one-step reaction of $TiCl_4$ with the bis(amino)phosphazanes $[P(\mu\text{-}N^tBu)HNR]_2$ (**1.34**, Chapter 1) in the presence of Et_3N, to form the dichloro-titanium complexes (**1.34-MCl_2**, Scheme 5.2).[30] Another method is the transmetallation of the lithiated bis(amido) ligand $[P(\mu\text{-}N^tBu)NR]_2[Li(thf)_2]_2$ with the metal tetrachlorides $HfCl_4$ or $ZrCl_4$, to give the hafnium and zirconium complexes.[162] These procedures were, however, only found to work with phosphazanes bearing ^{t}Bu groups on their imido substituents. A more general synthesis was developed by Repo *et al.* wherein a bis(amido) cyclophosphazane is reacted with a tetrakis(dimethylamido) metal precursor to form **1.34-M(NMe_2)$_2$** (Scheme 5.2), which is converted to the dichloro-metal species (**1.34-MCl_2**) by reaction with TMSCl.[26]

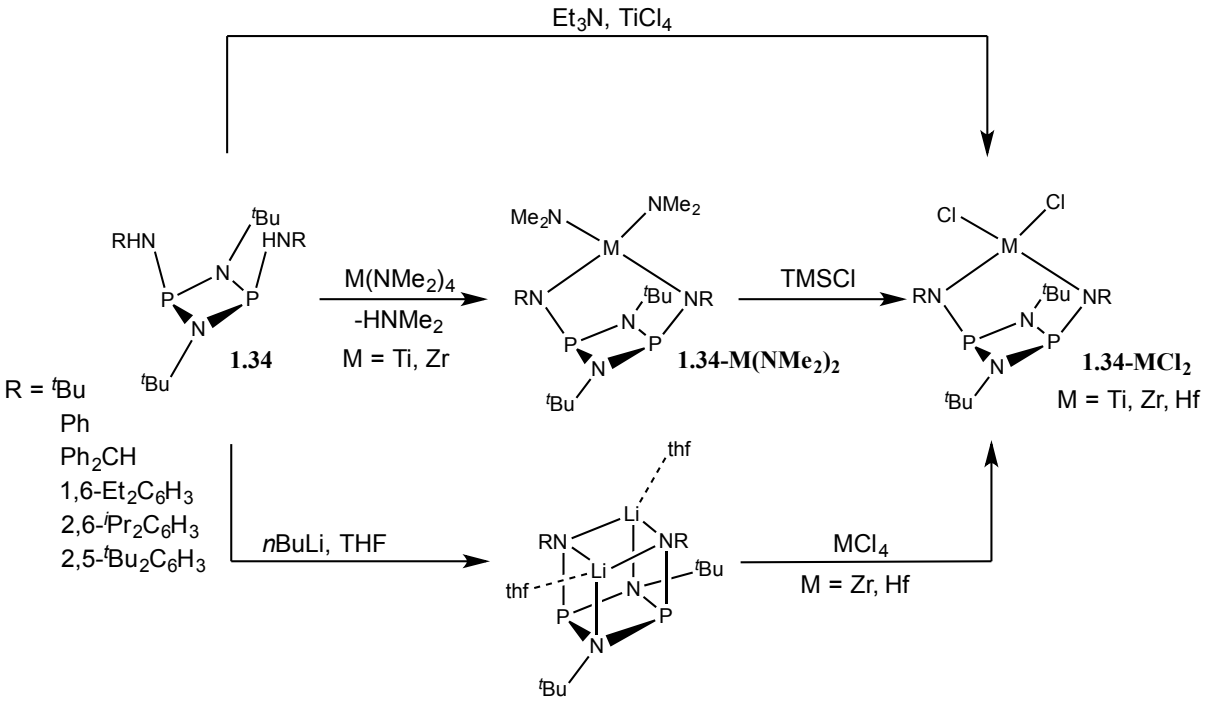

Scheme 5.2 Formation of complexes of bis(amido) phosphazanes with early transition metals.

In the studies by Repo *et al* employing bis(amino)cyclophosphazane metal complexes in alkene polymerisation MAO was used to activate the metal chloride species.[26,77] The reaction of amido-ligands with MAO is not unprecedented, especially when the steric bulk of the groups attached to nitrogen is reduced.[163] In order to circumvent this potential problem, bis-benzyl complexes were employed. These were obtained by reaction of the chloro-complexes **1.34-MCl$_2$** with BnMgCl to give the alkyl complexes **1.34-MBn$_2$** (Scheme 5.3).[164]

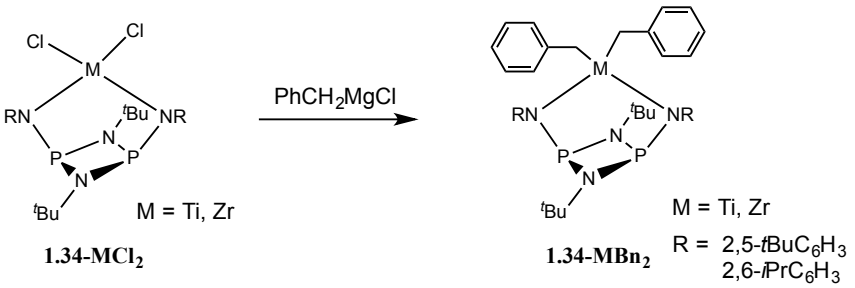

Scheme 5.3: Synthesis of alkyl Zr bis(amino) cyclophosphazane complexes 1.34-MBn$_2$.

These complexes showed low catalytic activity in $B(C_6F_5)_3$-activated polymerisation studies. This was attributed to their extremely air and moisture sensitive nature, which leads to rapid catalyst de-

activation if the conditions for polymerisation are not carefully controlled and all reagents rigorously dried prior to use.

Bis(amino) cyclophosphazanes present the advantage of having a modular synthesis, therefore allowing the introduction of a variety of groups near, or far from the metal coordination site (Figure 5.2). Bearing this in mind, we were interested in creating a range of novel bis(amino) cyclophosphazanes containing chiral and achiral groups with varying degrees of steric bulk in order to explore their coordination to metal centres and test their activity in olefin polymerisation.

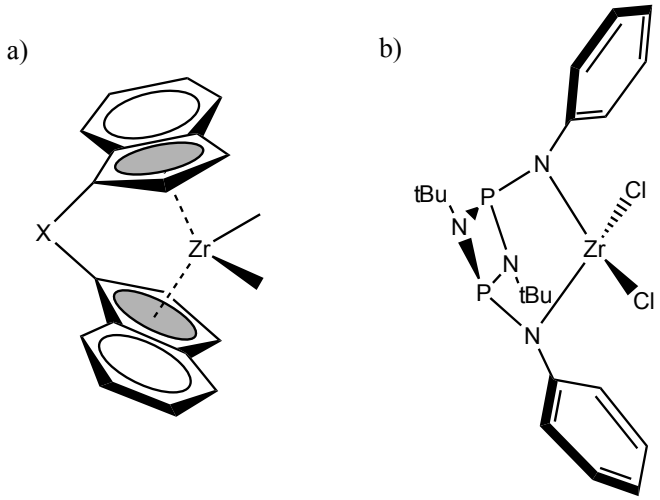

Figure 5.2: Comparison of a) Ziegler Natta type pre-catalyst, and b) bis(amino) cyclophosphazane Zr complex synthesised by Repo *et al.*

The metal coordination at the nitrogen in early transition metal bis(amino)cyclophosphazane complexes means that the chiral groups are next to the metal centre and should be able to transfer chirality to achiral substrates. [31]

5.2 Synthesis of Novel Bis(amino) Cyclophosphazanes

In order to create a library of novel cyclodiphosphazanes we first had to establish synthetic procedures that would allow the incorporation of chirality into the P_2N_2 unit. Based on the extensive work by Stahl *et al.* and Repo *et al.*, the substitution of the Cl-atoms in the ^{t}Bu dimer **2.1** by a range of amines was shown to proceed under a variety of conditions. Work by Gade *et al.* also showed that

substitution at species containing bulkier and more diverse imido-substituents in the P_2N_2 ring was also possible.

We therefore attempted to synthesise a range of bis(amino) cyclophosphazanes $[P(\mu\text{-}NR^1)NR^2]_2$ containing a variety of imido (R^1) and amino substituents (R^2) (Figure 5.3). The goal of the project was to use substituents that are chiral; however, in order to explore reactivity and stability of the compounds we also used non-chiral derivatives.

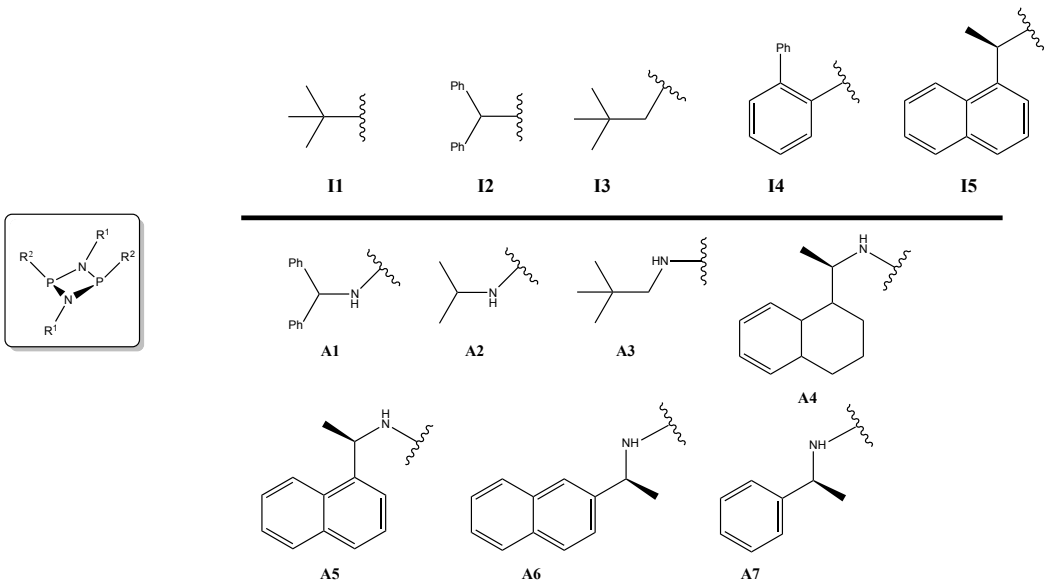

Figure 5.3: Summary of the imido and amino substituents used in this study.

The synthetic procedure was adapted from work by Stahl *et al.* and Repo *et al.* A primary amine RNH_2 (R = **A1-A7**) was added to a stirred solution of the appropriate chloro-dimer (**2.1-2.6**) in a solution of Et_3N (excess)/thf at 0 ºC. The formation of Et_3NHCl (a white precipitate) was almost immediate but the reaction was stirred for 24 hrs and warmed to ambient temperature to allow complete reaction (Scheme 5.4). There was no difference in the reactivity observed for the formation of *R*- over *S*- substituents, and therefore chiral groups used in this study were primarily (R) unless otherwise stated.

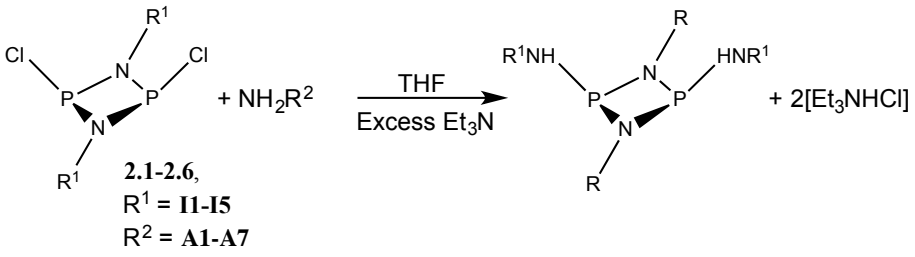

Scheme 5.4: Synthesis of bis(amino) cyclophosphazanes from chloro phosphazanes 2.1-2.6 (See Figure 5.3).

A full summary of selected condensation reactions attempted as well as the main ^{31}P NMR peaks are summarised in Table 7.1.

Table 5.1: Summary of selected bis(amino) cyclophosphazane syntheses and ^{31}P NMR (161.3 Hz, C_6D_6) of products obtained.

Imino	Amino	major ^{31}P-NMR (ppm)	minor ^{31}P-NMR (ppm)
I1	**A4**	97	-
I1	**A5**	98	-
I1	**A6**	96	-
I1	**A7**	96	-
I2	**A5**	171	14-16, 110
I3	**A4**	131	-
I3	**A6**	132	-
I3	**A7**	132	-
I4	**A5**	154	9
I5	**A1**	8-12	98(trace)
I5	**A2**	6-10	100-105
I5	**A3**	12-16	108

Combinations involving sterically bulky species **2.2** ([P(μ-N**I2**)Cl]$_2$) and **2.4** (R = [P(μ-N**I4**)Cl]$_2$) or with the chiral species **2.5** ([P(μ-N**I5**)Cl]$_2$) were unsuccessful giving a variety of unidentified products.

Reactions involving **2.2** ([P(μ-N**I2**)Cl]$_2$) or **2.4** ([P(μ-N**I4**)Cl]$_2$) all contained signals above δ = 150 ppm as the major product in their ^{31}P NMR spectra at ambient temperature. Although full characterisation of these species was not possible, it is likely that they result from the formation of chloride-substituted diamides, PCl(NHR)$_2$.[165] No purification method could be found to isolate these

products, and ^{13}C and ^{1}H NMR studies showed multiple signals, that could match a number of possible products.

In order to assess the reactivity of the chiral species **2.5** ([P(μ-N**I5**)Cl]$_2$) with regards to bulky substituents, a screening of reaction conditions using sterically bulky benzhydrylamine (**A1**NH$_2$) was undertaken. A variety of conditions were tested but only a trace amount of the desired product was obtained (Table 7.2). The ^{31}P NMR spectrum of the products after workup showed only a small signal in the expected region (*ca.* δ = 100 ppm) corresponding to the targeted bis(amino) cyclophosphazane ([P(μ-N**I5**)NH**A1**]$_2$) and a large amount of indistinguishable impurities between δ = 0-10 ppm. The lower region is typically of hydrolysed and oxidised phosphazane products; however, these signals appeared under several conditions and with rigorous exclusion of air and moisture. The ^{31}P-^{1}H coupled NMR spectrum of this region showed large $^{1}J_{P\text{-}H}$ coupling constants (up to 500 Hz), signifying a break-up of the P-N ring and formation of P-H bonded species.

Table 5.2: Screening of reaction conditions for reaction of benzhydrylamine (A1) with 2.5.

Solvent	Temperature (ºC)	Base (equiv.)	Amine (equiv.)
thf	0 to r.t.	Et_3N (4.0)	2.0
thf	0 to r.t.	Et_3N (40.0)	2.0
thf	-78 to r.t.	-	4.0
Et_2O	0 to r.t.	-	4.0

The steric bulk of the amine was not found to have a significant impact on the variety of products obtained when reacted with the chloro dimer **2.5**. By comparison of the relative integrations in the ^{31}P NMR spectra of the isolated products, the less sterically hindered *iso*-propyl amino substituent **A2** gives mostly decomposition products but still slightly more of the desired product than the bulkier benzhydrylamine **A1**.

Based on previous work by Repo *et al.* and Stahl *et al.*, we suspected that the attempted synthesis of chiral-amino species containing imido ^{t}Bu substituents would be successful. Reaction of the chloro-dimer **2.1** with chiral amine species **A4**, **A5**, **A6**, and **A7** in the presence of Et_3N gave bis(chiral-amino) cyclophosphazanes **5.1**, **5.2**, **5.3**, and **5.4** ([P(μ-N^{t}Bu)NH**A4-A7**]$_2$), respectively (Scheme 5.5). The ^{31}P NMR spectra of these species all contain broad singlets in the δ = 80-120 ppm region,

indicative of a the desired $[P(\mu\text{-}NR)NHR]_2$ species. The broad nature of the singlet in bis(amino) cyclophosphazane species is due to fluxional *cis*/*trans* inversion of the substituents on the P_2N_2 ring. This has been well documented in the literature for a variety of substituents.[23,28]

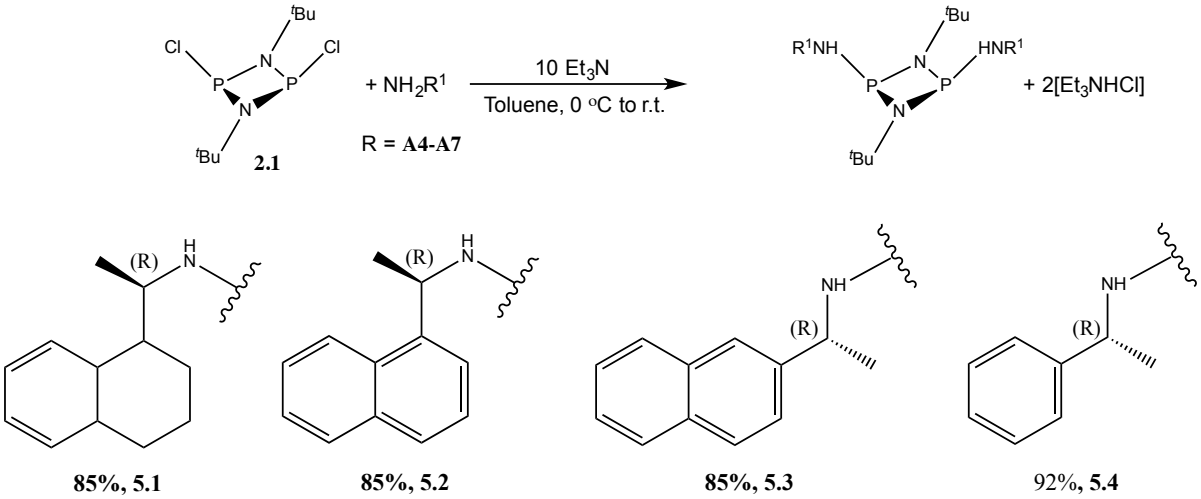

Scheme 5.5: Synthesis and yields of chiral bis(amino) cyclophosphazanes containing ^{t}Bu imino groups.

Crystals of **5.1** and **5.2** suitable for X-ray diffraction were grown from hexane/thf diffusion experiments. Crystals of **5.4** were obtained from a saturated thf solution at ambient temperature, whereas **5.3** crystallised from a pure oil product left at ambient temperature over the course of a few days. Solid state structures of **5.1**-**5.4** are shown in Figure 5.4.

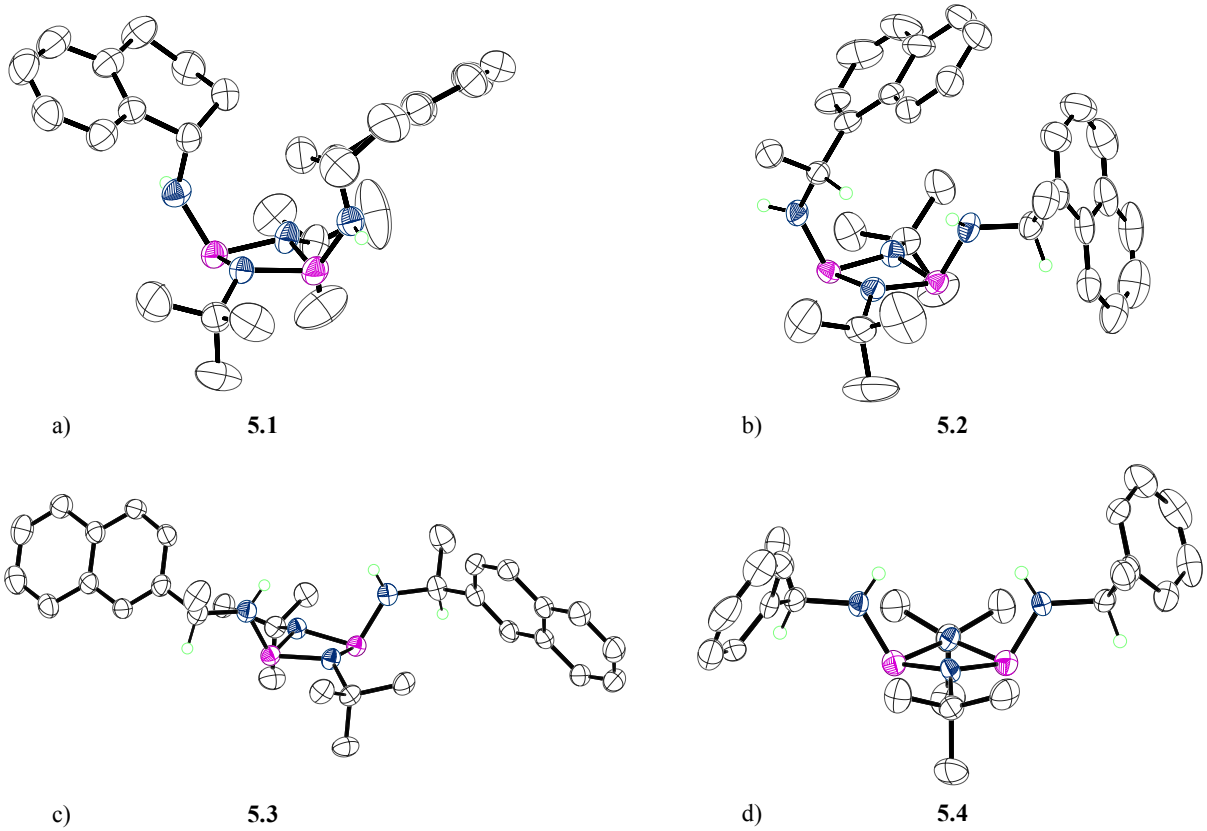

Figure 5.4: Solid state structures of chiral bis(amino) cyclophosphazanes bearing amino groups A4-A7. a) 5.1 (A4), b) 5.2 (A5), c) 5.3 (A6), and d) 5.4 (A7). Thermal ellipsoids set at the 50% probability level and selected hydrogens omitted for clarity.

Table 5.3: Selected bond lengths (Å) and angles (°) of compounds 5.1-5.4.

Compound	5.1	5.2	5.3	5.4
P-N average	1.7220	1.7122	1.7276	1.718
P-NH average	1.648	1.658	1.665	1.654
P···P	2.5773(15)	2.6007(12)	2.5973(10)	2.572(4)
PNP mean	96.89	98.81	97.44	97.2
NPN mean	108.61	105.88	106.38	105.9
PNNP torsion	161.06	167.54	161.77	161.96

Apart from internal steric factors within the dimers themselves, the configuration of the groups within these molecules is due to the different stacking/packing effects in the crystal lattices. For example, **5.3** contains the expected *exo*- configuration of the large R groups that minimises steric repulsion and allows for the formation of π-stacking interactions between molecules (Figure 5.5b). **5.1** on the other hand has P···H-N interactions (average P···HN intermolecular distance 2.93 Å) in the solid-state, resulting in the *exo*- configuration of the amino-hydrogens and the sterically bulky groups being

disposed *endo*- with respect to the P_2N_2 ring face (Figure 5.5a). **5.2** is fixed in a rare *endo*-,*exo* configuration, which is only seen in one other case for substituted phosphazanes (Figure 5.5b).[26]

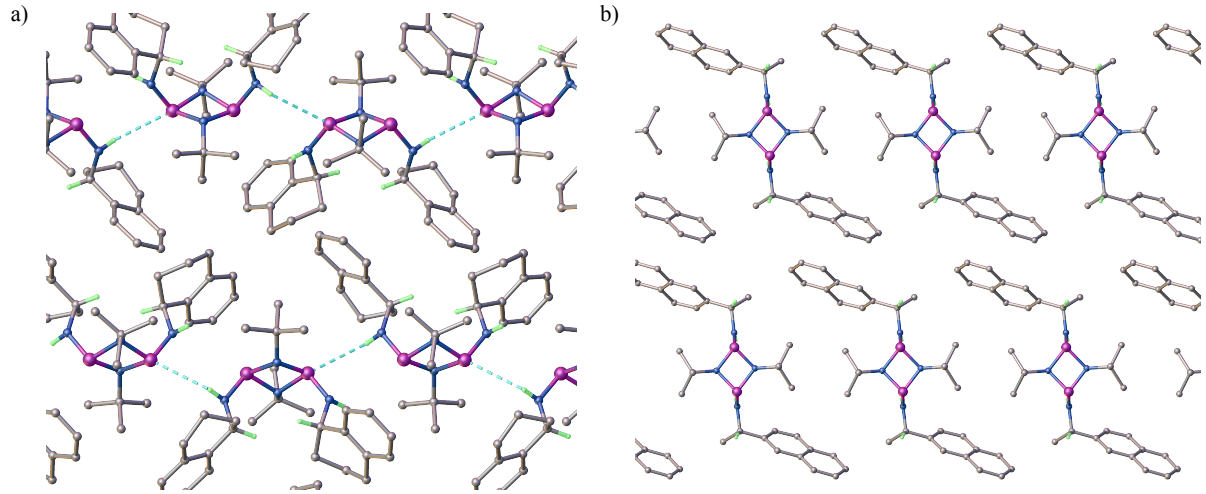

Figure 5.5: Packing diagrams of a) *endo*-5.1 (H-P intermolecular interactions show by dashed lines) and b) *exo*-5.3.

Synthesis of chiral species using the neopentyl chloro-dimer **2.3** ($[P(\mu\text{-}NCH_2{}^tBu)Cl]_2$ was used as a less sterically bulky derivative. The reaction with the chiral species **A4, A6** and **A7** gave products **5.1b**, **5.3b** and **5.4b**, respectively, with peaks at $\delta \approx 130$ ppm in their ^{31}P NMR spectra (Scheme 5.6).

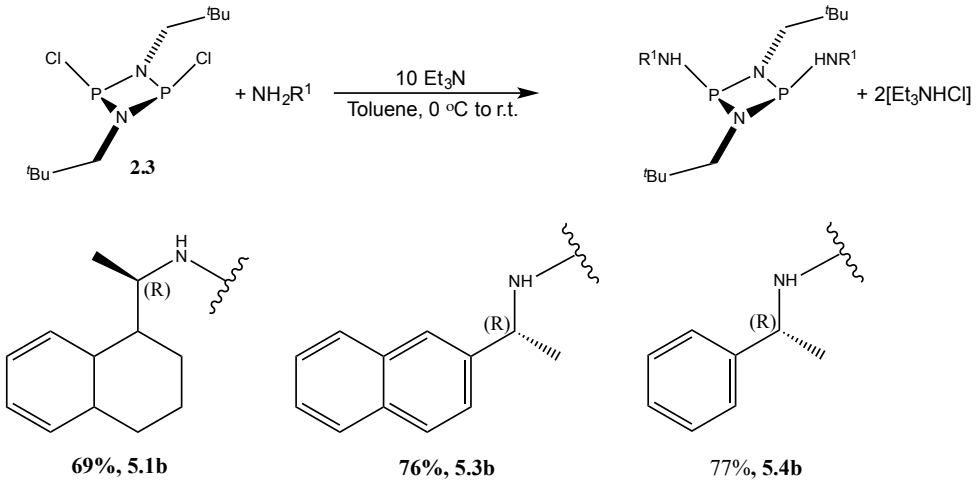

Scheme 5.6: Synthesis and yields of chiral bis(amino) cyclophosphazanes containing neopentyl imido groups.

These were initially assigned to be diamino-chloro species (RNH)(R′NH)PCl, similar to those found for other unsuccessful reactions. However, the shape of the ^{31}P NMR signals is similar to the broad

signals found for bis(amino) species **5.1**-**5.4** containing ^{t}Bu imido groups, suggesting that the P_2N_2 ring is still intact. Furthermore, the difference in the ^{31}P chemical shifts of **5.1b**, **5.3b** and **5.4b** relative to the ^{t}Bu derivatives **5.1**, **5.3**, and **5.4** ($\Delta\delta \approx 32$ ppm) is nearly identical in sign and magnitude to that found between respective dichloro-species **2.1** and **2.3** ($\Delta\delta = 32$ ppm). No crystal structures could be obtained, but we can say with some degree of certainty that these reactions give neopentyl chiral bis(amino) cyclophosphazanes. However, the formation of these species gives rise to very minor amounts of impurities in the ^{31}P NMR that could not be separated and the neopentyl group was therefore not used in further studies.

5.3 Metal Complexes of Chiral Bis(amino) Phosphazanes

Based on the unsuccessful attempts in synthesising species containing chiral imido groups, species **5.1**-**5.4** containing chiral amino and ^{t}Bu imido substituents were used in subsequent complexation reactions.

5.3.1 Lithium Complexes

In order to test the reactivity compared to other bis(amino)cyclophosphazanes, lithium complexes of **5.1** and **5.3** were synthesised by a similar route to that used by Repo *et al*. Addition of stoichiometric amounts of *n*BuLi to a solution of the chiral bis(amino) species in thf at -30 ºC followed by reflux for 3 hours gave formation of the lithiates. These are likely to have heterocubane structures (Type **I**, Chapter 1.2.1). The summary of this synthesis is shown in Scheme 5.7.

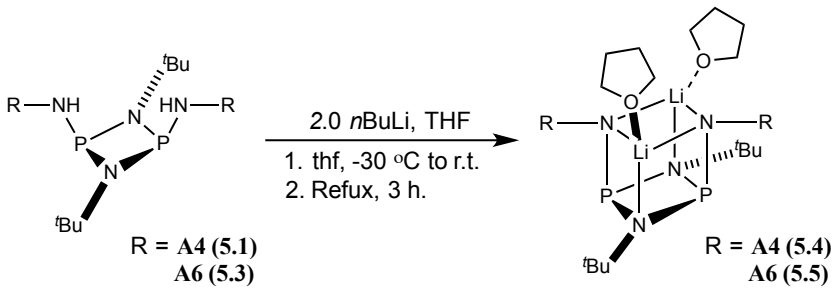

Scheme 5.7: Synthesis of lithiated cyclodiphosphazanes 5.4 and 5.5.

The progress of this reaction can be monitored by *in situ* ^{31}P NMR experiments. For example, the characteristic broad signal for the bis(amino) cyclophosphazane **5.3** ([P(μ-N^{t}Bu)HN**A2**]$_2$) at δ ≃ 95 ppm (Figure 5.6a) disappears after reflux and gives way to a sharp singlet for the lithiated species [P(μ-N^{t}Bu)N**A2**]$_2^{2-}$[Li$^+$]$_2$ at δ ≃ 165 ppm (Figure 5.6b).

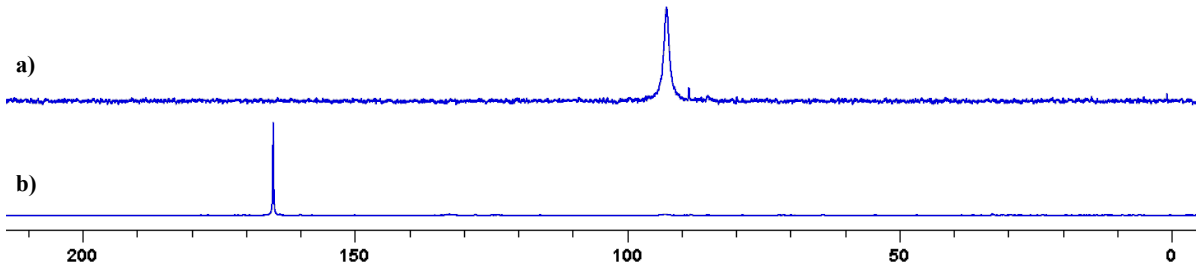

Figure 5.6: ^{31}P-NMR spectra (161.6 MHz, C_6D_6) of a) bis(amino) species 5.3 and b) the lithiated derivative 2.15.

If the reflux times are shortened, then the unsymmetrical *mono*-lithiate (Li-N**A2**)P(μ-N^{t}Bu)$_2$P(HN**A2)** can be seen in the *in situ* ^{31}P NMR at δ = 135 ppm. The sharp signal for the lithiated species is due to the now locked configuration with *cis* geometry of the *exo*-NR groups rather than the fluxional *cis*/*trans* equilibrium present in the bis(amino) starting materials [P(μ-N^{t}Bu)NHR]$_2$.

5.3.2 Gold and Copper Complexes

The reactivity of compounds **5.1** and **5.3** with DMSAuCl and DMSCuBr was also explored, in an analogous manner to the complexation reactions performed by Gade *et al.* in their studies of BINOL-substituted cyclophosphazanes.[31] The bis(amino) species **5.1** or **5.3** were dissolved in DCM and DMSAuCl was added as a solid to the stirred solution under a positive flow of nitrogen (Scheme 5.8). The mixtures were stirred for 30min and the products obtained as pure pale yellow or colourless solids after the removal of the solvent. Due to the light-sensitive nature of gold complexes, all steps were performed in light-protected flasks.

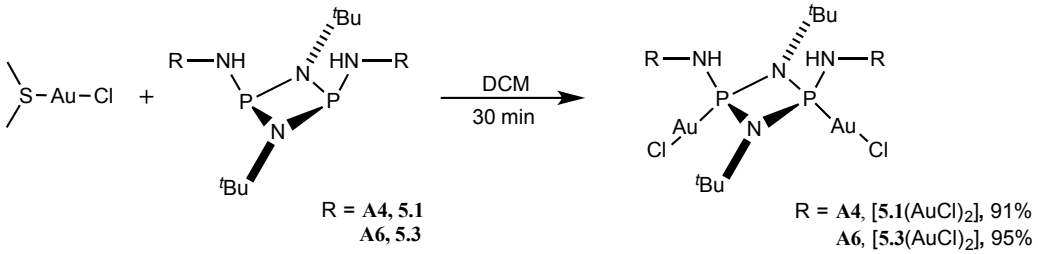

Scheme 5.8: Synthesis of chiral bis(amino) cyclophosphazane gold complexes.

In contrast to the lithiated species **5.4** and **5.5**, the ^{31}P NMR spectra of the gold complexes in DCM at ambient temperature consist of a broad singlet and the shift is significantly lower, in the region of δ = 80 ppm. Dissolving in d_6-DMSO gives rise to multiple signals in the ^{31}P NMR spectra in the δ = 60-80 ppm range. This is presumably due to the formation of DMSO-Au coordinated species through the (soft) sulfur lone pair.[166,167] Nonetheless the signal shape and especially the spectral region indicates that there is an *intact* P_2N_2 ring that is still coordinated to a metal centre. Furthermore, the starting bis(amino) ligands **5.1** and **5.3** were not found to decompose in DMSO. The ^{31}P NMR spectra of the gold complexes [**5.1**$(AuCl)_2$] and [**5.3**$(AuCl)_2$] in DCM and DMSO solvents can be seen in Figure 5.7. Despite the structural similarities, [**5.1**$(AuCl)_2$] and [**5.3**$(AuCl)_2$] have very different solubilities, the latter precipitates from DCM upon formation and could only be dissolved in DMSO.

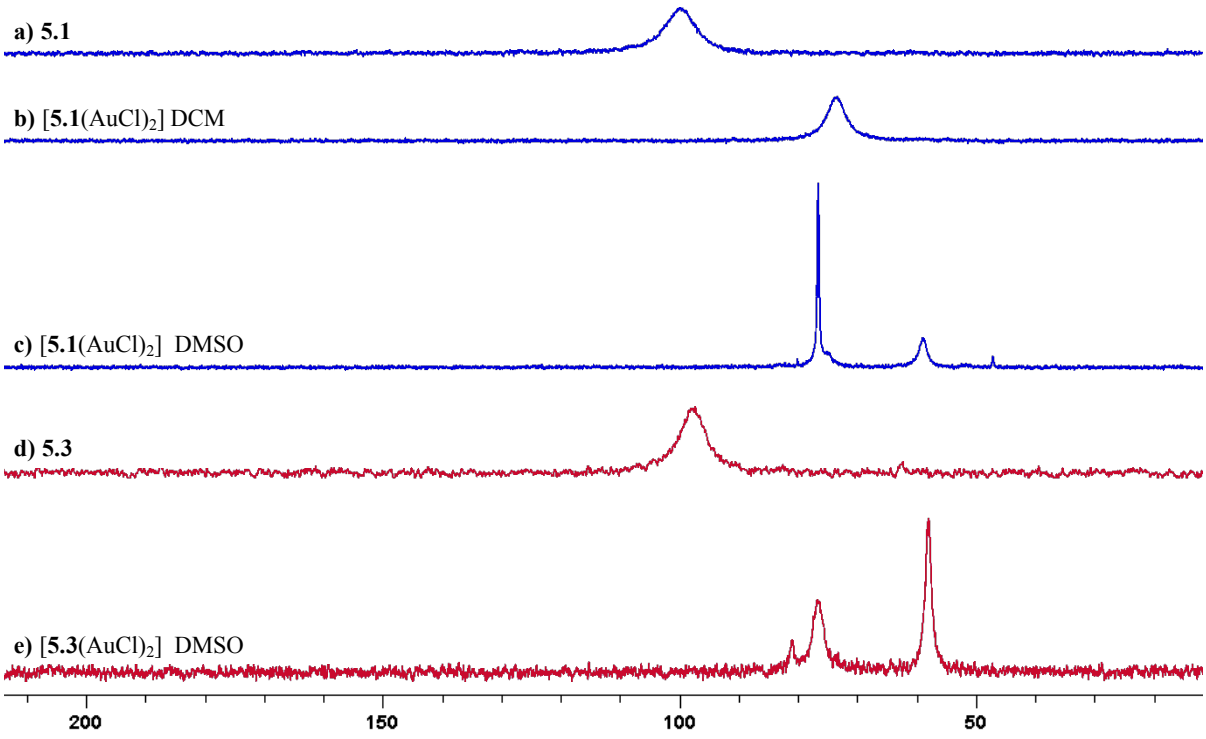

Figure 5.7: ^{31}P NMR (161 MHz) of ligands and their gold complexes. a) 5.1 in d_6-DMSO, b) [5.1(AuCl)$_2$] in CD_2Cl_2, c) [5.1(AuCl)$_2$] in d_6-DMSO, d) bis(amino) species 5.3 in d_6-DMSO, e) [5.3(AuCl)$_2$] in d_6-DMSO.

Copper complexes of **5.1** and **5.3** were formed by an analogous procedure to the reaction described for the gold complexes. Copper bromide was added to a stirred solution of the ligand in diethyl ether at ambient temperature The complexes [**5.1**(CuBr)$_2$] and [**5.3**(CuBr)$_2$] precipitate rapidly (*ca.* 5min) as colourless precipitates (Scheme 5.9). Although the species are obtained in excellent yields, they are only soluble in DMSO. The ^{31}P NMR spectra of [**5.1**(CuBr)$_2$] and [**5.3**(CuBr)$_2$] in d_6-DMSO showed similar patterns to those obtained in the analogous gold complexes due to presumed coordination of the DMSO solvent to the Cu atoms. The relative shifts are slightly higher than the corresponding gold complexes.

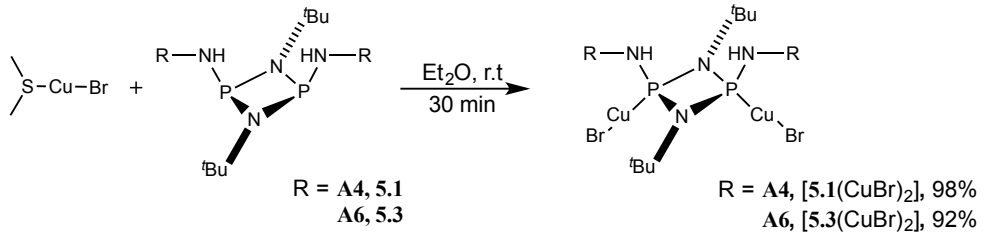

Scheme 5.9: Synthesis of chiral cyclophosphazane copper complexes [5.1(CuBr)$_2$] and [5.3(CuBr)$_2$].

No crystal structures of these coordination species could be obtained to give more information on the environment or the geometry of the gold or copper complexes.

5.3.3 Chiral Bis(amino) Cyclophosphazane Complexes of Zr

Following the work of Stahl *et al* and Repo *et al*, Zr complexes of chiral phosphazanes **5.1-5.4** were prepared. The reactions of bis(amino) species **5.1-5.4** ([P(μ-N^{t}Bu)NHR]$_2$, R = **A4-A7**) with Zr(NMe$_2$)$_4$ proceed selectively according to Scheme 5.10, giving [**5.1-5.4**·Zr(NMe$_2$)$_2$] in quantitative yields after removal of the solvent *in vacuo*.

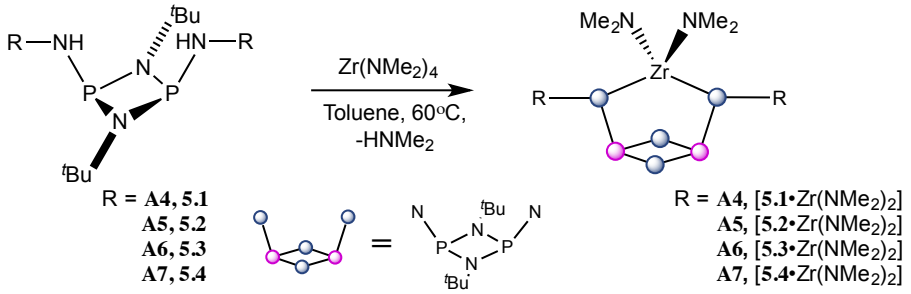

Scheme 5.10: Synthesis of ZrNMe$_2$ complexes of chiral bis(amino) cyclophosphazanes 5.1-5.4.

In situ ^{31}P NMR spectroscopic experiments show that as much as 80 % of the phosphazane is converted to the product after 30 minutes at ambient temperature, and the use of elevated temperature helps ensure the reaction goes to completion. All products were characterised by ^{1}H-, ^{13}C-, ^{31}P- NMR, and elemental analysis, however no crystal structures could be obtained.

The analogous reaction of **5.1** with Hf(NMe$_2$)$_4$ gives the phosphazane-metal complex in quantitative yield at ambient temperature. In contrast, reactions with the titanium precursor Ti(NMe$_2$)$_4$ showed low conversion at temperatures up to 80 ºC. This finding is in direct agreement with findings by Stahl *et al.* who showed that much higher temperatures were required for Ti complexes to form.[19] However, at least for these zirconium and hafnium complexes, low temperatures and short reaction times are key. If the reaction mixtures are left for too long, HNMe$_2$ eliminated during the reaction, and appears to lead to the decomposition of the complex – most likely due to cleavage of the phosphorus-nitrogen bond and exchange of the chiral amino group for the NMe$_2$ substituent.

In order to form effective precatalysts for alkene polymerisation, it was necessary to obtain either chloro- or alkyl- substituted zirconium complexes as precursors. The preparation of the chloro-zirconium species was adopted from previously published literature by Stahl *et al.* and Repo *et al.*[26,77] The subsequent alkylation was attempted according to previous studies on the synthesis of alkyl-zirconium complexes for Ziegler Natta polymerisation that employed simple organomagnesium reagents (eg. Bn_2Mg, BnMgCl) and organolithium (eg. $LiCH_2TMS$, *n*BuLi) to substitute the chloride position at the metal centre (Scheme 5.11).[164]

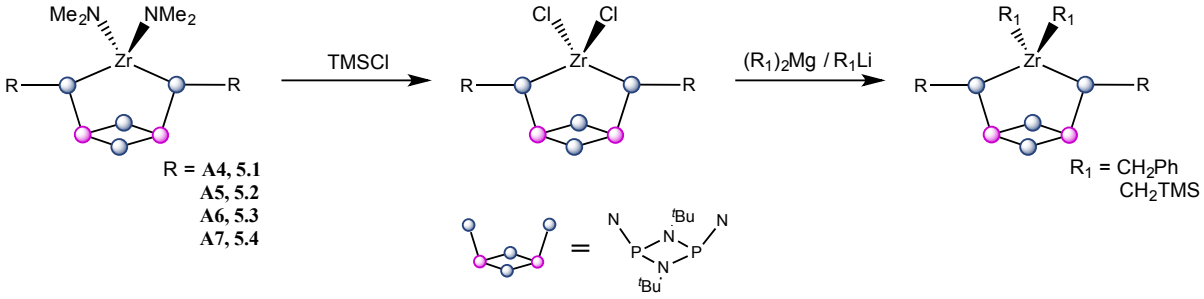

Scheme 5.11: Synthetic strategy for formation of bis-alkyl zirconium complexes.

According to the published procedure, TMSCl (excess) was added dropwise to a solution of the phosphazane-$Zr(NMe_2)_2$ complex in toluene. *In situ* ^{31}P NMR spectroscopy showed that the reaction occurred instantly and removal of the solvent *in vacuo* gave the products as white powders. ^{31}P NMR spectra of the isolated powders, however, showed that a number of side reactions had occurred during the reactions (for example, see Figure 5.8). The location of the impurity peaks in the spectra (δ = 112-124 ppm) shows that they are most likely similar complexes that contain an *intact* phosphazane ring. These impurities occurred reproducibly and regardless of reaction times and conditions. No suitable purification method could be found to exclude these impurities, which according to integration are 15-25% of the samples.

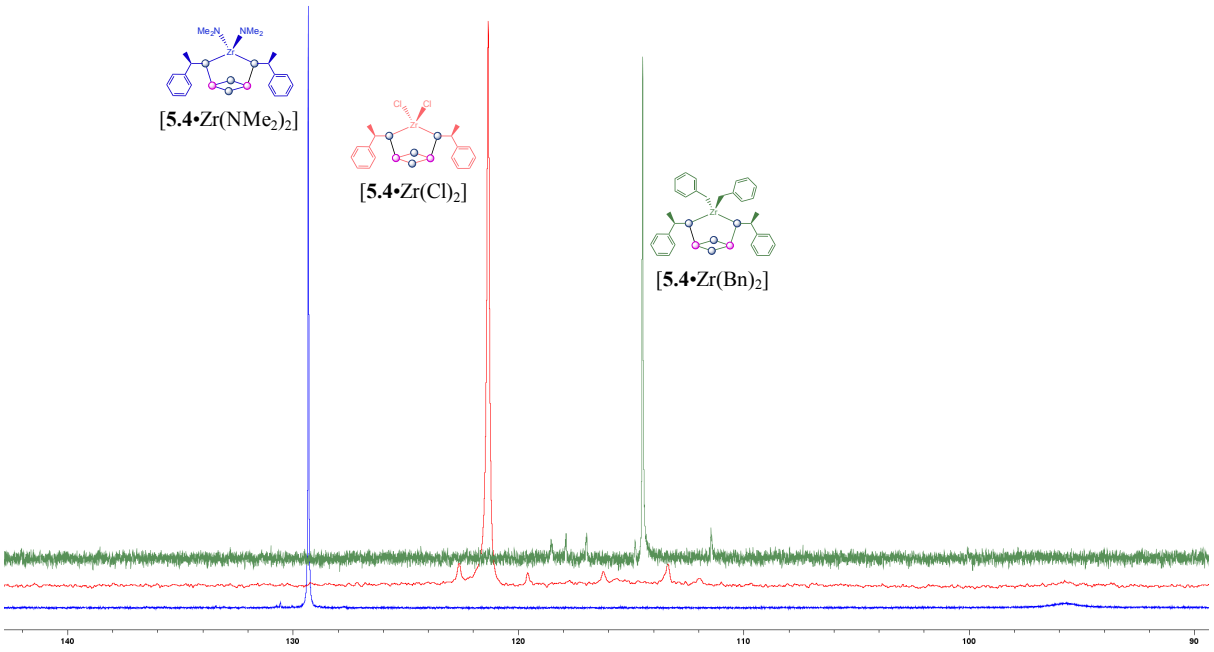

Figure 5.8: ^{31}P NMR spectrum (161.6 MHz, C_6D_6, 298 K) of [5.4·Zr(NMe$_2$)$_2$] (Blue), [5.4·Zr(Cl$_2$)] (Red), and [5.4·Zr(Bn)$_2$] (Green).

The impurity peaks arise from a presumed reaction with the $TMSNMe_2$ released during the reaction, a similar process to that seen in the formation of the [P(μ-NR)NR]$_2$-Zr(NMe$_2$)$_2$ complexes when the reaction mixture for extended periods of time. Attempted removal of the $TMSNMe_2$ by applying static vacuum during the addition with TMSCl failed due to its lower boiling point ($TMSNMe_2$: 87 ºC, TMSCl: 57 ºC) meaning the reactions did not proceed to completion.

Further analysis of the literature showed that the compounds isolated in the previous study by Repo *et al.* were not in fact 100% pure.[77,164] Similar impurity peaks were present in the ^{31}P NMR of the reported species, but not mentioned in the manuscript despite appearing in the spectrum of compounds in the supporting information.

Despite the presence of these side products, it was hoped that after alkylation some separation might be possible. Reaction of the chloro-complex [**5.4**·$ZrCl_2$] with either $LiCH_2TMS$ or Mg(Bn)$_2$(thf)$_2$ was attempted at low temperature. Analysis of the ^{31}P NMR spectrum of the alkyl-complexes [**5.4**·ZrR$^1_2$] (R = Bn, CH_2TMS) showed that although reaction had occurred, the impurities seen previously had increased in number and relative integration to the desired product. An expansion of the ^{31}P NMR

spectrum of [**5.4**·$Zr(Bn)_2$] can be seen in Figure 5.9, with relative integrations of the main species and side products.

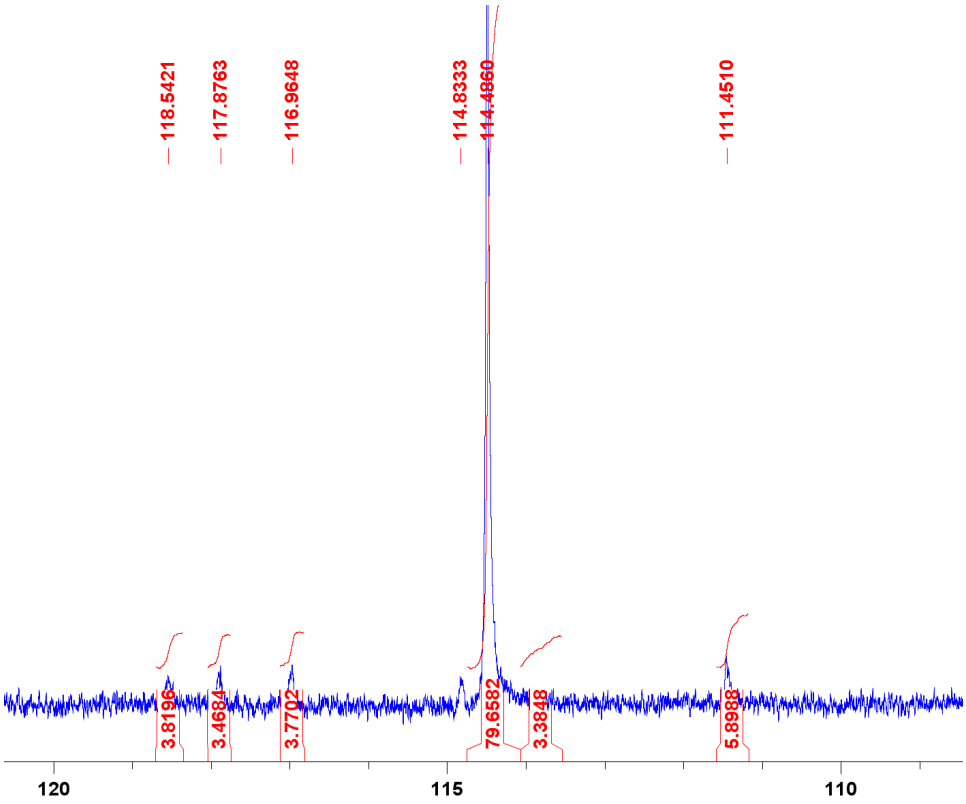

Figure 5.9: ^{31}P NMR (161.6 MHz, C_6D_6) spectrum of [5.4·$Zr(Bn)_2$].

Attempts to isolate the alkyl-zirconium complexes also failed. The products proved to be highly soluble in all organic.

Attempts to form complexes using other Zr^{IV} starting materials were also unsuccessful. Using the reactions of the lithiated starting materials **5.4** and **5.5** with a variety of chloro- and alkyl-bearing Zr centres only decomposition of the phosphazanes was observed. A summary of the different complexes used as starting materials is shown in Table 5.4.

Table 5.4: Zr complexes tested with lithiated bis(amino)cyclophosphazanes 5.5 and 5.6.

Zr complex	Ligand	Outcome
$ZrNMe_2Cl_2$	**5.5**/**5.6**	Decomp
$ZrCl_4$	**5.5**/**5.6**	Decomp
$Zr(CH_2TMS)_2Cl_2$	**5.5**/**5.6**	Decomp
$Zr(CH_2TMS)_2(NMe_2)_2$	**5.5**/**5.6**	Decomp
$Zr(CH_2Ph)_2Cl_2$	**5.5**/**5.6**	Decomp

The decomposition was apparent in *in situ* ^{31}P NMR spectroscopic studies, as multiple signals appearing throughout the spectrum due to complete break-up of the phosphazane ring. This is similar to the observations made by Repo *et al.* that the lithiated bis(amino)cyclophosphazanes do not form complexes with $TiCl_4$ or $ZrCl_4$ except in the case of the tertiary butyl amino-substituted [P(μ-N^{t}Bu)LiN^{t}Bu]$_2$.[30] This is attributed to the strong Lewis acidity of the tetrachlorides, which might attack the P-N bonds leading to destruction of the P_2N_2 unit. In our case, the presence of nucleophilic groups on the Zr centres as well as the Lewis acidity of the metals could lead to decomposition.

5.4 Conclusions

The tendency of zirconium bis(amido) complexes to be both moisture and thermally unstable is a strong limiting factor in terms of their applications. Typical purification methods such as column chromatography are not feasible, especially with the presence of a P^{III} centre on the P_2N_2 ring. Due to the impurities in the precatalyst alkyl complexes and the inability to isolate chiral species, olefin polymerisation reactions were not attempted. Although there is no doubt that the species would show some activity due to the presence of an active zirconium centre, there was no means of obtaining chiral control or selectivity towards forming isotactic or syndiotactic polymers.

Attempts to form the more thermally-stable titanium analogues led to incomplete complexation reactions even at higher temperatures. It was only possible to achieve at most 60% spectroscopic conversion by ^{31}P NMR and no separation of the remaining ligand from the metal complexes could be achieved.

Bis(amino) cyclophosphazanes have more recently been shown to form complexes with later transition metals.[168] The novel ligands presented here could therefore be of interest in late transition metal studies, where the increased thermal stability might allow for the clean formation of catalyst precursor complexes.

6. Conclusions and Further Work

6. Conclusions and Further Work

6.1 Conclusions

The broad aim of this thesis has been to explore the coordination and supramolecular chemistry of phospha(III,V)azanes. Chapter 2 presented the synthesis of key dimeric starting materials [ClP(μ-NR)]$_2$ for later synthetic elaboration. In Chapter 3, it was shown that the reaction of *in situ* generated LiSH with these chloro-phosphazanes gave the P^V species [S=P(H)(μ-NR)]$_2$. Interestingly, the ratio of *cis* to *trans* isomers of these species strong dependency on the R group of the phosphazane. Deprotonation of one of these new P^V precursors, [S=P(H)(μ-N^{t}Bu)]$_2$ (**3.1**), with *s*-block organometallic bases led to the formation of the new dianion [S-P(μ-N^{t}Bu)]$_2^{2-}$ (**3.5**). Structural studies suggest that this dianion has a versatile nature of this ligand due to the presence of hard (N) and soft (S) donor atoms. In Chapter 4, it was shown that oxidation of **3.5** with chalcogens gave the P^V dianions [S-P(=E)(μ-N^{t}Bu)]$_2^{2-}$ (E = S, Se, Te). These were shown to be robust ligands to a selection of main group and transition metal ions and excellent precursors for the formation of macrocyclic compounds. Finally, in Chapter 5 the use of phosphazane ligands to support single-site catalysis was investigated. The need to generate ligands of high purity for applications within pre-catalysts was highlighted.

6.2 Further work

The formation of the Na^+ metal salt of the P^{III} dianion **3.5** showed the potential of these species to form clusters and stabilise large architectures. The coordination of transition metal atoms has not, however, been successful to date, mainly due to the highly reducing nature of this dianion. Other methods of generating transition metal complexes could also be explored. For example, organo-transition metal bases could be used to deprotonate [S=P(H)(μ-N^{t}Bu)]$_2$ (**3.1**) (such as Cp_2Mn, Cp_2Cr, Cp_2Fe). Preliminary studies have shown that reaction of **3.1** with one equivalent of Cp_2Cr in thf gives a deep green solution however no product could be isolated, and due to the paramagnetic nature of the

metal centre no reliable NMR data could be obtained. The colour of the solution however implies the formation of a metal complex and the presence of an oxidised Cr centre. Isolation and crystallisation of the product would be necessary to determine its nature and might give a better indication of the validity of this route.

The formation of large cage compounds may also be possible using the P^V dianions $[S\text{-}P(=E)(\mu\text{-}N^tBu)]_2^{2-}$ (E= S, Se, Te). These new ligand sets provide the potential means of generating a range of new magnetic molecules and single molecular magnets. To date, only monomeric species have been observed from reactions with $[S\text{-}P(=E)(\mu\text{-}N^tBu)]_2^{2-}$; however, due to their increased stability over the P^{III} congeners they make attractive starting points for immediate future work. Considering the formation of stable Au and Ni complexes (**4.6** and **4.7**) containing organophosphorus ligands it is possible that using less bulky ligands might allow for aggregation, in a manner similar to the coinage metal bridged macrocycles observed by Chivers *et al*.[147]

Now that a series of simple methods have been developed for the synthesis of a range of phosphazane macrocycles, there is a clear potential for expanding the coordination of host-guest chemistry of these species. Further studies could involve not only the investigation of the complexation behaviour of these new macrocycles but also the gas absorption properties of these species, bearing in mind the presence of large molecular cavities in the solid state structures. Immediate work should focus on the generation of oxygen oxidised dianions (using HOOH or other peroxide) and the completion of the series to form the oxygen or sulfur bridge macrocycles (Scheme 6.1).

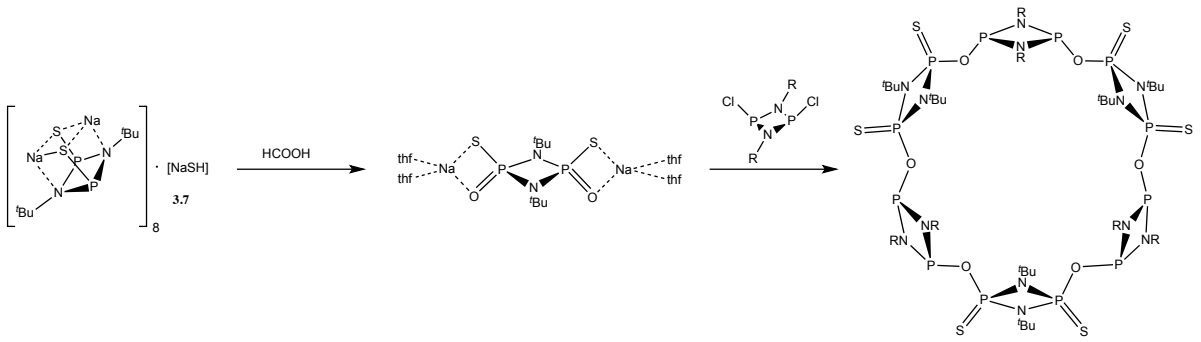

Scheme 6.1: Synthetic pathway to form oxygen bridged macrocycles. Bridging could equally occur *via* the sulfur atoms.

Once the chalcogen series is established a systematic approach to make different macrocycles containing not only different linker atoms but a variety of R groups should be undertaken. This study should focus on key R groups such as the ones already shown to form macrocycles in this study, which would provide a large library of matching/mismatching macrocycles. The presence of chiral and non-chiral R groups will be especially interesting with regards to any host/guest chiral selectivity.

In the case of the bis(amido) species presented in Chapter 5, a further avenue of research concerns switching to P^V ligand frameworks from P^{III}. Indeed, a very recent study by Stahl *et al*. showed that oxidation of bis(amido)cyclophosph(III)azane metal complexes with elemental sulfur was possible, and led to increased stability and activity in polymerisation studies (Scheme 6.2).[169]

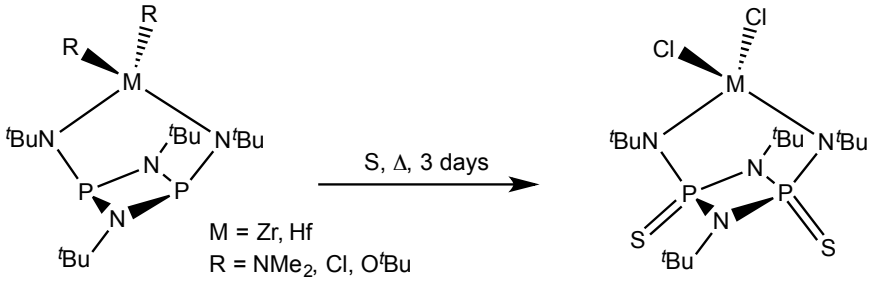

Scheme 6.2: Synthesis of the phosph(V)azane Zr/Hf metal complexes according to Stahl *et al.*

It is likely that any future developments in the area of ligands to support single-site catalysis will take advantage of P^V derivatives.

7. Experimental

7. Experimental

7.1 General Considerations

Inert atmosphere techniques

Compounds presented in this work were potentially air and moisture sensitive. P^{III} compounds are particularly susceptible to oxidation by atmospheric H_2O or in the presence of undried organic solvent. Standard inert atmosphere techniques were therefore used throughout this work.[170] All samples were stored under an inert dry-N_2 environment unless stated otherwise. Manipulations and synthesis were carried out using standard Schlenk techniques as well as in a dry-N_2 purged glovebox (Saffron Mk 2).

Starting materials and solvents

All commercially obtained solvents (toluene, thf, *n*-pentane, *n*-hexane, DCM, Et_3N) were freshly distilled from stills containing appropriate drying agents (Na/benzophenone/CaH_2) and liquid starting materials (PCl_3, amines, donors *etc*) were dried prior to use (CaH_2/Na/4.2 Å Mol Sieves) and handled under inert atmosphere at all times unless stated otherwise. This was particularly important for all primary amines, which even when provided as 99% pure required refluxing over CaH_2 followed by distillation under reduced pressure in order to avoid contamination through various amine decomposition species.

Elemental Analysis

C, H, N and Cl analysis were carried out on an Exeter Analytical CE-440 Elemental analyser. 1-2 mg of sample was sealed in pre-weighed aluminium boats under inert atmosphere using a press inside the glove box.

Mass spectroscopy

Mass spectra and high resolution mass spectra were measured by the University of Heidelberg Mass Spectrometry Facility. High-resolution mass spectra were acquired on Bruker ApexQe hybrid 9.4 T FT-ICR (ESI) and JEOL JMS-700 magnetic sector (FAB, EI, LIFDI) spectrometers

IR spectroscopy

Air stable samples were tested either on a Perkin Elmer FT-IR spectrometer fitted with an ATR head. Air sensitive samples were suspended in Nujol using a pestle and mortar and held between NaCl windows which were carefully wrapped in parafilm and quickly transferred to the spectrometer.

Nuclear Magnetic Resonance

Samples were either prepared in the glove box using pre dried spectroscopic grade deuterated solvents and sealed with tight fitting caps further wrapped in parafilm, or under air using standard techniques. *In situ* studies were carried out using Young's NMR tubes containing deuterated solvent, or reaction aliquots with a d_6-acetone capillary.

^{1}H, $^{31}P\{^{1}H\}$, $^{119}Sn\{^{1}H\}$, $^{77}Se\{^{1}H\}$ and $^{125}Te\{^{1}H\}$ NMR spectra were recorded on a Bruker Advance 400 QNP or Bruker Advance 500 MHz cryo spectrometer. All spectra were recorded with $SiMe_4$ (^{1}H), H_3PO_4 (^{31}P, 85% in D_2O), Me_4Sn (^{119}Sn, 90% in C_6D_6), Selenoxanthenone (^{77}Se, 0.1M, $CDCl_3$) and Me_2Te (^{125}Te, 0.1M, $CDCl_3$) as internal standards. All spectra were recorded at ambient temperature (298 K) unless stated otherwise.

X-ray diffraction studies

All compounds reported in this thesis were collected at low temperature (-180 K) in order to minimise lattice vibrations. Crystals were grown *via* a variety of methods as detailed in the experimental section. Crystals were held in place using perfluorinated polyether oil and cooled using a dry nitrogen gas stream.

Data were collected on a Nonius KappaCCD diffractometer, using graphite-monochromated MoKα radiation (λ = 0.7107 Å) or on a Bruker D8-QUEST diffractometer using an Incoatec IμS Cu microsource (λ = 1.5418 Å). Structures were solved using SHELXT[171] and refined using SHELXL[172] Structures were solved using direct methods[171] (unless stated otherwise) and refinements were by full matrix least squares techniques.[173] Images and minor refinements were also made using the Olex2 suite.[174]

7.2 Synthesis of Chlorophosphazanes and Standard Reagents

7.2.1 Synthesis of Chlorophosphazanes

Dichlorophosphazanes $[ClP(\mu\text{-}NR)]_2$ (**2.1-2.9)** were synthesised according to two general procedures (**GP 1** and **GP 2**, Scheme 7.1) depending on the R groups, with a modified procedure for **2.1** due to the large scale of the preparation.

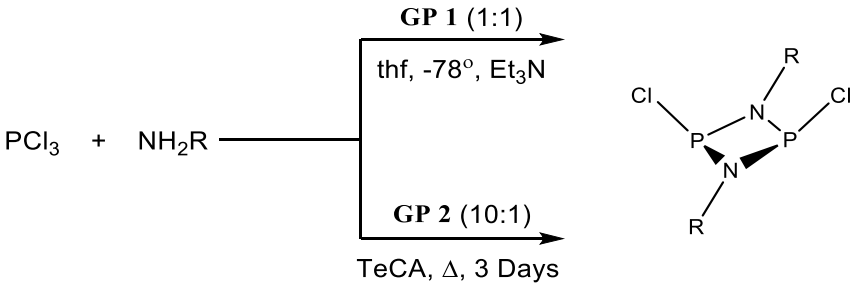

Scheme 7.1: Summary of synthetic routes to dichlorophosphazanes according to general procedures 1 and 2.

Synthesis of $[ClP(\mu\text{-}N^tBu)]_2$ (2.1)

An overhead stirrer was mounted on a 2L 3-neck flask fitted with a dropping funnel and a tap-adapter. PCl_3 (30 ml, 342 mmol) was added slowly to a solution of Et_3N (473ml (10 equiv.)) in thf (700 ml) at -78 ºC (so as to avoid excessive Et_3NHCl formation). ^{t}Butyl amine (36.1 ml, 342 mmol) was added dropwise with stirring and the solution was allowed to warm to ambient temperature slowly over 12hrs. A thick precipitate of Et_3NHCl was filtered off and washed with thf (3 x 50ml). The thf was removed and the residue taken in 200ml of toluene and filtered once more over celite to remove any trace salts. The toluene was removed *in vacuo* and the residue distilled carefully under vacuum. The resulting fluffy white powder was heated until dissolved and left to warm slowly to ambient temperature to afford **2.1** as large clear crystals (30 g, 64%).

General synthesis of Dichlorophosphazanes (General Procedure 1) $[ClP(\mu\text{-}NR)]_2$:

A stirred solution of Et_3N (10 equiv.) in thf was cooled to -78 ºC and PCl_3 (1 equiv.) added dropwise. Primary amine (1 equiv.) was added dropwise with vigorous stirring and the mixture left to warm to ambient temperature slowly overnight. The solution was filtered and the solvent removed under

reduced pressure. The white residue was taken in toluene and filtered to remove trace Et_3N. The toluene was removed under reduced pressure until precipitation of the product. Removal was continued well past precipitation and the suspension heated back into solution. Storage overnight at 5 ºC gave one crop of crystalline material. The remaining toluene solution was decanted off, and the material washed with *n*-pentane. Subsequent concentrations/crystallisations of the toluene solution yielded two more batches of the product as a crystalline white powder (typical yield of all batches ~80%).

General synthesis of Dichlorophosphazanes (General Procedure 2) [ClP(μ-NR)]$_2$:

PCl_3 (10 equiv.) and 1,1,2,2-tetrachloroethane (20 ml) were added to a flask fitted with a reflux condenser. Primary amine was added slowly at low temperature (0 ºC) and the mixture heated to reflux for 3 days. Due to the corrosive nature of PCl_3 frequent regreasing of the joints as well as the use of a Teflon tape seal was required. Removal of the excess solvent and PCl_3 *in vacuo* gave a slimy yellow mixture (it is important not to overheat the flask, as PCl_3 combusts spontaneously >80 ºC under reduced pressure). Extraction of this residue with toluene and filtration over Celite followed by removal of the solvent gave the product as a white powder. Recrystallisation from toluene gave a crystalline product.

[ClP(μ-NBenz)] (2.2)

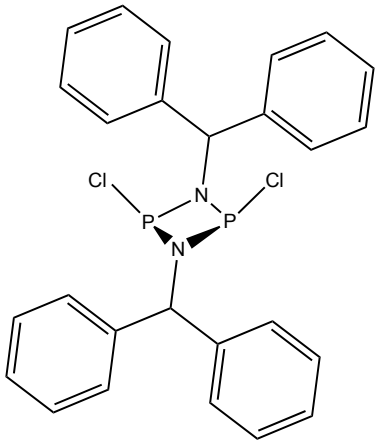

Synthesised according to **GP 1**

Crystallised from saturated toluene solution at -12 ºC yield: 40%

Purity verified by ^{1}H and ^{31}P NMR against literature material.[24]

[ClP(μ-NCH$_2$^{t}Bu)]$_2$ (Neopentyl) (2.3)

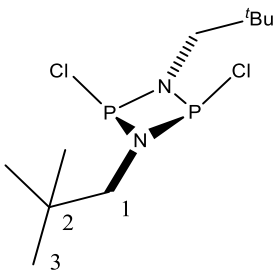

Synthesised according to **GP 1**, The solvent was then evaporated yielding a yellow oil. The crude product was purified *via* distillation in vacuo (0.5 mbar, 140 ºC). Crystalline material was obtained by sublimation.

Yield: 3.35 g colourless solid (11.1 mmol, 28%)

^{1}H NMR (400.13 MHz, C$_6$D$_6$, 298 K): δ (ppm) = 0.77 (s, 18H, CH$_3$), 2.60 (t, $^3J_{P\text{-}H}$ = 12Hz, 4H. CH$_2$)

^{13}C{^{1}H} NMR (100.61 MHz, C$_6$D$_6$, 298 K): δ (ppm) = 27.37 (t, $^4J_{CP}$ = 2.4 Hz, 6C, C-3), 32.02 (t, $^3J_{CP}$ = 2.5 Hz, 2C, C-2), 55.88 (t, $^1J_{PC}$ = 5.9 Hz, 2C, C-1)

^{31}P{^{1}H} NMR (161.96 MHz, C$_6$D$_6$, 298 K): δ (ppm) = 240.89 (s).

[ClP(μ-NC$_{12}$H$_9$)]$_2$ (2-Biphenyl) (2.4)

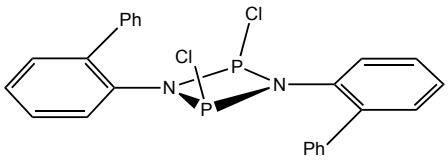

Synthesised according to **GP 1**.

Crystallised from saturated toluene solution at -12 ºC

Yield: 65%

Purity verified by ^{1}H and ^{31}P NMR against literature material.[24]

[ClP(μ-N(2-napthyl)]$_2$ (2.5)

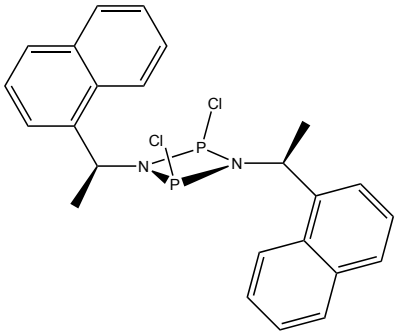

Synthesised according to **GP 1.**

Yield: 25%

Purity verified by ^{1}H and ^{31}P NMR against literature material.[24]

[ClP(μ-NMes)]$_2$ (2.6)

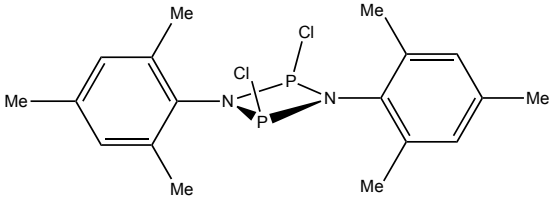

Synthesised according to **GP 1.**

Crystallised from saturated toluene solution at -12 ºC

Yield: 75%

Purity verified by ^{1}H and ^{31}P NMR against literature material.[22]

[ClP(μ-NDipp)]$_2$ (2.7)

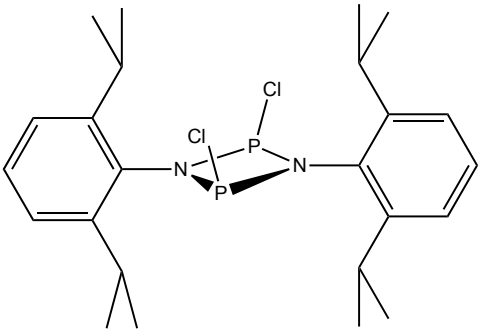

Synthesised according to **GP 1**

Crystallised from saturated toluene solution at -12 ºC.

Yield: 40%

Purity verified by ^{1}H and ^{31}P NMR against literature material.[24]

[ClP(μ-$NC_7H_6O_2$)]$_2$ (2.8)

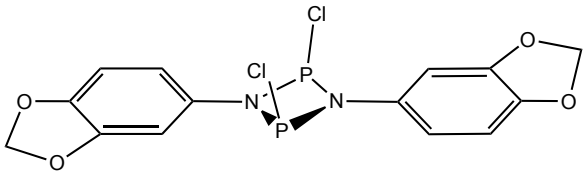

Synthesised according to **GP 2**

Yield: 41%

^{1}H NMR (400.13 MHz, C_6D_6, 298 K): δ (ppm) = 6.53 (2H, d, ^{1}J = 8.2Hz, H1), 5.98 (2H, d, ^{3}J = 2.14 Hz, H2), 5.72 (2H, dd, ^{2}J = 8.2; ^{3}J = 2.14, H3)

^{13}C{^{1}H} NMR (100.61 MHz, C_6D_6, 298 K): δ (ppm) = 97.92 (s, 2C, CH_2), 100.52 (s, 2C, Ar-C1), 106.66 (s, 2C, Ar-C1), 108.76 (s, 2C, Ar-C1), 140.43 (s, 2C, qAr), 142.39 (s, 2C, qAr), 148.73 (s, 2C, qAr)

^{31}P{^{1}H} NMR (161.96 MHz, C_6D_6, 298 K): δ (ppm) = 211.56 (s).

[ClP(μ-$NC_{10}H_{13}$)]$_2$ (4-^{t}BuPh) (2.9)

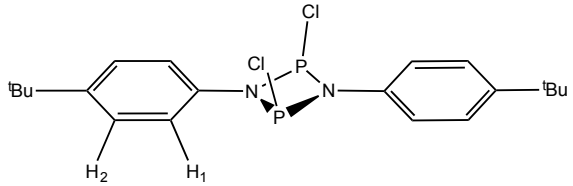

^{1}H NMR (400.13 MHz, C_6D_6, 298 K): δ (ppm) = 7.17 (2H, d, ^{2}J = 8.0 Hz, H1), 7.02 (2H, d, ^{2}J = 8.1 Hz, H2), 1.16 (s, ^{t}Bu)

^{31}P{^{1}H} NMR (161.96 MHz, C_6D_6, 298 K): δ (ppm) = 201.31 (s).

2.9 was synthesised according to a **General Procedure 2:**

Preparation adapted from work by Robert Zahn: 4-tert-butyl-Aniline (4 g, 1 equiv.) was added to a solution of PCl_3 (excess) in 1,1,2,2 tetrachloroethane (20ml) and heated to reflux for 2 days. The remaining solvent and PCl_3 was removed *in vacuo* and the resulting slurry extracted with toluene. The toluene fraction was filtered and the solvent removed until precipitation of a brown precipitate. This was heated back into solution and left to crystallise over night at r.t. A first batch of crystalline material was obtained (~40%) and subsequent concentrations/crystallisations of the remaining toluene solution yielded two more batches of the product as a crystalline white/brown powder (typical yield of all batches ~80%).

Synthesis of [(^{t}BuNH)P(μ-N^{t}Bu)$_2$PCl] (3.6)

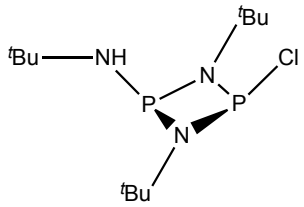

PCl_3 (12.5 ml, 143 mmol) was added dropwise to a stirred solution of ^{t}BuNH$_2$ (60 ml, 569 mmol) in thf (300 ml) at -78 ºC with immediate formation of white precipitate. The mixture was brought to ambient temperature and stirred for 1 hr before being filtered to remove ^{t}BuNH$_3$Cl. The solvent was removed under reduced pressure. The residue was extracted with toluene and filtered before removal of the toluene to give the crude product as a white powder. The crude was distilled under vacuum (86 ºC, *ca.* 0.2 mmHg) to afford the pure product as a white powder. Purity verified by comparison of literature spectroscopic data.[144]

7.2.2 Synthesis of Standard Reagents

Synthesis of BnK:

A method adapted from the literature prep of BnK by Wright *et al*. was used.[102] KO^{t}Bu (5 g, 44.56 mmol) was suspended in toluene (30 ml) and *n*BuLi (27.85 ml, 1.6M, 44.56 mmol) was added slowly with vigorous stirring. An immediate colour change to a bright red suspension was noted. The product was filtered off and washed with *n*-hexane (2 x 50 ml) and left under vacuum for 48hrs to

ensure complete dryness. Typical yield 5 g (86%), purity verified by ^{1}H and ^{7}Li NMR. The absence of any signals in the ^{7}Li NMR showed no remaining LiO^{t}Bu which can be a common contaminant in other preparations.

Synthesis of BnNa:

A method adapted from the literature prep of BnK by Wright *et al*. was used.[102] NaO^{t}Bu (5 g, 53 mmol) was suspended in toluene (30 ml) and *n*BuLi (32.52 ml, 1.6M, 53 mmol) was added slowly with vigorous stirring. An immediate colour change to a bright orange suspension was noted. The product was filtered off and washed with *n*-hexane (2 x 50 ml) and left under vacuum for 48hrs to ensure complete dryness. Typical yield 5.5 g (81%), purity verified by ^{1}H and ^{7}Li NMR.

7.3 Synthesis of Chapter 3

7.3.1 Synthesis of Novel $[S(H)P(\mu\text{-}NR)]_2$ Species

A range of novel Sulfur substituted dimers were carried out according to General Procedure 3.

General procedure 3 *n*BuLi (2 equiv. in hexanes) was added to thf (40 ml) and the solution cooled to -78 ºC. SH_2 gas was bubbled slowly though this solution for *ca.* 20 mins. The reaction was allowed to warm to ambient temperature and the thf removed completely under vacuum, to give white powder of LiSH (this step ensures excess SH_2 is removed from the reaction). The solid was resuspended in thf (40 ml) and cooled to -78 ºC. A solution of $[ClP(\mu\text{-}NR)]_2$ (1 equiv.) in thf (20 ml) was added slowly dropwise and the resulting mixture allowed to warm to ambient temperature and stirred for 72 hrs. The solvent was removed and the resulting solid was suspended in toluene (80 ml) and filtered. The solution was concentrated until the beginning of precipitation. The precipitate was gently warmed back into solution and the contents left to crystallise at -16 ºC overnight (heating over ~ 30 ºC can lead to decomposition).

1,3-di-tert-butyl-1,3,2,4-diazadiphosphetidine 2,4-disulfide [S=P(H)(μ-N^{t}Bu)] (3.1)

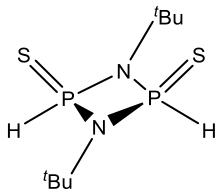

Synthesised according to **GP 3**, 1.37 g, 5mmol gave a first batch of white crystals was isolated (60%) followed by a second batch from a further concentration/crystallisation (Total yield: 1.15 g, 83%)

^{1}H NMR (500.2 MHz, $CDCl_3$, 298 K): δ (ppm)= *cis* isomer, 8.40 (2H, P-H, AA´XX´ mult. apparent J_{max} = 598 Hz), 1.38 (s., 18H, ^{t}Bu); *trans* isomer, 8.75 (P-H, AA´XX´ mult., *cis* isomer), 1.36 (s., ^{t}Bu), (ratio of *trans* : *cis* ≈ 1 : 50 from P-H integration)

^{31}P NMR (161.7 MHz, $CDCl_3$, 298 K): δ (ppm) = 36.3 (AA´XX´ mult., *cis* isomer), 40.7 A´XX´ mult., *trans* isomer)

IR (NaCl windows, Nu*J*ol mull), ν/cm^{-1} = 2360 (m) (P-H str.), 762 (s) (P=S str.)

Elemental Analysis (%): Calcd. 35.4, H 7.4, N 7.9; cald. for **3.1**, C 35.5, H. 7.5, N. 10.4

3.2, **3.3**, and **3.4**; The synthetic route employed was exactly the same as for **3.1** (**GP 3**) but immediately after the addition of the dimer the reactions were allowed to warm to ambient temperature. At this point, the solvent was removed under vacuum and the solid extracted in the same manner as for **3.1**.

1,3-bis(2,6-diisopropylphenyl)-1,3,2,4-diazadiphosphetidine 2,4-disulfide [S=P(H)(μ-Dipp)] (3.2)

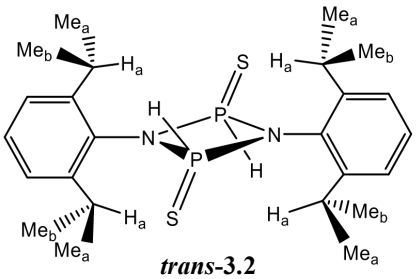

***trans*-3.2**

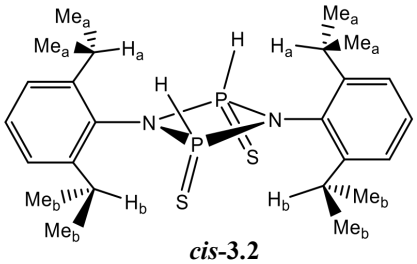

***cis*-3.2**

Yield: 200 mg of [ClP(μ-NDipp)]$_2$ (**2.5**), 30 mg of **3.2** produced after further crystallisation from *n*-pentane, 15%. Crystals of *trans*-**3.2** were grown from *n*-pentane at -16 ºC. Unit cell analyses of crystalline samples indicate that only the *trans* isomer crystallises under these conditions.

^{1}H NMR (500.2 MHz, d_8-toluene, 298 K): δ (ppm) = *cis* isomer 9.04 (mult., J_{max} = 593 Hz), 4.30 (sept., CH_b Dipp), 3.00 (sept., CH_a Dipp), 1.40 (d, Me Dipp), 0.86 (d, Me Dipp); *trans* isomer, 9.32 (mult., J_{max} = 591 Hz), 3.78 (sept., CH Dipp), 1.10 (d, Me Dipp), 0.98 (d, Me Dipp)

^{31}P NMR (161.7 MHz, d_8-toluene, 298 K): δ (ppm) = 53.1 (second-order mult., *trans* isomer, apparent $^{1}J_{P\text{-}H}$ = 594 Hz), 45.05 (second-order mult., *cis* isomer, apparent $^{1}J_{P\text{-}H}$ = 591 Hz) (ratio of *trans* : *cis* ≈ 1 : 1)

1,3-dimesityl-1,3,2,4-diazadiphosphetidine 2,4-disulfide [S=P(H)(μ-Mes)] 3.3

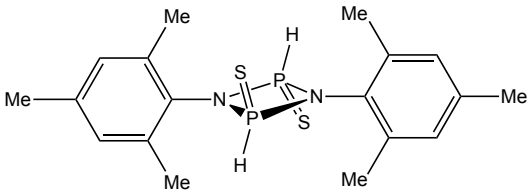

***trans*-3.3**

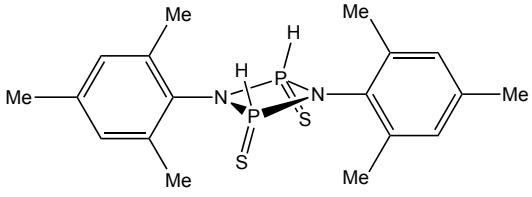

***cis*-3.3**

(200 mg of [ClP(μ-NMes)]$_2$, 0.144 g of **3.3** produced, 73%), crystals of *trans*-**3.3** were grown from *n*-hexane/thf at ambient temperature. Unit cell analyses of crystalline samples indicate that only the *trans* isomer crystallises under these conditions.

^{1}H NMR (500.2 MHz, d$_8$-toluene, 298 K): *cis* isomer, δ (ppm) = 9.07 (2H, mult., P-H *cis,* J_{max} = 592Hz), 6.72 (2H, s., C-H$_{aryl}$ Mes *cis*, 6.61 (2H, s, C-H$_{aryl}$ Mes *cis*) 3.03 (s., 6H, *o*-Me Mes *cis*), 2.08 (s., 12H, *p*-Me Mes *cis* and *trans*), 1.95 (s., 6H, *o*-Me Mes *cis*); *trans* isomer, δ(ppm) = 9.29 (2H, mult., P-H *trans,* J_{max} = 593 Hz), 6.65 (4H, s, C-H$_{aryl}$ Mes), 2.47 (12H, s, *o*-Me Mes *trans*)

^{31}P NMR (161.7 MHz, d$_8$-toluene, 298 K): δ (ppm) = 44.6 (second-order mult., *trans* isomer, apparent $^1J_{P-H}$ = 594 Hz; ^{31}P{1H} d., $^2J_{P-P}$ 2.0 Hz), 36.7 (second-order mult., *cis* isomer, apparent $^1J_{P-H}$ = 593 Hz) (ratio of *trans* : *cis* ≈ 1 : 1)

X Ray Data:

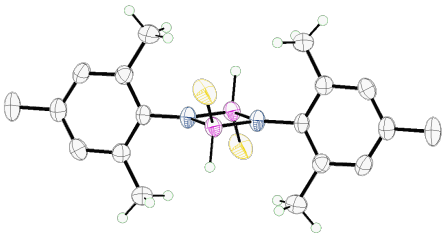

Empirical formula	$C_{18}H_{24}N_2P_2S_2$
Formula weight	394.45
Temperature/K	180(2)
Crystal system	monoclinic
Space group	$P2_1/c$
a/Å	10.4215(3)
b/Å	11.0475(3)
c/Å	9.3492(3)
α/°	90
β/°	109.462(2)
γ/°	90
Volume/Å^3	1014.89(5)
Z	2
ρ_{calc}g/cm^3	1.291
μ/mm^{-1}	3.878
F(000)	416
Crystal size/mm^3	0.190 × 0.090 × 0.060
Radiation	CuKα (λ = 1.54178)
2Θ range for data collection/°	9 to 133.186
Reflections collected	13746
Independent reflections	1755 [R_{int} = 0.0492, R_σ = 0.0319]
Data/restraints/parameters	1755/4/125
Goodness-of-fit on F^2	1.048
Final R indexes [I>=2σ (I)]	R_1 = 0.0456, wR_2 = 0.0941
Final R indexes [all data]	R_1 = 0.0647, wR_2 = 0.1095
Largest diff. peak/hole / e Å^{-3}	0.31/-0.36

The crystal structure of **3.3** contains a minor disorder component for the $[S=(H)PN]_2$ core:

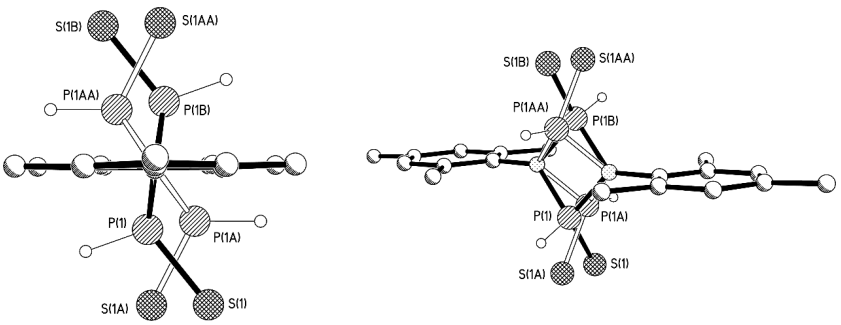

Major component: P(1),S(1),P(1B),S(1B) (suffix B generated from P(1),S(1) by inversion centre), solid bonds: site occupancy factor 0.923(3), dihedral angle between N_2P_2 plane and Mes plane 82.2°.

Minor component: P(1A),S(1A),P(1AA),S(1AA) (suffix AA generated from P(1A),S(1A) by inversion centre), open bonds: site occupancy factor 0.077(3), dihedral angle between N_2P_2 plane and Mes plane 55.6°. P(1A) and S(1A) were refined with isotropic displacement parameters.

Both conformations have (approximate) C_{2h} point symmetry.

This type of disorder was observed frequently in crystals of **3.2** and **3.3**.

1,3-dibenzhydryl-1,3,2,4-diazadiphosphetidine 2,4-disulfide [S=P(H)(μ-Benz)]$_2$ (3.4)

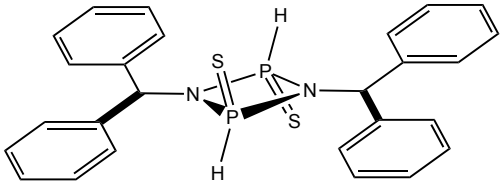

Synthesised according to **GP 3.**

Yield: 200mg of [ClP(μ-NCHPh$_2$)]$_2$, 0.109 g of **3.4** produced, 55%.

^{1}H NMR (500.2 MHz, $CDCl_3$, 298 K): δ (ppm) = 7.44 (2H, P-H, AA´XX´ mult. apparent J_{max} = 550 Hz), 6.9-7.7 (overlapping mult. Ph of Ph_2CH), 5.62 (dd., Ph_2CH)

^{31}P NMR (161.7 MHz, $CDCl_3$, 298 K): δ (ppm) = 40.0 (second-order mult., *trans* isomer, apparent $^1J_{P\text{-}H}$ = 556 Hz), 38.2 (br. d., *cis* isomer, apparent $^1J_{P\text{-}H}$ = 579 Hz) (ratio of *trans* : *cis* ≈ 9 : 1)

Synthesis of [Mg(3.5)·2thf] (3.6)

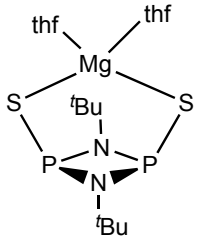

A solution of Bu_2Mg (0.185 ml, 0.5M in heptane, 92 mmol) was added to a solution of **3.1** (50 mg, 0.18 mmol) in thf (5 ml) at -78 ºC. The solution was warmed to ambient temperature with stirring and then solvent removed under vacuum. The resulting foamy powder produced was washed with *n*-pentane under vigorous stirring (2x10 ml) and the solid residue was suspended in toluene (10 ml) with

the slow addition of thf (ca 2 ml) and gentle heating until the powder was dissolved. The product crystallises as colourless clear crystals after storage at -12 ºC (16h).

Yield: 56 mg, 70%

^{1}H NMR (500.2 MHz, d_8-thf, 298 K): δ (ppm) = 3.61 (7.5H, bs, CH_2-thf), 1.75 (9.3H, br.s, CH_2-thf), 1.32 (18H, s, ^{t}Bu)

^{31}P NMR (161.7 MHz, d_8-thf, 298 K) δ (ppm) = 186.5 (br.s)

Elemental Analysis (%): Calcd. C, 44.0; H, 7.8; N, 6.4. Measured; C,43.8; H, 8.1; N, 5.3.

Synthesis of [Na_{16}(3.5)$_8$·NaSH·8thf] (**3.7**)

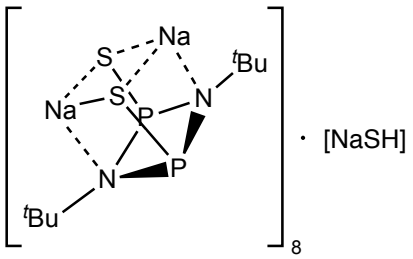

A solution of NaBn (84.43 mg, 0.74 mmol) in thf (10 ml) was added dropwise to a stirred solution of **3.1** (100 mg, 0.37 mmol) in thf (10 ml). A deep blue colour was generated initially but as addition continued this gave way to a clear solution. After stirring at ambient temperature for 1 h, storage at -12 ºC (16 h) gave colourless crystals of **3.7**. If the solvent was removed before crystallisation and the resulting powder washed with *n*-hexane (2 x 10 ml), 3 was obtained as a white powder (quantitative yield).

FTIR (Nujol): 2579 (S-H str)

^{1}H NMR (500.2 MHz, d_8-thf, 298 K): δ (ppm) = 3.4 (1.4 H, s, Na-SH) 1.29 (144H, s, ^{t}Bu)

^{31}P{^{1}H} NMR (161.7 MHz, d_8-thf, 298 K): δ (ppm) = 190.9 (s)

Elemental Analysis (%): Calcd**.** C, 36.6; H, 6.7; N, 7.1 Found C, 36.2; H, 6.6; N 5.1. Low nitrogen content probably due to metal nitride formation, as previously documented.[39]

X-Ray Data:

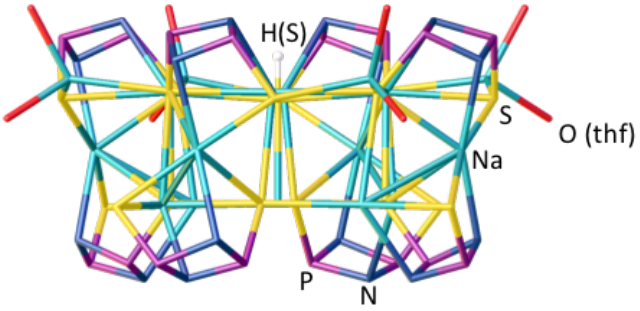

Empirical formula	$C_{96}H_{209}N_{16}Na_{17}O_8P_{16}S_{17}$
Formula weight	3147.15
Temperature/K	180(2)
Crystal system	tetragonal
Space group	P4*cc*
a/Å	23.7918(2)
b/Å	23.7918(2)
c/Å	37.5449(6)
α/°	90
β/°	90
γ/°	90
Volume/Å^3	21252.3(5)
Z	4
ρ_{calc}g/cm^3	0.984[a]
μ/mm^{-1}	0.365
F(000)	6640
Crystal size/mm^3	0.210 × 0.180 × 0.140
Radiation	MoKα (λ = 0.71073)
2Θ range for data collection/°	7.062 to 44.962
Reflections collected	39076
Independent reflections	12141 [R_{int} = 0.0877, R_σ = 0.0824]
Data/restraints/parameters	12141/197/769
Goodness-of-fit on F^2	1.027
Final R indexes [I>=2σ (I)]	R_1 = 0.0725, wR_2 = 0.1916
Final R indexes [all data]	R_1 = 0.1068, wR_2 = 0.2156
Largest diff. peak/hole / e Å^{-3}	0.34/-0.39
Flack parameter (Parsons)	-0.01(7)

[a] The SQUEEZE algorithm (Spek, 2015) has been applied to handle diffuse solvent regions.[140]

The crystals diffracted weakly, and the data set used for refinement is limited to 0.95 Å resolution. Numerous crystals were examined, also using the Cu microsource of the D8-QUEST instrument. The same unit cell was always obtained, but the MoKα data set produced the best refinement result. Numerous restraints are applied to the ^{t}Bu groups and coordinated thf molecules:

- N–C(CH_3)$_3$ bond distances 1.50(1) Å
- C–C bond distances in ^{t}Bu 1.54(1) Å

- C···C distances in ^{t}Bu 2.51(1) Å
- C–C and C–O bond distances in thf 1.48(1) Å
- ISOR restraint (esd 0.01) on C atoms of thf

The SH group is assigned on the basis of the additional characterisation information, as described in the main manuscript. For charge balance, the atom/group at the site must have a 1– charge. The refinement could be made equally well with Cl assigned, but this is ruled out by the elemental analysis. With the SH group independently identified, the H atom was placed on the 4-fold rotation axis (for both independent complexes) with S–H = 1.20 Å; only the *z* coordinate needs to be specified. The coordinates of these Hydrogen atoms were not refined in the final cycles, so small shifts in the S coordinates mean that the final S–H distances deviate slightly from the specified 1.20 Å.

There are two independent complexes in the structure, lying on crystallographic 4-fold axes, with basically identical geometry (aside from minor variations in the coordinated thf positions). An overlay of the two molecules (coloured red and blue) is shown:

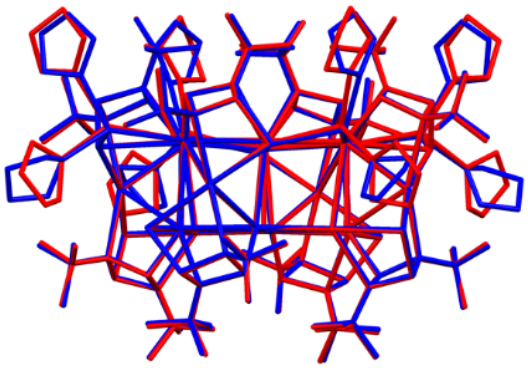

The structure contains substantial void space (SQUEEZE estimate, 1.2 Å probe radius = 6652 Å^3 = *ca* 30% of the unit-cell volume), within which it was not possible to resolve any solvent (thf) molecules. The SQUEEZE procedure has therefore been applied.[140] The procedure corrects for 3205 electrons per unit cell in voids, which corresponds to 80 thf molecules (C_4H_8O = 40 electrons). This is approximately consistent with the available void space, giving 6652 / (80*5) = 16.6 Å^3 per non-H atom.

The absolute structure, assessed using the quotient method of Parsons, is satisfactorily determined.

Synthesis of [K(3.5)] (3.8)

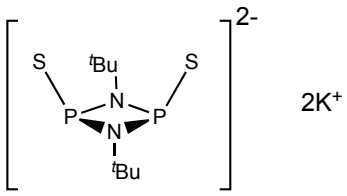

A solution of KBn (98 mg, 0.74 mmol) in thf (10 ml) was added dropwise to a stirred solution of **3.1** (100 mg, 0.37 mmol) in thf (10 ml). The deep orange solution quickly gave way to a clear solution. The solution was stirred for 2hrs during which a snow white precipitate formed. This powder was washed with *n*-pentane (2 x 10 ml) and with thf (15 ml) to yield the product as a white powder soluble only in DMSO and sparingly in acetonitrile and DMF.

Yield: quantitative.

^{1}H NMR (500.2 MHz, d_8-thf, 298 K): δ (ppm) = 1.29 (18H, s, ^{t}Bu).

^{31}P{^{1}H} NMR (161.7 MHz, 298 K): d_8-thf: δ (ppm) = 191.62 (broad s). d_6- DMSO: δ (ppm) = 188.06 (sharp s).

Elemental Analysis (%): Calcd**.** C, 27.73; H, 5.24; N, 8.08; Found; C, 27.80; H, 5.30; N, 7.50

Synthesis of [S=(H)P(μ-N^{t}Bu)$_2$P]$_2$(μ-S) (3.9)

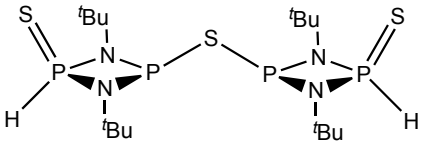

A solution of **3.7** was prepared *in situ* by the deprotonation of **3.1** (100 mg, 0.36 mmol) in thf (20 ml) with BnNa (2 equivalents). This solution was then added to solid of $ZnCl_2$ (49 mg, 0.36 mmol) at r.t. The solution stirred (1 h) during which a white precipitate formed that was filtered off. Evaporation of the solvent yielded **3.9** as a colourless solid. NMR evidence suggested that **3.9** was not isolated as a pure compound.

^{1}H NMR (500.2 MHz, CD_3CN, 298 K): δ (ppm) = 8.52 (2H, dd, $^{2}J_{P\text{-}H}$ = 555 Hz, $^{3}J_{P\text{-}H}$ = 4 Hz, PH) ,1.41 (s, 36H, ^{t}Bu)

$^{31}P\{^{1}H\}$ NMR (161.7 MHz, CD_3CN, 298 K): δ (ppm)= 134.8 (d, $^{2}J_{P\text{-}P}$ = 15 Hz, P^{III}), 44.3 (d, $^{2}J_{P\text{-}P}$ = 15 Hz, P^{V})

Synthesis of [S=(H)P(μ-^{t}Bu)$_2$PNH^{t}Bu] (3.11)

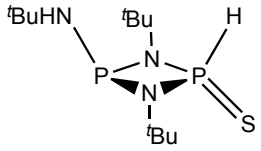

*n*BuLi (3.1 ml, 5 mmol, 1.6 M in *n*-hexane) was added to thf (40 ml) and the solution cooled to −78 ºC. H_2S gas was bubbled slowly though this solution for *ca.* 10 min. The reaction was allowed to warm to ambient temperature and the solvent and remaining gas removed completely under vacuum to give a white powder of LiSH. The solid was redissolved in thf (40 ml) and cooled to −78 ºC. A solution of **3.6** (1.55g, 5 mmol) in thf (20 ml) was added slowly dropwise and the resulting mixture allowed to warm to ambient temperature and stirred for 30 min. The solvent was removed and the resulting solid was suspended in *n*-hexane (80 ml) and filtered. The solvent was removed until precipitation of a white solid which was then redissolved by gentle heating. Storage at -16 ºC gave **3.11** as colourless crystals (1.17g, 75%) suitable for x-ray analysis.

^{1}H NMR (500.2 MHz, C_6D_6, 298 K): δ (ppm) = 9.62 (1H, dd, $^{1}J_{P\text{-}H}$ = 532 Hz, $^{3}J_{P\text{-}H}$ = 9 Hz, PH), 2.5 (1H, bs, NH), 1.38 (s, 18H, ^{t}Bu), 0.99 (9H, d, $^{4}J_{HH}$ = 1.7 Hz, ^{t}Bu)

$^{31}P\{^{1}H\}$ NMR (161.7 MHz, CD_3CN, 298 K): δ (ppm) = 50.7 (d, $^{2}J_{P\text{-}P}$ = 4 Hz, P^{V}), 128.7 (bs, P^{III})

Elemental Analysis (%): Calcd. C 46.6; H 9.5; N 13.6; found C 46.8, H 10.0, N 13.4

Synthesis of [S=(H)P(μ-^{t}Bu)$_2$PNH^{t}Bu] (3.12)

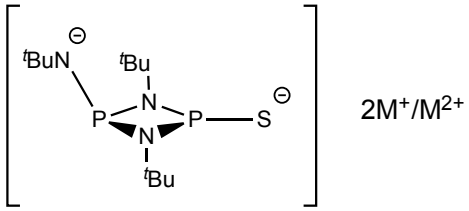

Organometallic base, Bu_2Mg (129 µl, 645 µmol, 0.5M in heptane), *n*BuLi (80.6 µl, 129 µmol, 1.6 in *n*-hexane) or solid BnNa (7 mg, 129 µmol), was added to a solution of **3.9** (20 mg, 65 µmol) in thf

(1 ml) at ambient temperature. In each case an aliquot was transferred to a Young's tap NMR tube and analysed by ^{31}P NMR spectrometry. In the case of the BnNa reaction, the solvent was left to evaporate and the sample extracted with *n*-hexane *via* a filter syringe.

Bu_2Mg: **^{31}P{^{1}H} NMR (161.7 MHz, d_8-thf, 298 K)**: = 187.3 (bs), 213.4 (bs)

Bn_2Na: **^{31}P{^{1}H} NMR (161.7 MHz, d_6-acetone capillary, 298 K)**: δ (ppm) = 152.7 (d, $^{2}J_{P\text{-}P}$ = 11 Hz, P-N), 169.7 (d, $^{2}J_{P\text{-}P}$ = 11 Hz, P-S)

*n*BuLi: **^{31}P{^{1}H} NMR (161.7 MHz, d_8-thf, 298 K)**: δ (ppm) = 188 (bs), 234 (bs)

Synthesis of [Ph_2Sn(3.5)] (3.13)

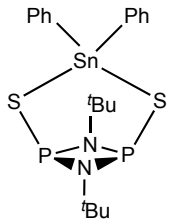

A solution of **3.6/3.7** was prepared *in situ* by the deprotonation of **3.1** (100 mg, 0.32 mmol) in thf (20 ml) with Bu_2Mg (1 equiv.) or BnNa (2 equiv.). This solution was then added dropwise to a solution of Ph_2SnCl_2 (109.4 mg, 0.32 mmol) in thf (20 ml) at -78 ºC. The solution was warmed to ambient temperature and stirred (1 h) and the solvent removed. The product was extracted into *n*-hexane (20 ml) and filtered. Removal of the solvent gave a white powder (151 mg, 88%). Crystals suitable for X-ray diffraction were grown from a concentrated *n*-hexane solution (r.t., 16 h).

^{1}H NMR (500.2 MHz, d_8-thf, 298 K): δ (ppm) = 7.73 (4H, m, *o*-Ph), 7.13-7.09 (4H, m, *m*-Ph), 7.09-7.06(2H, m, *p*-Ph), 1.27 (s, ^{t}Bu)

^{31}P{^{1}H} NMR (161.7 MHz, d_8-thf, 298 K): δ (ppm) = 206.7 (app t, $^{2}J_{P\text{-}Sn}$= 195 Hz).

Synthesis of [Ph_2Ge(3.5)] (3.14)

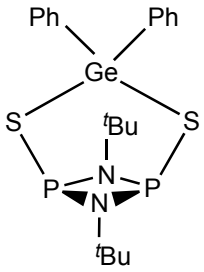

Synthesis proceeded in exactly the same way as for **3.13** using Ph_2GeCl_2 (0.32 mmol) instead. Product was isolated as an amorphous white powder (80%).

^{1}H NMR (500.2 MHz, d_8-thf, 298 K): δ (ppm) = 7.76 (4H, m, *o*-Ph), 7.20-7.13 (4H, m, *m*-Ph), 7.1-7.06 (2H, m, *p*-Ph), 1.29 (s, ^{t}Bu)

^{31}P{^{1}H} NMR (161.7 MHz, d_8-thf, 298 K): δ (ppm) = 215.4 (s)

7.4 Synthesis of Chapter 4

General Procedure 9: Synthesis of Oxidised Dianions $[S=P(E)(\mu\text{-}N^tBu)_2]_2^{2-}$ (E = S, Se, Te)

A solution of **3.7** was prepared *in situ* in thf and added to a suspension of elemental chalcogen (S, Se, Te) and an immediate colour change was noted. Any excess chalcogen was removed by filtration and the solvent removed under reduced pressure.

Synthesis of $[Na^+]_2[S=P(S)(\mu\text{-}N^tBu)_2]_2^{2-}$ 4.1·Na_2

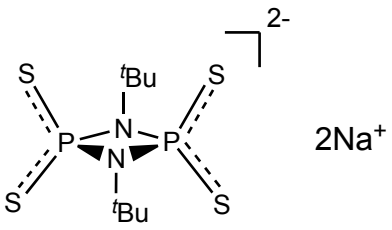

3.1 (100 mg, 364 µmol) in thf (10 ml) was added to solid Benzylsodium (84 mg, 726 µmol). The resulting pale green mixture was stirred for 5 minutes at ambient temperature before being added to elemental sulfur (23 mg, 726 µmol). This yellow solution was stirred at ambient temperature for 20 minutes. The solvent was removed slowly under reduced pressure until precipitation of a white solid. Toluene (20 ml) was added to the solution to fully precipitate the product. The suspension was collected by filtration and washed with toluene (10 ml) and dried under vacuum.

Yield: 133 mg white powder (95%)

^{1}H NMR (400 MHz, CD_3CN, 400 MHz, 298 K): δ (ppm) = 1.76 (18H, s)

^{31}P{^{1}H} NMR (161.7 MHz, CD_3CN, 298 K): δ (ppm) = 83.8 (s)

Elemental Analysis (%): Calcd. for 4.1·Na_2·0.5thf: C 29.3, H 5.3, N 6.0; found C 29.1, H 5.3, N 5.5

Synthesis of $[S=P(Se)(\mu\text{-}N^tBu)_2]_2^{2-}$ 4.2·Na_2

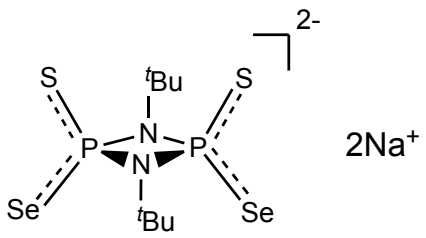

3.1 (100 mg, 364 µmol) in thf (10 ml) was added to solid BnNa (84 mg, 726 µmol). The resulting pale green mixture was stirred for 5 minutes at ambient temperature before the addition of elemental selenium (70 mg, 728 µmol). This suspension was stirred at ambient temperature for 20 minutes during which it turned dark brown. The solvent was removed slowly under reduced pressure until precipitation of a brown solid. Toluene (20 ml) was added to the solution to fully precipitate the product. The suspension was collected by filtration and washed with toluene (10 ml) and dried under vacuum.

Yield: Brown Powder (156 mg, 91%)

^{1}H NMR (400 MHz, CD_3CN, 298 K): δ (ppm) = 1.81 (18H, s)

^{31}P{^{1}H} NMR (161.7 MHz, CD_3CN, 298 K): δ (ppm) = 57.5 (2P, s, 2 satellites doublets arising from $^{1}J_{PSe}$= 703.1 Hz)

^{77}Se{^{1}H} NMR (95.4 MHz, CD_3CN, rel. Me_2Se, 298 K): 295.7 (d, $^{1}J_{PSe}$= 703.1 Hz)

Elemental Analysis (%): Calcd. for 4.2·Na_2·0.5thf: C 23.3, H 4.7, N 5.6 found C 23.0, H 4.5, N 5.3

Synthesis of $[S=P(Te)(\mu\text{-}N^tBu)_2]_2^{2-}$ 4.3

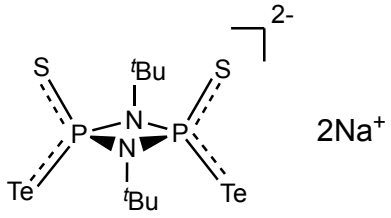

3.7 (100 mg, 364 µmol) in thf (10 ml) was added to solid BnNa (84 mg, 726 µmol). The resulting pale green mixture was stirred for 5 minutes at ambient temperature before the addition of elemental tellurium (94 mg, 726 µmol). The yellow solution was stirred at 50 ºC for 3hours before being cooled to r.t. and stored at -16 ºC. After 7 days a microcrystalline dark brown solid formed. The supernatant solution was removed by syringe and the remaining solid washed with *n*-hexane and dried under vacuum.

Yield: 55 mg brown solid (27%)

^{1}H NMR (400 MHz, CD_3CN, 298 K): δ (ppm) = 1.92 (18H, s)

^{31}P{^{1}H} NMR (161.7 MHz, CD_3CN, 298 K): δ (ppm) = -31.2 (2P, s, 2 satellites doublets arising from $^1J_{PTe}$= 1638.3 Hz)

^{125}Te{^{1}H} NMR (157.7 MHz, CD_3CN, rel. Me_2Te, 298 K): 419.4 (d, $^1J_{PTe}$= 1638.3 Hz)

Elemental Analysis: No satisfactory elemental analysis could be obtained due to the highly unstable nature of the compound.

Synthesis of $[Ph_2Sn(4.1)]$ 4.4

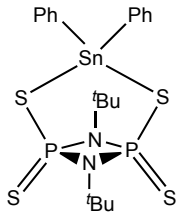

A solution of **4.1·Na2** (100 mg, 0.26 mmol) in thf (10 ml) was added to solid Ph_2SnCl_2 (89 mg, 0.26 mmol) at ambient temperature. The solution was stirred for 15 min at ambient temperature and the solvent removed. The product was extracted with *n*-hexane (20 ml) and filtered. The solvent was

removed until precipitation of a white solid which was dissolved by gentle heating. Storage at -16 ºC yielded [Ph_2Sn(**4.1**)] (**4.4**) as colourless crystals (95 mg, 60%). X-ray quality crystals were grown from a concentrated *n*-hexane solution.

^{1}H NMR (500.2 MHz, C_6D_6, 298 K): δ (ppm) = 7.48 - 7.24 (4H, m, *o*-Ph), 7.12-6.95 (6H, m, *m*-Ph + *p*- Ph), 1.67 (9H, s, ^{t}Bu).

^{31}P{^{1}H} NMR (161.7 MHz, CD_3CN, 298 K): δ (ppm) = 58.1 (app t, $^2J_{P\text{-}Sn}$= 49 Hz)

^{119}Sn{^{1}H} NMR (186.5 MHz, C_6D_6, 298 K) δ (ppm) = - 134.1 (t, $^2J_{P\text{-}Sn}$= 49 Hz)

Elemental Analysis (%): Calcd. C 39.7, H 4.7, N 4.6; found C 40.6, H 4.9, N 4.3

Synthesis of [Ph_2Sn(4.2)] 4.5

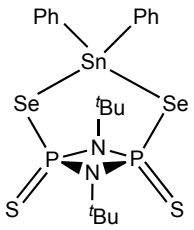

A solution of **4.2·Na_2** (100 mg, 0.21 mmol) in thf (10 ml) was added to solid Ph_2SnCl_2 (72 mg, 0.34 mmol) at ambient temperature. The solution was stirred for 15 min at ambient temperature and the solvent removed. The product was extracted with *n*-hexane (20 ml) and filtered. The solvent was removed until precipitation of a white solid which was dissolved by gentle heating. Storage at -16 ºC gave [Ph_2Sn(**4.1**)] (**4.4**) as a colourless crystalline solid (147 mg, 66%). X-ray quality crystals were grown from slow solvent evaporation of a saturated *n*-hexane solution under an inert atmosphere.

^{1}H NMR (500.2 MHz, C_6D_6, 298 K): δ (ppm) = 7.39 - 7.23 (4H, m, *o*-Ph), 7.09-6.94 (6H, m, *m*-Ph + *p*- Ph), 1.67 (9H, s, ^{t}Bu)

^{31}P{^{1}H} NMR (161.7 MHz, CD_3CN, 298 K): δ (ppm) = 36.9 (app t, $^1J_{P\text{-}Se}$ = 463 Hz, $^2J_{P\text{-}Sn}$= 69 Hz)

^{77}Se{^{1}H} NMR (95.4 MHz, CD_3CN, rel. Me_2Se, 298 K): δ (ppm) = 171.4 (d, $^1J_{PSe}$= 465 Hz)

^{119}Sn{^{1}H} NMR (186.5 MHz, C_6D_6, 298 K) δ (ppm) = - 54.2 (t, $^2J_{P\text{-}Sn}$= 69 Hz)

Elemental Analysis (%): Calcd. C 34.4, H 4.0, N 4.0; found C 34.5, H 4.0, N 4.2

Synthesis of [($Ph_3PAu)_2$(4.1)] (4.6)

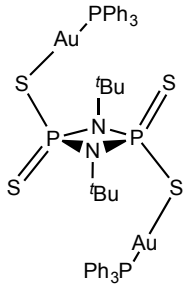

A solution of **4.1·Na$_2$** (100 mg, 0.26 mmol) in thf (10 ml) was added to solid Ph_3PAuCl (256 mg, 0.52 mmol) at ambient temperature. The reaction mixture was stored under exclusion of light at 6 ºC overnight during which **4.6** formed as colourless crystals suitable for X-ray diffraction (50 mg, 15 %).

^{1}H NMR (500.2 MHz, d$_8$-thf, 298 K): δ (ppm) = 6.93 - 6.77 (4H, m, Ph), 6.76-6.63 (7H, m, m-Ph + p-Ph), 6.53 – 6.36 (4H, m, Ph), 1.60 (s, 9H, ^{t}Bu)

^{31}P{^{1}H} NMR (161.7 MHz, d$_8$-thf, 298 K): δ (ppm) = 32.0 (bs), 78.2 (bs)

Elemental Analysis (%): Calcd. for 4.6·thf: C 43.6, H 4.3, N 2.1; found C 44.2, H 4.5, N 2.4

Synthesis of [dppeNi(4.2)] (4.7)

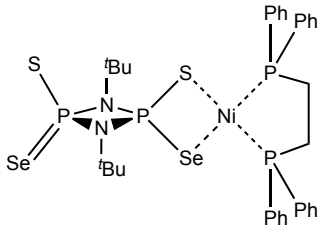

A solution of **4.2·Na$_2$** (100 mg, 0.26 mmol) in thf (10 ml) was added to solid $dppeNiCl_2$ (136 mg, 0.26 mmol) at ambient temperature. The solution was stirred for 15 min at ambient temperature and the solvent was removed. The product was extracted into dichloromethane (20 ml) and filtered. Evaporation of the solvent yielded **4.7** as a red solid (184 mg, 90%). X-ray quality crystals were grown from layering a saturated dichloromethane solution with *n*-hexane.

^{1}H NMR (500.2 MHz, CD$_3$CN, 298 K): δ (ppm) = 7.84 – 7.73 (8H, m, *o/m*-Ph), 7.70-7.64 (4H, m, *p*-Ph), 7.62-7.54 (8H, m, *o/m*-Ph), 2.72 – 2.47(4H, m, CH_2), 1.69 (18H, s, ^{t}Bu)

^{31}P{^{1}H} NMR (161.7 MHz, CD$_3$CN, 298 K): δ (ppm) = 39.5 - 40.4 (m), 65.2 (d, $^2J_{P\text{-}P}$ = 15 Hz), 66.7-65.3(m)

$^{31}P\{^{1}H\}$ NMR (161.7 MHz, d_6-acetone capillary, 298 K): δ (ppm) = 56.4 (2nd order AA'XX', $J_{A\text{-}A'}$= 133 Hz, $J_{X\text{-}X'}$= 137 Hz, $J_{A\text{-}X}$= 70 Hz, $J_{A\text{-}X'}$= -37 Hz), 47.9 (2nd order AA'XX')

Elemental Analysis (%): Calcd. C 41.7, H 5.4; found C 41.9, H 5.3 no sufficient nitrogen elemental data could be obtained, this is due to ceramic formation as previously reported.[31]

Synthesis of [{S=P^{V}(μ-N^{t}Bu)}$_2$(μ-S){P^{III}(μ-N^{t}Bu)}$_2$]$_3$ 4.8

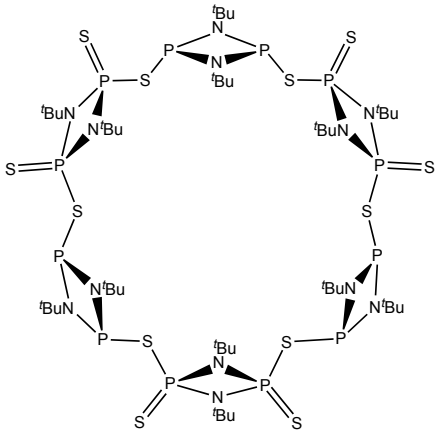

3.1 (100 mg, 363 µmol) in thf (10 ml) was added to solid BnNa (84 mg, 726 µmol). The resulting pale green mixture was stirred for 5 minutes at ambient temperature before the addition of elemental sulfur (12 mg, 726 µmol). This mixture was stirred at ambient temperature for 5 minutes during which the colour turned orange indicating the presence of the oxidised dianion [S=P(S)(μ-N^{t}Bu)]$_2^{2-}$. This solution was added dropwise to powder [ClP(μ-N^{t}Bu)]$_2$ (**2.1**) (100 mg, 363 µmol) at ambient temperature. The resulting pale yellow mixture was evaporated to dryness *in vacuo*, extracted with toluene (10 ml) and filtered to remove NaCl. The filtrate was evaporated to dryness, yielding **4.8** as a white powder (171 mg, 106 µmol). X-Ray quality crystals were grown from a saturated toluene solution at -16 ºC.

^{1}H NMR (500.12 MHz, d$_8$-toluene, 298 K): δ (ppm) = 1.41 (s, ^{t}Bu, P^{V} unit), 1.82 (s, ^{t}Bu, P^{III} unit);

^{31}P{^{1}H} NMR (161.7 MHz, d$_8$–toluene/d$_3$-acetonitrile mixture, 298 K) (ppm) = 60.7 (dd, $^{2}J_{P\text{-}P}$ = 16.7 Hz, $^{2}J_{P\text{-}P}$ = 27.2Hz), 229.8 (dd, $^{2}J_{P\text{-}P}$ = 16.7 Hz, $^{2}J_{P\text{-}P}$ = 27.2Hz)

Elemental Analysis (%): Calcd. C 35.8, H 6.7; found C 35.9, H 6.6; no sufficient nitrogen elemental data could be obtained, this is due to ceramic formation as previously reported.[31]

ATR-IR $\tilde{\nu}$ (cm^{-1}) = 1203 (w), 1089 (s), 1030 (s), 931 (w), 876 (m, P=S), 799 (m, P=S), 753 (w), 721 (w), 665 (w), 570 (w)

Synthesis of [{S=P^{V}(μ-N^{t}Bu)}$_2$(μ-S){P^{III}(μ-NCH$_2$^{t}Bu)}$_2$]$_3$ 4.9

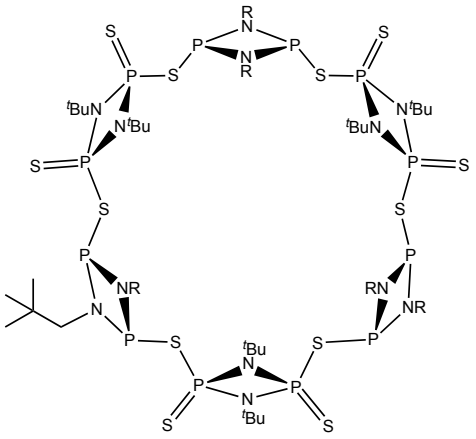

3.1 (100 mg, 363 µmol) in thf (10 ml) was added to solid BnNa (84 mg, 726 µmol). The resulting pale green mixture was stirred for 5 minutes at ambient temperature before the addition of elemental sulfur (12 mg, 726 µmol). This mixture was stirred at ambient temperature for 15 minutes during which the colour turned orange indicating the presence of the oxidised dianion [S=P(S)(μ-N^{t}Bu)$_2$]$_2^{2-}$. This solution was added dropwise to powder [ClP(μ-NCH$_2$^{t}Bu)]$_2$ (110 mg, 363 µmol) at ambient temperature. The resulting pale yellow mixture was evaporated to dryness *in vacuo*, extracted with toluene (10 ml) and filtered to remove NaCl. The filtrate was evaporated to dryness, yielding **4.9** as a white powder (180 mg, 104 µmol). X-Ray quality crystals were grown from a saturated d$_8$-toluene solution at r.t.

^{1}H NMR (500.12 MHz, d$_8$-toluene/CD$_3$CN mixture, 298 K): δ (ppm) = 1.48 (s, ^{t}Bu, P^{V} unit), 1.87 (s, Neopentyl-^{t}Bu); 2.90 (t, 2H, $^{2}J_{H\text{-}P}$ = 10.40 Hz, Neopentyl-CH$_2$)

^{31}P{^{1}H} NMR (161.7 MHz, d$_8$-toluene/CD$_3$CN mixture, 298 K): δ (ppm) = 61.7 (dd, $^{2}J_{P\text{-}P}$ = 21 Hz, $^{2}J_{P\text{-}P}$ = 30 Hz), 249.7 (dd, $^{2}J_{P\text{-}P}$ = 16 Hz, $^{2}J_{P\text{-}P}$ = 27 Hz, m on ^{1}H coupling)

Elemental Analysis (%): Calcd. C 38.4, H 7.2; found C 38.7, H 7.2; no sufficient nitrogen elemental data could be obtained, this is due to ceramic formation as previously reported.[31]

ATR-IR $\tilde{\nu}$ (cm^{-1}) = 1260 (w), 1050 (s), 1030 (s), 931 (w), 876 (m, P=S), 800 (m, P=S), 721 (w)

Synthesis of [{S=P^{V}(μ-N^{t}Bu)}$_2$(μ-S){P^{III}(μ-NCH$_2$^{t}Bu)}$_2$]$_3$ 4.10

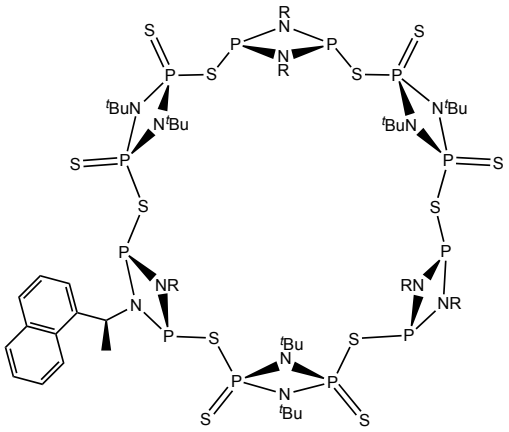

3.1 (100 mg, 363 µmol) in thf (10 ml) was added to solid BnNa (84 mg, 726 µmol). The resulting pale green mixture was stirred for 5 minutes at ambient temperature before the addition of elemental sulfur (23 mg, 726 µmol). This mixture was stirred at ambient temperature for 15 minutes during which the colour turned orange indicating the presence of the oxidised dianion [S=P(S)(μ-N^{t}Bu)$_2$]$_2^{2-}$. This solution was added dropwise to powder [ClP(μ-NCHCH$_2$Napthyl)]$_2$ (179 mg, 363 µmol) at ambient temperature. The resulting pale yellow mixture was evaporated to dryness *in vacuo*, extracted with toluene (10 ml) and filtered to remove NaCl. The filtrate was evaporated to dryness, giving **4.10** as a white powder (233 mg, 98 µmol).

^{1}H NMR (500.12 MHz, C$_6$D$_6$, 298 K): δ (ppm) = 1.69 (s, ^{t}Bu, P^{V} unit), 1.77 (d, CH$_3$, $^{3}J_{HH}$ = 6.6 Hz), 5.01 (q, $^{3}J_{HH}$ = 6.6 Hz, CH), 7.22 (m, 3H, Naphtyl), 7.58 (m, 3H, Naphtyl), 7.85 (s, 1H, Naphtyl)

^{31}P{^{1}H} NMR (161.7 MHz, C$_6$D$_6$, 298 K): δ (ppm) = 61.7 (dd, $^{2}J_{P\text{-}P}$ = 21 Hz, $^{2}J_{P\text{-}P}$ = 30 Hz), 249.7 (dd, $^{2}J_{P\text{-}P}$ = 16 Hz, $^{2}J_{P\text{-}P}$ = 27 Hz)

Elemental Analysis (%): Calcd. for 4.9·0.5 Toluene: C 55.0, H 5.9; found C 55.8, H 6.1; no sufficient nitrogen elemental data could be obtained, this is due to ceramic formation as previously reported.[31]

ATR-IR $\tilde{\nu}$ (cm^{-1}) = 1156 (w), 1030 (s), 1046 (s), 931 (w), 888 (m, P=S), 799 (m, P=S), 753 (w), 721 (w)

[{S=P^{V}(μ-N^{t}Bu)}$_2$(μ-S){S=P^{v}(μ-NCH$_2$^{t}Bu)}$_2$]$_3$ 4.11

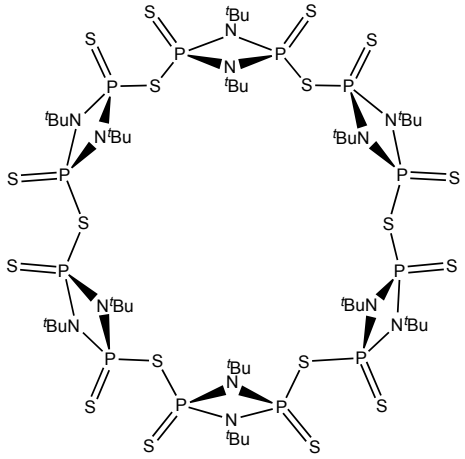

4.8 (171 mg, 106 µmol) was dissolved in toluene (20 ml) and added to elemental sulfur (12 mg, 726 µmol) at ambient temperature. The resulting suspension was refluxed overnight giving a yellow solution. The mixture was evaporated to dryness and washed with *n*-pentane yielding the product as a pale yellow solid (183 mg, quantitative).

^{1}H NMR (500.12 MHz, CD$_3$CN, 298 K): δ (ppm) = 1.74 (s, ^{t}Bu)

^{31}P {^{1}H} NMR (161.7 MHz, CD$_3$CN, 298 K): δ (ppm) = 63.5 (s)

Elemental Analysis (%): Calcd. C 32.6, H 6.2; found C 32.3, H 6.0; no sufficient nitrogen elemental data could be obtained, this is due to ceramic formation as previously reported.[31]

ATR-IR $\tilde{\nu}$ (cm^{-1}) = 1202 (w), 1091 (s), 1020 (s), 929 (w), 880 (m, P=S), 799 (m, P=S), 757 (w), 721 (w), 667 (w), 595 (w)

Synthesis of [{S=P^{V}(μ-N^{t}Bu)}$_2$(μ-Se){P^{III}(μ-NR)}$_2$]$_3$ 4.12

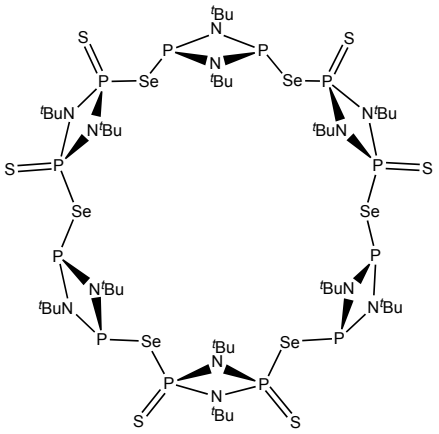

3.1 (100 mg, 363 µmol) in thf (10 ml) was added to solid BnNa (84 mg, 726 µmol). The resulting pale green mixture was stirred for 5 minutes at ambient temperature before the addition of elemental selenium (57 mg, 726 µmol). This mixture was stirred at ambient temperature for 15 minutes during which the colour turned orange indicating the presence of the oxidised dianion [Se=P(S)(μ-N^{t}Bu)$_2$]$_2^{2-}$. This solution was added dropwise to powder [ClP(μ-N^{t}Bu)]$_2$ (**2.1**) (100 mg, 363 µmol) at ambient temperature. The resulting pale yellow mixture was evaporated to dryness *in vacuo*, extracted with toluene (10 ml) and filtered to remove NaCl. The filtrate was evaporated to dryness, yielding **4.12** as a white powder (171 mg, 106 µmol). X-Ray quality crystals were grown from a saturated d_8-toluene solution at r.t.

^{1}H NMR (500.12 MHz, d_8-toluene, 298 K): δ (ppm) = 1.41 (s, ^{t}Bu, P^{V} unit), 1.82 (s, ^{t}Bu, P^{III} unit);

^{31}P{^{1}H} NMR (161.7 MHz, d_8-toluene, 298 K) δ (ppm) = 43.5 (pt accompanied by a set of ^{77}Se Satellites, $^{2}J_{P\text{-}P}$ = 20.5 Hz, $^{1}J_{PSe}$ = 484.7 Hz), 252.4 (dd accompanied by a set of ^{77}Se Satellites, $^{2}J_{P\text{-}P}$ = 16.4 Hz, $^{2}J_{P\text{-}P}$ = 25.2Hz, $^{1}J_{PSe}$ = 227.0 Hz)

This material was too insoluble in organic solvents to obtain a ^{77}Se spectrum.

Elemental Analysis (%): Calcd. C 30.5, H 5.8; found C 30.4, H 5.6; no sufficient nitrogen elemental data could be obtained, this is due to ceramic formation as previously reported.[31]

ATR-IR $\tilde{\nu}$ (cm^{-1}) = 1202 (w), 1091 (s), 1020 (s), 929 (w), 880 (m, P=S), 799 (m, P=S), 757 (w), 721 (w), 667 (w), 595 (w)

7.5 Synthesis of Chapter 5

7.5.1 Synthesis of Bis(amino)cyclodiphosphazanes

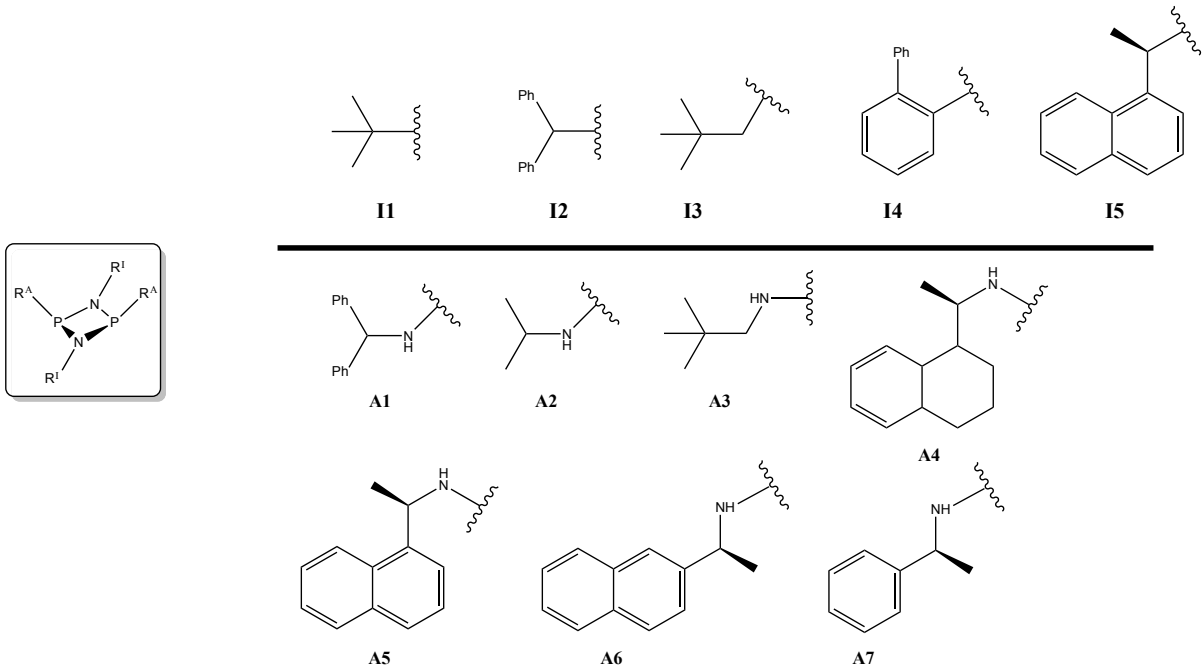

Figure 7.1: Reference table for substituent abbreviations

All reactions were carried out according to a General Procedure (**GP 4**, cf. Scheme 2.2).

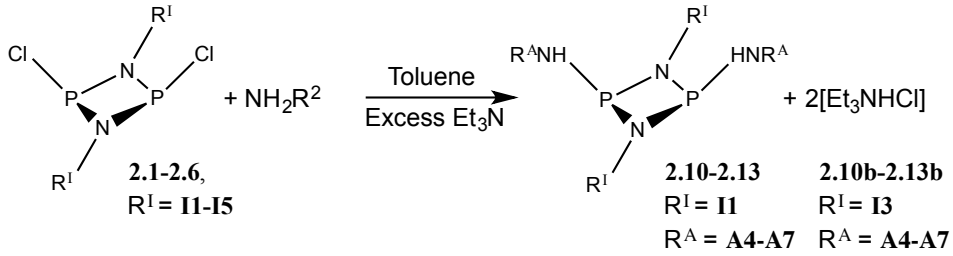

Scheme 7.2: Synthesis of chiral bis(amino)cyclodiphosphazanes according to GP 4.

General Procedure 4: In a Schlenk tube the dichloride dimer (0.36 mmol, 1.0 equiv.) was dissolved in 10 ml of dry toluene and cooled to 0 ºC. A solution of the amine (0.72 mmol, 2.0 equiv.) and Et_3N (7.20 mmol, 10 equiv.) in 10 ml of dry toluene was added dropwise and the mixture was allowed to warm to r. t. The reaction was stirred at r. t. for 18 h, forming a colourless precipitate of Et_3NHCl. The suspension was filtered and the solvent was removed under reduced pressure, yielding the desired

product as a colourless solid. Purification of the ligands was achieved through crystallisation from a mixture of toluene and *n*-hexane at -20 ºC.

[($C_{10}H_{10}NH$)P(μ-N^{t}Bu)]$_2$ (5.1)

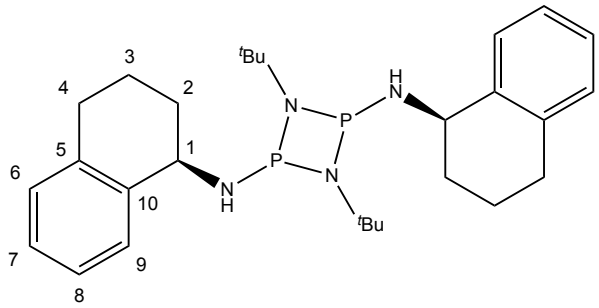

Yield: 1.35 g colourless solid (2.72 mmol, 85 %).

^{1}H NMR (400.13 MHz, C_6D_6, 298 K): δ (ppm) = 1.44–1.49 (m, 2H, H-4), 1.516 (s, 18H, H-12 (^{t}Bu)), 1.60– 1.72 (m, 2H, H-4), 1.75–1.85 (m, 2H, H-2), 1.91–2.02 (m, 2H, H-2), 2.39–2.49 (m, 2H, H-3), 2.50–2.59 (m, 2H, H-3), 2.83–2.96 (m, 2H, H-N), 4.59–4.68 (m, 2H, H-1), 6.89 (d, $^3J_{HH}$ = 7.2Hz, 2H, H-9), 7.02 (dt, $^3J_{HH}$ = 7.4 Hz, $^4J_{HH}$ = 1.2Hz, 2H, H-8), 7.09 (dt, $^3J_{HH}$ = 7.4 Hz, $^4J_{HH}$ = 1.3 Hz, 2H, H-7), 7.68 (d, $^3J_{HH}$ = 7.7 Hz, 2H, H-6)

^{13}C{^{1}H} NMR (100.61 MHz, C_6D_6, 298 K): δ (ppm) = 19.98 (s, 2C, C-4), 29.57 (s, 2C, C-3), 31.31 (t, $^3J_{CP}$ = 7.2Hz, 6 C, C-12), 34.28 (d, $^3J_{CP}$ = 1.6 Hz, 2C, C-2), 52.22 (t, $^2J_{CP}$ = 15.7 Hz, 2C, C-11), 126.13 (s, 2C, C-7), 126.88 (s, 2C, C-8), 129.22 (s, 4 C, C-6/9), 137.28 (s, 2C, C-5), 140.88 (d, $^3J_{CP}$ = 3.9 Hz, 2C, C-10)

^{31}P{^{1}H} NMR (161.96 MHz, C_6D_6, 298 K): δ (ppm) = 98.03 (br s)

HR-MS (ESI$^+$): $[M+H]^+ = C_{28}H_{43}N_4P^+_2$ Calcd.: 497.2958 found: 497.2978

[($C_{12}H_{11}NH$)P(μ-N^{t}Bu)]$_2$ (5.2)

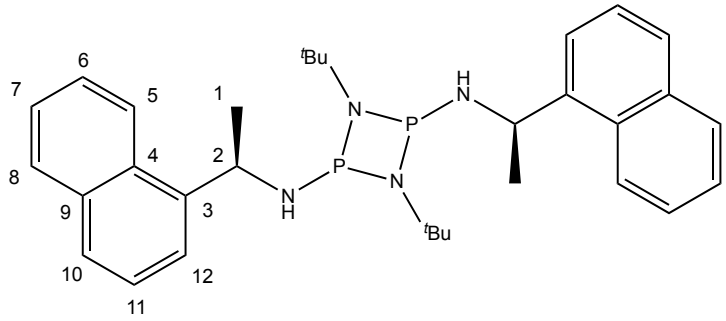

Yield: 993 mg colourless solid (1.85 mmol, 90 %).

^{1}H NMR (400.13 MHz, C_6D_6, 298 K): δ (ppm) = 1.21 (s, 18H, H-14), 1.38 (d, $^3J_{HH}$ = 6.8 Hz, 6 H, H-1), 3.07 (dd, $^2J_{HP}$ = 14.4 Hz, $^3J_{HH}$ = 9.9 Hz, 2H, H-N), 5.47–5.61 (m, 2H, H-2), 7.08–7.35 (m, 8H, H-Ar), 7.52–7.57 (m, 2H, H-Ar), 7.64–7.67 (m, 2H, H-Ar), 8.05–8.10 (m, 2H, H-Ar)

^{13}C{^{1}H} NMR (100.61 MHz, C_6D_6, 298 K): δ (ppm) = 26.92 (d, $^3J_{CP}$ = 3.1 Hz, 2C, C-1), 31.01 (t, $^3J_{CP}$ = 7.1 Hz, 6 C, C-14), 46.00 (br s, 2C, C-2), 51.82 (t, $^2J_{CP}$ = 14.9 Hz, 2C, C-13), 122.98 (s, 2C, C-Ar), 123.47 (s, 2C, C-Ar), 125.56 (s, 2C, C-Ar), 125.87 (s, 2C, C-Ar), 126.40 (s, 2C, C-Ar), 127.01 (s, 2C, C-Ar), 129.43 (s, 2C, C-Ar),130.49 (s, 2C, C-Ar), 134.35 (s, 2C, C-Ar), 143.79 (d, $^3J_{CP}$ = 1.6 Hz 2C, C-3)

^{31}P{^{1}H} NMR (161.96 MHz, C_6D_6, 298 K): δ (ppm) = 95.76 (br s)

HR-MS (ESI+): [M+H]$^+$= $C_{32}H_{43}N_4P_2^+$ Calcd.: 545.2958 found: 545.2992

[($C_{12}H_{11}NH$)P(μ-N^{t}Bu)]$_2$ (5.3)

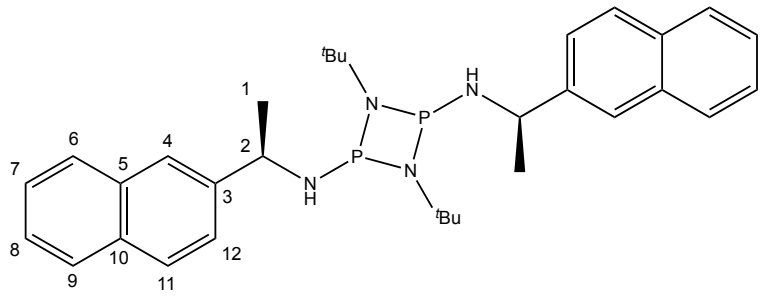

Yield: 1.65 g colourless solid (3.03 mmol, 98 %)

^{1}H NMR (400.13 MHz, C_6D_6, 298 K): δ (ppm) = 1.25 (s, 18H, H-14), 1.42 (d, $^3J_{HH}$ = 6.8 Hz, 6H, H-1), 3.14 (dd, $^2J_{HP}$ = 14.5 Hz, $^3J_{HH}$ = 9.2Hz, 2H, H-N), 4.76–4.91 (m, 2H, H-2), 7.21–7.30 (m, 6H, H-Ar), 7.49–7.55 (m, 2H, H-Ar), 7.55–7.61 (m, 4 H, H-Ar), 7.61–7.66 (m, 2H, H-Ar).

^{13}C{^{1}H} NMR (100.61 MHz, C_6D_6, 298 K): δ (ppm) = 27.27 (d, $^3J_{CP}$ = 3.3 Hz, 2C, C-1), 31.02 (t, $^4J_{CP}$ = 6.9 Hz, 6 C, C-14), 50.65 (d, $^2J_{CP}$ = 10.9 Hz, 2C, C-2), 51.84 (t, $^2J_{CP}$ = 15.0 Hz, 2C, C-13), 124.75 (s, 2C, C-Ar), 125.29 (s, 2C, C-Ar), 125.66 (s, 2C, C-Ar), 126.27 (s, 2C, C-Ar), 128.03 (s, 2C, C-Ar), 128.17 (s, 2C, C-Ar), 128.50 (s, 2C, C-Ar), 133.03 (s, 2C, C-Ar), 134.00 (s, 2C, C-Ar), 145.49 (d, $^3J_{CP}$ = 1.6 Hz, 2C, C-3)

^{31}P{^{1}H} NMR (161.96 MHz, C_6D_6, 298 K): δ (ppm) =96.75 (br s)

HR-MS (ESI+): $[M+H]^+ = C_{32}H_{43}N_4P^+_2$ Calcd.: 545.2958 found: 545.2992

[(C$_8$H$_9$NH)P(μ-N^{t}Bu)]$_2$ (5.4)

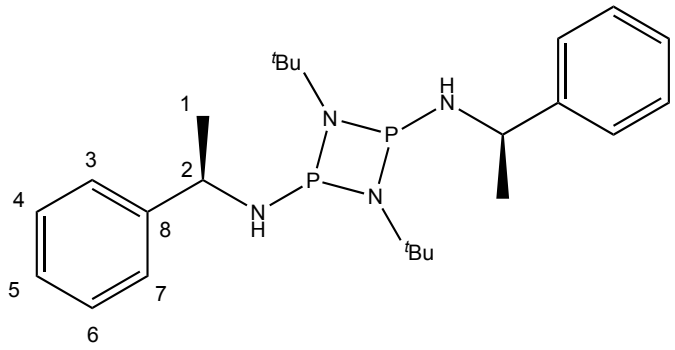

Yield: 4.01 g colourless solid (9.03 mmol, 92 %).

^{1}H NMR (400.13 MHz, C$_6$D$_6$, 298 K): δ (ppm) = 1.27 (s, 18H, H-10), 1.33 (d, $^3J_{HH}$ = 6.7 Hz, 6H, H-1), 2.98 (dd, $^2J_{HP}$ = 14.3 Hz, $^3J_{HH}$ = 9.4 Hz, 2H, H-N), 4.57–4.69 (m, 2H, H-2), 7.02–7.09 (m, 2H, H-Ar), 7.14–7.17 (m, 8H, H-Ar).

^{13}C{^{1}H} NMR (100.61 MHz, C$_6$D$_6$, 298 K): δ (ppm) = 27.23 (d, $^3J_{CP}$ = 3.4 Hz, 2C, C-1), 31.04 (t, $^3J_{CP}$ = 7.0 Hz, 6C, C-10), 50.53 (d, $^2J_{CP}$ = 12.8 Hz, 2C, C-2), 51.80 (t, $^2J_{CP}$ = 14.8 Hz, 2C, C-9), 126.51 (s, 2C, C-Ar), 126.72 (s, 1C, C-6), 128.60 (s, 2C, C-Ar), 148.05 (d, $^3J_{CP}$ = 1.9 Hz,1C, C-3)

^{31}P{^{1}H} NMR (161.96 MHz, C$_6$D$_6$, 298 K): δ (ppm) = 95.89 (br s)

HR-MS (ESI+): $[M+H]^+ = C_{24}H_{39}N_4P^+_2$ Calcd.: 445.2650 found: 445.2653

[($C_{10}H_{10}NH$)P(μ-$NCH_2{}^tBu$)]$_2$ 5.1b

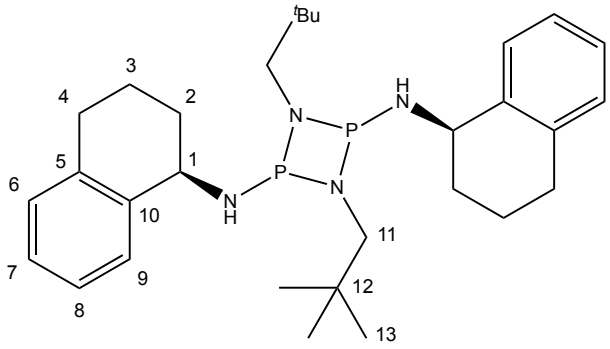

yield: 2.40 g colourless solid (4.57 mmol, 69 %).

^{1}H NMR (600.13MHz, C_6D_6, 298 K): δ (ppm) = 1.15 (s, 18H, H-13), 1.43–1.51 (m, 2H, H-Alk), 1.61–1.73 (m, 4H, H-Alk), 1.86–1.95 (m, 2H, H-Alk), 2.35–2.45 (m, 2H, H-Alk), 2.50–2.57 (m, 2H, H-Alk), 2.98–3.07 (m, 4H, H-Alk), 3.10 (dd, $^2J_{HP}$ = 8.9Hz, $^3J_{HH}$ = 8.9Hz, 2H, H-N), 4.45–4.53 (m, 2H, H-Alk), 6.86–6.90 (m, 2H, H-Ar), 6.98–7.03 (m, 2H, H-Ar), 7.08–7.12 (m, 2H, H-Ar), 7.64–7.70 (m, 2H, H-Ar)

^{31}P{1H} NMR (242.94 MHz, C_6D_6, 298 K): δ (ppm) = 131.57 (br s, 2 P)

MS (LIFDI$^+$): $[M]^+ = C_{30}H_{46}N_4P_2{}^+$ Calcd.: 524.32 found: 524.0

[((2-Napthyl)NH)P(μ-$NCH_2{}^tBu$)]$_2$ 5.3b

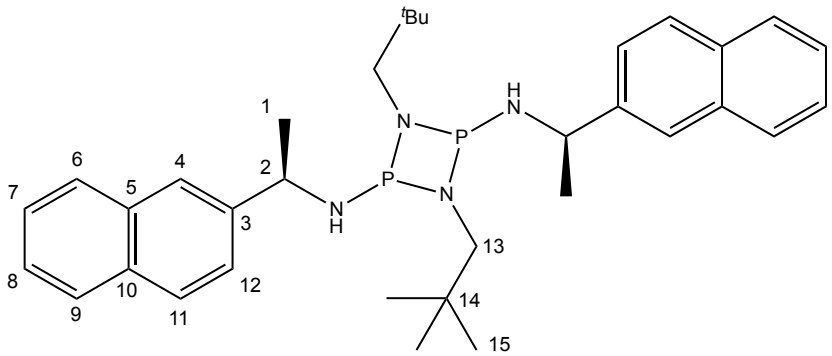

Yield: 1.45 g colourless solid (2.53 mmol, 76 %)

^{1}H NMR (600.13MHz, C_6D_6, 298 K): δ (ppm) = 0.90 (s, 18H, H-15), 1.41 (d, $^3J_{HH}$ = 7.3Hz, 6H, H-1), 2.31–2.82 (m, 4H, H-13), 3.34 (dd, $^2J_{HP}$ = 12.1Hz, $^3J_{HH}$ = 9.7Hz, 2H, H-N, 4.69–4.80 (m, 2H, H-2), 7.09–7.14 (m, 2H, H-Ar), 7.21–7.27 (m, 4H, H-Ar), 7.39–7.45 (m, 2H, H-Ar), 7.46–7.52 (m, 4H, H-Ar), 7.57–7.62 (m, 2H, H-Ar)

^{31}P{1H} NMR (242.94 MHz, C_6D_6, 298 K): δ (ppm) = 132.78 (br s, 2 P)

MS (LIFDI$^+$): $[M]^+ = C_{34}H_{46}N_4P_2^+$ Calcd.: 572.32 found: 572.1

$[(C_8H_9NH)P(\mu\text{-}NCH_2{}^tBu)]_2$ 5.4b

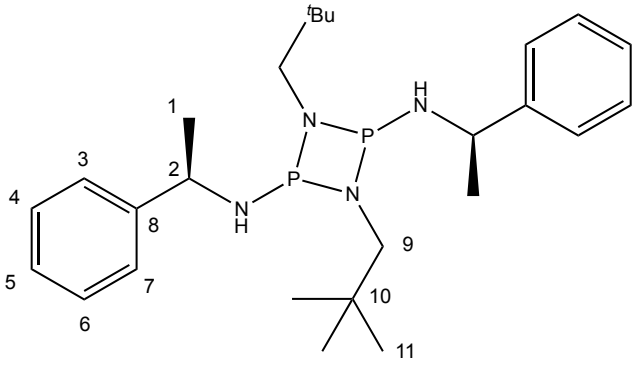

Yield: 1.20 g colourless solid (2.54 mmol, 77 %).

^{1}H NMR (600.13MHz, C_6D_6, 298 K): δ (ppm) = 0.96 (s, 18H, H-11), 1.32 (d, $^3J_{HH}$ = 6.8Hz, 6H, H-1), 2.50–2.70 (m, 4H, H-9), 3.23 (dd, $^2J_{HP}$ = 10.8Hz, $^3J_{HH}$ = 10.8Hz, H-N), 4.50–4.59 (m, 2H, H-2), 7.02–7.06 (m, 2H, H-Ar), 7.08–7.11 (m, 4H, H-Ar), 7.11–7.14 (m, 4H, H-Ar)

^{31}P{1H} NMR (242.94 MHz, C_6D_6, 298 K): δ (ppm) = 132.24 (br s, 2P)

MS (LIFDI$^+$): $[M]^+ = C_{26}H_{42}N_4P_2^+$ Calcd.: 472.29 found: 472.0

7.5.2 Lithiation of Bis(amino)cyclodiphosphazanes

Lithiation reactions were carried out according to a General Procedure (**GP 5).**

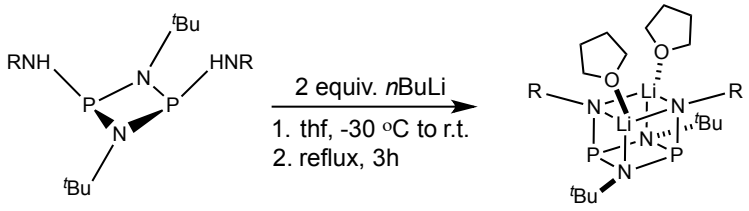

Scheme 7.3: Lithiation of chiral bis(amino)cyclodiphosphazanes according to GP 5.

General Procedure 5: This reaction was carried out according to an adapted literature procedure:[26,77] In a Schlenk tube the phosphazane (1.0 equiv.) was dissolved in dry thf and cooled to -30 ºC. A solution of *n*BuLi in *n*-hexane (1.6 M, 2.0 equiv.) was added dropwise. The mixture was allowed to

warm to r. t. slowly and was then heated to reflux for 3 h. The solvent was evaporated under reduced pressure and the crude was washed with *n*-pentane, yielding the desired product as a colourless to pale yellow solid.

2[Li(thf)$_2$]·[(2-Napthyl)N)P(μ-N^{t}Bu)]$_2$ (5.5)

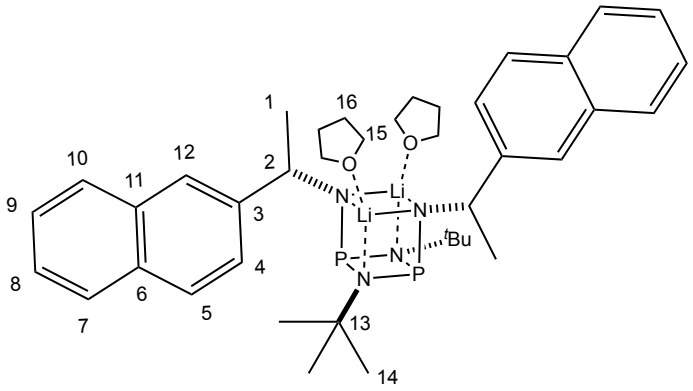

yield: 49.0 mg pale yellow solid (75.6 µmol, 75 %).

^{1}H NMR (400.13 MHz, C_6D_6, 298 K): δ (ppm) = 1.18–1.30 (m, 8H, H-14), 1.60–1.68 (s, 18H, H-12), 1.60–1.68 (m, 2H, H-2), 1.69–1.75 (m, 2H, H-4), 1.84–1.99 (m, 2H, H-4), 2.12–2.24 (m, 2H, H-2), 2.64–2.72 (m, 4H, H-3), 3.16–3.43 (m, 8H, H-13), 4.69–4.82 (m, 2H, H-1), 6.93–6.99 (m,4H, H-Ar), 7.02–7.08 (m, 2H, H-Ar), 7.75–7.84 (m, 2H, H-Ar)

^{13}C{^{1}H} NMR (100.61 MHz, C_6D_6, 298 K): δ (ppm) = 21.83 (s, 2C, C-4), 25.38 (s, 4C, C-14), 30.93 (t, $^3J_{CP}$ = 7.8Hz, 6C, C-12), 31.08 (s, 2C, C-3), 38.94 (d, $^3J_{CP}$ = 7.1 Hz, 2C, C-2), 52.80 (t, $^2J_{CP}$ = 15.0 Hz, 2C, C-11), 59.73 (d, $^2J_{CP}$ = 45.1 Hz, 2C, C-2), 68.06 (s, 4C, C-13), 124.91 (s, 2C, C-Ar), 125.29 (s, 2C, C-Ar), 128.20 (s, 2C, C-Ar) 130.87 (s, 2C, C-Ar), 136.12 (s, 2C, C-Ar), 148.39 (d, $^3J_{CP}$ = 9.3 Hz)

^{31}P{^{1}H} NMR (161.96 MHz, C_6D_6, 298 K): δ (ppm) = 166.89 (s)

HR-MS (ESI$^+$): Due to sensitivity towards moisture no suitable spectrum could be obtained.

2[Li(thf)$_2$]$^+$·[(C$_{10}$H$_{10}$N)P(μ-N^{t}Bu)]$_2$ (5.6)

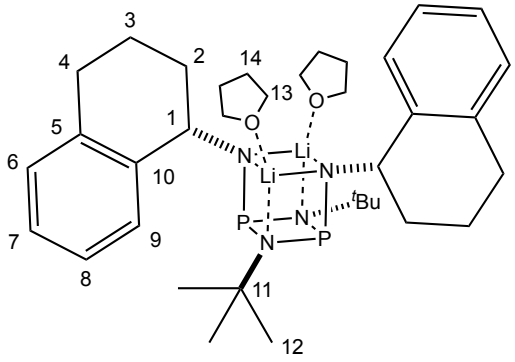

Yield: 52.0 mg pale yellow solid (74.4 µmol, 81 %)

^{1}H NMR (400.13 MHz, C$_6$D$_6$, 298 K): δ (ppm) = 1.02–1.09 (m, 8H, H-16), 1.58 (s, 18H, H-14), 1.69 (d, $^3J_{HH}$ = 6.5 Hz, 6H, H-1), 3.22–3.36 (m, 8H, H-15), 4.94–5.05 (m, 2H, H-2), 7.26–7.30 (m, 2H, H Ar), 7.31–7.37 (m, 2H, H-Ar), 7.67–7.74 (m, 6H, H-Ar), 7.76–7.81 (m, 2H, H-Ar), 7.88–7.91 (m, 2H, H-Ar)

^{13}C{^{1}H} NMR (100.61 MHz, C$_6$D$_6$, 298 K): δ (ppm) = 25.16 3(s, 4C, C-16), 30.58 (t, $^3J_{CP}$ = 7.4 Hz, 6C, C-14), 31.10 (d, $^3J_{CP}$ = 7.1 Hz, 2C, C-1), 52.80 (t, $^2J_{CP}$ = 14.7 Hz, 2C, C-13), 60.10 (d, $^2J_{CP}$ = 44.4 Hz, 2C, C-2), 68.28 (s, 4C, C-15), 123.94 (s, 2C, C-Ar), 124.92 (s, 2C, C-Ar), 125.81 (s, 2C, C-Ar), 127.45 (s, 2C, C-Ar), 127.58 (s, 2C, C-Ar), 127.88 (s, 2C, C-Ar), 127.96 (s, 2C, C-Ar), 132.74 (s, 2C, C-Ar), 134.47 (s, 2C, C-Ar), 152.11 (s, 2C, C-3)

^{31}P{^{1}H} NMR (161.96 MHz, C$_6$D$_6$, 298 K): δ (ppm) = 167.96 (s)

7.5.3 Synthesis of Chiral Zr Complexes

Complexation reactions with Zr were carried out according to a General Procedure (**GP 6**) and subsequent chlorinations and alkylations attempted according to General Procedures 7 and 8 (Scheme 7.4).

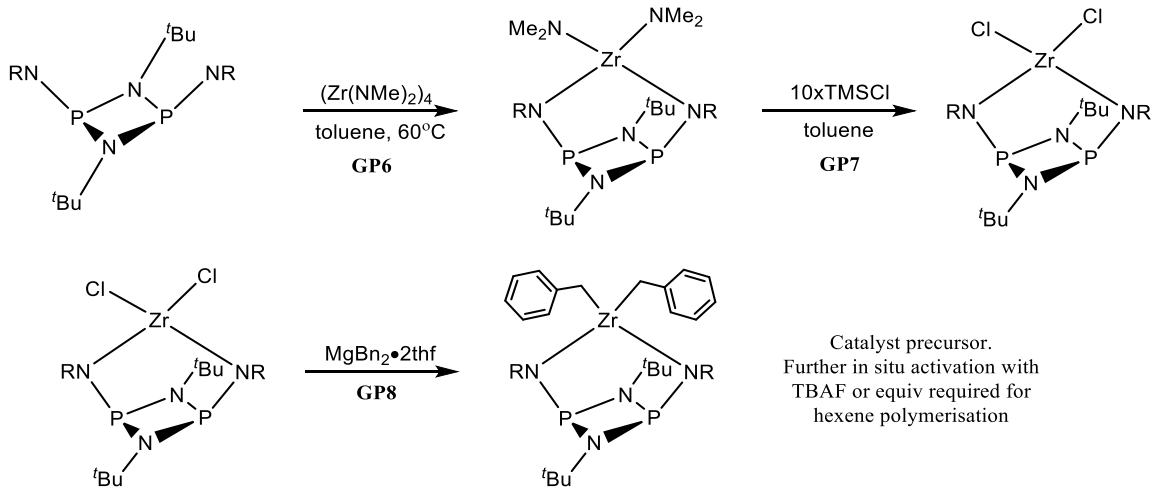

Scheme 7.4: Lithiation of chiral bis(amino)cyclodiphosphazanes and subsequent coordination to metal tetrakis-amide according to GP 6, 7 and 8.

General Procedure 6: A solution of chiral bis(amino)cyclophosphazane (**5.1**, **5.2**, **5.3**, **5.4**) was dissolved in toluene (150 ml) with $Zr(NMe_2)_4$ in a 1:1 ratio and heated under reflux with static vacuum for 3hrs. Static vacuum is necessary to remove $HNMe_2$ as it is generated. The solvent was removed *in vacuo* to yield the bis-amino metal complex $[NRP(\mu\text{-}N^tBu)]_2 \cdot M(NMe_2)_2$.

General Procedure 7: The bis-amino complex was dissolved in toluene (30 ml) and TMSCl (10 equivalents) was added dropwise and the solution stirred overnight. The solvent was removed and the residue washed with *n*-hexane to give the product as a white powder.

General Procedure 8: The dichloro metal complex was dissolved in toluene and a toluene solution of $Mg(Bn)_2(thf)_2$ added dropwise at -40 ºC. After 30min stirring at -40 ºC dioxane (1 ml) was added and the toluene removed. The resulting residue is washed with *n*-hexane to give the product as a white powder.

[5.1]·ZrNMe$_2$

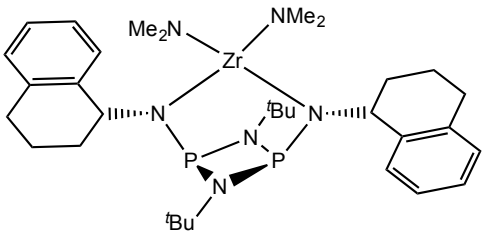

Synthesised according to **GP 6**

Yield: Yellow powder (quant.)

^{1}H-NMR (400.13 MHz, C_6D_6, 298 K): δ (ppm) = 1.39 (s, 18H, H-12), 1.61–1.74 (m, 2H, H-Alk), 1.91–2.03 (m, 2H, H-Alk), 2.03–2.15 (m, 4H, H-Alk), 2.62 (s, 12H, H-13), 2.72–2.84 (m, 2H, H-Alk), 4.66–4.79 (m, 2H, H-1), 6.94–6.99 (m, 2H, H-Ar), 7.03–7.09 (m, 2H, H-Ar), 7.11–7.15(m, 2H, H-Ar), 7.57–7.63 (m, 2H, H-Ar)

^{13}C{^{1}H} NMR (100.55 MHz, C_6D_6, 298 K): δ (ppm) = 20.68 (s, 2C, C-Alk), 29.95 (s, 2C, C-Alk), 30.17 (t, $^3J_{CP}$ = 7.2Hz, 6C, C-12), 34.79 (d, $^2J_{CP}$ = 6.4 Hz , 2C, C-2), 41.61 (s, 4C, C-13), 51.55 (t, $^2J_{CP}$ = 12.4 Hz, 2C, C-11), 59.82 (d, $^2J_{CP}$ = 29.2Hz, 2C, C-1), 125.66 (s, 2C, C-Ar), 126.58 (s, 2C, C-Ar), 129.02 (s, 2C, C-Ar), 137.01 (s, 2C, C-Ar), 142.75 (d, $^3J_{CP}$ = 6.5 Hz, 2C, C-10)

^{31}P{^{1}H} NMR (161.88 MHz, C_6D_6, 298 K): δ (ppm) = 128.65 (s)

HR-MS (ESI$^+$): $[M+H]^+$= $C_{24}H_{39}N_4P^+_2$ Calcd.: 445.2650 found: 445.2653

[5.2]·ZrNMe$_2$

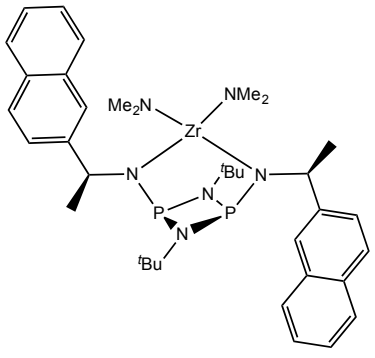

Yield: Pale yellow solid (quantitative).

^{1}H-NMR (400.13 MHz, C_6D_6, 298 K): δ (ppm) = 1.27 (s, 18H, H-14), 1.72 (d, $^{3}J_{HH}$ = 6.9Hz 6H, H-1), 2.63 (s, 12H, H-15), 4.75–4.87 (m, 2H, H-2), 7.25–7.31 (m, 2H, H-Ar), 7.62–7.76 (m, 8H, H-Ar), 7.80 (s, 2H, H-4)

^{13}C{^{1}H} NMR (100.55 MHz, C_6D_6, 298 K): δ (ppm) = 129.34 (s, 2 C)

Elemental Analysis (%): Calcd. C, 59.89, H, 7.26, N, 11.64; found: C, 60.05, H, 7.28, N, 11.21.

[5.3]·ZrNMe$_2$

Synthesised according to **GP 6**

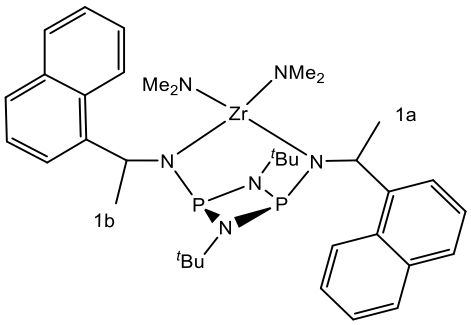

Yield: Pale yellow Powder (Quant.)

^{1}H-NMR (400.13 MHz, C_6D_6, 298 K): δ (ppm) = 1.29 (s, 18H, H-14), 1.79 (d, $^{3}J_{HH}$ = 6.8 Hz, 6H, H-1), 2.39 (s, 12H, H-15), 5.51–5.70 (m, 2H, H-2), 7.24–7.32 (m, 2H, H-Ar), 7.32–7.42 (m, 4H, H-Ar), 7.52–7.61 (d, $^{3}J_{HH}$ = 8.6 Hz, 2H, H-Ar), 7.62–7.73 (m, 4H, H-Ar), 8.45–8.55 (d, $^{3}J_{HH}$ = 7.8 Hz, 2H, H-Ar)

^{13}C{^{1}H} NMR (100.55 MHz, C_6D_6, 298 K): δ (ppm) = 26.23 (d, $^{3}J_{CP}$ = 11.3 Hz, 2C, C-1), 29.96 (t, $^{3}J_{CP}$ = 6.5 Hz, 6 C, C-14), 41.47 (s, 4C, C-15), 53.32 (s, 2C, C-2), 52.32 (t, $^{2}J_{CP}$ = 12.0 Hz, 2C, C-13), 123.82 (s, 2C, C-Ar), 124.43 (s, 2C, C-Ar), 125.60 (s, 2C, C-Ar), 125.82 (s, 2C, C-Ar), 127.36 (s, 2C, C-Ar), 129.14 (s, 2C, C-Ar),129.33 (s, 2C, C-Ar), 131.46 (s, 2C, C-Ar), 134.64 (s, 2C, C-Ar), 145.55 (s, 2C, C-Ar)

^{31}P{^{1}H} NMR (161.88 MHz, C_6D_6, 298 K): δ (ppm) = 133.06 (s)

Elemental Analysis (%): Calcd. C, 59.89, H, 7.26, N, 11.64; found: C, 60.54 H, 7.29, N, 10.96

[5.4]·ZrNMe$_2$

Synthesised according to **GP 6**

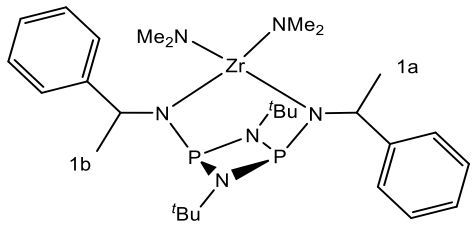

Yield: Pale yellow powder (Quant.)

^{1}H-NMR (600.13 MHz, C_6D_6, 298 K): δ (ppm) = 1.27 (s, 18H, H-10), 1.64 (d, $^3J_{HH}$ = 6.9 Hz, 6H, H-1), 2.71 (s, 12H, H-11), 4.61–4.69 (m, 2H, H-2), 7.05–7.11 (m, 2H, H-7), 7.19–7.24 (m, 4H, H-6/8), 7.36–7.43 (m, 4 H, H-5/9).

^{13}C{^{1}H} NMR (150.9 MHz, C_6D_6): δ (ppm) = 26.68 (d, $^3J_{CP}$ = 10.9 Hz, 2C, C-1), 29.78 (t, $^3J_{CP}$ = 7.0 Hz, 6C, C-10), 41.78 (s, 4C, C-11), 53.22 (t, $^2J_{CP}$ = 12.1 Hz, 2C, C-9), 60.64 (d, $^2J_{CP}$ = 27.6 Hz, 2C, C-2), 126.79 (s, 2C, C-7), 127.31 (s, 4 C, C-5/9), 128.60 (s, 4C, C-6/8), 149.56 (d, $^3J_{CP}$ = 6.6 Hz, 2C, C-3).

^{31}P{^{1}H} NMR (161.96 MHz, C_6D_6, 298 K): δ (ppm) = 129.3 (s)

Elemental Analysis (%): Calcd. C, 54.08, H, 7.78, N, 13.51; found: C, 53.91, H, 7.30, N, 12.78

Synthesis of [5.3]·ZrCl$_2$

Synthesised according to **GP 7**

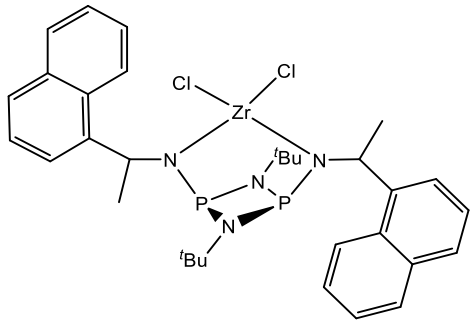

Yield: Pale yellow Powder (48%)

^{1}H-NMR (400.13 MHz, C_6D_6, 298 K): δ (ppm) = 0.99 (s, 18H, H-14), 1.41 (d, $^{3}J_{HH}$ = 6.8 Hz, 6H, H-1), 4.7-4.8 (m, 2H, H-2), 7.24–7.32 (m, 2H, H-Ar), 7.32–7.42 (m, 4H, H-Ar), 6.90–6.94 (d, $^{3}J_{HH}$ = 8.9 Hz, 2H, H-Ar), 7.08–7.11 (d, $^{3}J_{HH}$ = 8.9 Hz, 2H, H-Ar) 7.62–7.73 (m, 4H, H-Ar)

^{31}P{^{1}H} NMR (161.88 MHz, C_6D_6, 298 K): δ (ppm) = 121.08 (s, 82%) Impurities: 122.12 (s, 4.2%), 119.6 (s, 4.8%), 116.6 (s, 5.2%), 113 (s, 3.7%)

[5.4]·$ZrCl_2$

Synthesised according to **GP 7**

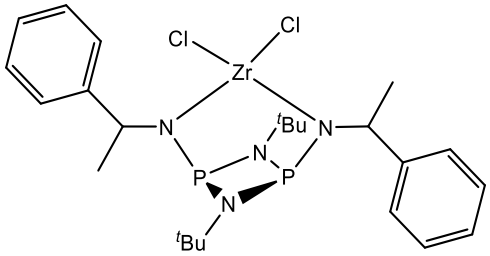

^{1}H-NMR (400.13 MHz, C_6D_6, 298 K): δ (ppm) = 1.20 (s, 18H, H-14), 1.33-1.46 (m, 70H, impurities NMe_2 + H-1, H-11), 2.39 (s, 12H, H-15), 4.70-4.80 (m, 2H, H-2), 7.24–7.32 (m, 2H, H-Ar), 7.32–7.42 (m, 4H, H-Ar), 7.52–7.61 (d, $^{3}J_{HH}$ = 8.6 Hz, 2H, H-Ar), 7.62–7.73 (m, 4H, H-Ar), 8.45–8.55 (d, $^{3}J_{HH}$ = 7.8 Hz, 2H, H-Ar)

^{31}P{^{1}H} NMR (161.88 MHz, C_6D_6, 298 K): δ (ppm) = 121.0 (s, 76%). Impurities: 122.09 (s, 7.4%), 119.5 (s, 2.1%), 116.2 (s, 3.4%), 113.8 (s, 5%)

Attempted synthesis using alternative Zr complexes.

Lithiated species **5.4** and **5.5** with $ZrCl_4$ gave no single products.

$ZrNMe_2Cl_2$

$Zr(CH_2TMS)_2Cl_2$

$Zr(CH_2TMS)_2(NMe_2)_2$

$Zr(CH_2Ph)_2Cl_2$

8. Appendix

8.1 X-Ray data for all compounds

Compound number	**2.2**	**2.8**
Empirical formula	$C_{92}H_{82}Cl_6N_6P_6$	$C_{14}H_{10}Cl_2N_2O_4P_2$
Formula weight	1670.16	403.08
Temperature/K	180(2)	200(2)
Crystal system	Monoclinic	Monoclinic
Space group	C2/c	C2/c
a/Å	59.385(2)	29.506(3)
b/Å	6.0660(2)	7.1129(7)
c/Å	23.5076(7)	17.0140(19)
α/°	90	90
β/°	91.988(1)	115.751(3)
γ/°	90	90
Volume/Å^3	8463.0(5)	3216.1(6)
Z	4	8
ρ_{calc}g/cm^3	1.311	1.665
μ/mm^{-1}	0.367	0.625
F(000)	3472	1632
Crystal size/mm^3	0.28 × 0.18 × 0.05	0.59 × 0.40 × 0.10
Radiation	MoKα (λ = 0.71073)	MoKα (λ = 0.71073)
2Θ range for data collection/°	7.02 to 44.92	4.84 to 50.08
Reflections collected	17967	16307
Independent reflections	5353 [R_{int} = 0.0675]	2844 [R_{int} = 0.0545]
Data/restraints/parameters	5353/0/497	2844/0/217
Goodness-of-fit on F^2	1.002	1.047
Final R indexes [I>=2σ (I)]	R_1 = 0.0579, wR_2 = 0.1271	R_1 = 0.0399, wR_2 = 0.1016
Final R indexes [all data]	R_1 = 0.0991, wR_2 = 0.1464	R_1 = 0.0499, wR_2 = 0.1091
Largest diff. peak/hole / e Å^{-3}	0.70/-0.77	0.37/-0.30
Flack parameter		
CCDC Number		

3.1	**3.2**	**3.3**
$C_8H_{20}N_2P_2S_2$	$C_{24}H_{36}N_2P_2S_2$	$C_{18}H_{24}N_2P_2S_2$
270.32	478.61	394.45
180(2)	200(2)	180(2)
triclinic	monoclinic	monoclinic
P-1	$P2_1/n$	$P2_1/c$
5.9112(2)	8.3695(19)	10.4215(3)
9.9768(3)	10.1458(17)	11.0475(3)
12.1132(3)	15.541(3)	9.3492(3)
85.594(2)	90	90
88.593(2)	101.646(7)	109.462(2)
79.0550(10)	90	90
699.27(4)	1292.5(4)	1014.89(5)
2	2	2
1.284	1.23	1.291
0.58	0.344	3.878
288	512	416
0.560 × 0.230 × 0.140	0.500 × 0.200 × 0.100	0.190 × 0.090 × 0.060
MoKα (λ = 0.71073)	MoKα (λ = 0.71073)	CuKα (λ = 1.54178)
7.46 to 54.988	4.826 to 45.552	9 to 133.186
6232	11418	13746
3108 [R_{int} = 0.0255, R_σ = 0.0381]	1743 [R_{int} = 0.0895, R_σ = 0.0591]	1755 [R_{int} = 0.0492, R_σ = 0.0319]
3108/0/141	1743/0/144	1755/4/125
1.115	1.016	1.048
R_1 = 0.0287, wR_2 = 0.0766	R_1 = 0.0392, wR_2 = 0.0763	R_1 = 0.0456, wR_2 = 0.0941
R_1 = 0.0305, wR_2 = 0.0779	R_1 = 0.0697, wR_2 = 0.0869	R_1 = 0.0647, wR_2 = 0.1095
0.29/-0.27	0.24/-0.23	0.31/-0.36
1062561	1062562	1062563

3.6	**3.7**	**3.13**
$C_{16}H_{34}MgN_2O_2P_2S_2$	$C_{96}H_{209}N_{16}Na_{17}O_8P_{16}S_{17}$	$C_{20}H_{28}N_2P_2S_2Sn$
436.82	3147.15	541.19
180(2)	180(2)	180(2)
monoclinic	tetragonal	triclinic
$P2_1/n$	P4*cc*	P-1
13.2446(2)	23.7918(2)	8.5948(4)
10.2823(2)	23.7918(2)	9.7615(4)
17.0713(3)	37.5449(6)	14.7996(6)
90	90	85.955(2)
97.7952(7)	90	87.786(2)
90	90	73.175(2)
2303.37(7)	21252.3(5)	1185.33(9)
4	4	2
1.26	0.984[a]	1.516
0.41	0.365	11.552
936	6640	548
0.500 × 0.350 × 0.250	0.210 × 0.180 × 0.140	0.200 × 0.190 × 0.110
MoKα (λ = 0.71073)	MoKα (λ = 0.71073)	CuKα (λ = 1.54178)
7.254 to 54.968	7.062 to 44.962	5.988 to 136.864
21092	39076	34420
5117 [R_{int} = 0.0374, R_σ = 0.0306]	12141 [R_{int} = 0.0877, R_σ = 0.0824]	4338 [R_{int} = 0.0445, R_σ = 0.0235]
5117/0/232	12141/197/769	4338/0/251
1.027	1.027	1.053
R_1 = 0.0332, wR_2 = 0.0733	R_1 = 0.0725, wR_2 = 0.1916	R_1 = 0.0200, wR_2 = 0.0480
R_1 = 0.0436, wR_2 = 0.0786	R_1 = 0.1068, wR_2 = 0.2156	R_1 = 0.0214, wR_2 = 0.0486
0.28/-0.30	0.34/-0.39	0.33/-0.61
	-0.01(7)	
1475941	1475943	1475942

4.4	**4.5**	**4.6**
$C_{20}H_{28}N_2P_2S_4Sn$	$C_{18}H_{28}N_2P_2S_2Se_2Sn$	$C_{38}H_{48}Au_2N_2OP_4S_4$
605.31	675.09	1194.83
180(2)	180(2)	180(2)
triclinic	triclinic	triclinic
P-1	P-1	P-1
10.8583(3)	11.0401(3)	9.4180(3)
14.3906(4)	14.4694(4)	12.4401(4)
17.0372(5)	17.0709(4)	13.3534(4)
97.746(2)	97.8430(10)	93.1200(10)
98.017(2)	98.7060(10)	107.0380(10)
90.464(2)	90.6030(10)	110.5230(10)
2611.14(13)	2668.98(12)	1379.15(8)
4	4	1
1.54	1.68	1.439
12.01	13.381	12.566
1224	1320	580
0.180 × 0.130 × 0.020	0.400 × 0.210 × 0.090	0.240 × 0.140 × 0.050
CuKα (λ = 1.54178)	CuKα (λ = 1.54178)	CuKα (λ = 1.54178)
5.288 to 133.412	5.288 to 133.726	7.032 to 133.528
60330	64023	32706
9221 [R_{int} = 0.0802, R_σ = 0.0485]	9457 [Rint = 0.0775, Rσ = 0.0454]	4872 [R_{int} = 0.0491, R_σ = 0.0293]
9221/0/523	9457/0/591	4872/40/298
1.012	1.039	0.932
R_1 = 0.0366, wR_2 = 0.0808	R1 = 0.0466, wR2 = 0.1206	R_1 = 0.0270, wR_2 = 0.0673
R_1 = 0.0532, wR_2 = 0.0872	R1 = 0.0574, wR2 = 0.1298	R_1 = 0.0314, wR_2 = 0.0731
1.12/-0.73	1.71/-2.70	1.09/-1.58

4.8	**4.10**	**5.1**
$C_{54}H_{120}N_{12}P_{12}S_{12}$	$C_{62}H_{123}N_{12}P_{12}S_6Se_6$	$C_{28}H_{42}N_4P_2$
1693.98	2074.48	495.61
220(2)	180(2)	199.15
triclinic	triclinic	orthorhombic
$P2_1$	P-1	$P2_12_12_1$
25.1072(5)	14.1175(5)	10.343(2)
27.6627(5)	16.9798(5)	13.287(2)
32.8288(6)	28.2307(9)	21.025(5)
90	89.0600(10)	90
108.2270(10)	89.647(2)	90
90	65.5640(10)	90
21656.6(7)	6160.2(3)	2889.5(10)
12	2	4
1.559	1.118	1.1392
6.273	4.776	0.172
10800	2118	1069.1
0.40 × 0.19 × 0.14	0.400 × 0.280 × 0.270	1 × 0.27 × 0.26
CuKα (λ = 1.54178)	CuKα (λ = 1.54178)	MoKα (λ = 0.71073)
4.26 to 133.76	5.718 to 133.468	3.62 to 43.78
278665	177320	24527
75480 [R_{int} = 0.0572, R_σ = 0.0204]	21743 [Rint = 0.0620, Rσ = 0.0319]	3471 [R_{int} = 0.0733, R_σ = 0.0494]
75480/1866/3556	21743/0/920	3471/0/320
1.261	1.03	1.053
R_1 = 0.0944, wR_2 = 0.2910	R1 = 0.0847, wR2 = 0.2461	R_1 = 0.0437, wR_2 = 0.1131
R_1 = 0.1132, wR_2 = 0.3175	R1 = 0.0898, wR2 = 0.2497	R_1 = 0.0666, wR_2 = 0.1392
2.55/-1.04	2.75/-0.93	0.27/-0.33
0.45(2)		

5.2	**5.3**	**5.4**
$C_{28}H_{41}N_4P_2$	$C_{32}H_{42}N_4P_2$	$C_{24}H_{38}N_4P_2$
495.61	544.64	444.54
199.15	180(2)	200.15
orthorhombic	monoclinic	monoclinic
$P2_12_12_1$	C2	C2
10.343(2)	19.3277(5)	26.731(7)
13.287(2)	5.8281(2)	5.8097(13)
21.025(5)	13.9080(4)	20.651(5)
90	90	90
90	97.904(2)	126.161(6)
90	90	90
2889.5(10)	1551.77(8)	2589.2(11)
4	2	4
1.1392	1.166	1.1403
0.172	0.167	0.185
1069.1	584	961.1
1 × 0.27 × 0.26	0.35 × 0.14 × 0.07	0.74 × 0.2 × 0.16
MoKα (λ = 0.71073)	MoKα (λ = 0.71073)	MoKα (λ = 0.71073)
3.62 to 43.78	7.3 to 54.96	2.44 to 41.06
24527	8671	2611
3471 [R_{int} = 0.0733, R_σ = 0.0494]	3114 [R_{int} = 0.0480, R_σ = 0.0440]	2611 [R_{int} = 0.0000, R_σ = 0.0769]
3471/0/320	3114/1/176	2611/0/278
1.053	1.062	1.377
R_1 = 0.0437, wR_2 = 0.1131	R_1 = 0.0392, wR_2 = 0.0855	R_1 = 0.0604, wR_2 = 0.1326
R_1 = 0.0666, wR_2 = 0.1392	R_1 = 0.0475, wR_2 = 0.0900	R_1 = 0.0849, wR_2 = 0.1615
0.27/-0.33	0.29/-0.20	0.50/-0.47
-0.06(15)	0.01(10)	-0.02(17)

8.2 Computational Studies on $[S=P(H)(\mu\text{-}NR)]_2$

General Information

Computational studies of the four different derivatives (R = ^{t}Bu, Dipp, Mes, Benz) were performed employing Gaussian 09 Rev. B.01 software package.[136] All structures were optimized at the B3LYP/cc-pVTZ (PCM = thf) level of theory.[132–135] Frequency calculations were performed to ensure that all found geometries correspond to energetic minima on the PES. Coordinates of optimized structures can be found in a separate geometry file. The following nomenclature has been used in this file:

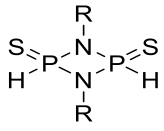
R_phn_s_*cis*

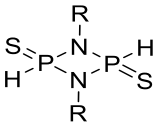
R_phn_s_*trans*

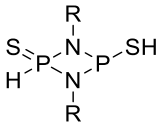
R_phn_sh_*cis*

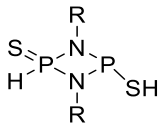
R_phn_sh_*trans*

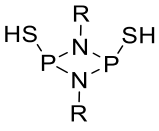
R_pn_sh_*cis*

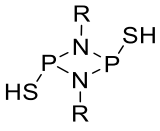
R_pn_sh_*trans*

Thermodynamic Data

Unless stated otherwise all energies are provided in atomic units.

R = ^{t}Bu	phn_s_*cis*	phn_s_*trans*	phn_sh_*cis*	phn_sh_*trans*	pn_sh_*cis*	sh_*trans*
E0	-1905,8641	-1905,8609	-1905,8576	-1905,8544	-1905,8478	-1905,8415
EZPE	0,2809	0,2809	0,2782	0,2781	0,2758	0,2756
Etot	0,2993	0,2993	0,2976	0,2975	0,2960	0,2958
Hcorr	0,3002	0,3002	0,2985	0,2984	0,2970	0,2968
Gcorr	0,2350	0,2352	0,2311	0,2306	0,2274	0,2275
E0+EZPE	-1905,5832	-1905,5800	-1905,5794	-1905,5763	-1905,5720	-1905,5659
E0+Etot	-1905,5648	-1905,5616	-1905,5600	-1905,5569	-1905,5518	-1905,5456
E0+Hcorr	-1905,5639	-1905,5607	-1905,5591	-1905,5560	-1905,5508	-1905,5447
E0+Gcorr	-1905,6291	-1905,6257	-1905,6265	-1905,6238	-1905,6204	-1905,6140
ΔE	0,0000	0,0032	0,0066	0,0097	0,0163	0,0227
ΔE kJ/mol	0,00	8,52	17,20	25,56	42,85	59,50

ΔH	0,0000	0,0032	0,0048	0,0079	0,0131	0,0192
ΔH kJ/mol	0,00	8,42	12,62	20,72	34,28	50,40
ΔG	0,0000	0,0034	0,0026	0,0053	0,0087	0,0152
ΔG kJ/mol	0,00	9,04	6,91	14,01	22,85	39,82

R = Dipp	phn_s_*cis*	phn_s_*trans*	phn_sh_*cis*	phn_sh_*trans*	pn_sh_*cis*	sh_*trans*
E0	-2525,4231	-2525,4233	-2525,4166	-2525,4169	-2525,4069	-2525,4054
EZPE	0,5551	0,5548	0,5524	0,5523	0,5501	0,5494
Etot	0,5889	0,5887	0,5871	0,5871	0,5856	0,5853
Hcorr	0,5898	0,5897	0,5881	0,5881	0,5865	0,5863
Gcorr	0,4896	0,4882	0,4845	0,4851	0,4824	0,4792
E0+EZPE	-2524,8680	-2524,8685	-2524,8642	-2524,8646	-2524,8568	-2524,8561
E0+Etot	-2524,8342	-2524,8346	-2524,8295	-2524,8298	-2524,8213	-2524,8201
E0+Hcorr	-2524,8333	-2524,8337	-2524,8286	-2524,8289	-2524,8203	-2524,8191
E0+Gcorr	-2524,9335	-2524,9351	-2524,9321	-2524,9318	-2524,9244	-2524,9262
ΔE	0,0000	-0,0002	0,0065	0,0062	0,0162	0,0177
ΔE kJ/mol	0,00	-0,58	17,03	16,25	42,64	46,44
ΔH	0,0000	-0,0004	0,0047	0,0044	0,0129	0,0141
ΔH kJ/mol	0,00	-1,03	12,38	11,58	33,97	37,10
ΔG	0,0000	-0,0016	0,0014	0,0017	0,0091	0,0073
ΔG kJ/mol	0,00	-4,22	3,69	4,35	23,82	19,08

R = Mes	phn_s_*cis*	phn_s_*trans*	phn_sh_*cis*	phn_sh_*trans*	pn_sh_*cis*	sh_*trans*
E0	-2289,5382	-2289,5382	-2289,5325	-2289,5331	-2289,5236	-2289,5227
EZPE	0,3828	0,3832	0,3805	0,3804	0,3781	0,3778
Etot	0,4100	0,4101	0,4084	0,4083	0,4068	0,4067
Hcorr	0,4109	0,4111	0,4094	0,4093	0,4078	0,4076
Gcorr	0,3231	0,3240	0,3199	0,3201	0,3168	0,3164
E0+EZPE	-2289,0956	-2289,0957	-2289,0914	-2289,0924	-2289,0842	-2289,0835
E0+Etot	-2289,0685	-2289,0688	-2289,0635	-2289,0645	-2289,0555	-2289,0546
E0+Hcorr	-2289,0675	-2289,0678	-2289,0626	-2289,0636	-2289,0545	-2289,0537
E0+Gcorr	-2289,1553	-2289,1549	-2289,1520	-2289,1527	-2289,1455	-2289,1449
ΔE	0,0000	0,0000	0,0056	0,0050	0,0145	0,0155

ΔE kJ/mol	0,00	-0,05	14,72	13,17	38,13	40,57
ΔH	0,0000	-0,0003	0,0050	0,0039	0,0130	0,0138
ΔH kJ/mol	0,00	-0,88	13,00	10,28	34,11	36,29
ΔG	0,0000	0,0004	0,0033	0,0026	0,0098	0,0105
ΔG kJ/mol	0,00	1,00	8,64	6,84	25,71	27,45

R = Benz	phn_s_*cis*	phn_s_*trans*	phn_sh_*cis*	phn_sh_*trans*	pn_sh_*cis*	sh_*trans*
E0	-2594,4608	-2594,4647	-2594,4581	-2594,4586	-2594,4528	-2594,4481
EZPE	0,4378	0,4373	0,4354	0,4349	0,4326	0,4324
Etot	0,4663	0,4660	0,4647	0,4645	0,4630	0,4628
Hcorr	0,4672	0,4670	0,4656	0,4654	0,4639	0,4638
Gcorr	0,3733	0,3704	0,3702	0,3683	0,3647	0,3641
E0+EZPE	-2593,9586	-2593,9606	-2593,9575	-2593,9571	-2593,9524	-2593,9475
E0+Etot	-2593,9300	-2593,9318	-2593,9282	-2593,9275	-2593,9220	-2593,9171
E0+Hcorr	-2593,9291	-2593,9309	-2593,9273	-2593,9265	-2593,9210	-2593,9161
E0+Gcorr	-2594,0230	-2594,0275	-2594,0227	-2594,0237	-2594,0202	-2594,0158
ΔE	0,0000	-0,0039	0,0027	0,0022	0,0080	0,0127
ΔE kJ/mol	0,00	-10,31	7,20	5,87	21,03	33,24
ΔH	0,0000	-0,0018	0,0018	0,0026	0,0081	0,0130
ΔH kJ/mol	0,00	-4,61	4,81	6,71	21,21	34,07
ΔG	0,0000	-0,0044	0,0004	-0,0006	0,0028	0,0073
ΔG kJ/mol	0,00	-11,60	0,94	-1,62	7,39	19,06

Geometries

R = ^{t}Bu

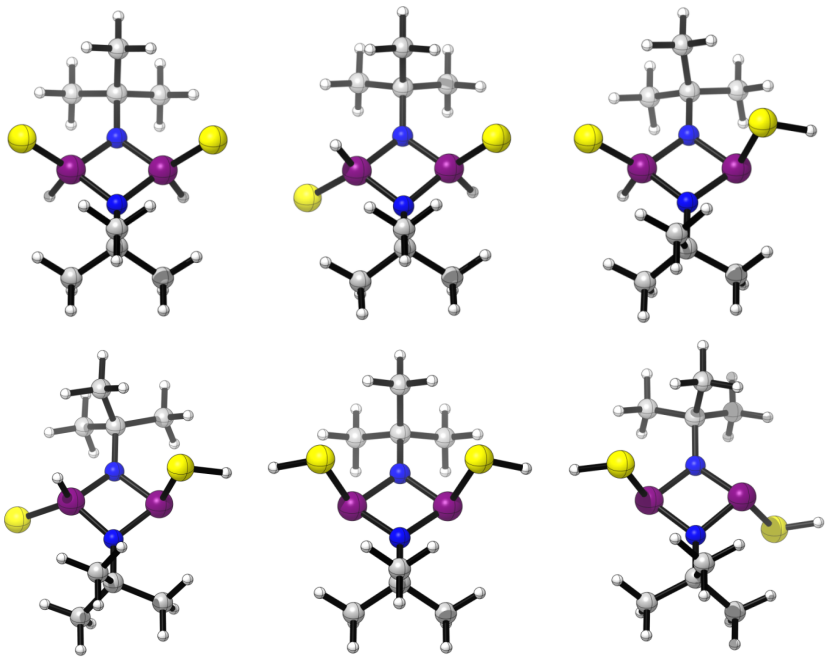

R = Dipp

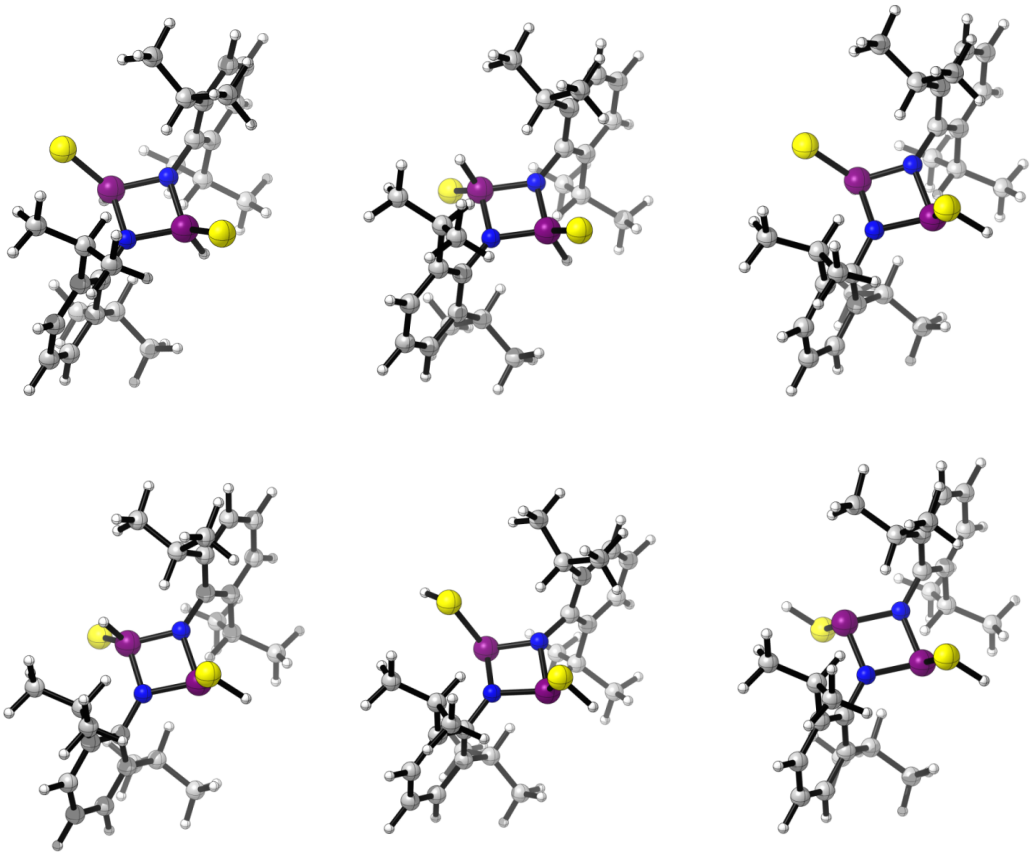

R = Mes

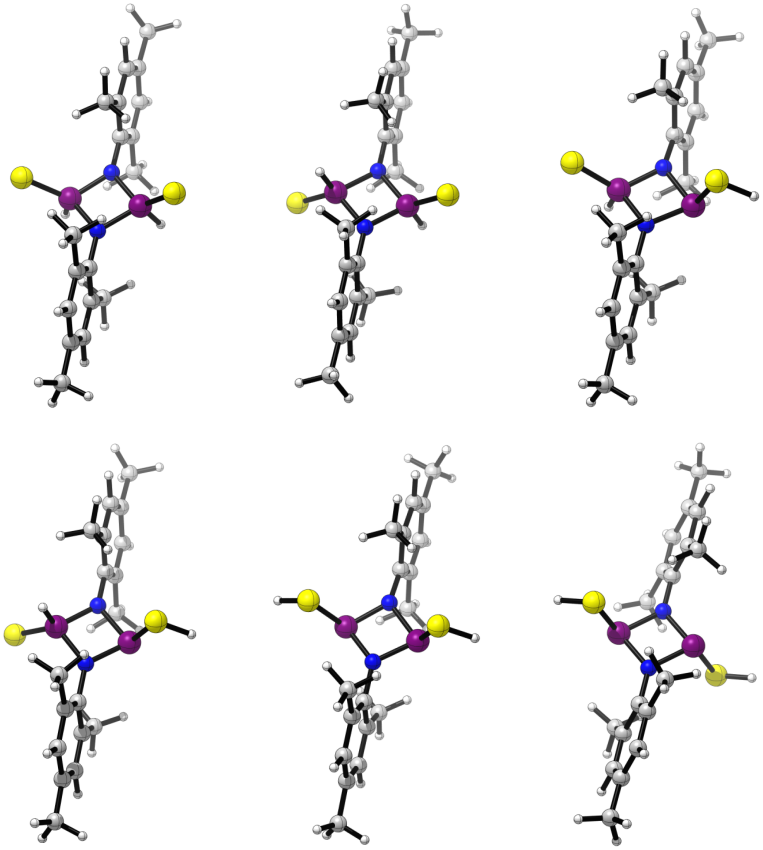

R = Benzhydryl

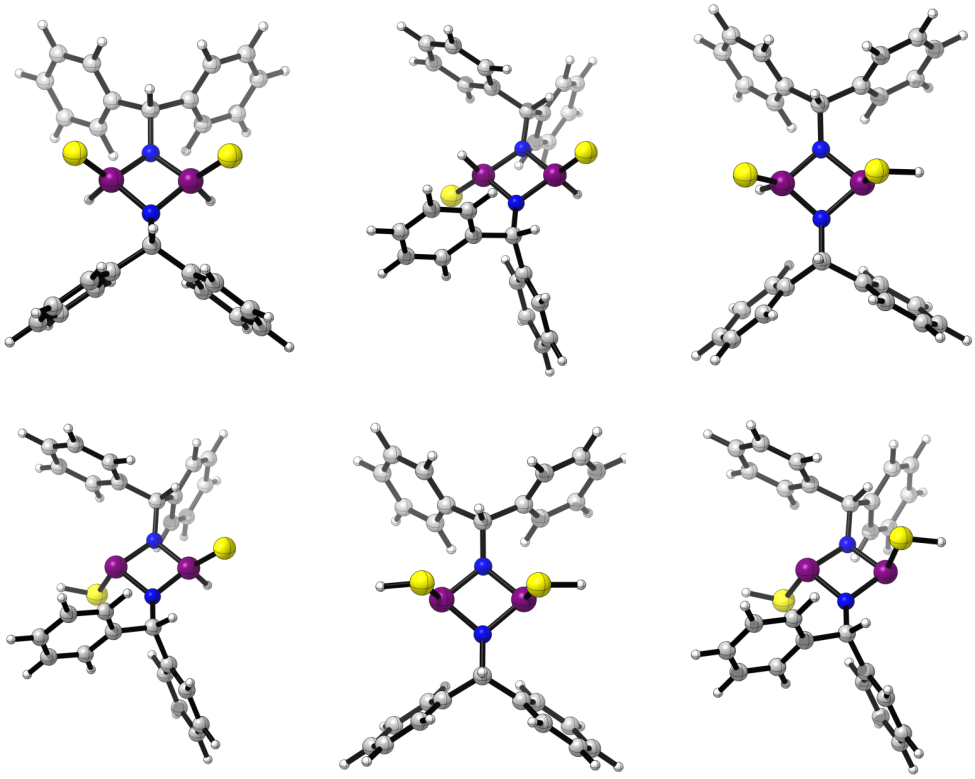

Activation Barriers

Calculations have been performed for the isomer bearing a ^{t}Bu substituent. The same basis set, functional and solvent as for the previous calculations has been used. The following intramolecular inversion mechanisms have been considered: (i) direct inversion of the tetrahedral phosphorus centres (marked in red, *via* TS1, Figure 10.1) and (ii) proton shift from P to S (*via* TS2) followed by lone-pair inversion at the P centre (*via* TS3, vertex inversion). Transition states have been optimized and their nature has been confirmed by frequency calculations giving one imaginary frequency.

	TS1	**TS2**	**TS3**
E0	-1905,7748	-1905,7950	-1905,7843
EZPE	0,2793	0,2771	0,2754
Etot	0,2973	0,2960	0,2943
Hcorr	0,2983	0,2969	0,2952
Gcorr	0,2341	0,2309	0,2288
E0+EZPE	-1905,4955	-1905,5178	-1905,5089
E0+Etot	-1905,4775	-1905,4990	-1905,4900
E0+Hcorr	-1905,4765	-1905,4980	-1905,4891
E0+Gcorr	-1905,5407	-1905,5641	-1905,5554
ΔE	0,0893	0,0692	0,0798
ΔE kJ/mol	234,49	181,58	209,62
ΔH	0,0874	0,0658	0,0748
ΔH kJ/mol	229,34	172,88	196,47
ΔG	0,0884	0,0651	0,0737
ΔG kJ/mol	232,17	170,89	193,52

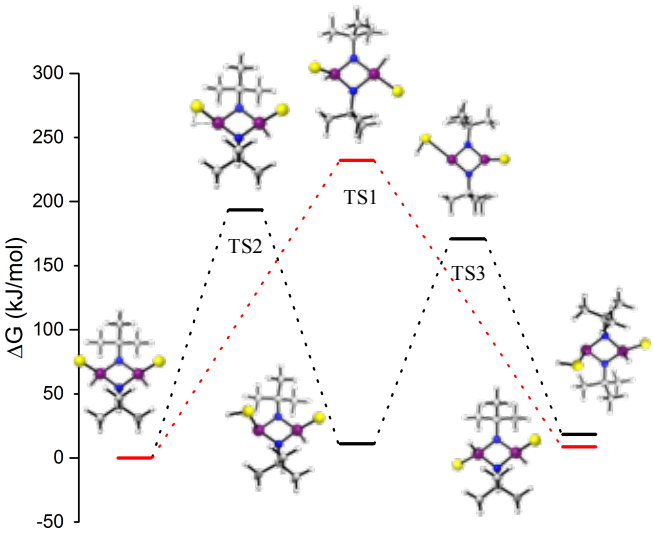

Figure 8.1: Transition state calculations- (i) a concerted pathway in which *cis*-3.1 is converted into *trans*-3.1 directly *via* rotation of one P(H)=S fragment (red); (ii) a stepwise pathway involving P(H)=S/P-SH tautomerism and phosphorus lone pair inversion (black

9. References

1. E. Niecke, M. Nieger, and F. Reichert, *Angew. Chemie Int. Ed.*, 1988, **27**, 1715–1716.

2. D. Gudat, E. Niecke, G. Grossmann, and K. Kruger, *Magn. Reson. Chem.*, 1999, **37**, 43–47.

3. A. B. Chaplin, J. A. Harrison, and P. J. Dyson, *Inorg. Chem.*, 2005, **44**, 8407–8417.

4. E. Magnusson, *J. Am. Chem. Soc.*, 1993, **115**, 1051–1061.

5. A. A. Korkin, *Russ. Chem. Rev.*, 1992, **61**, 473–483.

6. K. A. R. Mitchell, *Chem. Rev.*, 1969, **69**, 157–178.

7. H. Allcock and C. Crane, *Inorg. Chem.*, 1999, **38**, 280.

8. V. Chandrasekhar, P. Thilagar, and B. Murugesa Pandian, *Coord. Chem. Rev.*, 2007, 251, 1045–1074.

9. H. R. Allcock, *Soft Matter*, 2012, **8**, 7521.

10. H. R. Allcock, *Appl. Organomet. Chem.*, 2013, **27**, 620–629.

11. V. Blackstone, A. J. Lough, M. Murray, and I. Manners, *J. Am. Chem. Soc.*, 2009, **131**, 3658–3667.

12. M. Bendle, R. Kuzora, I. Manners, P. Rupar, A. Schulz, and A. Villinger, *Eur. J. Inorg. Chem.*, 2014, **2014**, 1735–1744.

13. I. N. Zhmurova and A. V Kirsanov, *Zhurnal Obs. Khimii*, 1959, **29**, 1687–1694.

14. H. Thönnessen, T. Siedentop, P. G. Jones, and R. Schmutzler, *Zeitschrift für Anorg. und Allg. Chemie*, 2001, **627**, 731–741.

15. A. F. Grapov, N. N. Mel'nikov, and L. V Razvodovskaya, *Russ. Chem. Rev.*, 1970, **39**, 20–30.

16. O. J. Scherer and P. Klusmann, *Angew. Chemie*, 1969, **81**, 743–744.

17. A.-L. Wang, S.-J. Lu, H.-X. Fu, H.-Q. Wang, and X.-Y. Huang, *Carbohydr. Res.*, 1996, **281**,

301–305.

18. J. F. Nixon and B. Wilkins, *Zeitschrift für Naturforsch. B*, 1970, **25**, 649–650.

19. L. Stahl, *Coord. Chem. Rev.*, 2000, **210**, 203–250.

20. F. Garcia, R. A. Kowenicki, L. Riera, and D. S. Wright, *Dalt. Trans.*, 2005, 2495–2496.

21. R. A. Kowenicki, Thesis, University of Cambridge (United Kingdom), 2005.

22. A. L. Brazeau, M. M. Hänninen, H. M. Tuononen, N. D. Jones, and P. J. Ragogna, *J. Am. Chem. Soc.*, 2012, **134**, 5398–5414.

23. N. Burford, S. T. Cameron, K. D. Conroy, B. Ellis, M. Lumsden, C. L. B. Macdonald, R. McDonald, A. D. Phillips, P. J. Ragogna, R. W. Schurko, D. Walsh, and R. E. Wasylishen, *J. Am. Chem. Soc.*, 2002, **124**, 14012–14013.

24. N. Burford, T. S. Cameron, K. D. Conroy, B. Ellis, C. L. B. Macdonald, R. Ovans, A. D. Phillips, P. J. Ragogna, and D. Walsh, *Can. J. Chem. Can. Chim.*, 2002, **80**, 1404–1409.

25. H. J. Chen, R. C. Haltiwanger, T. G. Hill, M. L. Thompson, D. E. Coons, and A. D. Norman, *Inorg. Chem.*, 1985, **24**, 4725–4730.

26. K. V. Axenov, V. V. Kotov, M. Klinga, M. Leskelä, and T. Repo, *Eur. J. Inorg. Chem.*, 2004, 695–706.

27. C. R. Groom, I. J. Bruno, M. P. Lightfoot, and S. C. Ward, *Acta Crystallogr. Sect. B Struct. Sci. Cryst. Eng. Mater.*, 2016, **72**, 171–179.

28. I. Silaghi-Dumitrescu and I. Haiduc, *Phosphorus. Sulfur. Silicon Relat. Elem.*, 1994, **91**, 21–36.

29. E. L. Doyle, University of Cambridge, 2004.

30. D. F. Moser, C. J. Carrow, L. Stahl, and R. J. Staples, *J. Chem. Soc. Dalt. Trans.*, 2001, 1246–1252.

31. T. Roth, H. Wadepohl, D. S. Wright, and L. H. Gade, *Chem. - A Eur. J.*, 2013, **19**, 13823–13837.

32. I. Schranz, L. Stahl, and R. J. Staples, *Inorg. Chem.*, 1998, **37**, 1493–1498.

33. I. Schranz, L. P. Grocholl, L. Stahl, R. J. Staples, and A. Johnson, *Inorg. Chem.*, 2000, **39**, 3037–41.

34. D. Moser, L. Grocholl, L. Stahl, and R. Staples, *Dalt. Trans.*, 2003, 1402–1410.

35. G. R. Lief, C. J. Carrow, L. Stahl, and R. J. Staples, *Organometallics*, 2001, **20**, 1629–1635.

36. A. Bashall, A. D. Bond, E. L. Doyle, F. García, S. Kidd, G. T. Lawson, M. C. Parry, M. McPartlin, A. D. Woods, and D. S. Wright, *Chem. - A Eur. J.*, 2002, **8**, 3377–3385.

37. S. G. Calera, S. González Calera author., and S. G. Calera, PhD Thesis, University of Cambridge, 2013.

38. W. T. K. Chan, D. Eisler, F. García, S. Gonzalez-Calera, M. McPartlin, J. V Morey, R. E. Mulvey, S. Singh, A. Steiner, and D. S. Wright, *Chem. Commun. (Camb).*, 2008, 2251–3.

39. A. Bashall, E. L. Doyle, C. Tubb, S. J. Kidd, M. Mcpartlin, D. Anthony, and D. S. Wright, *Chem. Commun.*, 2001, **2**, 2542–2543.

40. E. L. Doyle, F. García, S. M. Humphrey, R. A. Kowenicki, L. Riera, A. D. Woods, and D. S. Wright, *Dalt. Trans.*, 2004, 807–812.

41. M. H. Holthausen and J. J. Weigand, *J. Am. Chem. Soc.*, 2009, **131**, 14210–14211.

42. N. Burford, K. D. Conroy, J. C. Landry, P. J. Ragogna, M. J. Ferguson, and R. McDonald, *Inorg. Chem.*, 2004, **43**, 8245–8251.

43. R. J. Davidson, J. J. Weigand, N. Burford, T. S. Cameron, A. Decken, and U. Werner-Zwanziger, *Chem. Commun.*, 2007, 4671.

44. F. Reiß, A. Schulz, A. Villinger, and N. Weding, *Dalt. Trans.*, 2010, **39**, 9962.

45. T. Beweries, R. Kuzora, U. Rosenthal, A. Schulz, and A. Villinger, *Angew. Chemie Int. Ed.*, 2011, **50**, 8974–8978.

46. A. Hinz, A. Schulz, and A. Villinger, *Chem. - A Eur. J.*, 2014, **20**, 3913–3916.

47. A. Hinz, R. Kuzora, U. Rosenthal, A. Schulz, and A. Villinger, *Chem. - A Eur. J.*, 2014, **20**, 14659–14673.

48. A. Hinz, A. Schulz, and A. Villinger, *Chem. Commun.*, 2013, **0**, 1–3.

49. Y. X. Shi, R. Z. Liang, K. A. Martin, N. Weston, S. Gonzalez-Calera, R. Ganguly, Y. Li, Y. Lu, A. J. M. Ribeiro, M. J. Ramos, P. A. Fernandes, and F. García, *Inorg. Chem.*, 2015, **54**, 6423–6432.

50. J. Weiss and G. Hartmann, *Zeitschrift für Naturforsch. B*, 1966, **21**, 891–892.

51. E. H. M. Ibrahim and R. A. Shaw, *Chem. Commun. (London)*, 1967, **0**, 244–245.

52. M. B. Peterson and A. J. Wagner, *J. Chem. Soc., Dalt. Trans.*, 1973, 106–111.

53. R. Keat, D. S. Rycroft, and D. G. Thompson, *J. Chem. Soc. Dalt. Trans.*, 1979, **19**, 1224.

54. R. Keat and D. G. Thompson, *J. Chem. Soc. Dalt. Trans.*, 1980, **1**, 928.

55. M. Vijjulatha, S. Kumaraswamy, K. C. K. Swamy, and U. Engelhardt, *Polyhedron*, 1999, **18**, 2557–2562.

56. P. Kommana and K. C. K. Swamy, *Inorg. Chem.*, 2000, **39**, 4384–4385.

57. M. Chakravarty, P. Kommana, and K. C. K. Swamy, *Chem. Commun.*, 2005, **28**, 5396.

58. T. Chivers, M. Krahn, M. Parvez, and G. Schatte, *Inorg. Chem.*, 2001, **40**, 2547–2553.

59. J. S. Ritch and T. Chivers, *Dalt. Trans.*, 2008, **2**, 957–962.

60. P. J. W. Elder, T. Chivers, and R. Thirumoorthi, *Eur. J. Inorg. Chem.*, 2013, **2013**, 2867–2876.

61. L. Jeremias, M. Babiak, V. Kubát, M. J. Calhorda, Z. Trávníček, and J. Novosad, *RSC Adv.*, 2014, **4**, 15428.

62. J. Konu, H. M. Tuononen, and T. Chivers, *Inorg. Chem.*, 2009, **48**, 11788–11798.

63. T. Chivers, M. Krahn, and M. Parvez, *Chem. Commun.*, 2000, **5**, 463–464.

64. A. Nordheider, K. S. Athukorala Arachchige, A. M. Z. Slawin, J. D. Woollins, T. Chivers, K. S. A. Arachchige, A. M. Z. Slawin, J. D. Woollins, and T. Chivers, *Dalt. Trans.*, 2015, **44**, 8781–8783.

65. A. Nordheider, J. D. Woollins, and T. Chivers, *Chem. Rev.*, 2015, 115, 10378–10406.

66. R. Noyori, *Angew. Chemie Int. Ed.*, 2002, **41**, 2008.

67. A. Suzuki, *Angew. Chemie Int. Ed.*, 2011, **50**, 6722–6737.

68. C. C. C. Johansson Seechurn, M. O. Kitching, T. J. Colacot, and V. Snieckus, *Angew. Chemie Int. Ed.*, 2012, **51**, 5062–5085.

69. E. Negishi, *Angew. Chemie Int. Ed.*, 2011, **50**, 6738–6764.

70. S. Lühr, J. Holz, and A. Börner, *ChemCatChem*, 2011, **3**, 1708–1730.

71. A. Börner, *Phosphorus Ligands in Asymmetric Catalysis*, Wiley-VCH Verlag, Weinheim, 1st Editio., 2008.

72. M. Van den Berg, A. J. Minnaard, E. P. Schudde, J. Van Esch, A. H. M. De Vries, J. G. De Vries, and B. L. Feringa, *J. Am. Chem. Soc.*, 2000, 122, 11539–11540.

73. B. L. Feringa, *Angew. Chemie Int. Ed.*, 1996, **35**, 2374–2376.

74. B. L. Feringa, M. Pineschi, L. A. Arnold, R. Imbos, and A. H. M. De Vries, *Angew. Chemie Int. Ed.*, 1997, **36**, 2620–2623.

75. A. Alexakis, J. Frutos, and P. Mangeney, *Tetrahedron: Asymmetry*, 1993, **4**, 2427–2430.

76. A. Gillon, K. Heslop, D. J. Hyett, A. Martorell, A. Guy Orpen, P. G. Pringle, C. Claver, and E. Fernandez, *Chem. Commun.*, 2000, **2**, 961–962.

77. K. V. Axenov, M. Klinga, M. Leskelä, V. Kotov, and T. Repo, *Eur. J. Inorg. Chem.*, 2004,

4702–4709.

78. K. V. Axenov, M. Leskelä, and T. Repo, *J. Catal.*, 2006, **238**, 196–205.

79. J. Burckett, B. St. Laurent, P. B. Hitchcock, and J. F. Nixon, *J. Organomet. Chem.*, 1983, **249**, 243–254.

80. in *IUPAC Compendium of Chemical Terminology*, IUPAC, Research Triagle Park, NC.

81. L. . Lindoy, *The Chemistry of Macrocyclic Ligand Complexes*, Cambridge University Press, Cambridge, 1991.

82. A. Bianchi, K. Bowman-James, and E. García-España, *Supramolecular Chemistry of Anions*, Wiley-VCH, 1997.

83. J. W. Steed and J. L. Atwood, *Supramolecular Chemistry*, Wiley, 2009.

84. J. N. Davidson, *The Biochemistry of the Nucleic Acids*, Springer Netherlands, 6th edn., 1969.

85. L. R. Snyder, J. J. Kirkland, and J. L. Glajch, *Practical HPLC Method Development*, Wiley, 1997.

86. Z. Zheng, C. B. Knobler, and M. F. Hawthorne, *J. Am. Chem. Soc.*, 1995, **117**, 5105–5113.

87. J. L. Atwood, L. J. Barbour, A. Jerga, and B. L. Schottel, *Science*, 2002, **298**, 1000–1002.

88. J. Melorose, R. Perroy, and S. Careas, in *Climate Change 2013 - The Physical Science Basis*, ed. Intergovernmental Panel on Climate Change, Cambridge University Press, Cambridge, 2015, vol. 1, pp. 1–30.

89. S. Rackley, *Carbon Capture and Storage*, Elsevier Science, 2009.

90. K. L. Lim, H. Kazemian, Z. Yaakob, and W. R. W. Daud, *Chem. Eng. Technol.*, 2010, **33**, 213–226.

91. L. Schlapbach and A. Züttel, *Nature*, 2001, **414**, 353–358.

92. K. Sumida, D. L. Rogow, J. A. Mason, T. M. McDonald, E. D. Bloch, Z. R. Herm, T.-H. H.

Bae, and J. R. Long, *Chem. Rev.*, 2012, **112**, 724–781.

93. P. K. Thallapally, G. O. Lloyd, T. B. Wirsig, M. W. Bredenkamp, J. L. Atwood, and L. J. Barbour, *Chem. Commun. (Camb).*, 2005, 5272–4.

94. P. K. Thallapally, T. B. Wirsig, L. J. Barbour, and J. L. Atwood, *Chem. Commun. (Camb).*, 2005, 4420–2.

95. S. J. Dalgarno, P. K. Thallapally, L. J. Barbour, and J. L. Atwood, *Chem. Soc. Rev.*, 2007, **36**, 236–245.

96. I. V. Bodrenko, A. V. Avdeenkov, D. G. Bessarabov, A. V. Bibikov, A. V. Nikolaev, M. D. Taran, and E. V. Tkalya, *J. Phys. Chem. C*, 2012, **116**, 25286–25292.

97. N. S. Venkataramanan, R. Sahara, H. Mizuseki, and Y. Kawazoe, *J. Phys. Chem. C*, 2008, **112**, 19676–19679.

98. S. Alavi, T. K. Woo, A. Sirjoosingh, S. Lang, I. Moudrakovski, and J. A. Ripmeester, *Chem. - A Eur. J.*, 2010, **16**, 11689–11696.

99. N. C. Norman, *Periodicity and the s- and p-Block Elements*, Oxford University Press, Oxford, 1997.

100. R. E. Mulvey, *Chem. Commun.*, 2001, 1049–1056.

101. W. Clegg, K. W. Henderson, A. R. Kennedy, R. E. Mulvey, C. T. O'Hara, R. B. Rowlings, and D. M. Tooke, *Angew. Chemie Int. Ed.*, 2001, **40**, 3902–3905.

102. D. Hoffmann, W. Bauer, F. Hampel, N. J. R. van Eikema Hommes, P. v. R. Schleyer, P. Otto, U. Pieper, D. Stalke, D. S. Wright, and R. Snaith, *J. Am. Chem. Soc.*, 1994, **116**, 528–536.

103. N. Etkin, M. C. Fermin, and D. W. Stephan, *J. Am. Chem. Soc.*, 1997, **119**, 2954–2955.

104. W. C. Marsh and J. Trotter, *J. Chem. Soc. A Inorganic, Phys. Theor.*, 1971, 1482.

105. J. P. O'Brien, R. W. Allen, and H. R. Allcock, *Inorg. Chem.*, 1979, **18**, 2230–2235.

106. J. S. Ritch and T. Chivers, *Angew. Chemie Int. Ed.*, 2007, **46**, 4610–4613.

107. M. A. Beswick, M. K. Davies, M. A. Paver, P. R. Raithby, A. Steiner, and D. S. Wright, *Angew. Chemie Int. Ed.*, 1996, **35**, 1508–1510.

108. R. Bryant, S. C. James, J. C. Jeffery, N. C. Norman, A. G. Orpen, and U. Weckenmann, *J. Chem. Soc. Dalt. Trans.*, 2000, 4007–4009.

109. F. García, D. J. Linton, M. McPartlin, A. Rothenberger, A. E. H. Wheatley, and D. S. Wright, *J. Chem. Soc. Dalt. Trans.*, 2002, **2**, 481–483.

110. J. E. Huheey, E. a. Keiter, and R. L. Keiter, *Inorganic Chemistry: Principles of Structure and Reactivity (4th Edition)*, Harper Collins, 4th edn., 1993.

111. W. C. Marsh, N. L. Paddock, C. J. Stewart, and J. Trotter, *J. Chem. Soc. D Chem. Commun.*, 1970, 1190.

112. N. L. Paddock, T. N. Ranganathan, S. J. Rettig, R. D. Sharma, and J. Trotter, *Can. J. Chem.*, 1981, **59**, 2429–2434.

113. K. D. Gallicano, N. L. Paddock, S. J. Rettig, and J. Trotter, *Can. J. Chem.*, 1981, **59**, 2435–2440.

114. O. J. Scherer, K. Andres, C. Krüger, Y.-H. Tsay, and G. Wolmerhäser, *Angew. Chemie Int. Ed.*, 1980, **19**, 571–572.

115. J. K. Brask, T. Chivers, M. L. Krahn, and M. Parvez, *Inorg. Chem.*, 1999, **38**, 290–295.

116. R. E. Allan, M. A. Beswick, N. L. Cromhout, M. A. Paver, P. R. Raithby, A. Steiner, M. Trevithick, and D. S. Wright, *Chem. Commun.*, 1996, 1501–1502.

117. F. García, J. P. Hehn, R. A. Kowenicki, M. McPartlin, C. M. Pask, A. Rothenberger, M. L. Stead, and D. S. Wright, *Organometallics*, 2006, **25**, 3275–3281.

118. E. L. Doyle, L. Riera, and D. S. Wright, *Eur. J. Inorg. Chem.*, 2003, **2003**, 3279–3289.

119. M. S. Balakrishna, D. J. Eisler, and T. Chivers, *Chem. Soc. Rev.*, 2007, **36**, 650–664.

120. P. Chandrasekaran, J. T. Mague, R. Venkateswaran, and M. S. Balakrishna, *Eur. J. Inorg. Chem.*, 2007, **2007**, 4988–4997.

121. P. Chandrasekaran, J. T. Mague, and M. S. Balakrishna, *Dalt. Trans.*, 2009, **36**, 5478.

122. M. S. Balakrishna, *Dalt. Trans.*, 2016, **45**, 12252–12282.

123. S. G. Calera and D. S. Wright, *Dalt. Trans.*, 2010, **39**, 5055–5065.

124. M. Shionoya, H. Furuta, V. Lynch, A. Harriman, and J. L. Sessler, *J. Am. Chem. Soc.*, 1992, **114**, 5714–5722.

125. F. García, J. M. Goodman, R. A. Kowenicki, I. Kuzu, M. McPartlin, M. A. Silva, L. Riera, A. D. Woods, and D. S. Wright, *Chem. - A Eur. J.*, 2004, **10**, 6066–6072.

126. A. D. Bond, E. L. Doyle, F. García, R. A. Kowenicki, M. McPartlin, L. Riera, and D. S. Wright, *Chem. Commun.*, 2003, **8**, 2990–2991.

127. S. Gonzalez Calera, D. J. Eisler, J. M. Goodman, M. McPartlin, S. Singh, and D. S. Wright, *Dalt. Trans.*, 2009, **2**, 1293.

128. A. D. Bond, E. L. Doyle, F. García, R. A. Kowenicki, D. Moncrieff, M. McPartlin, L. Riera, A. D. Woods, and D. S. Wright, *Chem. - A Eur. J.*, 2004, **10**, 2271–2276.

129. S. González-Calera, D. J. Eisler, J. V. Morey, M. McPartlin, S. Singh, and D. S. Wright, *Angew. Chemie Int. Ed.*, 2008, **47**, 1111–1114.

130. D. Bawari, B. Prashanth, S. Ravi, K. R. Shamasundar, S. Singh, and D. S. Wright, *Chem. - A Eur. J.*, 2016.

131. R. Zahn, *Towards New Phosphazane Macrocycles*, 2011.

132. P. J. Stephens, F. J. Devlin, C. F. Chabalowski, and M. J. Frisch, *J. Phys. Chem.*, 1994, **98**, 11623–11627.

133. S. H. Vosko, L. Wilk, and M. Nusair, *Can. J. Phys.*, 1980, **58**, 1200–1211.

134. C. Lee, W. Yang, and R. G. Parr, *Phys. Rev. B*, 1988, **37**, 785–789.

135. A. D. Becke, *J. Chem. Phys.*, 1993, **98**, 5648.

136. D. J. Frisch, M. J.; Trucks, G.W.; Schlegel, H. B.; Scuseria, G. E.; Robb, M. A.; Cheeseman, J. R.; Scalmani, G.; Barone, V.;Mennucci, B.; Petersson, G. A.; Nakatsuji, H.; Caricato, M.; Li, X.; Hratchian, H. P.; Izmaylov, A. F.; Bloino, J.; Zheng, G.; Sonnenber, *Gaussian, Inc. Wallingford CT*, 2010, 2–3.

137. G. G. Briand, T. Chivers, and M. Krahn, *Coord. Chem. Rev.*, 2002, **233**–**234**, 237–254.

138. G. G. Briand, T. Chivers, M. Parvez, and G. Schatte, *Inorg. Chem.*, 2003, **42**, 525–531.

139. H. Jacobs, U. Metzner, R. Kirchgässner, H. D. Lutz, and K. Beckenkamp, *Zeitschrift für Anorg. und Allg. Chemie*, 1991, **598**, 175–192.

140. A. L. Spek, *Acta Crystallogr. Sect. C Struct. Chem.*, 2015, **71**, 9–18.

141. E. Pretsch, P. Bühlmann, and M. Badertscher, *Structure Determination of Organic Compounds*, Springer, Berlin, Heidelberg, 2009.

142. R. Linguerri, N. Komiha, J. Fabian, and P. Rosmus, *Zeitschrift für Phys. Chemie*, 2008, **222**, 163–176.

143. R. Steudel, Ed., *Topic in Current Chemistry*, Springer, Berlin, Heidelberg, 2003, vol. 231.

144. R. Jefferson, J. F. Nixon, T. M. Painter, R. Keat, and L. Stobbs, *J. Chem. Soc. Dalt. Trans.*, 1973, 1414–1419.

145. M. Vijjulatha, K. C. Kumara Swamy, J. J. Vittal, and L. L. Koh, *Polyhedron*, 1999, **18**, 2249–2254.

146. A. Nordheider, K. Hüll, J. K. D. Prentis, K. S. Athukorala Arachchige, A. M. Z. Slawin, J. D. Woollins, and T. Chivers, *Inorg. Chem.*, 2015, **54**, 3043–3054.

147. A. Nordheider, K. Hüll, K. S. Athukorala Arachchige, A. M. Z. Slawin, J. D. Woollins, R. Thirumoorthi, and T. Chivers, *Dalt. Trans.*, 2015, **44**, 5338–5346.

148. A. Nordheider, T. Chivers, R. Thirumoorthi, K. S. Athukorala Arachchige, A. M. Z. Slawin, J. D. Woollins, and I. Vargas-Baca, *Dalt. Trans.*, 2013, **42**, 3291–3294.

149. A. Nordheider, T. Chivers, R. Thirumoorthi, I. Vargas-Baca, and J. D. Woollins, *Chem. Commun.*, 2012, **48**, 6346.

150. A. J. Plajer, University of Cambridge, 2016.

151. M. M. Siddiqui, S. M. Mobin, J. T. Mague, and M. S. Balakrishna, *Polyhedron*, 2015, **101**, 179–184.

152. D. H. O'Brien, N. Dereu, C. K. Huang, K. J. Irgolic, and F. F. Knapp, *Organometallics*, 1983, **2**, 305–307.

153. N. Sandblom, T. Ziegler, and T. Chivers, *Can. J. Chem.*, 1996, **74**, 2363–2371.

154. *http://www.chem.wisc.edu/areas/reich/nmr/h-data/hdata.html*.

155. H. J. Reich, *J. Chem. Educ.*, 1995, **72**, 1086.

156. D. Coucouvanis and J. P. Fackler, *Inorg. Chem.*, 1967, **6**, 2047–2053.

157. Y. X. Shi, R. Z. Liang, K. A. Martin, D. G. Star, J. Díaz, X. Y. Li, R. Ganguly, and F. García, *Chem. Commun.*, 2015, **51**, 16468–16471.

158. G. J. P. Britovsek, V. C. Gibson, and D. F. Wass, *Angew. Chemie Int. Ed.*, 1999, **38**, 428–447.

159. V. C. Gibson and S. K. Spitzmesser, *Chem. Rev.*, 2003, **103**, 283–315.

160. R. F. Jordan, R. E. LaPointe, C. S. Bajgur, S. F. Echols, and R. Willett, *J. Am. Chem. Soc.*, 1987, **109**, 4111–4113.

161. W. Kuran, *Principles of Coordination Polymerisation: Heterogeneous and Homogeneous Catalysis in Polymer Chemistry-Polymerisation of Hydrocarbon, Heterocyclic, and*

Heterounsaturated Monomers, John Wiley, 2001.

162. G. R. Lief, D. F. Moser, L. Stahl, and R. J. Staples, *J. Organomet. Chem.*, 2004, **689**, 1110–1121.

163. H. Mack and M. S. Eisen, *J. Organomet. Chem.*, 1996, **525**, 81–87.

164. K. V. Axenov, I. Kilpeläinen, M. Klinga, M. Leskelä, and T. Repo, *Organometallics*, 2006, **25**, 463–471.

165. F. Reiß, A. Schulz, and A. Villinger, *Eur. J. Inorg. Chem.*, 2012, **2012**, 261–271.

166. B. R. James, E. Ochiai, and G. L. Rampel, *Inorg. Nucl. Chem. Lett.*, 1971, **7**, 781–784.

167. B. A. Schoenfelner and R. A. Potts, *A mixed valence complex of gold with dimethyl sulfoxide*, Pergamon, 1981, vol. 43.

168. K. V. Axenov, M. Klinga, O. Lehtonen, H. T. Koskela, M. Leskelä, and T. Repo, *Organometallics*, 2007, **26**, 1444–1460.

169. M. E. Otang, G. R. Lief, and L. Stahl, *J. Organomet. Chem.*, 2016, **820**, 98–110.

170. D. F. Shriver, *The Manipulation of Air-sensitive Compounds*, Wiley, 1969.

171. G. M. Sheldrick, *Acta Crystallogr. Sect. A Found. Adv.*, 2015, **71**, 3–8.

172. G. M. Sheldrick, *Acta Crystallogr. Sect. C Struct. Chem.*, 2015, **71**, 3–8.

173. G. M. Sheldrick, *Acta Crystallogr.*, 2008, 112–122.

174. O. V. Dolomanov, L. J. Bourhis, R. J. Gildea, J. A. K. Howard, and H. Puschmann, *J. Appl. Crystallogr.*, 2009, **42**, 339–341.